CLATHRATION BY DIOL HOSTS: THERMODYNAMICS AND STRUCTURE

by

Leonard James Barbour

Thesis presented to the

UNIVERSITY OF CAPE TOWN

for the degree of

DOCTOR OF PHILOSOPHY

Department of Chemistry

February 1994

Acknowledgements

I would like to express my gratitude to the following:

Professor Luigi Nassimbeni for many things, but mostly for his enthusiastic supervision and support of this work;

Associate Professor Mino Caira for his expert assistance with structure elucidation and for proofreading;

The Foundation for Research Development for partial financial support;

Mr Klaus Achleitner for combining his electronic talents with his keen enjoyment for problem-solving;

My parents for having me;

My wife Corinne for making me eat vegetables.

Publications and Conferences

The following publications have arisen from this work:

1 L. J. Barbour, K. Achleitner and J. R. Greene
A system for studying gas-solid reaction kinetics in controlled atmospheres
Thermochim. Acta, 1992,**205**,171

2 E. Weber, K. Skobridis and A. Wierig, L. J. Barbour, M. R. Caira and L. R. Nassimbeni,
Synthesis and solid-state inclusion properties of bis(diarylhydroxymethyl)-substituted 1,1'-binaphthyls. Crystal structures of a host and its pyridine clathrate.
Chem. Ber., 1993,**126**,1141

3 L. J. Barbour, S. A. Bourne, M. R. Caira, L. R. Nassimbeni, E. Weber, K. Skobridis and A. Wierig
Complexation with diol host compounds. Part 14. Inclusion compounds of 2,2'-bis(9-hydroxy-9-fluorenyl)biphenyl with acetonitrile, cyclohexanone, di-n-propylamine and dimethylformamide
Supramol. Chem., 1993,**1**,331

4 L. J. Barbour, M. R. Caira and L. R. Nassimbeni
Enclathration of diethyl ether
J. Chem. Soc., Perkin Trans. 2, 1993,1413

5 L. J. Barbour, M. R. Caira and L. R. Nassimbeni
Kinetics of Inclusion
J. Chem. Soc., Perkin Trans. 2, 1993,2321

Work was presented at the following conferences:

1 6th International Symposium on Molecular Recognition and Inclusion
Berlin, FRG, September 10 - 14, 1990

2 31st Convention of the South African Chemical Institute
Grahamstown, 23 - 27 June 1991

3 Conference on Molecular Recognition and Synthetic Design
University of Cape Town, 12 - 14 February 1992

4 4th International Summer School on Supramolecular Chemistry
Sobieszewo, Poland, 14 - 25 June 1993

5 Conference on Molecular Recognition and Synthetic Design
University of Cape Town, 9 - 11 February 1994

Abstract

Inclusion properties of the following seven diol host compounds were investigated:

Host 1 9,9′-bis(9,9′-dihydroxy-fluorene)

Host 2 1,1′-binaphthyl-2,2′-bis(diphenylhydroxymethyl)

Host 3 2,2′-bis(9-hydroxy-9-fluorenyl)biphenyl

Host 4 *trans*-9,10-dihydroxy-9,10-diphenyl-9,10-dihydroanthracene

Host 5 *trans*-9,10-dihydroxy-9,10-di-p-tolyl-9,10-dihydroanthracene

Host 6 *trans*-9,10-dihydroxy-9,10-di-p-*tert*-butylphenyl-9,10-dihydroanthracene

Host 7 *trans*-9,10-dihydroxy-9,10-di-α-naphthyl-9,10-dihydroanthracene

These compounds all possess molecular planes with bulky substituents and opposing hydroxyl moieties as probes for possible coordination to guest molecules by means of hydrogen bonding. Sixteen different inclusion compounds were formed with common organic solvents as the guests. Various characterisation techniques were used and the crystal structures of the inclusion compounds and of the α-phases of Hosts 2 and 5 were elucidated using single crystal X-ray diffraction methods.

Thermal decomposition studies using thermogravimetry and differential scanning calorimetry (DSC) were carried out in order to relate the strength of the host-guest interactions to the structures of the inclusion compounds. Owing to practical limitations, the DSC technique is not suitable for the measurement of ΔH for the decomposition of an inclusion compound where the guest is relatively volatile. Therefore an apparatus was devised to yield accurate ΔH° values for this process.

Some inclusion compounds are able to form as a result of a solid-gas reaction between the solid host and gaseous guest. Thus a second apparatus was devised in order to measure the kinetics of inclusion and to evaluate the activation energy for the solid-gas inclusion reaction. This apparatus also enables investigation of isothermal decomposition kinetics of inclusion compounds.

Potential energy calculations were carried out on crystallographically independent guest molecules of a selected inclusion compound. The decomposition pattern of the compound was then related to the different guest topologies within the structure.

In addition, several computer programs were developed in order to record, analyse and present crystallographic, thermal and kinetic data.

Abbreviations and Symbols

Most of the abbreviations and symbols used in this dissertation are widely accepted. Many relate to the well-documented discipline of crystallography and will thus not be explained here except to avoid possible ambiguities.

A	Arrhenius preexponential or frequency factor
ADC	analogue to digital converter
A.M.D.	accurate molecular mass determination
Ar	aryl moiety
CFOM	combined figure of merit
CSD	Cambridge Structural Database
D_m, D_c	measured and calculated density respectively
DEK	diethyl ketone
DMSO	dimethyl sulphoxide
DSC	differential scanning calorimetry
E	normalised structure factor
E	activation energy
G	guest
H	host
ΔH^o	standard state enthalphy change
I.R.	infrared spectroscopy
k	rate constant
K	equilibrium constant
L	litre (although "l" is the correct notation, "L" is used to avoid confusion with the number "1")
Ln	natural logarithm ("ln" is the correct notation but "Ln" has been used in diagrams to avoid confusion)
M_r	molecular mass
M.P.	melting point
M.S.	mass spectrometry

NMR	nuclear magnetic resonance spectroscopy
P	pressure
PC	personal computer
Ph	phenyl moiety
PTFE	polytetrafluoroethylene (teflon)
R	gas constant = 8.31441 J K^{-1} mol^{-1}
ΔS^{o}	standard state entropy change
T	temperature (in K or °C)
TG	thermogravimetry
V	cell volume
VGA	video graphics array
XRD	X-ray powder diffraction
Z	number of structural units per unit cell

α	the angle between the b and c unit cell axes, extent of reaction, or the phase of a potential host compound with no guest included
β	the angle between the a and c unit cell axes, or a known phase of an inclusion compound
γ	the angle between the a and b unit cell axes, or an intermediate phase of an inclusion compound
τ	torsion angle
$\simeq$	aromatic bond
···	non-bonded contact
$\angle$	angle

Contents

Chapter 1 Introduction

Historical overview

The history of inclusion compounds is traced back to 1811 when Davy[1] observed a chlorine clathrate hydrate, the preparation of which was later reported by Faraday.[2] Other significant early preparations of inclusion compounds are summarised in Table 1.1. From these reports, it is apparent that the nature of inclusion compounds was not well understood and none of the authors ventured to propose a structure.

Table 1.1 Chronology of important early studies of inclusion compounds

Year	System studied	Reference
1841	graphite intercalates	3
1849	β-quinol H_2S clathrate	4
1891	cyclodextrin inclusion compounds	5
1897	nickel cyanide ammonia inclusion of benzene	6
1906	inclusion compounds of triphenylmethane	7
1909	tri-*o*-thymotide inclusion of benzene	8
1914	clathrates of Dianin's compound	9
1916	inclusion compounds of cholic acids	10
1935	phenol clathrates	11
1940	urea inclusion compounds	12
1946	amylose inclusion compounds	13

The advent of X-ray structural studies of inclusion compounds is generally considered to be a milestone in the development of the field. In 1927, Caspari[14] determined the unit cell dimensions and space group for a quinol clathrate with methanol, but did not attempt to determine atomic coordinates. Then, in 1945, Palin and Powell[15] reported a preliminary structure of the host framework of the sulphur dioxide adduct of quinol using X-ray techniques (see Figure 1.1). They suggested that the SO_2 molecules are situated in the cavities formed as a result of the hydrogen bond linkages between the quinol molecules. Two years later these authors published details of an X-ray crystal structure determination showing conclusively that the sulphur dioxide molecules were indeed located in the cavities at non-linked distances from the quinol molecules.[16] The following year Powell[17] published a survey of known inclusion compounds and coined the term "*clathrate*" to describe compounds where one component is enclosed within the framework of another.

Since the pioneering work of Powell, the study of inclusion compounds has become a well-established branch of chemistry. This is mostly due to the increasing accessibility of X-ray crystallographic methods, because an understanding of the nature of inclusion compounds is largely dependent on knowledge of the spatial arrangements of their components. Over the last 45 years, the number of published studies of inclusion compounds has increased dramatically. This is evidenced by the

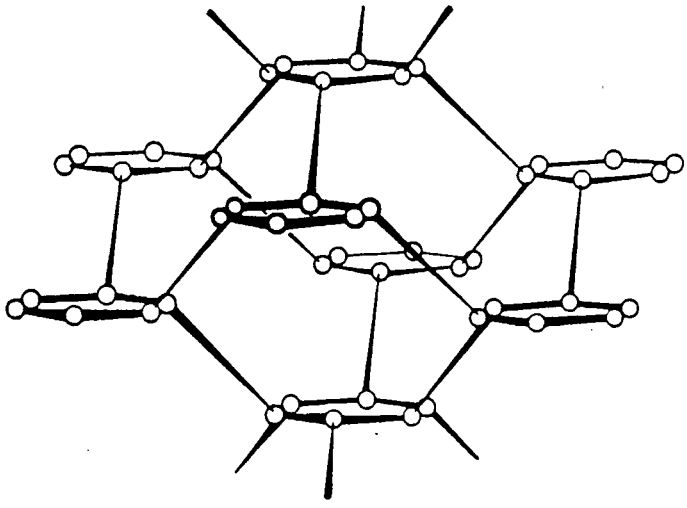

Figure 1.1 Host framework of the quinol/SO_3 inclusion compound. Hexagons denote hydrogen bonds and each of the longer sloping lines connecting different hexagons represents the oxygen-oxygen axis of a quinol molecule for which the benzene ring has been omitted for clarity.[15]

recent institution of two new journals, *viz.* the *Journal of Inclusion Phenomena* in 1983 and *Supramolecular Chemistry* in 1992. In addition, several volumes and review articles on the subject have been published.[18-30] However, perhaps the most significant indication of the importance of the study of inclusion compounds was the awarding of the 1987 Nobel Prize in Chemistry to D.J. Cram,[31] J.-M. Lehn[32] and C.J. Pederson[33] for their work in this field.

Classification of inclusion compounds

Inclusion compounds can be defined as compounds in which one type of molecule (the *host*) is able to enclose another molecule (the *guest*) within its structure whilst leaving the bonding network of each compound unchanged.

Today, two major directions of interest in inclusion phenomena can be identified as shown in Figure 1.2. The first deals with the binding or complexation of guest species by unimolecular hosts in *solution*. It should be noted that these compounds generally crystallise as inclusion compounds and are extensively studied in their solid state. Examples are the naturally-occurring cyclodextrins[34-36] and the synthetic crown ethers.[28] The second major aspect of inclusion chemistry relates to the study of multimolecular *crystalline* inclusion compounds.[18-26] The latter can further be subdivided into three groups:

i **clathrates**

Guest molecules act as templates in solution and induce, on crystallisation, orientation of the host molecules to form guest-specific voids, e.g. β-quinol clathrates.[18,19]

ii **channel** inclusion compounds
Guest species are accommodated in continuous channels running through the crystal, e.g. inclusion compounds formed by urea and thiourea.[37]

iii **layered** inclusion compounds
Guest species are accommodated between bands or layers of the host compound, e.g. intercalation compounds formed by graphite[38] and kaolinite.[39]

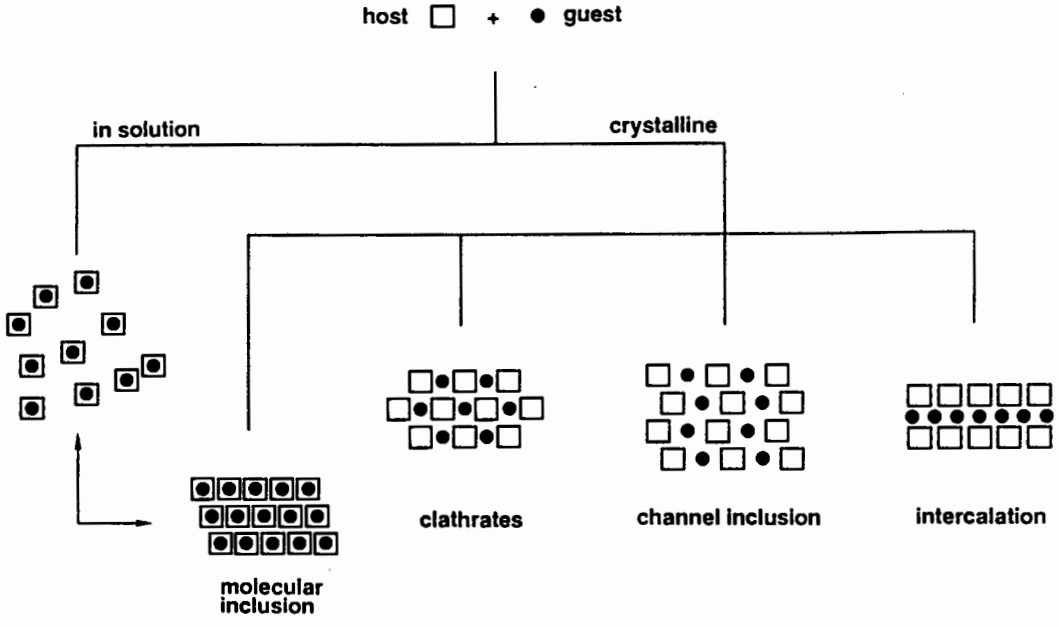

Figure 1.2 Classification of inclusion compounds.

The industrially important inorganic zeolites[40] form an intermediate class of inclusion compound since they possess cavities which are interconnected by channels. It should also be noted that although the occurrence of clathrates is normally limited to the solid state, clathrate formation in the liquid state has been reported.[41-46]

Owing to the relatively recent upsurge in interest in inclusion phenomena, there has been much confusion in the literature over terminology. Weber has recognised the need for a universal method of classification and nomenclature and has proposed a system based on host-guest *interactions* and the *topology* of the host-guest aggregate.[20,47]

Types of inclusion compounds

A growing number of types of inclusion compounds can be distinguished where diversity within a class is achieved by modification of the host compound by means of chemical substitution, or by alteration of the guest. Since justice cannot be done to all the known classes in one chapter, a few of the more widely studied host-guest systems are described briefly in an attempt to make the unfamiliar reader aware of the diversity and current trends of the field of inclusion chemistry :

A Inorganic hosts

i **Zeolites**[49] consist of a large group of porous tectosilicates with about sixty different framework topologies which occur naturally or have been synthesised. Each different framework is characterised by its unique system of channels and cavities giving rise to guest-shape-specific properties. This, coupled with their high stability, makes these compounds extremely versatile for industrial applications.

ii **Intercalation compounds**[39] are formed by the insertion of mobile atomic or molecular guest species into a solid host layered structure and are of interest as reversible battery electrodes, electrochromic displays, hydrogen storage devices, shape-selective heterogeneous catalysts, electro-catalysts and electronic conductors.

iii **Hofmann inclusion compounds**[50] have the general formula $M(NH_3)_2M'(CN)_4 \cdot 2G$ (M = Mn, Fe, Co, Ni, Cu, Zn or Cd; M′ = Ni, Pd or Pt; G is a small aromatic molecule). The metal complex hosts can include five- or six-membered aromatic molecules without bulky substituents. As shown in Figure 1.3, the host molecules form planar layers containing the metal atoms and the cyanide groups, but with the NH_3 moieties protruding above and below the planes. The latter then define a void within which the guest molecule is accommodated. Size selectivity is a characteristic of this host structure since the *c* dimension is relatively constant (a notable exception has M = Mn, M′ = Ni and G = biphenyl).

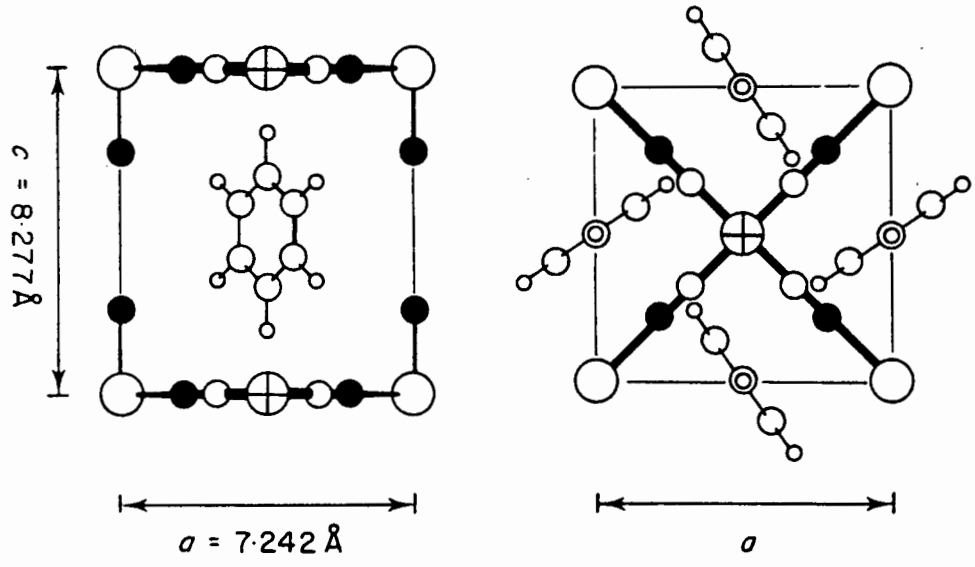

Figure 1.3 Structure of Hofmann's benzene clathrate $Ni(NH_3)_2Ni(CN)_4 \cdot 2C_6H_6$. Large open circle, six-coordinate Ni; crossed large circle, square-planar Ni; solid circle, N; open circle, C; small open circle, H. Host H atoms are not shown.[50]

iv **Werner clathrates**[51] consist of a wide range of inclusion compounds where the host component is a coordination compound with the general formula MX_2A_4 (M = Fe, Co, Ni, Cu, Zn, Cd, Mn, Hg or Cr; X = NCS^-, NCO^-, CN^-,NO_3^-, NO_2^-,Cl^-, Br^- or I^-; A is a neutral substituted pyridine and G is a small aromatic molecule). Irregular octahedral coordination about the metal atom and non-bonded repulsions in the densely populated central region result in a limited number of stable conformations of the host molecules. Schaeffer[52] has shown that these host structures are selective towards the isomers of disubstituted benzenes, and this property has been utilised in the chromatographic separation of these isomers.[53]

B Organic hosts

i **Urea**[37] forms inclusion compounds with *n*-alkanes and *n*-alkenes where $n \geq 6$ (substitution of the carbon chain is allowed to a small degree). The urea molecules hydrogen bond to one another forming long helical chains. This produces hollow channels (shown in cross-section in Figure 1.4) in which the guests can be accommodated. **Thiourea** inclusion compounds are analogous to those of urea. They have a larger channel diameter, thus allowing the inclusion of highly branched hydrocarbons. However, *n*-paraffins fit too loosely in the channels and are not included.

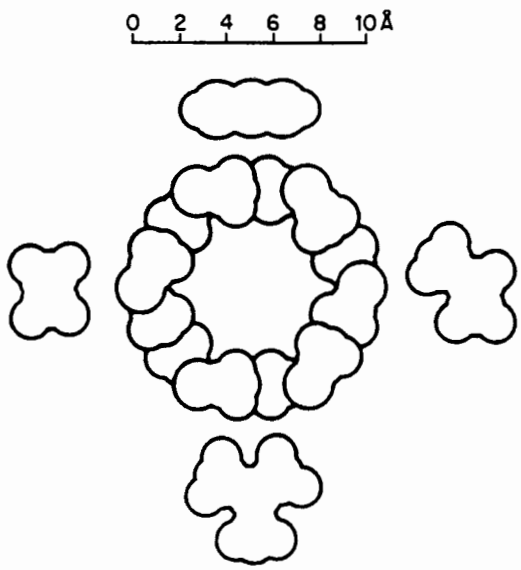

Figure 1.4 Van der Waals cross section of the cavity in the urea channel compared with the size of n-octane (left), benzene (top), 3-methylheptane (right) and 2,2,4-trimethylpentane (bottom).[54]

ii **Dianin's compound**, **hydroquinone** and **phenol** are precursors of an important class of host molecules which possess at least one phenolic hydroxyl group.[55] Dianin's compound [**1**] is a good example of a known clathrate host that has

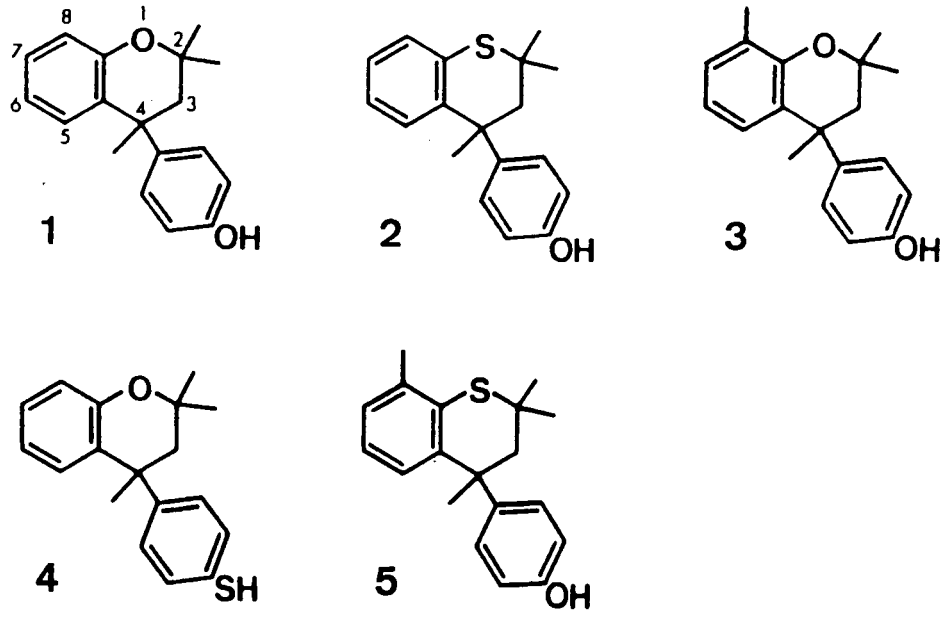

been structurally modified as a design strategy for new multimolecular host systems. Systematic studies have shown that the cage geometry can be altered markedly by replacement of the heteroatom[56] (e.g. [2]), substitution of the ring skeleton[57,58] (e.g. [3]), modification of the substitution at C(2) and C(4),[59,60] changing the hydrogen-bond functionality[61,62] (e.g. [4]), or combinations of the above (e.g. [5]). This is illustrated in Figure 1.5 which shows the difference in cavity shape between [2] and [5].

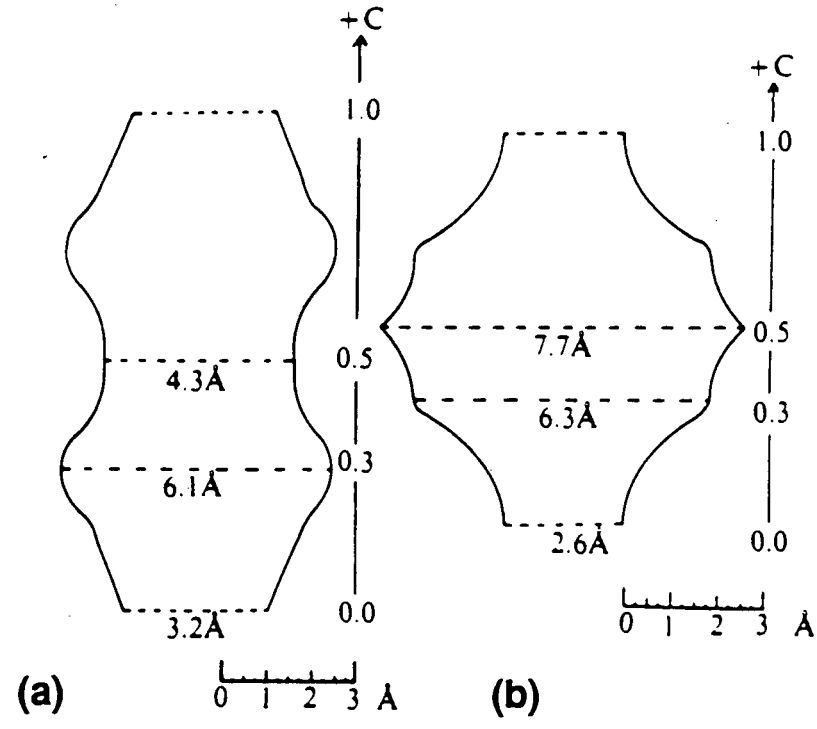

Figure 1.5 Section through the van der Waals surface of the cavity formed by (a) [2] and (b) [5].[63]

iii **Deoxycholic acid**[64] is a chiral compound isolated from the biles of some animals. Its remarkable properties as a versatile host are attributed to the existence of both hydrophilic and hydrophobic regions and it forms channel inclusion compounds with a wide variety of molecules (e.g. aliphatic, aromatic and alicyclic hydrocarbons, alcohols, ketones, fatty acids, esters, ethers, phenols, azo dyes, nitriles, peroxides and amines).

iv The **cyclodextrins**[30,65] are torus-shaped oligosaccharides made up of different numbers of α-1,4-linked d-glucopyranose units, α-, β- and γ-cyclodextrin comprising six, seven and eight units respectively (see Figure 1.6). They have an endolipophilic cavity, but are water-soluble owing to the many outward-pointing hydroxyl moieties. Host-guest interactions are found both in solution and in the crystalline state and with regard to the latter, both cage-type and channel-type inclusion compounds are formed. Cyclodextrins are relatively unselective, the most important factor governing inclusion compound formation being the size of the guest, and 1:1 complexes are usually formed. As hosts, they are used to encapsulate light- and oxygen-sensitive substances, fragrances, drugs and toxic compounds. In addition, their properties as "artificial enzymes" have received much attention.[23]

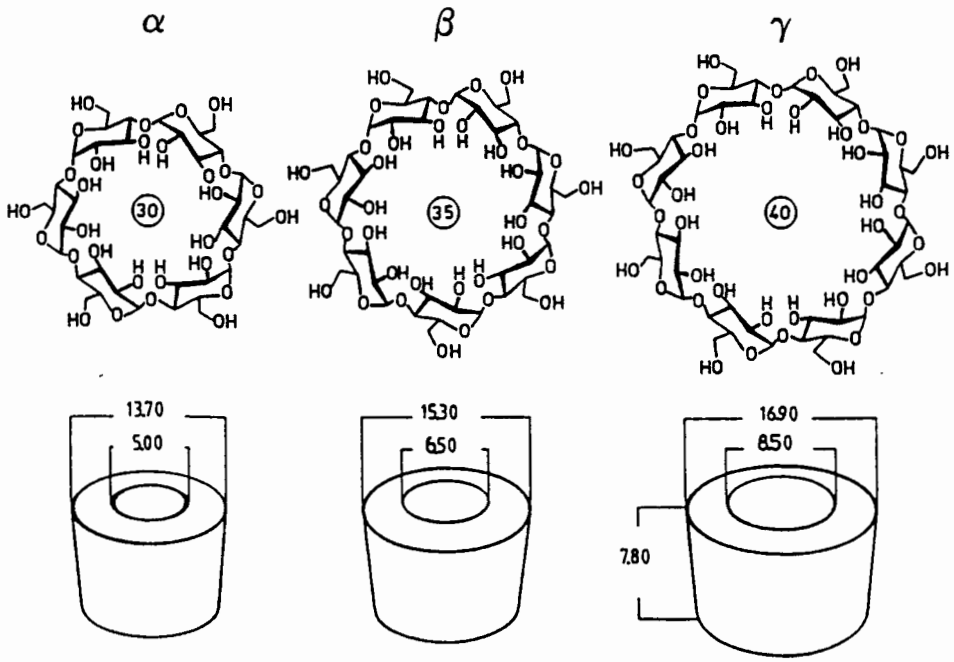

Figure 1.6 The structures and molecular dimensions of the α-, β- and γ-cyclodextrins. Lengths are in Å and the circled numbers indicate the ring-sizes (i.e. the number of atoms forming the ring).[23]

v **Crown ethers**,[28] a chance discovery,[33] also comprise a class of inclusion compound displaying host-guest interactions (usually 1:1) in solution as well as in the solid state. They are macrocyclic oligo-ethylene glycol ethers which can exist in many forms. Since their IUPAC names are rather cumbersome, Pederson's simplistic nomenclature has become accepted. Some examples of crown ethers are shown in Figure 1.7, [12]crown-4 being the smallest crown

ether capable of guest inclusion. For every hydrophilic oxygen atom, there exists a lipophilic ethylene moiety. Thus crown ethers are soluble in hydrophilic or lipophilic media. However, the type of solvent used determines the conformation of the macrocycle as shown in Figure 1.8. In a hydrophilic medium, the oxygen atoms point outwards, creating a lipophilic hydrocarbon core. Conversely, in a lipophilic medium, the oxygen atoms are forced inwards, forming a hydrophilic electron-rich cavity into which cations can be coordinated. By suitable modification of the ring-size and donor sites, crown ethers can be "fine-tuned" for guest-selectivity. The two main directions of interest in the utilisation of crown ethers are (a) separation and determination of ions for analytical purposes, and (b) synthesis involving ions or ionic intermediates. Other host-guest systems related to crown ethers, but which will not be discussed here, include **cryptands**, **podands** and **spherands**.

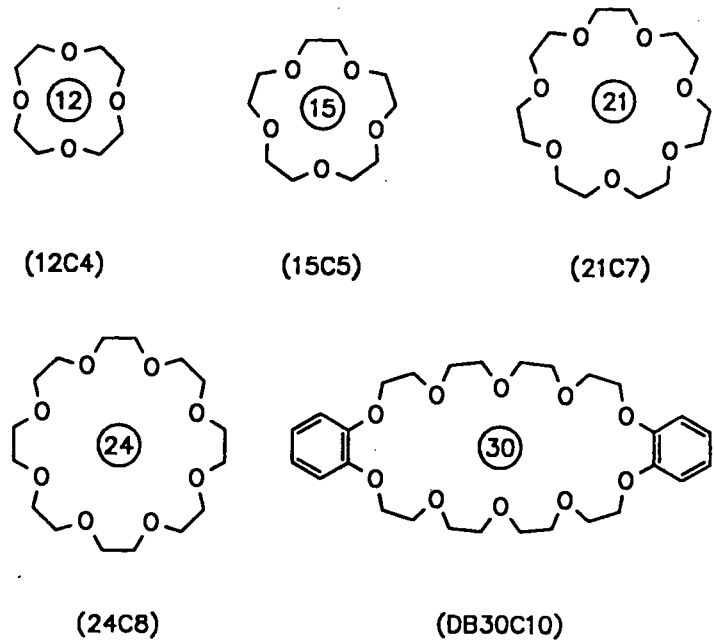

Figure 1.7 Crown-ethers with different ring sizes (circled) and numbers of donor atoms.[23]

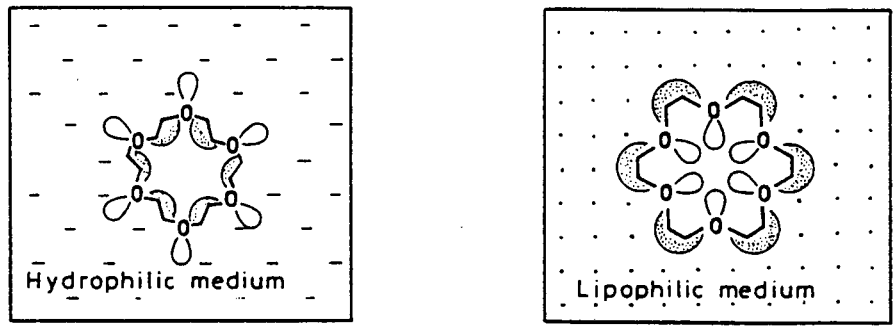

Figure 1.8 The effect of hydrophilic and lipophilic media on the conformation of [18]crown-6.[23]

vi **Cyclophanes**[29] are cyclic compounds containing non-fused aromatic rings and evolved from the study of bridged aromatic compounds.[65] They have neutral intramolecular cavities, giving them the ability to include a wide range of non-polar molecules. **Calixarenes**,[27,67] a subset of the cyclophanes, were developed specifically as mimics of enzyme activity.

vii In 1972, MacNicol and Wilson[68] considered whether, based on the knowledge of the crystal structures of known inclusion compounds, it is possible to design and synthesise new hosts which are unrelated to any known host compounds. They noted that the clathrates formed by hydroquinone, phenol, Dianin's compound and related systems share a common feature in the linking of the OH groups of six host molecules by a network of hydrogen bonds such that the oxygen atoms form a hexagonal arrangement as shown in Figure 1.9(a). However, a limitation of directed host design using these compounds is that the integrity of the hydrogen-bonded grouping depends on R. Thus the so-called "**hexa-host**" strategy was conceived whereby the hydrogen-bonded ring is replaced by a suitably hexasubstituted benzene molecule as shown in Figure 1.9(b). Using this strategy the permanent nature of the aromatic ring is exploited in order to avoid collapse of the hexamer. Since 1972 many inclusion compound hosts have been successfully synthesised based on the hexa-host strategy.[69] The significance of this work is that it has shown that new types of hosts can be actively sought or designed by applying the knowledge gained from structural investigations of known host-guest systems.

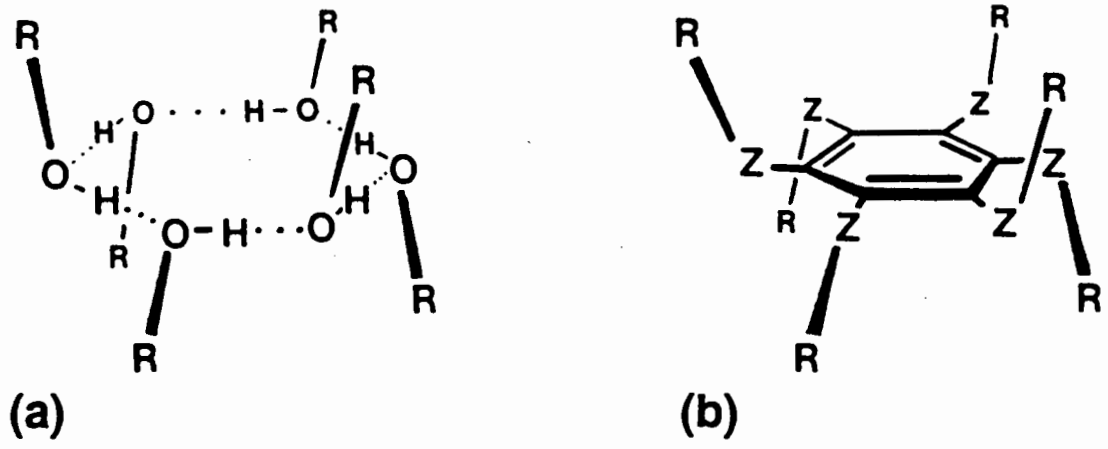

Figure 1.9 Comparison of (a) a hydrogen-bonded hexamer unit with (b) a hexasubstituted benzene analogue. Z is any bridging group or atom (usually CH_2).[69]

Directed host design

The majority of host compounds known to date have been discovered accidentally. The starting point of directed host design was the modification of known hosts like Dianin's compound in order to change or "fine-tune" their inclusion properties. However, Weber[20] suggests that true *directed host design* means the synthesis of *new* classes of host as exemplified by MacNicol's pioneering work on hexa-hosts. He has devised a strategy based on the formation of what he terms "*coordinatoclathrates*" in order to achieve chemoselective guest inclusion. The two main features of this strategy, as illustrated in Figure 1.10, are (a) the presence of a bulky skeleton to prevent close packing, and (b) the inclusion of functional moieties which can actively partake in coordinative host-guest interactions. Following these principles, a number of successful host types have been designed, the most notable being hosts of scissor-like and of roof-shaped appearance (Figures 1.11 (a) and (b) respectively), both of which have C_2 symmetry. For example, the scissor-shaped compound 1,1′-binaphthyl-2,2′-dicarboxylic acid and its structurally modified derivatives meet the requirements for a coordinatoclathrate host and have indeed been found to include a wide variety of organic guests.[21]

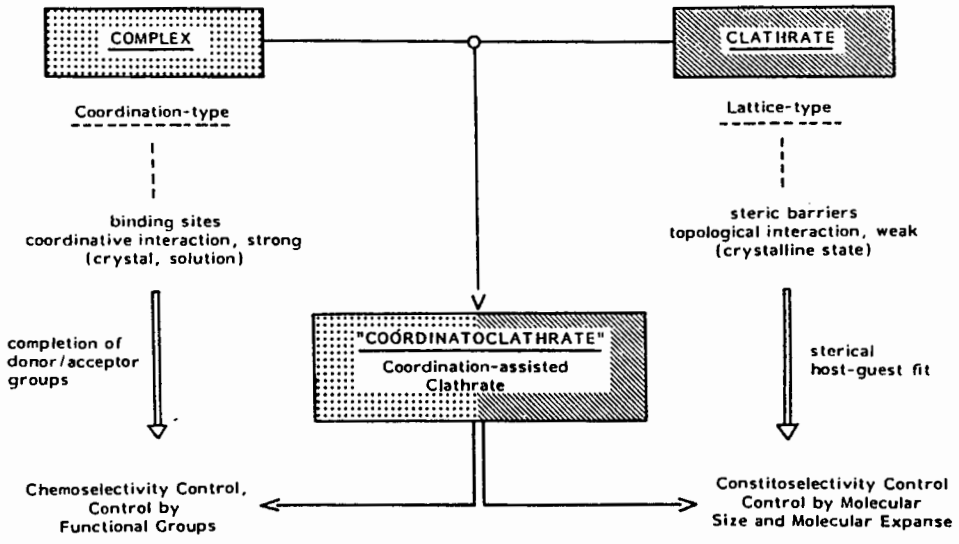

Figure 1.10 Schematic diagram of Weber's coordinatoclathrate approach to directed host design.[70]

In 1968 Toda *et al.*[71] reported on the clathrate properties of the diacetylene diol 1,6-dihydroxy-1,1,6,6-tetraphenylhexa-2,4-diyne. In 1984 Hart *et al.*[72] introduced various structural modifications to this host compound, thus giving rise to the so-called "*wheel-and-axle*" hosts which consist of a long molecular axis with bulky groups and functional moieties at each end. Since then, the molecular axis concept has been extended to include molecular planes. In this vein, Toda has designed new potential hosts using rigid molecules with an *anti*-diol function and with bulky hydrophobic (e.g. aromatic) groups (e.g. compounds **[6]** to **[8]**). These compounds were found to be good inclusion hosts,[73] usually featuring hydrogen-bonded host-guest interactions,[74-77] although non-polar guests are also included by clathration.[78]

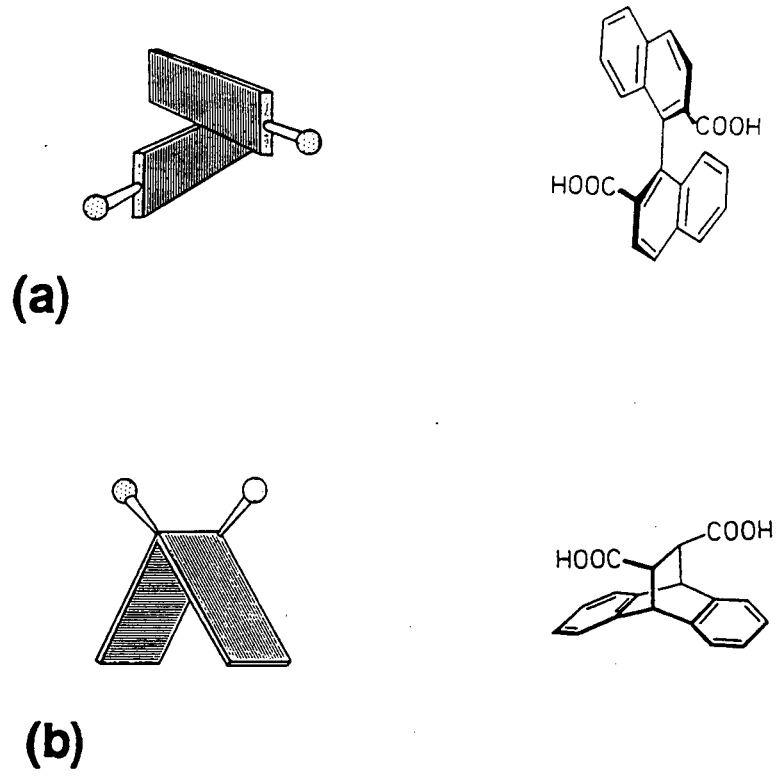

Figure 1.11 Graphic conceptions of (a) scissor- and (b) roof-shaped coordinatoclathrate hosts.[70]

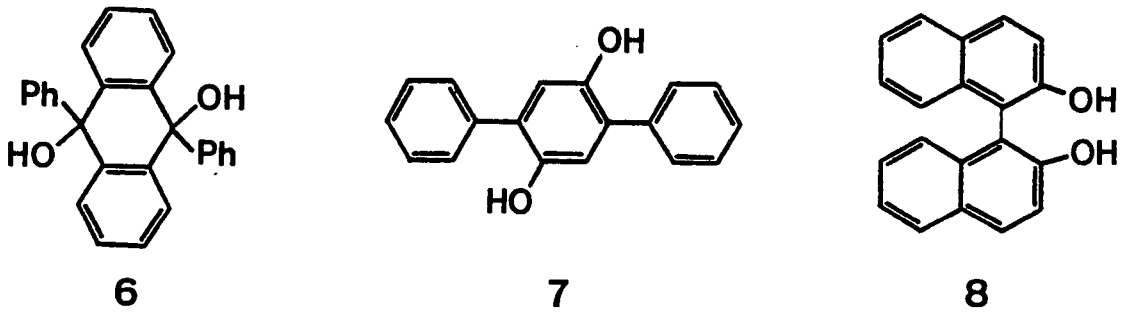

6 7 8

Some applications of inclusion compounds

An important property of host compounds is their ability to interact selectively with molecules which have a particular spatial arrangement and, in many cases, coordinative nature. This process is commonly termed "*molecular recognition*" and is the essence behind the exploitation of inclusion phenomena.

One of the most important applications of inclusion compounds is in the field of **separation** chemistry. For example, unbranched fatty acids can be isolated from various animal and vegetable oils through the formation of adducts with urea[79-81] and this method has also been used for the extraction of *n*-alkanes from crude oil fractions.[82] Applications in chromatography have been well documented[83,84] and have proved successful for the separation of structural isomers e.g. the separation of *ortho*-, *meta*- and *para*-nitrotoluene (Figure 1.12). Similarly, chiral hosts can be used for the separation of enantiomers in racemic mixtures.[20,85]

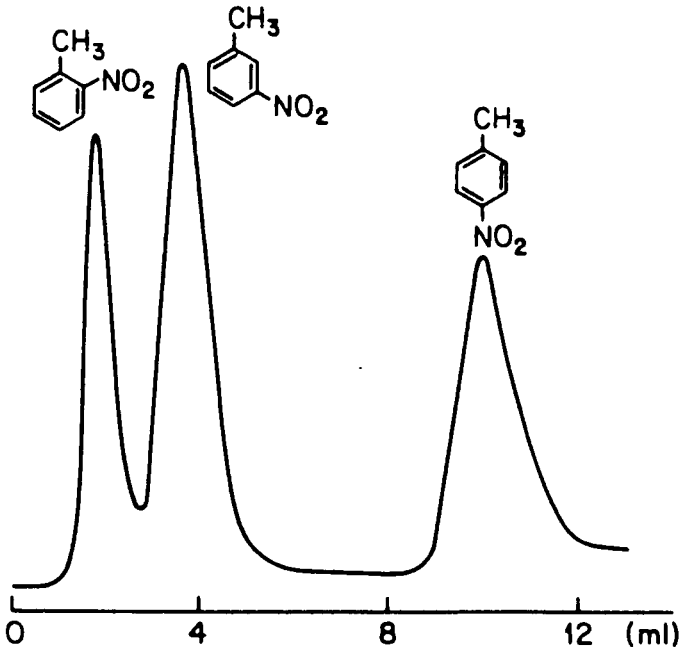

Figure 1.12 Elution trace showing the separation of a mixture of *o*-, *m*- and *p*-nitrotoluene by a clathrate chromatographic system using a Werner-type compound.[85]

Toda[21] has used inclusion compounds for the **control and acceleration of reactions** between guest molecules. An example of this type of catalytic behaviour of the host is illustrated in Figure 1.13.

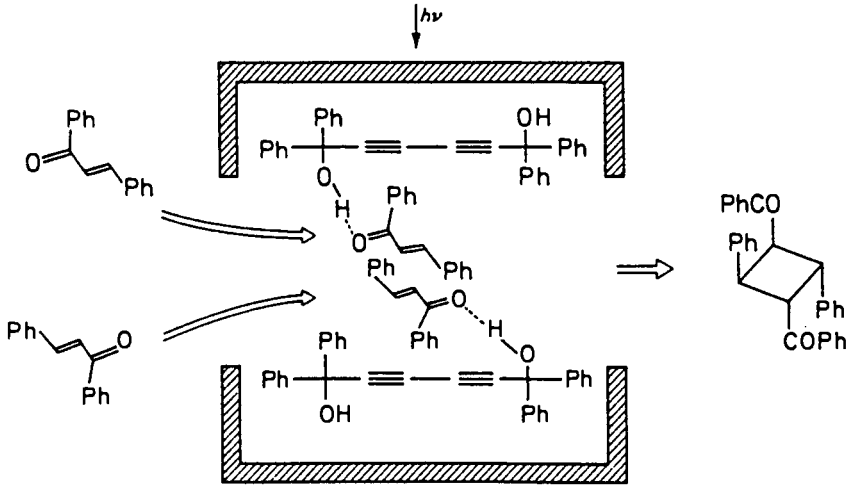

Figure 1.13 Irradiation of a 1:4 mixture of 1,6-dihydroxy-1,1,6,6-tetraphenylhexa-2,4-diyne and chalcone for 72 hours yields the product shown in 87% yield.[21]

Another area of interest related to guest-guest reactions is that of **inclusion polymerisation** which was developed in the latter half of the 1950s as an alternative to Ziegler-Natta coordination polymerisation.[86] The first example appeared in 1956 when Clasen[87] reported the polymerisation of 2,3-dimethylbutadiene included in

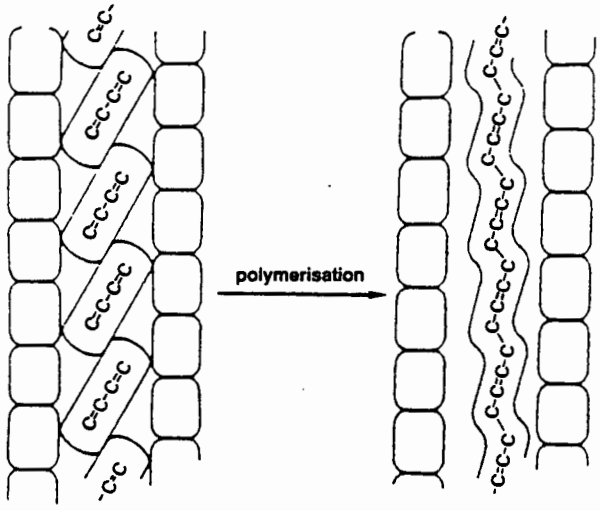

Figure 1.14 Polymerisation of 2,3-dimethylbutadiene as a guest-guest reaction in the thiourea channel.[88]

thiourea. No initiating agent was used and the polymerisation was extremely slow. Brown and White[88,89] extended this study and found that high energy radiation such as β-, γ- or X-rays are excellent initiators and that the resultant polymers exhibit considerable chemical and steric regularity (see Figure 1.14). Despite much interest in inclusion polymerisation, this method has not yet developed sufficiently to produce polymers on an industrial scale. Farina suggests that this is due to the limited availability of suitable hosts and the low yields which are generally obtained.[86]

Some recent patents show how inclusion compounds can be employed as **slow-release agents** for microbicides[90,91] and bactericides[92,93] and this concept is also of interest for the controlled release of drugs,[94] fragrances,[95] pheromones[96] and insecticides.[97] There are also possibilities for the **storage** of unstable,[98] toxic[99] or radioactive[100] compounds as guests in stable host structures for ease of handling.
Many other possible uses of inclusion compounds have been suggested and are too numerous to describe here. However, of particular interest, Weber and co-workers recently published a report which describes how organic clathrate-forming compounds can be used as highly selective **sensors** for the detection of solvent vapours.[101] They coated a quartz oscillator with the compounds [**9**] and [**10**] and detected a change in frequency of the oscillator as the compounds absorb organic solvent vapours, thus gaining mass. A linear relationship between the change in frequency and the extent of the solid-gas enclathration reaction was found to exist.

These findings have important implications for the development of chemical sensors for medical, industrial and environmental purposes (i.e. for warning and safety systems and for environmental analysis). The further development of this field

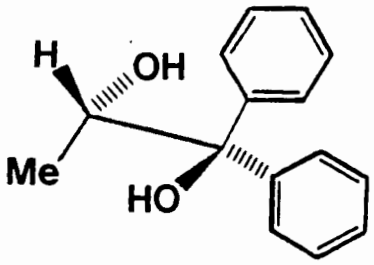

9

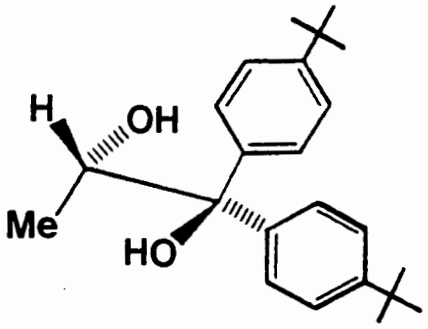

10

of interest depends on a sound understanding of the kinetics and pressure/temperature relationships of solid-gas enclathration reactions, and how these factors relate to structural aspects of the host-guest system considered. At present, there is a distinct void in this area with respect to studies of inclusion phenomena, perhaps due to the difficulties involved in measurement and the subsequent interpretation of results.

Objectives of the present study

This study is concerned with an exploratory investigation of structure/thermodynamic relationships of some diol inclusion compounds. The host compounds selected (Hosts 1 to 7 shown below) all conform to the design criteria described above, having molecular planes with opposing hydroxyl moieties and bulky aromatic groups to prevent close-packing. Host 1 is an example of a roof-shaped molecule and Hosts 2 and 3 are scissor-shaped. Host 4 is a well known host compound,[102] while hosts 5 to 7 are its structurally-modified analogues. The guest molecules used are common organic solvents and, with the exception of benzene, have the potential for participation in hydrogen-bond formation.

The approach taken in this study is to elucidate the structures of the selected inclusion compounds and to carry out various physico-chemical measurements such as their kinetics of formation and decomposition, and the enthalpy changes accompanying the guest-release reaction. Attempts will be made to correlate the structure of a compound at the molecular level with its physical properties at the macro level, and to thus understand the basis of its enclathration and declathration reactions.

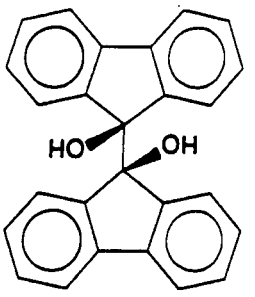

Host 1

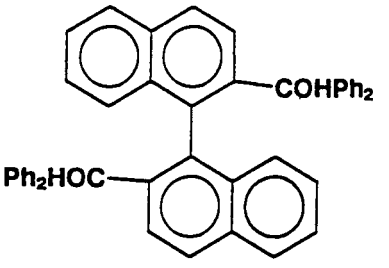

Host 2

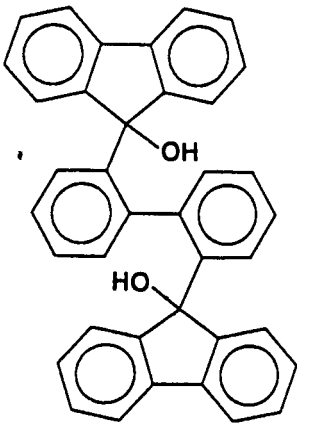

Host 3

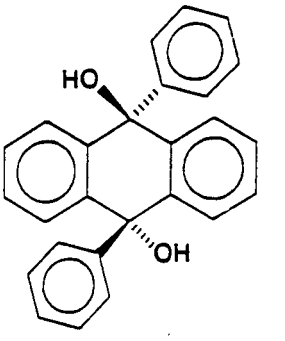

Host 4

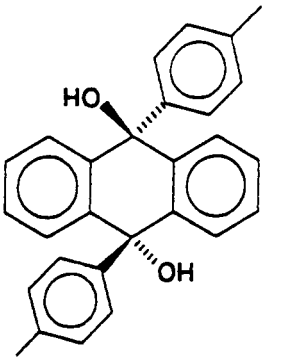

Host 5

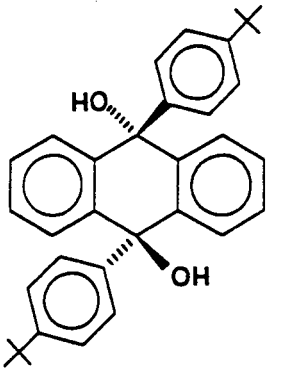

Host 6

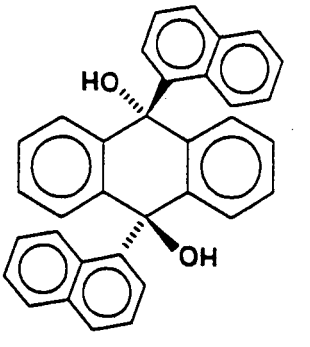

Host 7

References

1 H. Davy, *Philos. Trans. R. Soc. London*, 1811,**101**,1

2 M. Faraday, *Quart. J. Sci.*, 1823,**15**,71

3 C. Schafhäutl, *J. Prakt. Chem.*, 1841,**21**,129

4 F. Wohler, *Ann. Chem. Liebigs*, 1849,**69**,297

5 A. Villiers, *C. R. Hebd. Sceances Acad. Sci.*, 1891,**112**,536

6 K.A. Hofmann and F. Küspert, *Z. Anorg. Allg. Chem.*, 1897,**15**,204

7 H. Hartley and N.G. Thomas, *J. Chem. Soc.*, 1906,1013

8 R. Spallino and G. Provenzal, *Gazz. Chim. Ital.*, 1909,**39**,325

9 A.P. Dianin, *J. Soc. Phys. Chem. Russe*, 1914,**46**,1310

10 H. Wieland and H. Sorge, *Z. Phisiol. Chem. Hoppe-Seyler's*, 1916,**97**,1

11 E. Terres and W. Vollmer, *Z. Petroleum*, 1935,**31**,1

12 M.F. Bengen, German Patent Application, OZ123438 (March 18, 1940)

13 F.F. Mikus, R.M. Hixon and R.E. Rundle, *J. Am. Chem. Soc.*, 1946,**63**,1115

14 W.A. Caspari, *J. Chem. Soc.*, 1927,1093

15 D.E. Palin and H.M. Powell, *Nature*, 1945,**156**,334

16 D.E. Palin and H.M. Powell, *J. Chem. Soc.*, 1947,208

17 H.M. Powell, *J. Chem. Soc.*, 1948,61

18 M. Hagan, "Clathrate Inclusion Compounds", Reinhold, New York, 1962

19 L. Mandelcorn (Ed.), "Non-Stoichiometric Compounds", Academic Press, New York, 1964

20 E. Weber (Ed.), "Molecular Inclusion and Molecular Recognition - Clathrates I", in "Topics in Current Chemistry", Vol 140, M.J.S. Dewar, J.D. Dunitz, K. Hafner, E. Heilbronner, S. Ito, J.-M. Lehn, K. Niedenzu, K.N. Raymond, C.W. Rees, F. Vögtle and G. Wittig (Eds), Springer-Verlag, Berlin, 1987

21 E. Weber (Ed.), "Molecular Inclusion and Molecular Recognition - Clathrates II", in "Topics in Current Chemistry", Vol 149, M.J.S. Dewar, J.D. Dunitz, K. Hafner, E. Heilbronner, S. Ito, J.-M. Lehn, K. Niedenzu, K.N. Raymond, C.W. Rees, F. Vögtle and G. Wittig (Eds), Springer-Verlag, Berlin, 1988

22 J.L. Atwood, J.E.D. Davies and D.D. MacNicol (Eds), "Inclusion Compounds", Vol 1-3, Academic Press, London, 1984 and Vol 4-5, Oxford University Press, Oxford, 1991

23 F. Vögtle, "Supramolecular Chemistry", John Wiley & Sons, Chichester, 1991

24 D.D. MacNicol, J.J. McKendrick and D.R. Wilson, *Chem. Soc. Rev.*, 1978,7,65

25 J.E.D. Davies, *J. Mol. Struc.*, 1981,**75**,1

26 J.E.D. Davies, W. Kemula, H.M. Powell and N.O. Smith, *J. Incl. Phenom.*, 1983,**1**,3

27 C.D. Gutsche, "Calixarenes" in "Monographs in Supramolecular Chemistry", J.F. Stoddart (Ed.), The Royal Society of Chemistry, Cambridge, 1989

28 G. Gokel, "Crown Ethers and Cryptands" in "Monographs in Supramolecular Chemistry", J.F. Stoddart (Ed.), The Royal Society of Chemistry, Cambridge, 1991

29 F. Diederich, "Cyclophanes" in "Monographs in Supramolecular Chemistry", J.F. Stoddart (Ed.), The Royal Society of Chemistry, Cambridge, 1991

30 J.F. Stoddart and R. Zarzycki, "Cyclodextrins" in "Monographs in Supramolecular Chemistry", J.F. Stoddart (Ed.), The Royal Society of Chemistry, Cambridge, 1992

31 D.J. Cram, *Angew. Chem. Int. Ed. Engl.*, 1988,**27**,1009

32 J.-M. Lehn, *Angew. Chem. Int. Ed. Engl.*, 1988,**27**,89

33 C.J. Pedersen, *Angew. Chem. Int. Ed. Engl.*, 1988,**27**,1021

34 D.W. Griffiths and M.L. Bender, *Adv. in Catalysis*, 1973,**23**,209

35 F. Cramer and H. Hettler, *Naturwiss*, 1967,**54**,625

36 J.A. Thoma and L. Stewart in "Starch: Chemistry and Technology", Vol. 1, R.L. Whistler and E.F. Paschall (Eds), Academic Press, New York, 1965

37 K. Takemoto and N. Sonoda, "Inclusion Compounds of Urea, Thiourea and Selenourea" in "Inclusion Compounds", Vol 2, J.L. Atwood, J.E.D. Davies and D.D. MacNicol (Eds), Academic Press, London, 1984

38 F.R. Gamble and T.H. Geballe, in "Treatise on Solid State Chemistry", Vol. 3, "Crystalline and Noncrystalline Solids", N.B. Hannay, (Ed.), Plenum Press, New York, 1976

39 R. Schöllhorn, "Intercalation Compounds" in "Inclusion Compounds", Vol 1, J.L. Atwood, J.E.D. Davies and D.D. MacNicol (Eds), Academic Press, London, 1984

40 D.W. Breck, *J. Chem. Ed.*, 1964,**41**,678

41 J.L. Atwood, "Liquid Clathrates" in "Inclusion Compounds", Vol 1, J.L. Atwood, J.E.D. Davies and D.D. MacNicol (Eds), Academic Press, London, 1984

42 J.L Atwood, U.S. Pat. 4,024,170, 1977

43 D.C. Hrncir, L.M. Barden, M.R. Wells and P.C. Stark, *J. Incl. Phenom.*, 1988,**6**,425

44 M.V. Gaudet, D.C. Peterson and M.J. Zaworotko, *J. Incl. Phenom.*, 1988,**6**,425

45 J.L. Atwood, S.G. Bott, A.W. Coleman, K.D. Robinson, S.B. Whetstone and C.M. Means, *J. Am. Chem. Soc*, 1987,**109**,8100

46 D.R. Bond, G.E. Jackson, H.C. Joao, M.N. Hofmeyr, T.A. Modro and L.R. Nassimbeni, *J. Chem. Soc., Chem Commun.*, 1989,1910

47 E. Weber and H.-P. Josel, *J. Incl. Phenom.*, 1983,**1**,79

48 M.I. Hart and N.O. Smith, *J. Am. Chem. Soc.*, 1962,**84**,1816

49 R.M. Barrer, "Zeolite Inclusion Compounds" in "Inclusion Compounds", Vol 1, J.L. Atwood, J.E.D. Davies and D.D. MacNicol (Eds), Academic Press, London, 1984

50 T. Iwamoto, "The Hofmann-type and Related Inclusion Compounds" in "Inclusion Compounds", Vol 1, J.L. Atwood, J.E.D. Davies and D.D. MacNicol (Eds), Academic Press, London, 1984

51 L. Lipkowski, "Inclusion compounds formed by Werner MX_2A_4 coordination complexes" in "Inclusion Compounds", Vol 1, J.L. Atwood, J.E.D. Davies and D.D. MacNicol (Eds), Academic Press, London, 1984

52 W.D. Schaeffer, W.S. Dorsey, D.A. Skinner and C.G. Christian, *J. Am. Chem. Soc.*, 1957,**79**,5870

53 J. Lipkowski, M. Pawlowska and D. Sybilska, *J. Chromatogr.*, 1979,**176**,43

54 W. Schlenk, *Justus Liebigs Ann. Chem.*, 1949,**565**,204

55 D.D. MacNicol, "Structure and Design of Inclusion Compounds: the Clathrates of Hydroquinone, Phenol, Dianin's Compound and Related Systems" in "Inclusion Compounds", Vol 2, J.L. Atwood, J.E.D. Davies and D.D. MacNicol (Eds), Academic Press, London, 1984

56 D.D. MacNicol, H.H. Mills and F.B. Wilson, *J. Chem. Soc., Chem. Commun.*, 1969,1332

57 A.D.U. Hardy, J.J. McKendrick and D.D. MacNicol, *J. Chem. Soc., Chem. Commun.*, 1974,972

58 A.D.U. Hardy, J.J. McKendrick and D.D. MacNicol, *J. Chem. Soc., Perkin Trans. 2*, 1979,1072

59 A.D.U. Hardy, J.J. McKendrick and D.D. MacNicol, *J. Chem. Soc., Chem. Commun.*, 1976,355

60 J.H. Hall, A.D.U. Hardy, J.J. McKendrick and D.D. MacNicol, *J. Chem. Soc., Perkin Trans. 2*, 1979,376

61 A.D.U. Hardy, J.J. McKendrick, D.D. MacNicol and D.R. Wilson, *Tetrahedron Lett.*, 1975,4711

62 A.D.U. Hardy, J.J. McKendrick, D.D. MacNicol and D.R. Wilson, *J. Chem. Soc., Perkin Trans. 2*, 1979,729

63 D.D. MacNicol, A.D.U. Hardy and J.J. McKendrick, *Nature*, 1975,**256**,343

64 E. Giglio, "Inclusion Compounds of Deoxycholic Acid" in "Inclusion Compounds", Vol 2, J.L. Atwood, J.E.D. Davies and D.D. MacNicol (Eds), Academic Press, London, 1984

65 W. Saenger, "Structural Aspects of Cyclodextrins and their Inclusion Complexes" in "Inclusion Compounds", Vol 2, J.L. Atwood, J.E.D. Davies and D.D. MacNicol (Eds), Academic Press, London, 1984

66 D.J. Cram, *Acc. Chem. Res.*, 1971,**4**,204

67 C.D. Gutsche, *Acc. Chem. Res.*, 1983,**16**,161

68 D.D. MacNicol and D.R. Wilson, *J. Chem. Soc., Chem. Commun.*, 1976,494

69 D.D. MacNicol, "Structure and Design of Inclusion Compounds: the Hexahosts and Symmetry Considerations" in "Inclusion Compounds", Vol 2, J.L. Atwood, J.E.D. Davies and D.D. MacNicol (Eds), Academic Press, London, 1984

70 E. Weber, I. Csöregh, B. Stensland and M. Czugler, *J. Am. Chem. Soc.*, 1984,**106**,3297

71 F. Toda and K. Akagi, *Tetraherdon Lett.*, 1968,3695

72 H. Hart, L.T.W. Lin and D.L. Ward, *J. Am. Chem. Soc.*, 1984,**106**,4043

73 F. Toda, K. Tanaka, G. Ulibarri Daumas and M.C. Sanches, *Chem. Lett.*, 1983,1521

74 F. Toda, K. Tanaka, M.C. Wong and T.C.W. Mak, *Chem. Lett.*, 1987,2069

75 F. Toda, K. Tanaka, M.C. Wong and T.C.W. Mak, *Chem. Lett.*, 1989,1921

76 D.R. Bond, L. Johnson, L.R. Nassimbeni and F. Toda, *J. Sol. State. Chem.*, 1991,**92**,68

77 D.R. Bond, F. Toda, *Acta Cryst.*, 1991,**C47**,348

78 F. Toda, K. Tanaka, Y. Wang, G.-H. Lee, *Chem. Lett.*, 1986,109

79 R.T. Holman and S. Ener, *J. Nutr.*, 1954,**53**,461

80 W.E. Parker and D. Swern, *J. Amer. Oil Chem. Soc.*, 1957,**34**,43

81 T.N. Mehta and S.N. Shah, *J. Amer. Oil Chem. Soc.*, 1957,**34**,587

82 W.J. Zimmerschied, R.A. Dinerstein, A.W. Weitkamp and R.F. Marschner, *Ind. Eng. Chem.*, 1950,**42**,1300

83 E. Smolkova-Keulemansova and S. Krysl, *J. Chromatogr.*, 1980,**184**,347

84 D. Sybilska and E. Smolkova-Keulemansova, "Applications of Inclusion Compounds in Chromatography" in "Inclusion Compounds", Vol 3, J.L. Atwood, J.E.D. Davies and D.D. MacNicol (Eds), Academic Press, London, 1984

85 R. Arad-Yellin, B.S. Green, M. Knossow and G. Tsoucaris, "Enantiomeric Selectivity of Host Lattices" in "Inclusion Compounds", Vol 3, J.L. Atwood, J.E.D. Davies and D.D. MacNicol (Eds), Academic Press, London, 1984

86 M. Farina, "Inclusion Polymerisation" in "Inclusion Compounds", Vol 3, J.L. Atwood, J.E.D. Davies and D.D. MacNicol (Eds), Academic Press, London, 1984

87 H. Clasen, *Elektrochem.*, 1956,**60**,982

88 J.F. Brown and D.M. White, *J. Am. Chem. Soc.*, 1960,**82**,5671

89 D.M. White, *J. Am. Chem. Soc.*, 1960,**82**,5678

90 A. Sekikawa, H. Sugi, K. Tawara and F. Toda, Japanese Patent JP 62,175,401, 1986

91 A. Sekikawa, H. Sugi and R. Takahashi, Eur. Pat. Appl. EP 326,261, 1988

92 A. Sekikawa, T. Kawamura, S. Hirano, Y. Wakamatsu, M. Yamamoto and F. Amano, Japanese Patent JP 63,175,068, 1988

93 A. Sekikawa, R. Takahashi, H. Sugi and K. Tahara, Eur. Pat. Appl. EP 332,336, 1988

94 J. Szejtli, "Topics in Inclusion Science - Cyclodextrin Technology", Chapter 3, Dordrecht, The Netherlands, Kluwer Academic Publishers, 1988

95 A. Sopkova E. Hanzel'ova, Z. Ondrikova, J. Hvizdak and E. Buciova, Proc. 4th Intern. Seminar: Inclusion Compounds, 17-21 June 1991, Stara Lesna, CSFR, 1991,p.57

96 A. Botsi., K., Yannakopoulou and E. Hadjoudis, *Carbohydrate Res.*, 1993,**241**,37

97 J. Bubanec, A. Sopkova and L. Cerveny, Abstract Book, 4th Intern. Seminar: Inclusion Compounds, 17-21 June 1991, Stara Lesna, CSFR, 1991,p.64

98 T. Iwamoto, M. Kiyoki and N. Matsura, *Bull. Chem. Soc. Jpn.*, 1978,**51**,390

99 R.J. Cross, J.J. McKendrick and D.D. MacNicol, *Nature*, 1973,**245**,146

100 D.J. Chleck and C.A. Ziegler, *Nucleonics*, 1959,**17**,130

101 A. Ehlem, C. Wimmer, E. Weber and J. Bargon, *Angew. Chem. Int. Ed. Engl.*, 1993,**32**,110

102 F. Toda, K. Tanaka, S. Nagamatsu and T.C.W. Mak, *Isr. J. Chem.*, 1985,**25**,346

Chapter 2 Experimental

Several routine experimental procedures were used during this study. Since the literature abounds with the theory and practice of these methods, no attempt will be made here to give a general background description or even to direct the reader to specific references. In this chapter the standard equipment used, together with pertinent details concerning operating conditions and sample preparation, will be described briefly. The non-standard experimental techniques which have been developed will be described in detail in Chapters 8 and 9.

Melting point determination

Melting points were determined on a Linkam TH600 hot stage fitted to a Nikon AFX-II microscope equipped with a polarising transilluminator and an overhead light. Temperature was controlled using a Linkam CO600 controller. The calibration of the hot stage was verified using phenolphthalein (263°C, Reichert test substance) and melting points were recorded without correction.

Preliminary tests for inclusion compound formation were also performed using this apparatus. In general, single crystals of the types of inclusion compounds considered here can be observed to cloud over at temperatures between the boiling point of the guest and the melting point of the host. This clouding over is supposedly due to the formation of microfractures in the crystal associated with the inevitable phase change as the guest is volatilised and lost. These observations could subsequently be corroborated by TG and DSC.

Nuclear Magnetic Resonance Spectroscopy

Samples were dissolved in deuterated chloroform or acetone and ^1H NMR spectra were recorded at either 200 MHz (Varian VXR200) or 400 MHz (Varian Unity 400) with tetramethylsilane as reference.

Infrared Spectroscopy

Samples were ground with nujol into a mull and placed between two CsI plates. Spectra were recorded in the range 4000 to 400 cm^{-1} using a Perkin Elmer 983 double beam spectrometer.

Microanalysis

Analyses were performed using an Heraeus Universal CHN-RAPID combustion analyser.

Mass Spectrometry

Mass spectra were recorded using a VG Micromass 16F mass spectrometer with a VG System 2000 PDP-8/a microprocessor. Accurate mass determination was performed by peak matching using a Kratos High Resolution mass spectrometer.

Synthesis of host compounds

The host compounds (+) and (±) 1,1′-binaphthyl-2,2′-bis(diphenylhydroxymethyl),[1] 9,9′-bis(9,9′-dihydroxy-fluorene)[2] and (±) 2,2′-bis(9-hydroxy-9-fluorenyl)biphenyl[3] were synthesised and supplied by Professor E. Weber formerly of Bonn University and are assigned the codes **W12, W14** and **W15** respectively.

The compound *trans*-9,10-dihydroxy-9,10-diphenyl-9,10-dihydroanthracene was first synthesised by Haller and Guyot in 1904.[4] Since then the syntheses by various methods of this compound[5-10] and several other 9,10-substituted-9,10-anthracenediols including *trans*-9,10-dihydroxy-9,10-di-p-tolyl-9,10-dihydroanthracene[5,9,10] and *trans*-9,10-dihydroxy-9,10-di-α-naphthyl-9,10-dihydroanthracene[11] have been reported.

Hosts 4 to 7 were synthesised using the Grignard method with anthraquinone as starting material.[5] The Grignard reagents were prepared from the appropriate aryl bromide (ArBr) compounds where Ar = phenyl, 4-tolyl, α-naphthyl or 4-*tert*-butylphenyl. Details of the general synthetic methodology follow:

The diethyl ether used during all the preparations was dried by refluxing over sodium wire (using benzophenone as an indicator) followed by distillation.

A solution of 100 mmol ArBr in 30 ml diethyl ether was prepared. An initial volume of 5 ml of this solution was added to a heated and stirred mixture of 2.4 g (98.7 mmol) of magnesium and 10 ml diethyl ether. When it was apparent that the reaction had commenced, the remainder of the solution was added dropwise to the reacting mixture which was then allowed to reflux for one to two hours. The resulting Grignard reagent was then added dropwise to a stirred and heated suspension of 4 g (19.2 mmol) of anthraquinone (recrystallised from glacial acetic acid) in 100 ml diethyl ether. The reaction was allowed to continue under reflux for about 15-20 hours. Acidification to a pH of 2 using 2.5 M HCl whilst cooling on ice resulted in a grey-green precipitate. This precipitate was added to 500 ml boiling acetone and the mixture filtered hot after further heating for 10 minutes. The insoluble residue was discarded and the filtrate transferred to a round bottomed flask. A rotary evaporator was used to distil off about 400 ml of the acetone. The remaining solution was then allowed to cool on ice, resulting in precipitation of the reaction product. This product was purified by repeated recrystallisation from acetone until a sharp melting point was observed, and then finally recrystallised from benzene to yield a white powder. Melting points were determined after desorption of included solvent in a drying pistol (Büchi TO-51) at 120°C under vacuum. In general, yields between 30 and 40 % were achieved.

The purified reaction products were characterised using various techniques and the results are summarised in Table 2.1.

Formation of the new compound was conveniently verified by disappearance of the anthraquinone C=O stretch at 1660-1670 cm^{-1} with concomitant appearance of an O-H stretch at 3530-3580 cm^{-1} and a C-O stretch at 1000-1170 cm^{-1} in the infrared spectrum.

Crystal growth

Crystals of inclusion compounds were formed by first dissolving the host powder in the guest solvent that was to be included. These solutions were then forced through 0.5 μm Millex-LCR filters by means of a syringe to prevent solid debris from providing an excessive number of nucleation sites. The solutions were kept in glass

vials and the solvent was allowed to evaporate slowly at room temperature until suitably large crystals were formed.

The compounds **W12** and **DM** were grown in the same manner using diethyl ether and benzene as solvents respectively. However, in these two cases the solvents were not included and single crystals of the pure hosts (α-forms) were obtained.

Density measurement

After being removed from its mother liquor, a crystal was blotted dry and immersed in an aqueous solution of potassium iodide. Additions of a saturated solution of KI or of water were made until the density of the mixture was equal to the density of the crystal, as evidenced by free flotation of the latter. The density of the solution was then measured using a Paar DMA35 digital density meter. Owing to the possibility of crystal decomposition, this procedure had to be performed rapidly, although good agreement was achieved between calculated and measured densities (see Table 2.3).

X-ray powder diffraction

Inclusion compound crystals were ground under mother liquor into a fine powder, but not sieved owing to their increased thermal instability with decreased particle size. Two different powder diffraction systems, each employing nickel-filtered copper K_α incident radiation (λ = 1.5418Å), were used :

The first system consisted of a Philips PW1050/80 vertical goniometer with a PW1394 motor control unit and a PW1390 channel control unit. The goniometer assembly was mounted on a PW1130/90 X-ray generator operating at 45 kV and 30 mA. Diffracted rays were collected in a scintillation counter after collimation with divergence and receiving slits of ½° each and an anti-scatter slit of 1°. A range of $6° \leq 2\theta \leq 40°$ was scanned in steps of 0.1° (2θ) with a time constant of 2 s . Intensities were recorded with $2\theta°$ by means of an IBM compatible personal computer and stored on disk for subsequent manipulation. For this system, powdered samples were pressed into a shallow recess in an aluminium sample holder constructed specifically for use with unstable inclusion compounds. The sample could be covered with domestic polyethylene film to slow down the rate of guest desorption during the scan. The polyethylene film did not introduce extraneous peaks to the powder pattern of the sample.

The second system employed a Debye-Scherrer powder camera with a radius of 57.31 mm mounted on a Philips PW1010/25 X-ray generator which was operated at 50 kV and 25 mA. The powdered sample was packed into a 5 mm Lindemann glass capillary. Traces of relative intensity vs 2θ were produced by scanning the powder patterns photometrically.

Thermal analysis

TG and DSC were performed using a Perkin Elmer PC Series 7 system. The TG analyser was calibrated using built-in procedures for furnace and weight calibration. In addition, the Curie points for alumel (163°C) and perkalloy (596°C) were used to calibrate the furnace. This technique was primarily used to determine host-guest stoichiometry from the percentage weight loss recorded on heating the inclusion

compound. The TG results for the inclusion compounds studied are summarised in Table 2.2.

The DSC analyser was calibrated using the melting points of indium (156.4°C) and zinc (419.5°C) as well as the enthalpy of melting of indium (28.5 J g^{-1}). This technique could be used to evaluate the number of phase changes and the temperatures at which they occur. It should also be possible to use DSC to evaluate enthalpies associated with phase changes. However, this procedure is dependent on factors such as the geometry of the calorimeter, particle size distribution, heating rates and flow velocity of the purging gas.

Both TG and DSC served to indicate roughly the temperatures at which guest-loss occurred, although the experiments were not carried out under the same geometrical conditions: TG experiments were performed with the sample in an open platinum pan while DSC samples were placed in crimped, vented aluminium pans. TG and DSC measurements were made under the following conditions:

Crushed samples initially weighing between 2 and 10 mg were heated at a constant rate of 10 °C min^{-1} from 30 to 300 °C while a continuous stream of nitrogen gas was passed over the samples at a flow rate of 30 $mLmin^{-1}$. An empty aluminium pan was used as the reference for DSC.

Crystal structure analysis

Once suitably large crystals of the desired compound had been grown, a single crystal which extinguished plane polarised light uniformly was selected and cut to a suitable size if necessary. It was then wedged firmly into a 0.3 or 0.5 mm Lindemann capillary tube. A small quantity of mother liquor was introduced, in order to limit guest desorption and both ends of the capillary were flame-sealed (see Photograph 1, Appendix D). Since some of the solvents used were very volatile and flammable (e.g. diethyl ether), flame-sealing proved to be difficult and sealing wax was used instead. The capillary was then glued into a brass pin which in turn fitted into a goniometer head. This arduous procedure was not necessary for the compounds **W12** and **DM** and these crystals could simply be glued to the ends of thin Lindemann glass rods.

Approximate cell parameters and space group symmetry were determined by means of oscillation and Weissenberg photography using a Stoë camera and Nickel filtered copper K_α radiation.

Accurate cell parameters were determined by least-squares analysis of the setting angles of 24 high θ (ususlly in the range 16 to 17 °) reflections collected and centred on an Enraf-Nonius CAD4 diffractometer. Intensity data were collected at 293K using graphite-monochromated molybdenum K_α radiation (λ = 0.7107Å). The ω-2θ scan mode, with a final acceptance limit of 20σ at 20 °min^{-1} and a maximum recording time of 40 seconds was used. The vertical aperture length was fixed at 4 mm. The aperture width was set at (1.12 + 1.05tanθ) mm and the scan width at (x + 0.35tanθ)° in ω (see Table 2.3 for values of x). The intensities and orientation of reference reflections were monitored periodically to check crystal stability and orientation and instrumental stability. Data reduction included corrections for Lorentz and polarization effects. The values for the product μR, where μ is the linear absorption coefficient and R is the maximum radius of the crystal, were less than 0.1 for all crystals. Thus the absorption correction factors, A*, for all the reflections were virtually unity over the θ-range covered and empirical absorption

corrections were not applied to the data.[12] Final refinements were based on only those reflections that satisfied the condition $I > 2\sigma(I)$. Crystal data, experimental and refinement parameters are given in Table 2.3.

Computation

Structure solution and refinement computations were mainly performed using a remote VAX mainframe computer running the VMS 5.4 operating system (later upgraded to a MicroVAX 3100-90 with VMS 5.5) at the University of Cape Town Computing Centre. All structures were solved by direct methods using SHELX-86[13] and refined using SHELX-76[14] which employs the atomic radii derived by Pauling.[15] The complex neutral atom scattering factors for non-hydrogen atoms were based on values reported by Cromer and Mann[16] while values for hydrogen atoms were taken from Stewart *et al.*[17] Dispersion corrections were made according to Cromer and Lieberman.[18]

Agreement between the observed (F_o) and calculated (F_c) structure factors is expressed by the residual index, R, which is defined as

$$R = \frac{\Sigma \, | \, |F_o| - |F_c| \, |}{\Sigma \, |F_o|}$$

$$= \frac{\Sigma \, |\Delta F|}{\Sigma \, |F_o|}$$

Agreement may also be expressed in terms of the weighted residual, R_w,

$$R_w = \frac{\Sigma \, w^{1/2} \, |\Delta F|}{\Sigma \, w^{1/2} |F_o|} \qquad \text{where} \quad w = \frac{1}{\sigma^2(F_o) + gF_o^2}$$

The generalised residual used for the application of the Hamilton test is given as

$$R_G = \frac{\Sigma w \, |\Delta F|^2}{\Sigma \, |F_o|^2}$$

Geometrical molecular structure parameters were calculated using the PARST program.[19] Molecular and packing diagrams were produced using the IBM PC version of PLUTO.[20] The Cambridge Structural Database[21] was used to search, retrieve and analyse crystallographic data.

The program HEENY[22] was used to calculate intermolecular non-bonded interactions. HEENY is a modified version of EENY[23] and calculates atom-pair potentials using van der Waals energy of the form

$$U(r) = a \exp(-br)/r^d - c/r^6$$

where r is the distance in Å between any pair of atoms and a,b,c and d are coefficients calculated by Giglio[24] and Pavel *et al.*[25] to yield U(r) in kcal mol^{-1}. Hydrogen bonding is taken into account using the function

$$U_{hb} = [(A/R^{16}) - (C/R^{10})] \cos^2 \theta$$

where U_{hb} is the energy associated with the hydrogen bond, R the distance between the hydrogen atom and the acceptor, θ the angle donor–H···acceptor and the constants A and C are related to the well-depth U_{min} and the equilibrium distance R_0 by

$$A = -5R_0^{12}U_{min} \qquad \text{and} \qquad C = -6R_0^{10}U_{min}$$

A "mixing scheme" was introduced to allow the full non-bonded potential U_{norm} to take effect as θ deviates from the ideal angle of 180° such that

$$U_{total} = U_{hb} + (1 - \cos^2 \theta)U_{norm}.$$

Powder diffraction patterns were calculated from single-crystal X-ray structure data using the program LAZY PULVERIX.[26] The program MOLMAP was written by the author (see Appendix A) and was used to plot "slices" through unit cells in order to determine the shape of guest cavities or channels formed by host molecules.

All the programs developed by the author were written using the Turbo Pascal[27] programming language running on an IBM compatible computer with an 80286 processor, an 80287 numeric co-processor, VGA graphics capability and several other standard features. Details of these programs are discussed in Appendix A.

Structure solution and refinement

For any given structure, systematically absent and "unobserved" reflections, i.e. where $F_o \leq 4\sigma(F_o)$, are suppressed. The number of unique data as a function of resolution in the range 1.1 to 1.2 Å is examined. In order for the direct methods to succeed for a centrosymmetric structure, it is generally necessary for the number of observed reflections to be greater than one quarter of the number of theoretically possible reflections. For non-centrosymmetric structures this fraction increases to one half. Equivalent reflections (including Friedel opposites) are averaged and a figure of merit, R_{int}, for the reflection data set is calculated[13] where,

$$R_{int} = \frac{\Sigma|F_o^2-(F_o^2)_{mean}|}{\Sigma F_o^2}$$

Mean $|E^2-1|$ values (**E** is the normalised structure factor) for the zonal reflections *0kl, h0l, hk0* and the remainder are checked for consistency with space group symmetry. For centrosymmetric space groups $|E^2-1|$ should be close to 0.968 whereas for acentric space groups $|E^2-1|$ should be 0.736. The program then selects a reflection subset for the initial phase refinement on the basis of α_{est} and the number of negative quartets this subset generates. The "best" 10% of the subset

phase permutations are then subjected to multisolution tangent refinement. Two figures of merit, R_α and NQUAL, are calculated for all refined phase permutations:

$$R_\alpha = \frac{\Sigma w[(\alpha-\alpha_{est})]^2}{\Sigma w[(\alpha_{est})]^2}$$

where the weight $w = (\alpha_{est} + 5)^{-1}$

and

$$NQUAL = \frac{\Sigma[\Sigma(E_1E_2)\Sigma(E_3E_4E_5)]}{\Sigma[|\Sigma(E_1E_2)||\Sigma(E_3E_4E_5)|]}$$

where the outer summations are performed over all refined reflections and the inner summations over triplets and negative quartet relations involving a given reflection. A combined figure of merit is then calculated:

$$CFOM = R_\alpha + [\,0 \text{ or } (NQUAL-wn), \text{ whichever is greater}]^2$$

where wn is a structure-dependent constant which should be about 0.1 more negative than the anticipated value of NQUAL. CFOM should be a minimum for the "best" solution which is retained for calculating an E-map. This "best" solution is extended by further tangent expansion. After one cycle of E-Fourier recycling, the point atom R-factor based on E-values (R_E) is evaluated.[13] If $R_E < 0.3$, the structure is considered correct, provided that it is also chemically sensible. Most, if not all, of the non-hydrogen atoms in the various structures were found this way, and the correctness of each structure was confirmed by a sharp cutoff in the list of peak heights, and by successful subsequent refinement.

The atoms located by direct methods were input into SHELX-76 for least-squares refinement which involves minimisation of $\Sigma w(|F_o| - |F_c|)^2$. In most cases, full-matrix least-squares refinement was employed but, in cases where the number of variables exceeded 500, large block least-squares refinement was performed.

The final model usually involved anisotropic refinement of all non-hydrogen atoms. Non-hydroxyl hydrogen atoms were geometrically constrained in a riding model to 1.00Å from their parent atoms and refined with common temperature factors. Hydroxyl hydrogen atoms were located in difference Fourier maps and they were refined with independent isotropic temperature factors and bond length constraints. These hydrogen atoms were fixed at set lengths from their parent oxygen atoms according to a function of O···O (or O···N) vs O–H distance.[28]

A weighting scheme, where $w = (\sigma^2(F_o) + gF_o^2)^{-1}$, was employed in the final stages of refinement to yield a constant distribution of $<w(\Delta F)^2>$ with $\sin\theta$ and $(F_o/F_{o,max})^{½}$. The analyses of variance obtained in this fashion are given in Appendix F.

Chapters 3 to 6 describe the solution and refinement of the structures elucidated in this study. The structures were all essentially treated as described above and only interesting features in the refinement of each will be expounded. Final atomic coordinates, tables of bond lengths, angles and torsion angles and observed and calculated structure factors are provided on diskette as part of Appendix F.

Table 2.1 Characterisation of synthesised compounds

Compound	Microanalysis				I.R. (cm^{-1})	^1H NMR * 200 MHz, $CDCl_3$ † 400 MHz, $(CD_3)_2CO$	M.P. (°C)	M.S. (*m/z*)	A.M.D. (*m/z*)
	%C_c	%H_c	%C_o	%H_o					
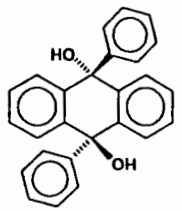	85.7	5.5	85.5	5.3	3569 (O-H) 1594, 1565 (Ar) 1151 (C-O)	δ = 7.26 (m,18H,Ar-H) * δ = 2.57 (s,2H,O-H)	260-261	364 (M^+) 330 287 209	—
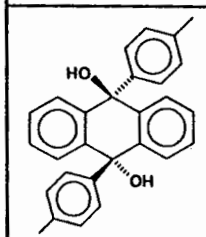	85.7	6.2	85.4	5.9	3555 (O-H) 1507, 1520 (Ar) 1161 (C-O)	δ = 7.25 (m,16H,Ar-H) * δ = 2.63 (s,2H,O-H) δ = 2.30 (s,6H,2×CH_3)	273-274	392 (M^+) 358 301 209	—
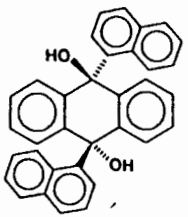	87.9	5.2	87.7	5.1	3537 (O-H) 1506 (Ar) 1041 (C-O) 799, 779, 767 (Ar-H)	δ = 8.83;8.36;7.95;7.83; 7.15;7.01 (d,16H,Ar-H) † δ = 7.77;7.26;7.03 (t,6H,Ar-H) δ = 5.20;2.78 (s,2H,O-H)	304-306	447 (M^+ - OH) 431 320 209	—
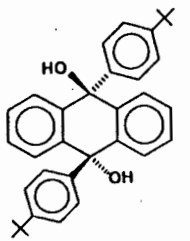	85.7	7.6	85.6	7.8	3570 (O-H) 1600, 1594, 1580 (Ar) 1005 (C-O)	δ = 7.24 (m,16H,Ar-H) * δ = 2.55 (s,2H,O-H) δ = 1.21 (s,18H,6×CH_3)	274-275	447 (M^+) 443 343 326 209	Found: 476.2710 Calc.: 476.2715

Table 2.2 Determination of inclusion compound stoichiometry by TG

Compound	Wt. loss (%)	H/G
W14et	27.1	1.973
W14bu	8.9	1.918
W14py	17.8	0.994
W12py	27.7	0.333
W15ch	27.5	0.498
DPac	23.7	0.490
DPdek	18.7	0.979
DPdmso	30.0	0.500
DP2bu	16.6	0.982
DMac	22.8	0.499
DMde	27.1	0.495
DMpy	29.1	0.507
DBac	32.5	0.248
DBde	23.6	0.497
DBbz	32.8	0.332
DNbz	14.1	0.980

Table 2.3 Crystal data, data collection and final refinement parameters

	W14et	W14bu	W14py	W12	W12py	W15ch
CRYSTAL DATA						
Compound	Ethanol	n-Butanol	Pyridine	-	Pyridine	Cyclohexanone
Guest	$2(C_{26}H_{18}O_2)\cdot C_2H_6O$	$2(C_{26}H_{18}O_2)\cdot C_4H_{10}O$	$C_{26}H_{18}O_2\cdot C_5H_5N$	$C_{46}H_{34}O_2$	$C_{46}H_{34}O_2\cdot 3(C_5H_5N)$	$C_{38}H_{26}O_2\cdot 2(C_6H_{10}O)$
Molecular formula	770.92	798.98	441.53	618.78	856.08	710.91
M_r	PĪ	PĪ	P2/n	$P2_12_12_1$	PĪ	$P2_1/c$
Space group	2	2	8	4	2	4
Z	10.639(11)	12.911(2)	20.439(15)	8.080(1)	12.541(3)	13.980(3)
a (Å)	14.058(6)	13.262(1)	9.199(1)	16.709(4)	12.643(5)	11.768(5)
b (Å)	14.608(12)	13.287(1)	27.060(1)	24.032(5)	15.684(2)	23.487(11)
c (Å)	71.64(5)	93.57(1)	90	90	82.78(2)	90
α (°)	74.27(9)	111.57(1)	108.94(6)	90	76.05(1)	98.77(3)
β (°)	88.57(7)	95.15(1)	90	90	82.76(2)	90
γ (°)	1992(3)	2096.9(4)	4812(5)	3245(1)	2382(1)	3819(2)
Volume (Å^3)	1.28(1)	1.26(1)	1.22(1)	1.27(1)	1.19(1)	1.23(1)
D_m (gcm^{-3})	1.285	1.265	1.219	1.266	1.193	1.236
D_c (gcm^{-3})	0.75	0.74	0.71	0.71	0.67	0.72
μ (Mo K_α) (cm^{-1})	812	844	1856	1304	904	1512
F(000)						
DATA COLLECTION PARAMETERS						
Crystal dimensions (mm)	0.41×0.41×0.47	0.47×0.47×0.44	0.28×0.31×0.38	0.16×0.16×0.38	0.41×0.41×0.47	0.31×0.25×0.44
θ range scanned (°)	1-23	1-23	1-23	1-23	1-23	1-23
Range of indices h,k,l	±11,±15,16	±14,±14,14	±22,10,29	8,18,26	±13,±13,17	±15,15,12
Total exposure time (hrs)	41.0	37.9	47.7	27.1	77.0	38.1
Overall intensity variation (%)	-8.2	20.4	-0.2	1.2	-1.8	54.1
Scan width, x in $(x + 1.05\tan\theta)°$	0.85	0.85	0.80	0.80	0.80	0.80
# Unique reflections collected	4874	5341	5141	2091	5457	4193
# Observed reflections with $I_{rel} > 2\sigma I_{rel}$	3650	4662	3296	1434	3955	2830
FINAL REFINEMENT PARAMETERS						
Number of variables	286	315	369	442	165	494
R	0.093	0.043	0.077	0.043	0.052	0.112
R_w	0.099	0.044	0.087	0.038	0.061	0.111
g in $w = (\sigma^2(F_o) + g(F_o)^2)^{-1}$	0.008	0.0001	0.1	0	0.003	0.01
S (goodness of fit parameter)	1.43	2.50	0.76	2.17	1.25	3.71
Max. shift/e.s.d.	0.011	0.004	0.037	0.043	0.481	0.002
Avg. shift/e.s.d.	0.001	0.000	0.001	0.002	0.064	0.000
Max., min. heights in difference Fourier (eÅ^{-3})	0.64, -0.20	0.19, -0.26	0.34, -0.35	0.16, -0.20	0.19, -0.27	0.45, -0.39

Table 2.3 *continued*

	DPac	DPdek	DPdmso	DP2bu	DM	DMac
CRYSTAL DATA						
Compound					-	
Guest	Acetone	Diethyl ketone	DMSO	(±)2-Butanol		Acetone
Molecular formula	$C_{26}H_{20}O_2 \cdot 2(C_3H_6O)$	$C_{26}H_{20}O_2 \cdot C_5H_{10}O$	$C_{26}H_{20}O_2 \cdot 2(C_2H_6OS)$	$C_{26}H_{20}O_2 \cdot C_4H_{10}O$	$C_{28}H_{24}O_2$	$C_{28}H_{24}O_2 \cdot 2(C_3H_6O)$
M_r	480.60	450.58	520.71	438.57	392.50	508.66
Space group	$P\bar{1}$	$P\bar{1}$	$P2_1/n$	$P\bar{1}$	$P2_1/c$	$P\bar{1}$
Z	1	1	2	1	2	2
a (Å)	8.689(14)	8.038(2)	8.706(3)	7.990(1)	5.876(2)	9.494(4)
b (Å)	9.466(6)	8.846(2)	9.838(2)	8.954(1)	21.349(9)	11.961(4)
c (Å)	9.448(6)	9.248(2)	16.206(3)	9.007(1)	8.971(2)	12.771(8)
α (°)	92.60(5)	109.36(2)	90	108.90(1)	90	95.69(4)
β (°)	114.85(9)	95.79(2)	94.31(2)	96.19(1)	108.70(1)	101.75(4)
γ (°)	107.46(9)	99.19(3)	90	101.37(1)	90	99.80(3)
Volume (Å^3)	659(1)	604.0(3)	1384(1)	587.3(1)	1066(1)	1413(1)
D_m (gcm^{-3})	1.21(1)	1.24(1)	1.25(1)	1.23(1)	1.22(1)	1.21(1)
D_c (gcm^{-3})	1.211	1.239	1.249	1.240	1.223	1.195
μ (Mo K_α) (cm^{-1})	0.73	0.73	2.15	0.39	0.70	0.72
F(000)	256	240	552	234	416	544
DATA COLLECTION PARAMETERS						
Crystal dimensions (mm)	0.28×0.28×0.56	0.31×0.31×0.44	0.16×0.22×0.38	0.41×0.38×0.44	0.06×0.19×0.25	0.50×0.50×0.50
θ range scanned (°)	1-23	1-25	1-25	1-25	1-20	1-25
Range of indices h,k,l	±9,±10,10	±9,±10,11	±10,11,19	±9,±9,10	±5,20,8	±11,±14,15
Total exposure time (hrs)	16.4	13.8	17.0	13.6	9.4	34.6
Overall intensity variation (%)	-11.9	1.4	-0.4	-0.9	-0.5	0.6
Scan width, x in (x + 1.05tanθ)°	0.85	0.85	0.80	0.85	0.85	0.80
# Unique reflections collected	2055	1908	1870	1852	836	4219
# Observed reflections with $I_{rel} > 2\sigma I_{rel}$	1673	1626	1171	1556	621	3150
FINAL REFINEMENT PARAMETERS						
Number of variables	174	150	174	145	142	372
R	0.085	0.107	0.069	0.072	0.047	0.052
R_w	0.098	0.141	0.073	0.096	0.061	0.065
g in w = $(\sigma^2(F_0) + g(F_0)^2)^{-1}$	0.0008	0.02	0.00074	0.0064	0.11	0.012
S (goodness of fit parameter)	8.53	1.36	3.98	1.60	0.058	0.76
Max. shift/e.s.d.	0.554	0.088	0.001	0.001	2.664	1.863
Avg. shift/e.s.d.	0.021	0.006	0.000	0.000	0.582	0.064
Max., min. heights in difference Fourier (eÅ^{-3})	0.36, -0.34	0.76, -0.60	0.33, -0.24	0.57, -0.58	0.18, -0.18	0.26, -0.22

Table 2.3 *continued*

CRYSTAL DATA						
Compound	**DMde**	**DMpy**	**DBac**	**DBde**	**DBbz**	**DNbz**
Guest	Diethyl ether	Pyridine	Acetone	Diethyl ether	Benzene	Benzene
Molecular formula	$C_{28}H_{24}O_2 \cdot 2(C_4H_{10}O)$	$C_{28}H_{24}O_2 \cdot 2(C_5H_5N)$	$C_{34}H_{36}O_2 \cdot 4(C_3H_6O)$	$C_{34}H_{36}O_2 \cdot 2(C_4H_{10}O)$	$C_{34}H_{36}O_2 \cdot 3(C_6H_6)$	$C_{34}H_{24}O_2 \cdot C_6H_6$
M_r	540.74	550.70	708.98	624.91	711.00	542.68
Space group	$P2_1/n$	$P2_1/n$	$P2_1/c$	$P2_1/a$	$P2_1/c$	$P\bar{1}$
Z	2	2	2	2	2	1
a (Å)	8.706(2)	9.661(1)	8.996(2)	8.771(2)	8.970(4)	7.254(2)
b (Å)	10.911(2)	9.724(2)	27.139(6)	25.132(5)	17.128(2)	9.003(3)
c (Å)	16.614(6)	16.398(4)	9.245(4)	9.042(3)	13.275(2)	11.882(3)
α (°)	90	90	90	90	90	108.13(2)
β (°)	94.90(3)	95.61(2)	109.16(3)	104.75(2)	90.26(2)	97.40(2)
γ (°)	90	90	90	90	90	101.29(2)
Volume (Å^3)	1572(1)	1533(1)	2132(1)	1928(1)	2040(1)	708.0(3)
D_m (gcm^{-3})	1.11(1)	1.19(1)	1.09(1)	1.07(1)	1.15(1)	1.27(1)
D_c (gcm^{-3})	1.142	1.193	1.104	1.076	1.157	1.273
μ (Mo K_α) (cm^{-1})	0.68	0.68	0.67	0.63	0.64	0.72
F(000)	584	584	768	680	764	286
DATA COLLECTION PARAMETERS						
Crystal dimensions (mm)	0.31×0.31×0.34	0.22×0.22×0.25	0.22×0.38×0.41	0.34×0.38×0.44	0.44×0.41×0.34	0.22×0.22×0.31
θ range scanned (°)	1-25	1-25	1-25	1-25	1-25	1-25
Range of indices *h,k,l*	±10,13,9	±11,11,19	±10,32,11	±10,29,10	±10,20,15	±8,±10,14
Total exposure time (hrs)	20.3	18.5	28.1	26.8	26.0	18.1
Overall intensity variation (%)	2.5	-6.4	-1.1	-50.6	-14.3	-0.2
Scan width, x in $(x + 1.05\tan\theta)^\circ$	0.85	0.80	0.85	0.85	0.85	0.85
# Unique reflections collected	2165	1954	2919	2710	2883	2186
# Observed reflections with $I_{rel} > 2\sigma I_{rel}$	1411	1240	1859	1830	2040	1771
FINAL REFINEMENT PARAMETERS						
Number of variables	197	200	147	230	264	196
R	0.057	0.058	0.144	0.070	0.097	0.050
R_w	0.064	0.062	0.164	0.071	0.108	0.064
g in $w = (\sigma^2(F_0) + g(F_0)^2)^{-1}$	0.0026	0.00084	0.006	0.00019	0.0027	0.05
S (goodness of fit parameter)	1.72	2.86	11.76	6.77	4.64	0.40
Max. shift/e.s.d.	0.153	0.028	0.001	0.658	0.158	0.015
Avg. shift/e.s.d.	0.009	0.001	0.000	0.033	0.013	0.002
Max., min. heights in difference Fourier (eÅ^{-3})	0.22, -0.26	0.23, -0.17	1.13, -0.44	0.28, -0.26	0.36, -0.34	0.20, -0.27

References

1 E. Weber, K. Skobridis, A. Wierig, L.J. Barbour, M.R. Caira and L.R. Nassimbeni, *Chem. Ber.*, 1993,**126**,1141

2 M. Gomberg and W.E. Bachmann, *J. Am. Chem. Soc.*, 1927,49,236
and
E. Weber, K. Skobridis, A. Wierig, L.J. Barbour, M.R. Caira and L.R. Nassimbeni, in preparation

3 E.Weber, K. Skobridis, A. Wierig, S. Stathi, L.R. Nassimbeni and M.L. Niven, *Angew. Chem. Int. Ed. Engl.*, 1993,32,606

4 A. Haller and A. Guyot, *Compt. Rend.*, 1904,**138**,327

5 C.K. Ingold and P.G. Marshall, *J. Chem. Soc.*, 1926,3080

6 C. Dufraise and J. Houpillart, *Compt. Rend.*, 1937,**205**,740

7 C.F. Koelsch, *J. Org. Chem.*, 1938,**3**,456

8 A. Willemart, *Bull. Soc. Chim.*, 1942,**2**,772

9 A. Mustafa, *J. Chem. Soc.*, 1949,1662

10 A. Mustafa, *J. Chem. Soc.*, 1952,2435

11 A. Willemart, *Bull. Soc. Chim.*, 1937,**4**,357

12 A.J.C. Wilson (Ed.), "International Tables for Crystallography", Volume C, Kluwer Academic Publishers, Dordrecht, 1992, pp 521-529

13 G.M Sheldrick in "Crystallographic Computing 3", G.M. Sheldrick, C. Kruger and R. Goddard (Eds), Oxford University Press, 175, 1985
and
G.M. Sheldrick, *Acta Cryst.*, 1990,**A46**,467

14 G.M Sheldrick in "Computing in Crystallography", H. Schenk, Olthof-Hazekamp, J. von Konigsveld and G.C. Bassi (Eds), Delft University Press, 34, 1978

15 L. Pauling in "The Nature of the Chemical Bond", Cornell University Press, Ithaca, New York, 1955

16 D.T. Cromer and J.B. Mann, *Acta Crystallogr.*, 1986,**A24**,321

17 R.F. Stewart, E.R. Davidson and W.T. Simpson., *J. Chem. Phys.*, 1965,**42**,3175

18 D.T. Cromer and D. Lieberman, *J. Chem. Phys.*, 1970,**53**,1891

19 M. Nardelli, *Comput. Chem.*, 1983,**7**,95

20 W.D.S. Motherwell in "PLUTO and PLUTOX - programs for plotting molecular and crystal structures", Cambridge University, England, unpublished,
Modified by E.J. Dodson, and G.D. Smith, further modified by M. Webster and E.J. Gabe, NRC, Canada, 1985

21 Cambridge Structural Database & Cambridge Structural Database System, Version 4.4 (January 1991) to Version 5.06 (October 1993), Cambridge Crystallographic Data Centre, University Chemical Laboratory, Cambridge, England

22 C.F. Marais, "HEENY - Modification of EENY to allow H-bonding calculations", University of Cape Town, 1990

23 W.D.S. Motherwell in "EENY - Potential Energy Program", Cambridge University, England, 1974 (unpublished)

24 E. Giglio, *Nature*, 1969,**222**,339

25 N.V. Pavel, C. Quagliata and N. Scarcelli, *Z. Kristallogr.*, 1976,**144**,64

26 K. Yvon, W. Jeitschko and E. Parthe, *J. Appl. Cryst,* 1977,**10**,73

27 Turbo Pascal, Version 6.0, 1990, Borland International Inc., Scotts Valley, CA, USA

28 P. Schuster, G. Zundel and C. Sanderfly, (Eds), "The Hydrogen Bond II. Structure and Spectroscopy", Chapter 8, North Holland Publishing Co., Amsterdam, 1976

Chapter 3 Structure solution - Hosts 1 to 3

Crystal structures of complexes with Hosts 1 to 3 are discussed in this chapter. For each compound, the molecular formula, space group and cell geometry are summarised together with the guest labelling scheme. This is followed by a brief description of its structure solution and refinement and then by a description of its molecular structure and guest conformation. Key bond lengths reported here can be compared with published average values based on X-ray and neutron diffraction results. Such values as are relevant to this study are reproduced in Appendix E. Crystal data, data collection and final refinement parameters for all the structures are given in Table 2.3.

Host 1

The atom labelling scheme for Host 1 is shown in Figure 3.1. Where the asymmetric unit contains two host molecules, the suffixes "A" and "B" are appended to their atom labels respectively. Similarly, crystallographically independent guest molecules are assigned numeric suffixes after the letter "G".

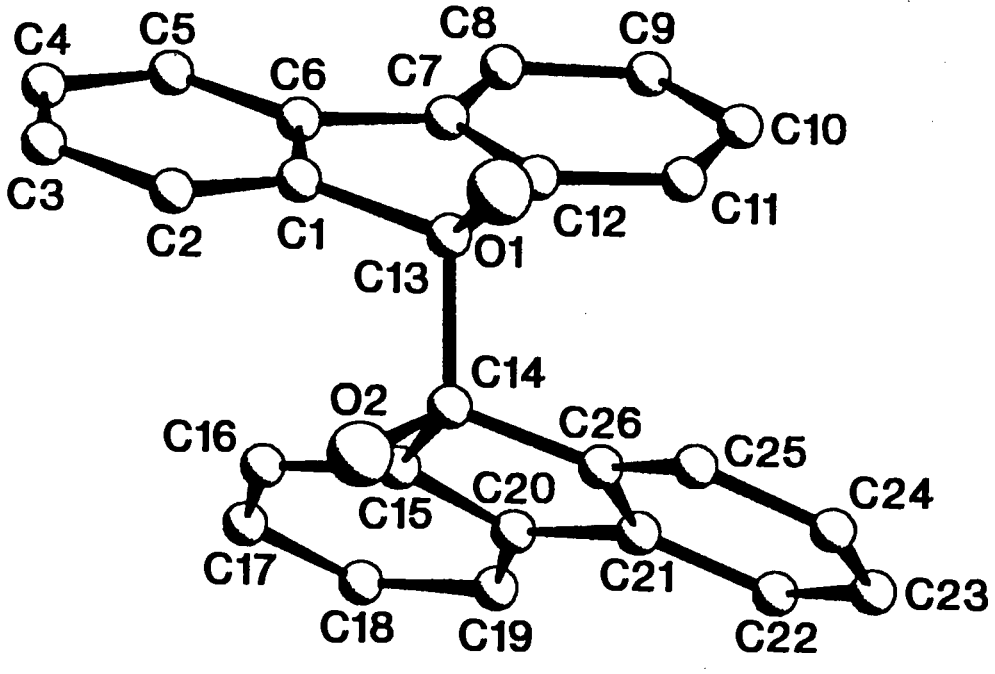

Figure 3.1 Atom numbering scheme for bis-(9,9′dihydroxy-9,9′-difluorene).

W14et $(C_{26}H_{18}O_2)_2 \cdot C_2H_6O$
Guest : Ethanol
Space group : $P\bar{1}$
a = 10.64(1)Å $\quad \alpha = 71.64(5)°$
b = 14.058(6)Å $\quad \beta = 74.27(9)°$
c = 14.61(1)Å $\quad \gamma = 88.57(7)°$
V = 1992(3)Å^3
Z = 2

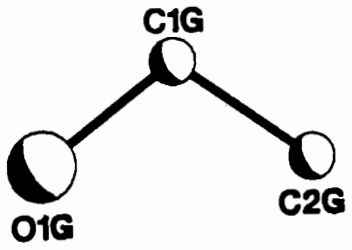

A host:guest ratio of 2:1 was established by TG (see Table 2.2). The triclinic system was indicated by $\bar{1}$ Laue symmetry of the X-ray diffraction record and the intensity statistics (mean $|E^2-1|$ for the general *hkl* reflections = 0.996) indicated $P\bar{1}$ as the correct space group rather than P1. Furthermore, determination of the unit cell volume and the crystal density suggested two host molecules and one guest molecule in the asymmetric unit, with Z = 2.

Direct methods yielded all non-hydrogen atoms in the asymmetric unit. Large-block least-squares refinement was necessary in order to limit the number of parameters. The guest hydrogen atoms were omitted owing to the relatively high temperature factors of their parent atoms. Since the guest atoms were poorly resolved, it was necessary to refine them with isotropic temperature factors and to constrain the distances O(1G)–C(1G) (1.43Å), C(1G)–C(2G) (1.53Å) and O(1G)–C(2G) (2.42Å). These distances subsequently refined to values of 1.45(1), 1.48(2) and 2.38(2) Å respectively.

A hydrogen bonded network was inferred from short O···O distances (see Table 3.1) and a close examination of the difference electron density map in the regions of the oxygen atoms revealed only H(2B), associated with parent atom O(2B). This atom was subsequently refined with a suitable bond length constraint and its own temperature factor. The final R value was 0.093.

Molecular structure

The asymmetric unit of **W14et** is shown in Figure 3.2 and hydrogen bond details are given in Table 3.1.

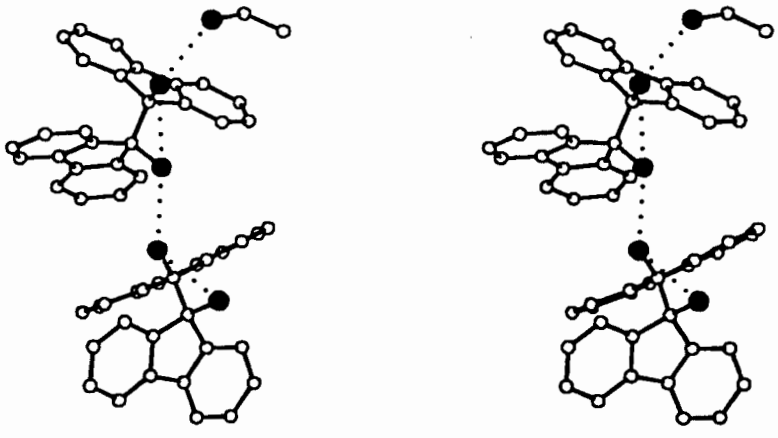

Figure 3.2 Stereoview of the asymmetric unit of **W14et** - hydrogen atoms are omitted and hydrogen bonds are indicated as dotted lines.

H(2B) forms part of an intermolecular hydrogen bond from O(2B) to O(2A). This implies that the donor → acceptor chain direction is O(1G) → O(1A) → O(2A) → O(2B) → O(1B). The ethanol molecules are situated in double cavities, linked by a narrow constriction located at a centre of inversion at ½,0,0 (Wyckoff position *d*) as shown in Figure 3.3. The relative positions of the host and guest molecules, all of which are situated on general positions in the unit cell, can be seen in Figure 3.4. From Figures 3.3 and 3.4 it can be seen that the ethanol molecules are situated with their hydrophilic ends together (the O···O distance is 3.450(9)Å) across the centre of inversion at ½,0,0 and the hydrophobic ends similarly positioned across 0,0,0. The guest cavities are enclosed by the fluorenyl moieties of the host molecules.

Since the geometry of the ethanol molecule was set by bond length constraints during refinement, any discussion about its conformation can be considered meaningless.

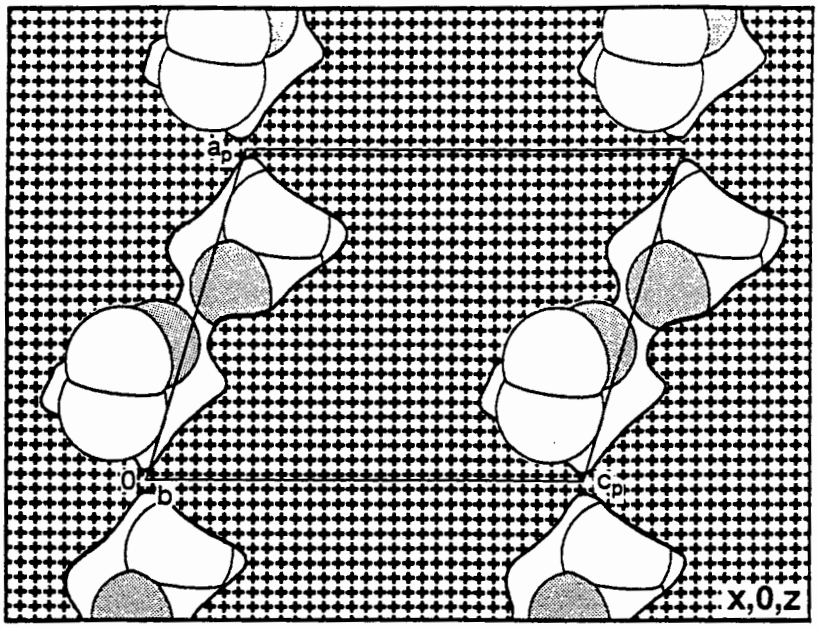

Figure 3.3 Projected cross-section of the host molecules (hatched area) of **W14et** on (010) showing the guest molecules (with oxygen atoms shaded) in cavities.

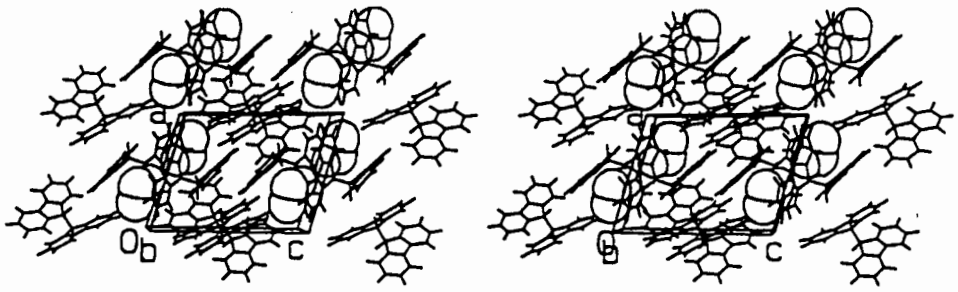

Figure 3.4 Stereoview of **W14et** viewed along [010].

W14bu $(C_{26}H_{18}O_2)_2 \cdot C_4H_{10}O$
Guest : n-Butanol
Space group : $P\bar{1}$
a = 12.911(2)Å α = 93.57(1)°
b = 13.262(1)Å β = 111.57(1)°
c = 13.287(1)Å γ = 95.15(1)°
V = 2096.9(4)Å^3
Z = 2

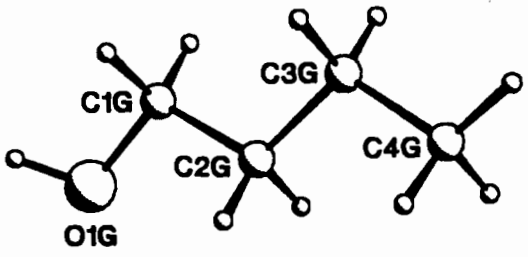

A host:guest ratio of 2:1 was established by TG (see Table 2.2). The triclinic system was indicated by $\bar{1}$ Laue symmetry of the X-ray diffraction record and the intensity statistics (mean $|E^2-1|$ for the general *hkl* reflections = 0.955) indicated $P\bar{1}$ as the correct space group rather than P1. As with the previous structure, determination of the unit cell volume and the crystal density suggested two host molecules and one guest molecule in the asymmetric unit, with Z = 2.

Direct methods yielded all non-hydrogen atoms in the asymmetric unit. Large-block least-squares refinement was necessary in order to limit the number of parameters. All the hydroxyl hydrogen atoms were located and refined with bond length constraints and individual temperature factors. Refinement proceeded uneventfully and the final R value was 0.043.

Molecular structure

The asymmetric unit of **W14bu** is shown in Figure 3.5 and hydrogen bond details are given in Table 3.1.

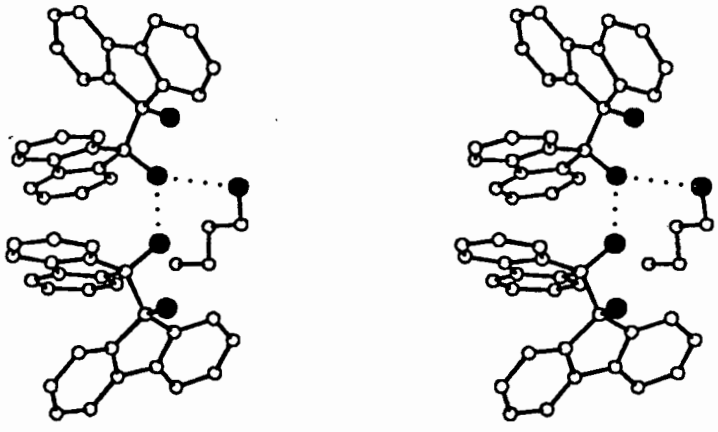

Figure 3.5 Stereoview of the asymmetric unit of **W14bu** - hydrogen atoms are omitted and hydrogen bonds are indicated as dotted lines.

The complete hydrogen bonding scheme is illustrated in Figure 3.6(a). The hydrogen bonds are shown as dotted lines which link host and guest molecules in double ribbons running along [010]. Figure 3.7 shows the butanol guest molecules in constricted channels parallel to [100] with 2 guest molecules (placed end-to-end with their hydrophobic groups together) per constriction. The packing diagram along

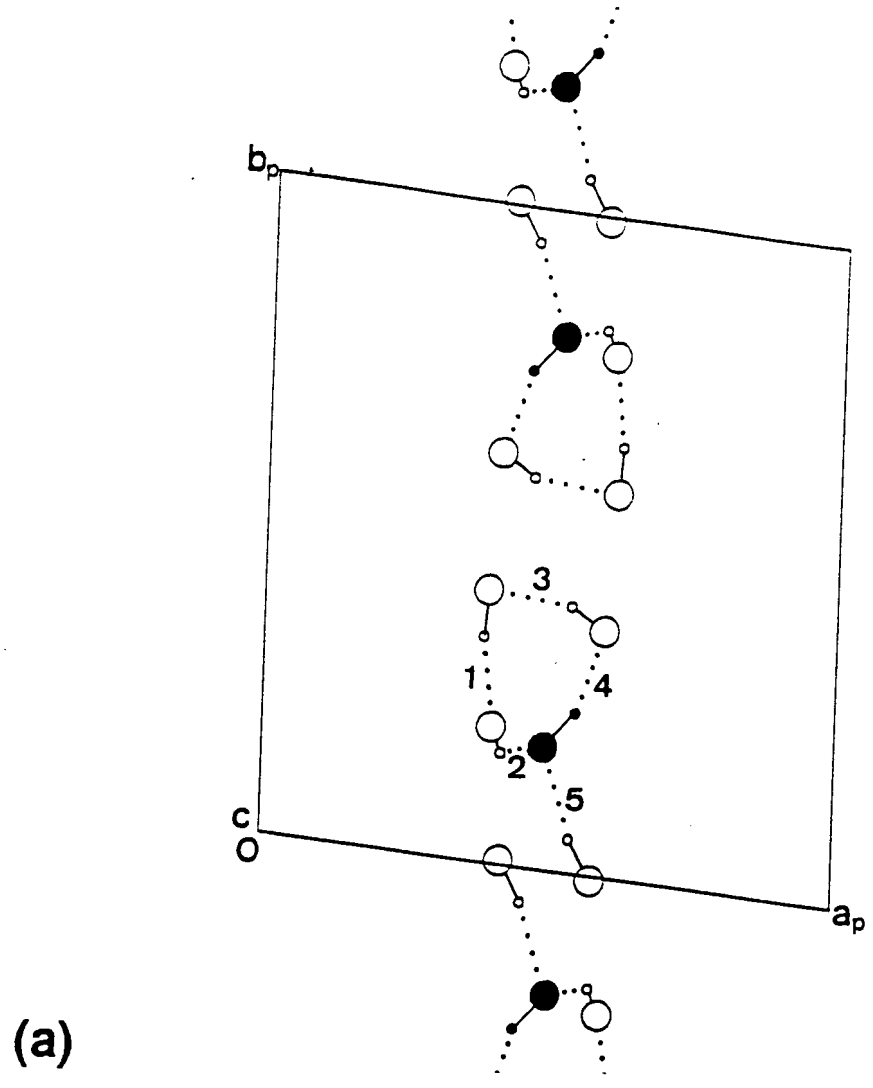

(a)

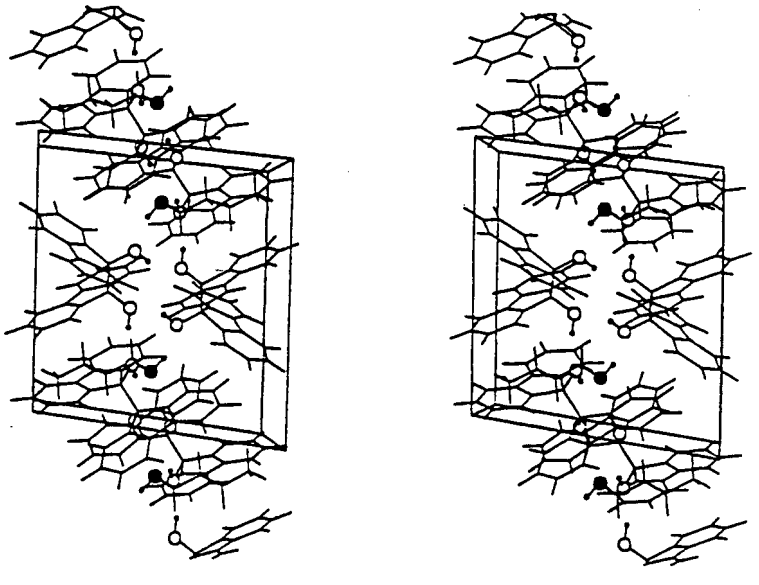

(b)

Figure 3.6 Projections of **W14bu** along [001] showing (a) the oxygen atoms with the unique hydrogen bonds numbered 1 to 5 and (b) the packing between host and guest molecules (the guest atoms are shaded).

[001], Figure 3.6(b), shows the relationship between the host and guest molecules, all of which occupy general positions in the unit cell.

The three bond angles formed by the non-hydrogen atoms of the butanol molecule are O(1G)-C(1G)-C(2G) (109.0(2)°), C(1G)-C(2G)-C(3G) (114.2(2)°) and C(2G)-C(3G)-C(4G) (111.2(2)°) and the torsion angles O(1G)-C(1G)-C(2G)-C(3G) and C(1G)-C(2G)-C(3G)-(C(4G) are 178.6(2)° and 178.7(2)° respectively. The O(1G)–C(1G) distance is 1.443(3)Å and the average C–C bond length is 1.511(3)Å.

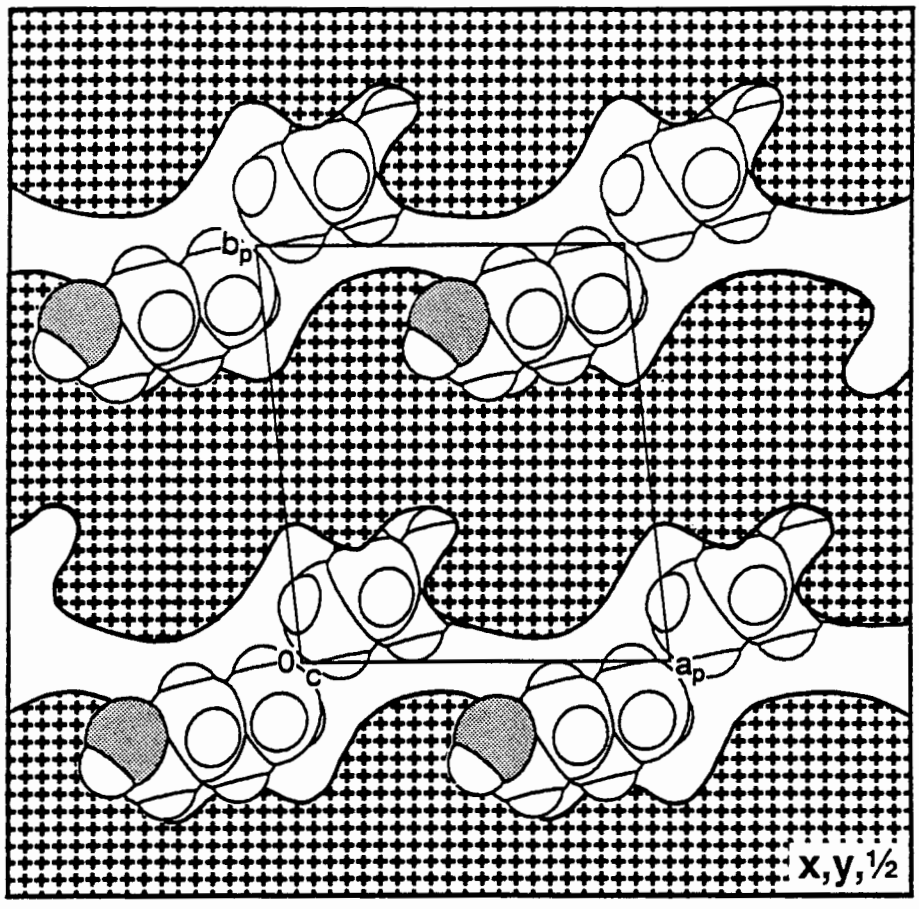

Figure 3.7 Projected cross-section of the host molecules (hatched area) of **W14bu** on (002) showing the guest molecules (with oxygen atoms shaded) in constricted channels.

W14py $C_{26}H_{18}O_2 \cdot C_5H_5N$
Guest : Pyridine
Space group : P2/n
a = 20.44(2)Å
b = 9.199(1)Å β = 108.94(6)°
c = 27.06(2)Å
V = 4812(5)Å^3
Z = 8

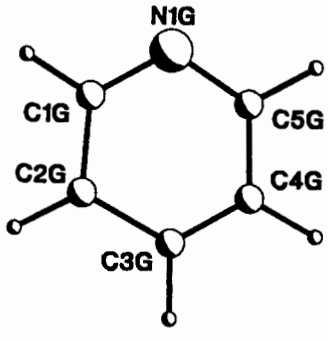

A host:guest ratio of 1:1 was established by TG (see Table 2.2). Preliminary oscillation and Weissenberg photography established **W14py** as belonging to the

monoclinic system (2/*m* Laue symmetry). Crystal reflection data exhibited the following non-extinction conditions:

hkl	:	none
h0l	:	$h+l = 2n$
0k0	:	none

and the space group could thus be narrowed down to either Pn or P2/n. Inspection of the intensity statistics (mean $|E^2-1|$ for the *0kl* (1.090), *h0l* (0.985), *hk0* (0.918) and general *hkl* reflections (1.002)) indicated that the space group was centric, hence P2/n was assumed to be the correct choice.

Determination of the unit cell volume and the crystal density suggested eight host and eight guest molecules per unit cell. The space group then requires the asymmetric unit to consist of two host molecules and two guest molecules.

Direct methods yielded all non-hydrogen atoms in the asymmetric unit. Large-block least-squares refinement was necessary in order to limit the number of parameters. The hydroxyl hydrogen atoms could not be located unambiguously but a hydrogen bonded network was inferred from several short O···O and O···N distances. Refinement proceeded uneventfully and the final R value was 0.077.

Molecular structure

The asymmetric unit is shown in Figure 3.8 and hydrogen bonds details are given in Table 3.1.

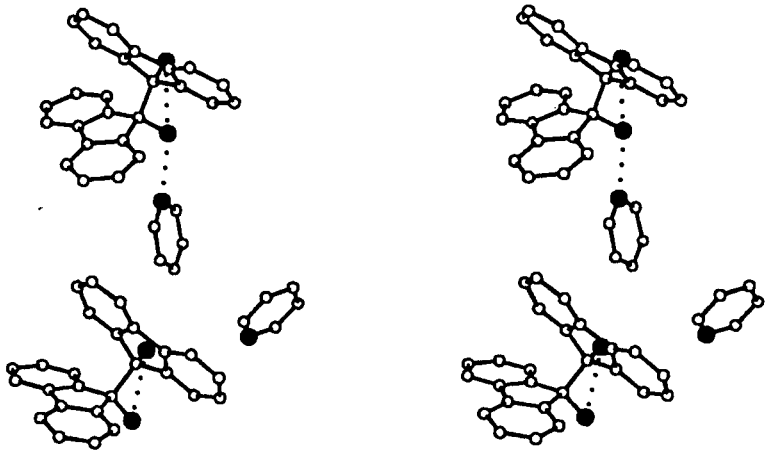

Figure 3.8 Stereoview of the asymmetric unit of **W14py** - hydroxyl hydrogen atoms are omitted and hydrogen bonds are indicated as dotted lines.

All the molecules occupy general positions in the unit cell. The host molecules are hydrogen bonded into dimers across the diads (at $\frac{1}{4}$,y,$\frac{1}{4}$, $\frac{1}{4}$,y,$\frac{3}{4}$, $\frac{3}{4}$,y,$\frac{1}{4}$ and $\frac{3}{4}$,y,$\frac{3}{4}$) and form two crystallographically independent columns parallel to [010] as shown in Figure 3.9. These in turn allow channels to form (Figure 3.10), into which the pyridine guest molecules are packed and held to the host molecules by O–H···N hydrogen bonds. Figure 3.11 shows the stacking of the guest molecules stereographically viewed along [001].

The two crystallographically independent pyridine molecules are planar; the maximum deviation of any atom from the least-squares planes through each of the guest molecules is 0.02(2)Å. The C≃N bond length range is 1.30(1) to 1.35(1) Å while the C≃C bond lengths range from 1.30(3) to 1.45(2) Å. The internal angles (in °) of the pyridine molecules are: 117(1) and 118(1) for C≃N≃C, 123(1) to 124(1) for N≃C≃C and 115(1) to 121(1) for C≃C≃C.

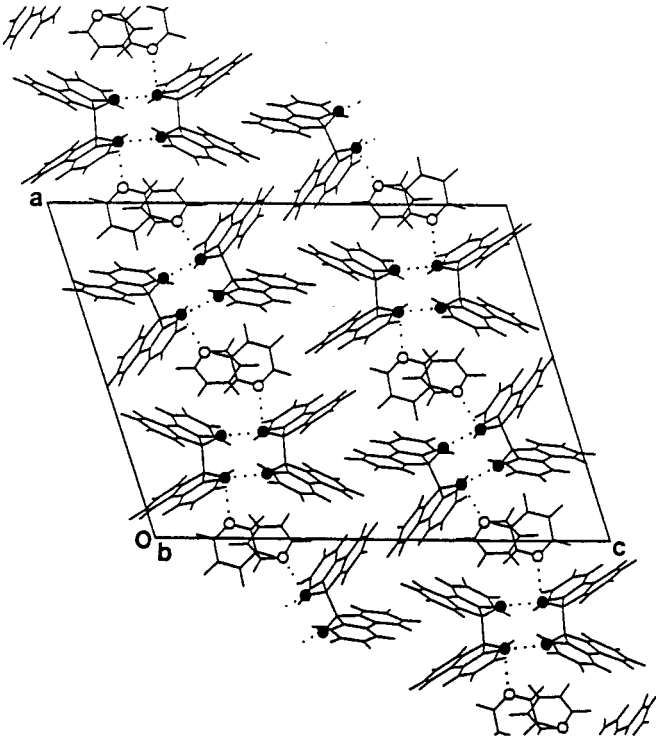

Figure 3.9 Projection of **W14py** viewed along [010] with oxygen atoms shaded and hydrogen bonds indicated as dotted lines.

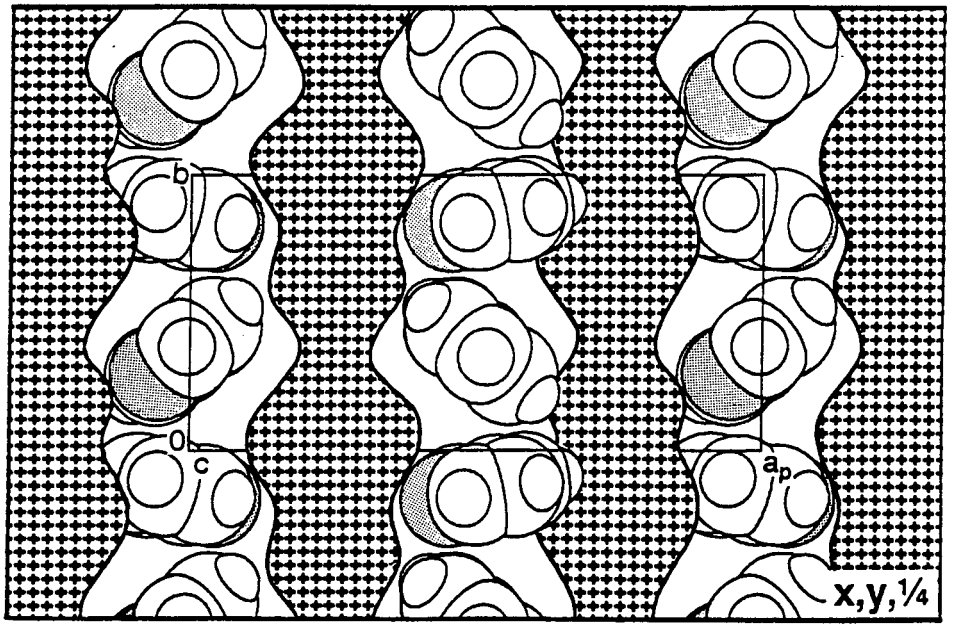

Figure 3.10 Projected cross-section of the host molecules (hatched area) of **W14py** on (004) showing the guest molecules in channels parallel to [010].

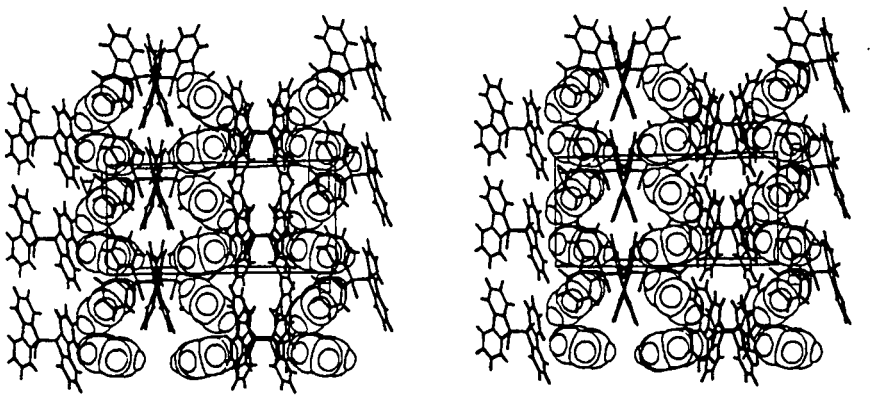

Figure 3.11 Stereographic projection of **W14py** viewed along [001] (guest molecules are drawn with van der Waals radii).

Host 2

The crystal structure **W12** is that of the R-enantiomer of 1,1′-binaphthyl-2,2′-bis(diphenylhydroxymethyl) while **W12Py** represents the pyridine solvate of the racemic mixture of the same compound. The atom labelling scheme for this host is shown in Figure 3.12. The asymmetric unit of **W12py** contains three guest molecules and the suffixes "1", "2" and "3" are appended to their atom labels respectively after the letter "G".

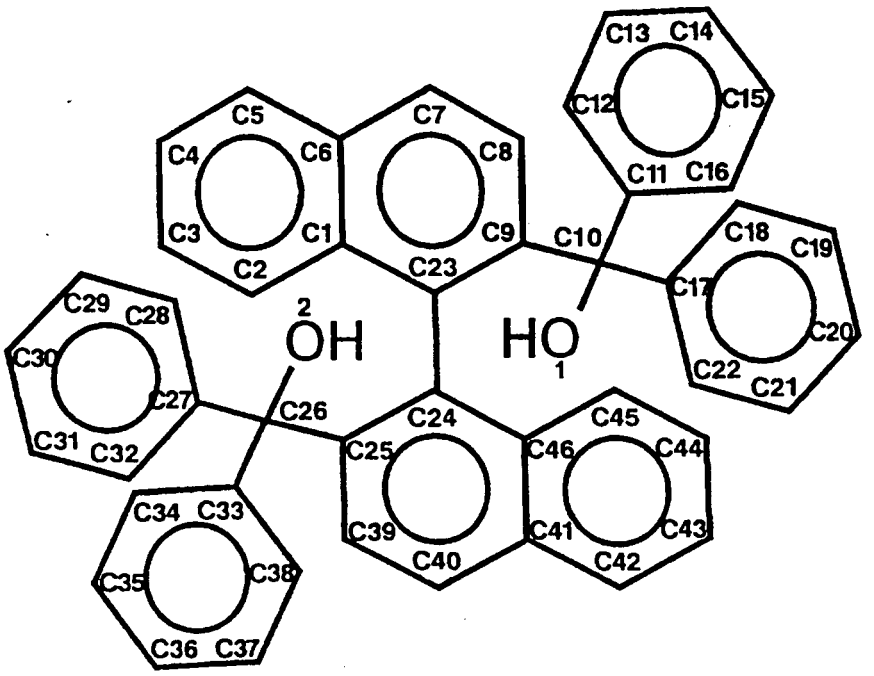

Figure 3.12 Atom numbering scheme for 1,1′-binaphthyl-2,2′-bis(diphenylhydroxymethyl).

W12 $C_{46}H_{34}O_2$
Guest : None
Space group : $P2_12_12_1$
a = 8.080(1)Å
b = 16.709(4)Å
c = 24.032(5)Å
V = 3245(1)Å^3
Z = 4

Crystals were grown by slow evaporation of a solution of the compound in diethyl ether. It was established by TG that the diethyl ether had *not* been included and the crystals were therefore of the pure form of the compound. Preliminary oscillation and Weissenberg photography established **W12** as belonging to the orthorhombic system (*mmm* Laue symmetry). Crystal reflection data exhibited the following non-extinction conditions:

hkl	:	none
h00	:	*h* = 2n
0k0	:	*k* = 2*n*
00l	:	*l* = 2n

indicating that the space group was $P2_12_12_1$. Determination of the unit cell volume and the crystal density suggested 4 molecules per unit cell. The space group then requires the asymmetric unit to consist of one complete molecule. These observations are consistent with the knowledge that the compound is chiral by virtue of steric hindrance to rotation about C(23)-C(24).

Direct methods yielded all non-hydrogen atoms in the asymmetric unit. The hydroxyl hydrogen atoms were located in difference electron density maps and refined with bond length constraints and individual isotropic temperature factors. Refinement proceeded uneventfully and, despite the poor overdetermination ratio (i.e. the ratio of the number of observed reflections to the number of parameters used) the final R value was 0.043.

Molecular structure

The asymmetric unit of **W12** is shown in Figure 3.13 and details of the hydrogen bond are given in Table 3.1.

The molecules occupy general position in the unit cell and Figure 3.14 shows a packing diagram of **W12** viewed along [100]. There are no intermolecular hydrogen bonds, but the structure is tightly packed, with a packing factor of 16.9Å^3 per non-hydrogen atom. The intramolecular hydrogen bond between O(1) and O(2) will be discussed in Chapter 7 together with other aspects of the molecular conformation.

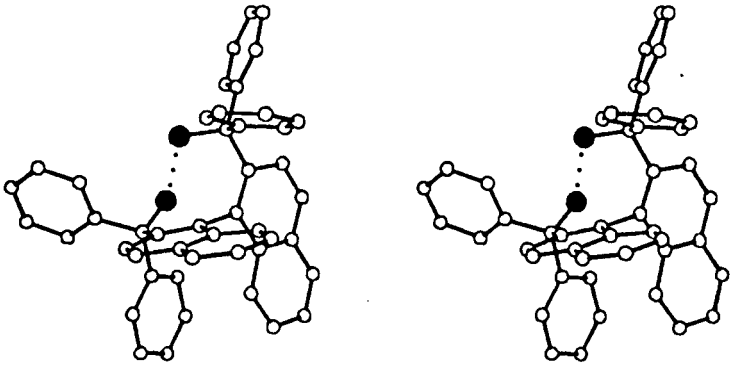

Figure 3.13 Stereoview of the asymmetric unit of **W12** - hydrogen atoms are omitted and hydrogen bonds are indicated as dotted lines.

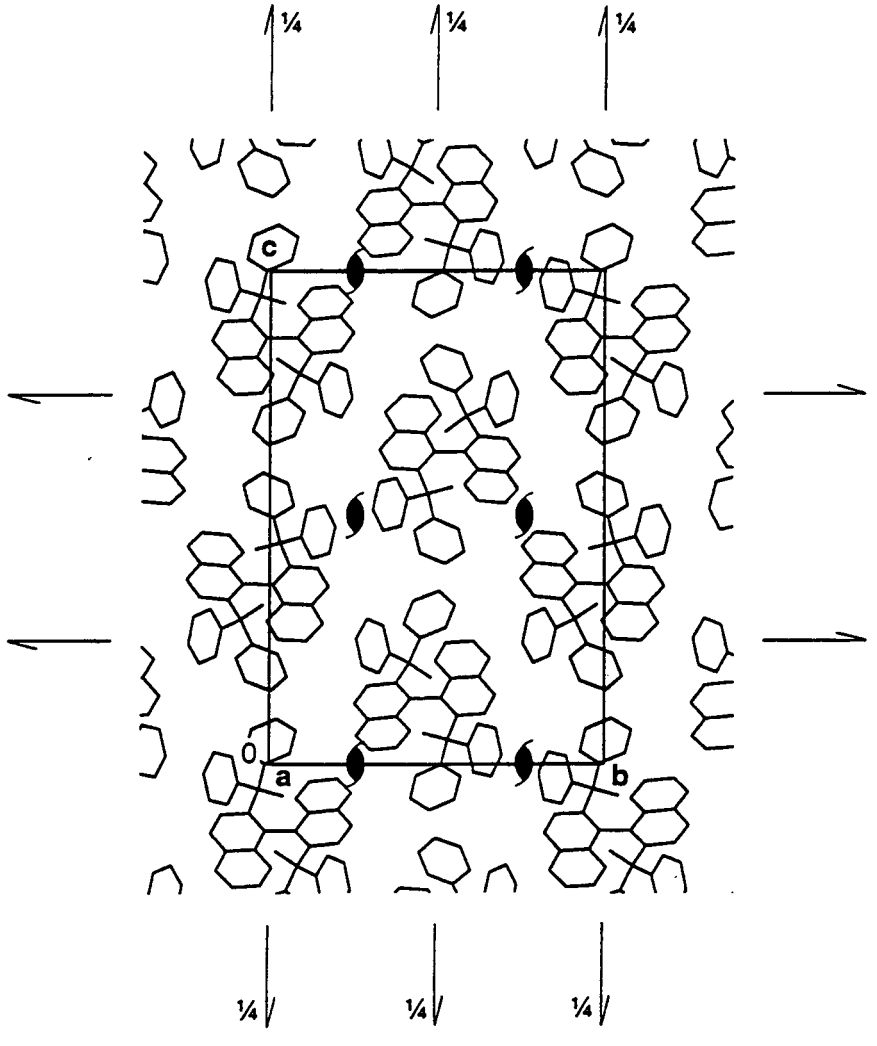

Figure 3.14 Packing diagram of **W12** viewed along [100] with hydrogen atoms omitted and with screw axes shown symbolically.

W12py $C_{46}H_{34}O_2 \cdot (C_5H_5N)_3$
Guest : Pyridine
Space group : $P\bar{1}$
a = 12.541(3)Å α = 82.78(2)°
b = 12.643(5)Å β = 76.05(1)°
c = 15.684(2)Å γ = 82.76(2)°
V = 2382(1)Å^3
Z = 2

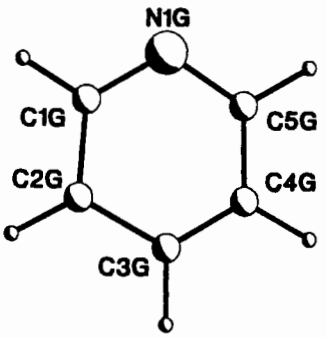

Crystals were grown from a solution of the racemic mixture of the host compound in pyridine. A host:guest ratio of 1:3 was established by TG (see Table 2.2). The triclinic system was indicated by $\bar{1}$ Laue symmetry of the X-ray diffraction record and the intensity statistics (mean $|E^2-1|$ for the general *hkl* reflections = 1.044) indicated $P\bar{1}$ as the correct space group rather than P1. Furthermore, determination of the unit cell volume and the crystal density suggested one host molecule and three guest molecules in the asymmetric unit, with Z = 2.

Direct methods yielded all non-hydrogen atoms in the asymmetric unit. Large-block least-squares refinement was necessary in order to limit the number of parameters. The hydroxyl hydrogen atoms were located in difference electron density maps and refined with bond length constraints and individual isotropic temperature factors. Refinement proceeded uneventfully and the final R value was 0.052.

Molecular structure

The asymmetric unit of **W12py** is shown in Figure 3.15 and hydrogen bond details are given in Table 3.1.

All the molecules occupy general positions in the unit cell. Figure 3.16 shows the projection of **W12py** viewed along [001] with the crystallographically independent guest molecules shaded uniquely. Guest molecules 1 and 2 are both situated in symmetry-related channels running parallel to [100] at x,0,$\frac{1}{4}$ and x,0,-$\frac{1}{4}$. The channels at x,0,$\frac{1}{4}$ are shown in Figure 3.17(a). These two channels are linked by cavities centered at the cell origin. The latter are depicted in Figure 3.17(b) where it can be seen that each cavity contains two molecules of Guest 3. The cavities themselves run along [010], almost forming channels with constrictions at 0,$\frac{1}{2}$,0. For further clarity, the cavities are also shown on (100) and (010) in Figures 3.18 (a) and (b) respectively.

There is an intramolecular hydrogen bond from O(1) to O(2) of the host molecule. O(2) in turn forms a hydrogen bond to N(1G2), belonging to one of the guest molecules situated in the channel as described above. The C≃N bond length range is 1.25(2) to 1.40(2) Å while the C≃C bond lengths range from 1.31(1) to 1.38(1) Å. The internal angles (in °) of the pyridine molecules are: 117(1) to 119(1) for C≃N≃C, 119(1) to 129(1) for N≃C≃C and 112(2) to 123(1) for C≃C≃C.

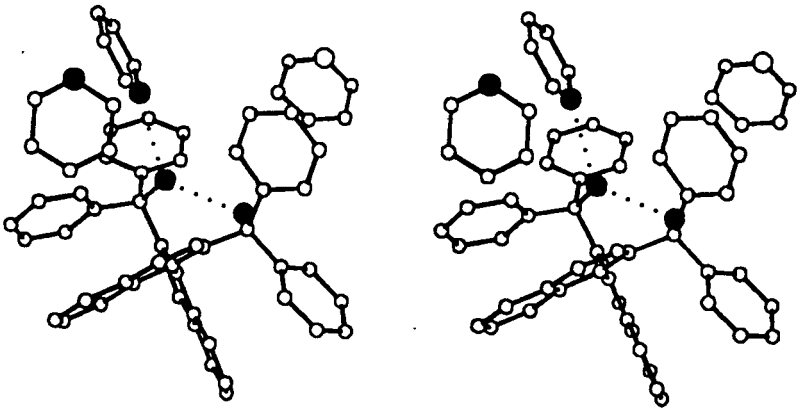

Figure 3.15 Stereoview of the asymmetric unit of **W12py** - hydrogen atoms are omitted and hydrogen bonds are indicated as dotted lines.

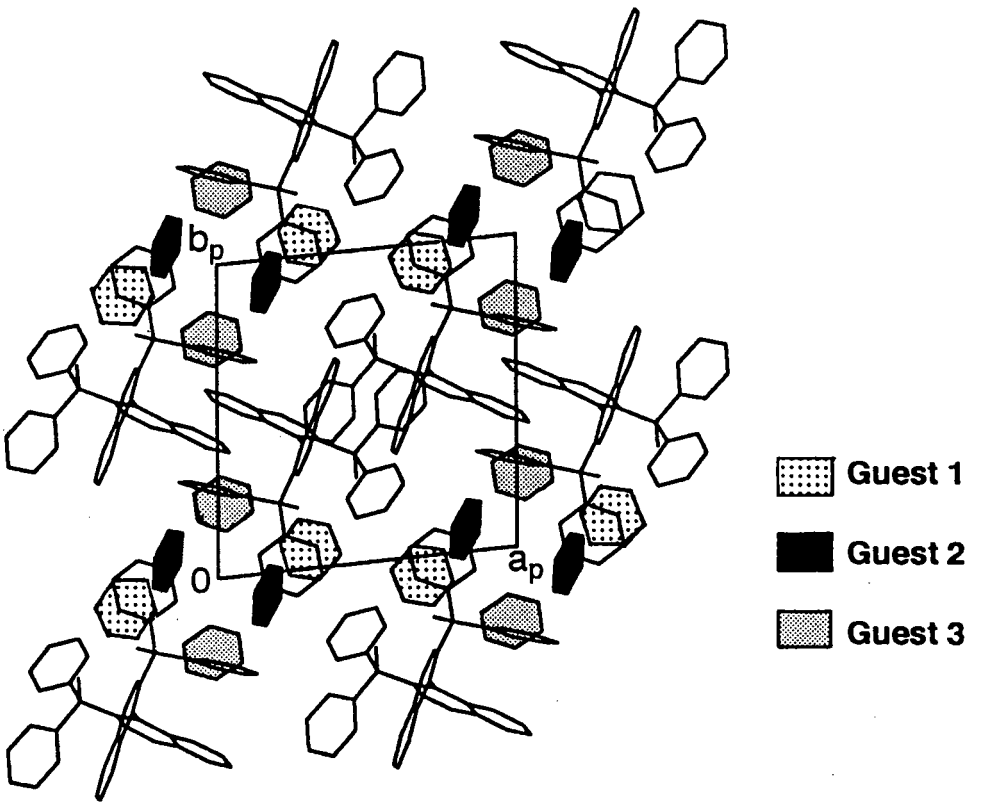

Figure 3.16 Projection of **W12py** along [001] with hydrogen atoms omitted and guest molecules shaded.

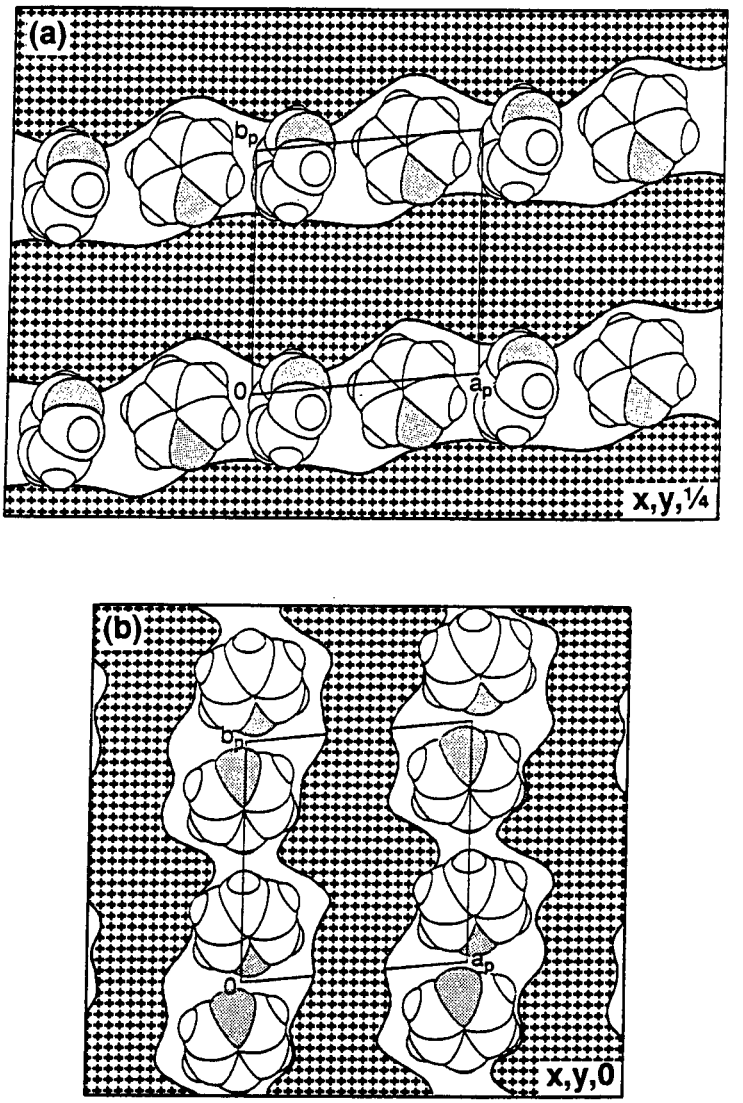

Figure 3.17 Projected cross-section of the host molecules (hatched area) of **W12py** on (a) (004), showing Guests 1 and 2 in channels, and (b) (001) showing Guest 3 in cavities.

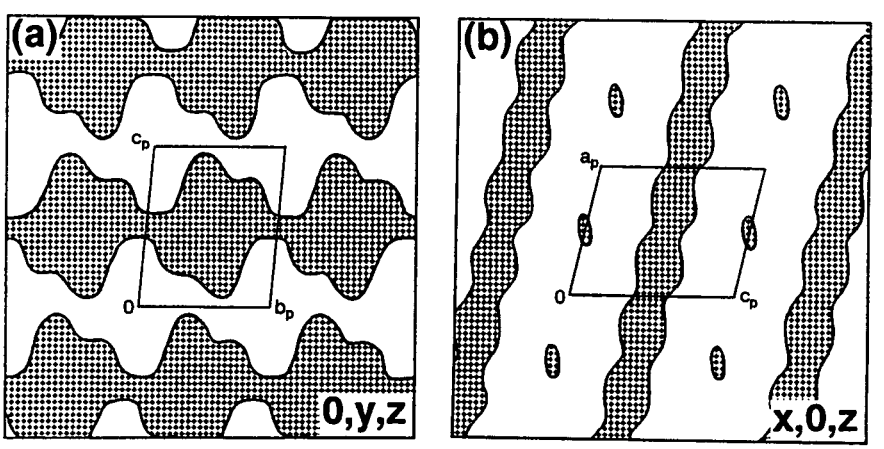

Figure 3.18 Projected cross-section of the host molecules (hatched area) of **W12py** on (a) (100) and (b) (010).

Host 3

The atom labelling scheme for Host 3 is shown in Figure 3.20. It is possible for this compound to exist in two enantiomeric forms owing to restricted rotation about C(19)–C(20). However, only one inclusion compound structure with the racemic mixture of this host was elucidated and the two crystallographically unique guest molecules are labelled with the suffixes "1" and "2" respectively after the letter "G".

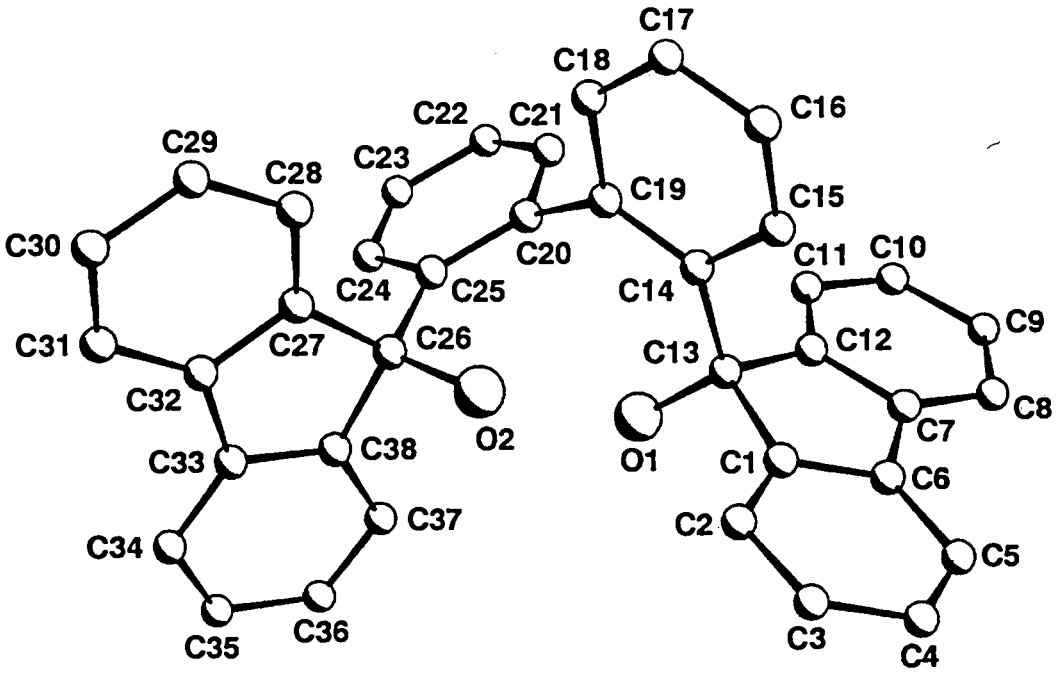

Figure 3.20 Atom numbering scheme for 2,2′-bis(9-hydroxy-9-fluorenyl)biphenyl.

W15ch $C_{38}H_{34}O_2 \cdot (C_6H_{12}O)_2$
Guest : Cyclohexanone
Space group : $P2_1/c$
a = 13.980(3)Å
b = 11.768(5)Å β = 98.77(3)°
c = 23.487(11)Å
V = 3819(2)Å^3
Z = 4

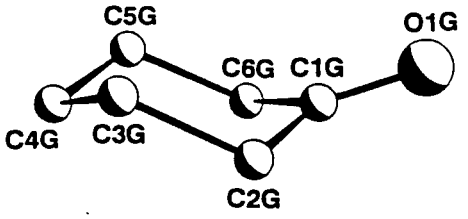

A host:guest ratio of 1:2 was established by TG (see Table 2.2). Preliminary oscillation and Weissenberg photography established **W15ch** as belonging to the monoclinic system (2/*m* Laue symmetry). Crystal reflection data exhibited the

following non-extinction conditions:

hkl : none
$h0l : l = 2n$
$0k0 : k = 2n$

indicating that the space group was $P2_1/c$. Determination of the unit cell volume and the crystal density suggested four formula units per unit cell.
During intensity data collection, it was necessary for the crystal to be re-centred three times. Periodic monitoring of three standard reflections indicated inconsistencies in the intensity data - an overall increase in intensity of 54.1% was observed. The increase in intensity was not linear but stepped in accordance with the re-centering of the crystal.

The reflection data set was appropriately corrected for intensity and direct methods yielded all non-hydrogen atoms in the asymmetric unit. The hydroxyl hydrogen atoms were located in difference electron density maps and refined with bond length constraints and individual temperature factors. In spite of an intermolecular hydrogen bond from O(2) to O(1G), the atoms of Guest 1 displayed a much higher degree of thermal motion than the atoms of Guest 2. Nevertheless, refinement proceeded uneventfully and the final R value was 0.112.

Molecular structure
The asymmetric unit of **W15ch** is shown in Figure 3.21 and hydrogen bond details are given in Table 3.1.

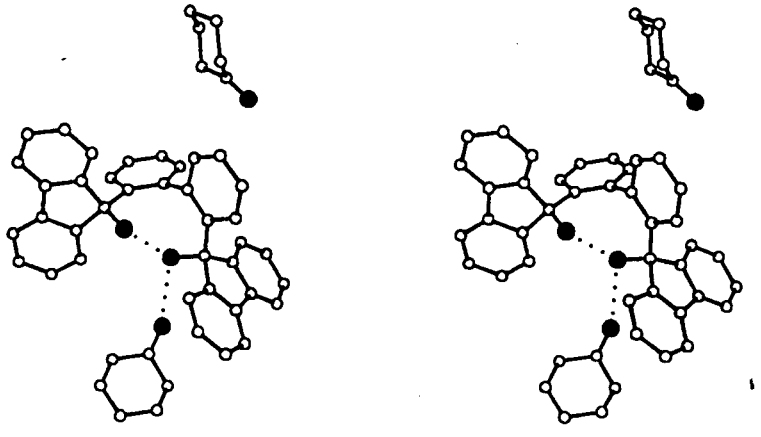

Figure 3.21 Stereoview of the asymmetric unit of **W15ch** - hydrogen atoms are omitted and hydrogen bonds are indicated as dotted lines.

All the molecules occupy general positions in the unit cell. There is an intramolecular hydrogen bond from O(1) to O(2) and an intermolecular hydrogen bond from O(2) to O(1G1). The guest molecules are situated in two symmetry-

related channels as shown in Figure 3.22(a). Careful inspection of the figure will show how the channels traverse the unit cell from A1 to A2 and from B1 to B2, running along [-110] and [110] respectively. Figure 3.22(b) shows the same projection stereographically with hydrogen atoms omitted, the host molecules in stick, and guest molecules in ball-and-stick representation. Only one of the guest molecules is hydrogen bonded to the host.

The C=O bond lengths of the guest molecule are both 1.22(2) Å while the C–C bond lengths range from 1.33(3) to 1.56(2) Å. The angles within the cyclohexyl ring range from 106(2) to 123(3) °.

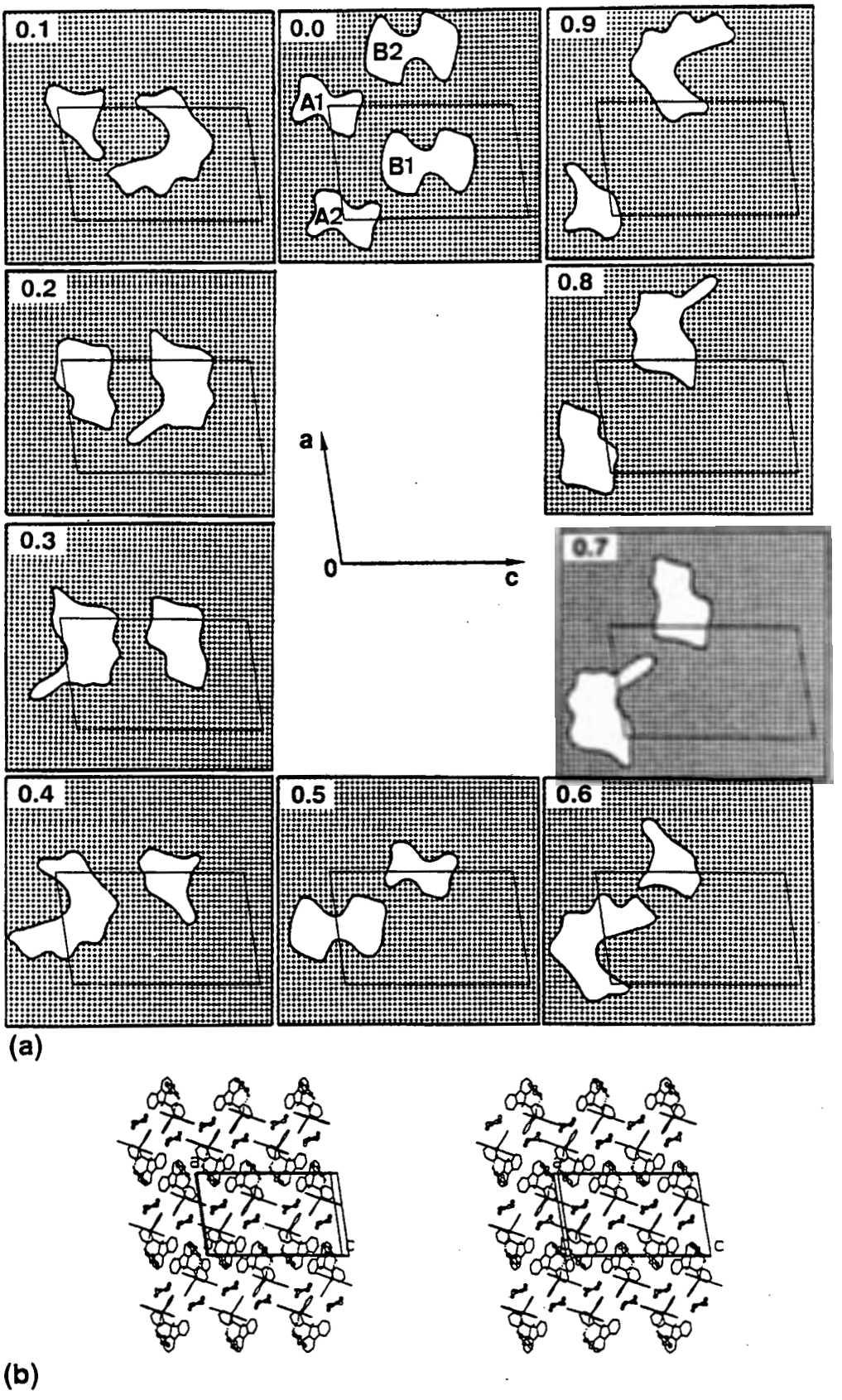

Figure 3.22 (a) Sections at intervals of 0.1b through **W15ch**, viewed parallel to [010] and (b) stereographic representation of the same projection.

Table 3.1 Hydrogen bond details for structures with Hosts 1 to 3

Compd.	(D)onor	(A)cceptor	D–H(Å)	D···A(Å)	H···A(Å)	D–H···A(°)
W14et	O(1B)	O(2B)		2.727(6)		
	O(2B)	O(2A)	0.97(2)	2.771(6)	1.95(4)	141(3)
	O(2A)	O(1A)		2.775(7)		
	O(1A)	O(1G)		2.715(8)		
W14bu	O(1A)	O(1B)	0.97(1)	2.772(2)	1.83(1)	163(2)
	O(1B)	O(1G)	0.96(2)	2.859(2)	2.04(2)	142(2)
	O(2A)	O(1A)[1]	0.96(3)	2.921(2)	2.01(2)	158(3)
	O(1G)	O(2A)[1]	0.96(2)	2.797(2)	1.91(2)	153(2)
	O(2B)	O(1G)[2]	0.95(2)	2.902(2)	1.96(2)	169(2)
W14py	O(1A)	N(1G1)		2.69(1)		
	O(2A)	O(1A)		2.753(8)		
	O(1B)	O(2B)		2.765(8)		
	O(2B)	N(1G2)[3]		2.73(1)		
	O(2A)	O(1A)[3]		2.803(7)		
	O(1B)	O(2B)[3]		2.835(8)		
W12	O(1)	O(2)	0.97(3)	2.759(7)	1.81(3)	167(6)
W12py	O(1)	O(2)	1.03(3)	2.679(4)	1.65(3)	175(3)
	O(2)	N(1G2)	0.97(3)	2.776(5)	1.81(3)	174(3)
W15ch	O(1)	O(2)	0.988(5)	2.755(7)	1.819(5)	156.9(3)
	O(2)	O(1A)	0.97(5)	2.76(1)	1.81(5)	163(5)

1 transformed by -x+1,-y+1,-z+1

2 transformed by -x+1,-y,-z+1

3 transformed by -x+½,y,-z+½

Chapter 4 Structure solution - Host 4

Crystal structures of complexes with Host 4 are discussed in this chapter. For each compound the molecular formula, space group and cell geometry are summarised together with the guest labelling scheme. This is followed by a brief description of its structure solution and refinement and then by a description of its molecular structure and guest conformation. Key bond lengths reported here can be compared with published average values based on X-ray and neutron diffraction results. Such values as are relevant to this study are reproduced in Appendix E. Crystal data, data collection and final refinement parameters for all the structures are given in Table 2.3.

The atom labelling scheme for Host 4 is shown in Figure 4.1. Where necessary, crystallographically independent guest molecules are assigned numeric suffixes after the letter "G".

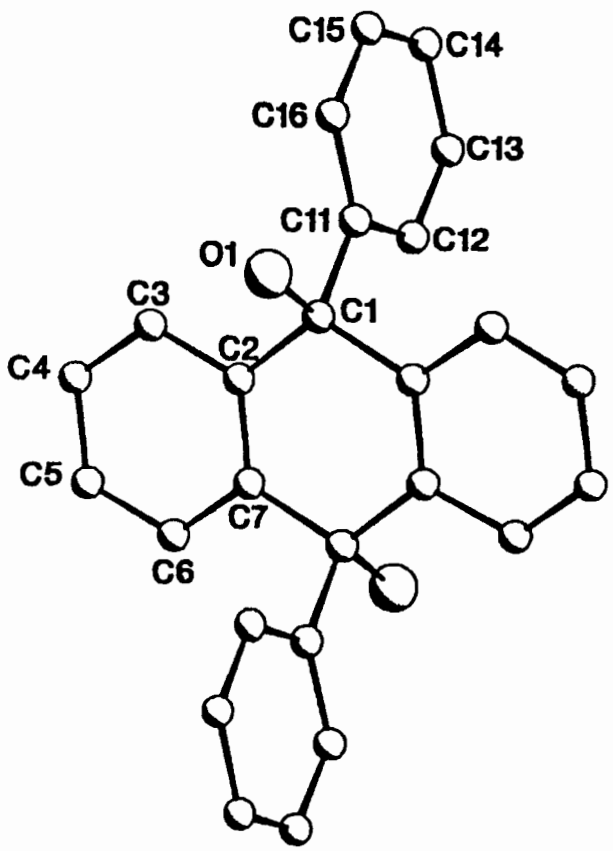

Figure 4.1 Atom numbering scheme for *trans*-9,10-dihydroxy-9,10-diphenyl-9,10-dihydroanthracene.

DPac $C_{26}H_{20}O_2 \cdot (C_3H_6O)_2$
Guest : Acetone
Space group : $P\bar{1}$
a = 8.689(14)Å α = 92.60(5)°
b = 9.466(6)Å β = 114.85(9)°
c = 9.448(6)Å γ = 107.46(9)°
V = 659(1)Å^3
Z = 1

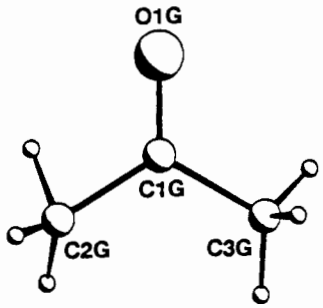

A host:guest ratio of 1:2 was established by TG (see Table 2.2). The triclinic system was indicated by $\bar{1}$ Laue symmetry of the X-ray diffraction record and the intensity statistics (mean $|E^2-1|$ for the general *hkl* reflections = 1.071) indicated $P\bar{1}$ as the correct space group rather than P1. Determination of the unit cell volume and the crystal density suggested one half of a host molecule and one complete guest molecule in the asymmetric unit, with Z = 1.

Direct methods yielded all non-hydrogen atoms in the asymmetric unit. The hydroxyl hydrogen atom was located in a difference electron density map and was refined with a bond length constraint and its own temperature factor. Refinement proceeded uneventfully and the final R was 0.085.

Molecular structure

The molecular structure of **DPac** is shown in Figure 4.2 and hydrogen bond details are given in Table 4.1.

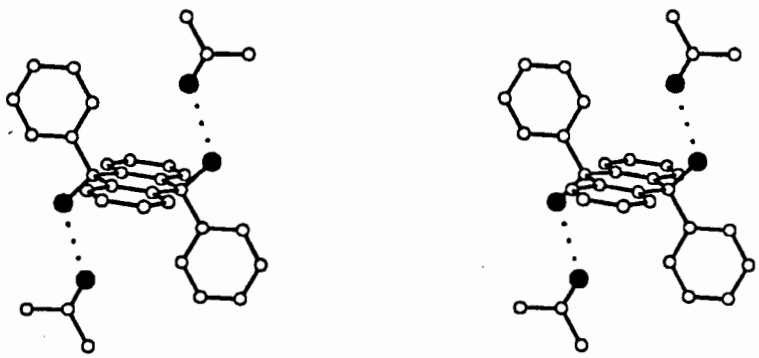

Figure 4.2 Stereoview of the molecular structure of **DPac** - hydrogen bonds are indicated as dotted lines.

With respect to the chosen unit cell, the host molecule is situated at $0,\frac{1}{2},0$ (Wyckoff position *c*). The guest molecules lie in channels running parallel to [010] at $\frac{1}{2},y,\frac{1}{2}$ and are held in place by the hydrogen bond O(1)–H(1O)···O(1G). The channels can be seen in Figures 4.3 (a) and (b) which show the projected cross-section of the host molecules on (002) viewed along [001] and on (200) viewed along [100], respectively. Figure 4.4 shows the relative positions of the host and guest molecules.

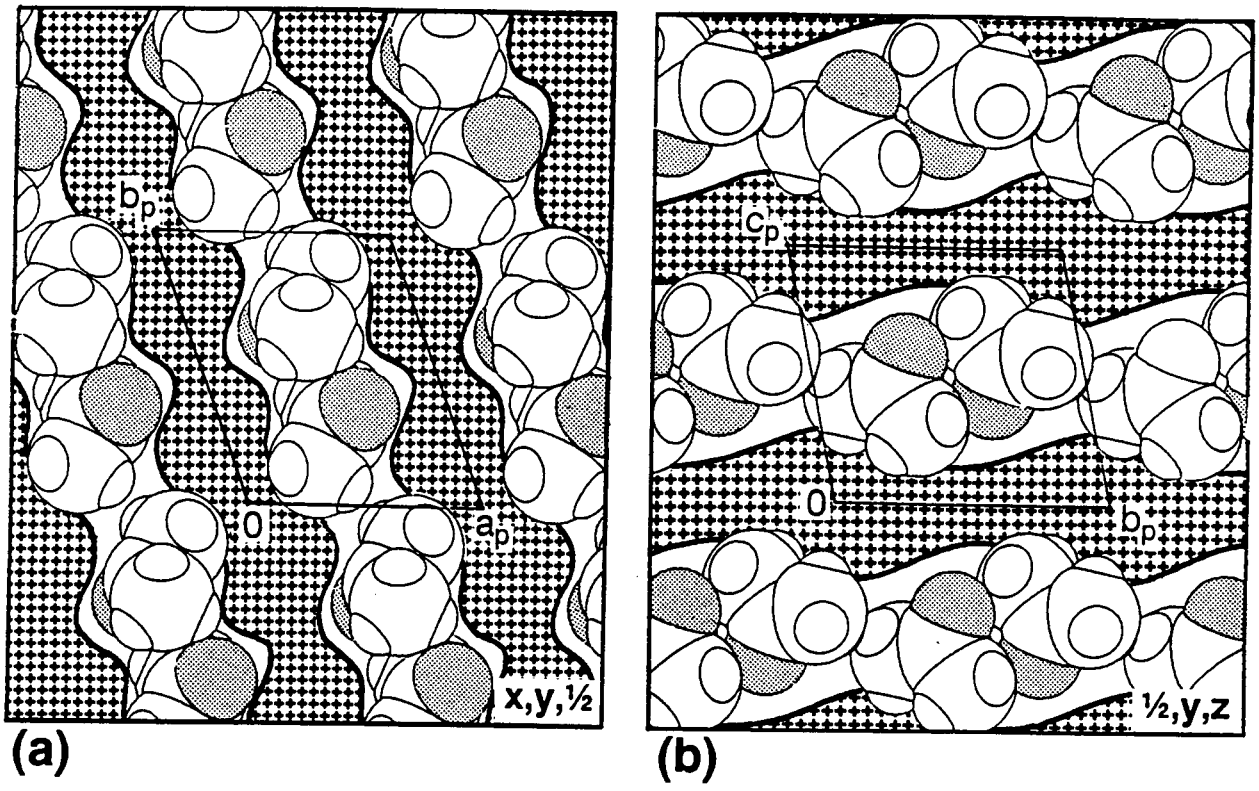

Figure 4.3 Projected cross-sections of the host molecules (hatched area) of **DPac** (a) along [001] on (002) and (b) along [100] on (200) - guest molecules are shown in van der Waals representation with the oxygen atoms shaded.

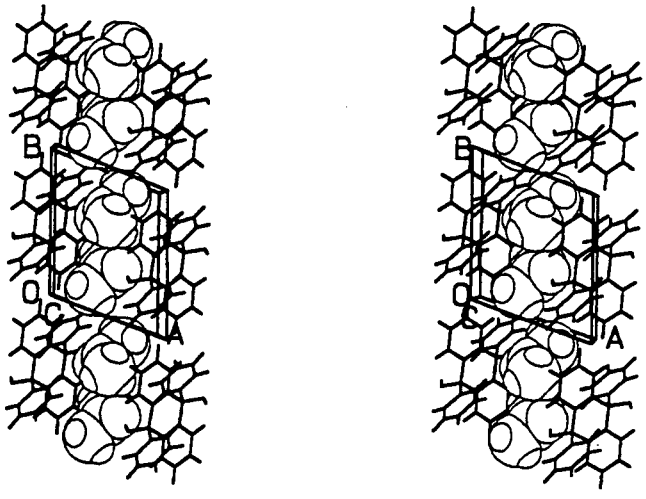

Figure 4.4 Stereoview of **DPac** viewed along [001] - guest molecules are shown with van der Waals radii and host molecules are shown in stick representation.

The three angles around the central carbon atom of the guest molecule range from 119.2(6) to 120.4(7) °, the C=O distance is 1.186(5) Å and the two C_{sp^3}–C_{sp^2} bond lengths are 1.46(1) and 1.44(1) Å respectively. These features of the guest geometry are in good agreement with values reported in the literature.

DPdek $C_{26}H_{20}O_2 \cdot C_5H_{10}O$
Guest : Diethyl ketone
Space group : $P\bar{1}$
a = 8.038(2)Å α = 109.36(2°
b = 8.846(2)Å β = 95.79(3)°
c = 9.248(2)Å γ = 99.19(3)°
V = 604.0(3)Å^3
Z = 1

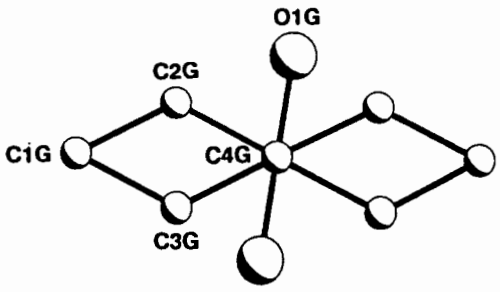

A host:guest ratio of 1:1 was established by TG (see Table 2.2). The triclinic system was indicated by $\bar{1}$ Laue symmetry of the X-ray diffraction record and the intensity statistics (mean $|E^2-1|$ for the general *hkl* reflections = 1.033) indicated $P\bar{1}$ as the correct space group rather than P1. Determination of the unit cell volume and the crystal density suggested one half of a host molecule and one half of a guest molecule in the asymmetric unit, with Z = 1.

Direct methods yielded all non-hydrogen host atoms in the asymmetric unit. The guest atoms were located in difference electron density maps and exhibited disorder which was successfully modelled. The sp^2 carbon atom, C(4G), is situated at $\frac{1}{2},0,\frac{1}{2}$ (Wyckoff position *f*), allowing the guest molecule to take on two possible arrangements as shown in the guest numbering scheme above. The atoms C(4G), O(1G), C(2G) and C(3G) were each assigned site-occupancy factors of 0.5 while C(1G) was modelled as one complete atom. These atoms were all refined isotropically with appropriate bond length constraints and the position of C(4G) was fixed at $\frac{1}{2},0,\frac{1}{2}$. Owing to the disorder of the guest molecule, no attempt was made to place its hydrogen atoms. The host hydroxyl hydrogen atom was located in a difference electron density map and refined with a bond length constraint and its own isotropic temperature factor. The maximum and minimum heights in the difference Fourier map were 0.76 and -0.60 eÅ^{-3} respectively. This reflects the fact that not all the atoms had been accounted for in the final model and that the guest atoms were refined isotropically. A relatively high final R value of 0.107 was obtained for the same reasons.

Molecular structure

The molecular structure of **DPdek** is shown in Figure 4.5 and hydrogen bond details are given in Table 4.1.

Both the host and the guest molecules are situated on centres of symmetry; i.e. at $0,\frac{1}{2},\frac{1}{2}$ and $\frac{1}{2},0,\frac{1}{2}$, Wyckoff positions *g* and *f*, respectively. Each of the two configurations of the disordered guest molecule forms a hydrogen bond with the host molecule, i.e. O(1)–H(1O)···O(1G) as shown in Figure 4.6.

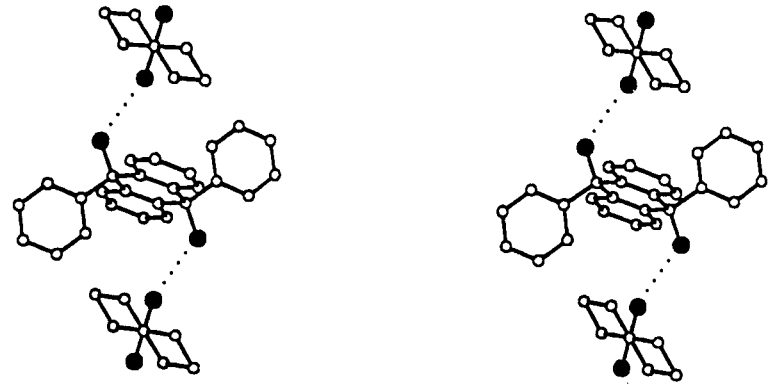

Figure 4.5 Stereoview showing the molecular structure of **DPdek** - hydrogen bonds are indicated as dotted lines.

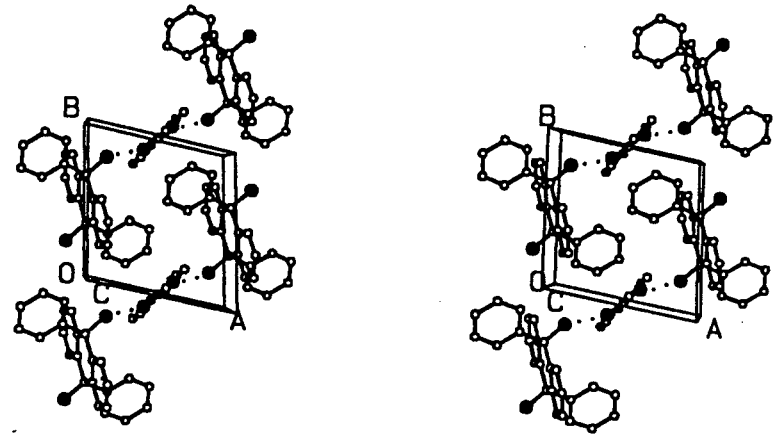

Figure 4.6 Stereoview of **DPdek** viewed along [001] - hydrogen atoms are omitted and hydrogen bonds are indicated as dotted lines.

The guest molecules are situated in cavities centred at $\frac{1}{2},0,\frac{1}{2}$. These cavities can be seen in projection in Figures 4.7 (a), (b) and (c) which show the guest molecules in van der Waals representation and the host molecules in cross section on (200), (010) and (002) respectively.

Since the geometry of the diethyl ketone molecule was set by bond length constraints during refinement, any discussion about its final conformation (other than the disorder described above) can be considered meaningless.

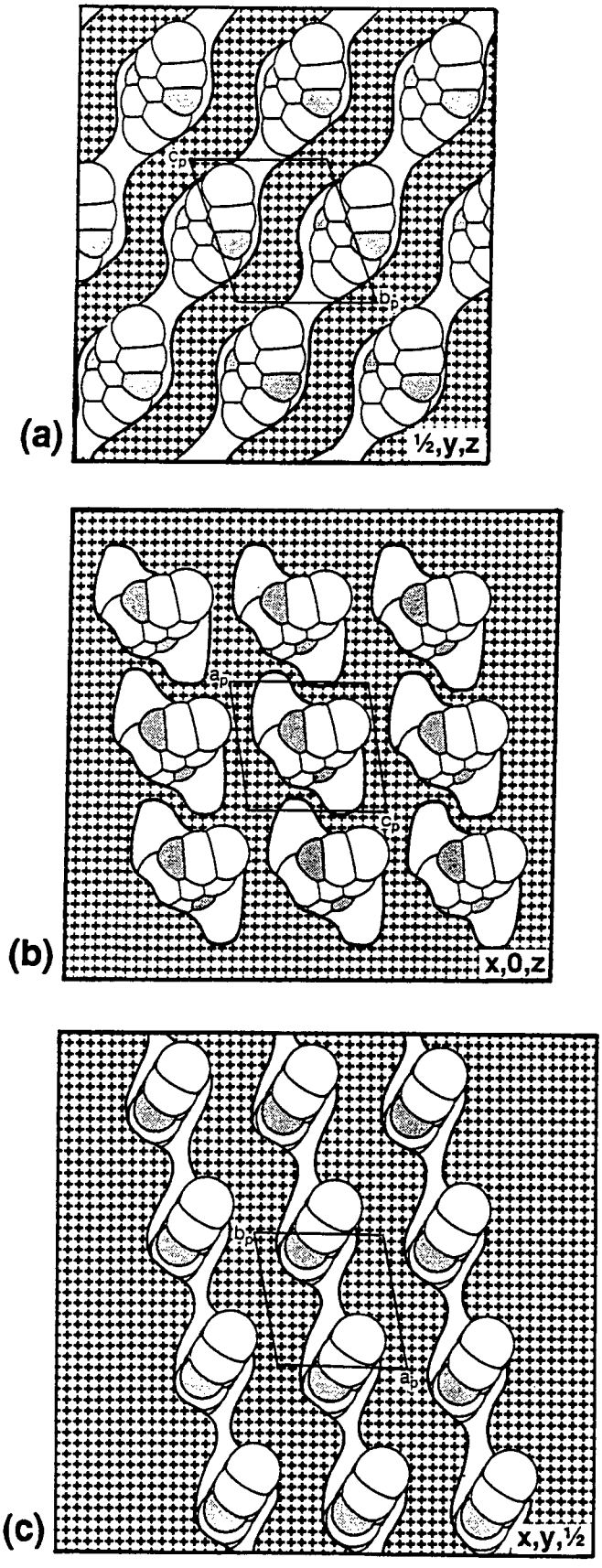

Figure 4.7 Projections of the host molecules of **DPdek** (hatched area) on (a) (200) viewed along [100], (b) (010) viewed along [010] and (c) (002) viewed along [001] - the guest molecules are shown in van der Waals representation with the oxygen atoms shaded.

DPdmso $C_{26}H_{20}O_2 \cdot (C_2H_6OS)_2$
Guest : Dimethyl sulphoxide
Space group : $P2_1/n$
a = 8.706(3)Å
b = 9.838(2)Å β = 94.31(2)°
c = 16.206(3)Å
V = 1384(1)Å^3
Z = 2

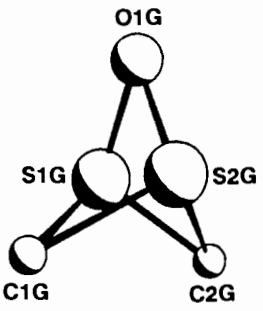

A host:guest ratio of 1:2 was established by TG (see Table 2.2). Preliminary oscillation and Weissenberg photography established **DPdmso** as belonging to the monoclinic system (2/*m* Laue symmetry). Crystal reflection data exhibited the following non-extinction conditions:

hkl	:	none
h0l	:	$h+l$ = 2n
0k0	:	k = 2n

indicating that the space group was $P2_1/n$. Determination of the unit cell volume and the crystal density suggested two formula units per unit cell. The space group then requires the host molecules to be situated at special positions with the asymmetric unit consisting of one half of a host molecule and one complete guest molecule.

Direct methods yielded all non-hydrogen host atoms in the asymmetric unit. The guest atoms were located in a difference electron density map which also showed that the guest molecule occupies a general position in the unit cell (as indeed required by the space group symmetry). The sulphur atom of the guest molecule is disordered and was located in two positions. The final model incorporated both positions for the sulphur atom and the site-occupancy factors were refined with starting values of 0.4 and 0.6 respectively. These values had been derived from relative peak heights in the electron density map and refined to 0.41 and 0.59 respectively. The two possible arrangements of the guest molecule are shown in the guest numbering scheme above. The guest atoms were modelled anisotropically but hydrogen atoms were omitted owing to the disorder of the S-C bonds. The host molecule refined uneventfully. Its hydroxyl hydrogen atom was located in a difference electron density map and refined with a bond length constraint and its own isotropic temperature factor. The final R value was 0.069.

Molecular structure

The molecular structure of **DPdmso** is shown in Figure 4.8 and hydrogen bond details are given in Table 4.1.

The host molecules are situated at 0,0,$\frac{1}{2}$ and $\frac{1}{2}$,$\frac{1}{2}$,0 (Wyckoff position *b*). The DMSO molecules are located in general positions in undulating, symmetry-related channels running parallel to [010] at approximately $\frac{1}{4}$,y,$\frac{1}{4}$ and $\frac{3}{4}$,y,$\frac{3}{4}$ as shown in Figures 4.9 (a) and (b) respectively and are held in place by the O(1)–H(1O)···O(1G) hydrogen bond. Figures 4.9 (c) and (d) show the packing of the host and guest molecules respectively.

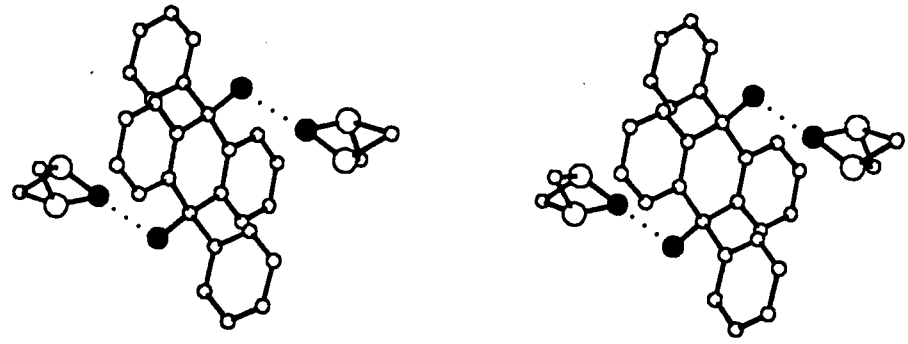

Figure 4.8 Stereoview of the molecular structure of **DPdmso** - hydrogen atoms are omitted and hydrogen bonds are indicated as dotted lines.

The S=O bond lengths in the disordered DMSO molecule are 1.488(6) and 1.475(9) Å, the S···S distance is 1.280(7) Å and the average C(1G)–S and C(2G)–S bond lengths are 1.77(1) and 1.64(1) Å respectively. Disorder of the DMSO molecule, either as a ligand or as an inclusion compound guest, is not uncommon[1-9] and the particular type of disorder observed here has been reported by Nassimbeni *et al.*[4] and Bond *et al.*[3]

DP2bu $C_{26}H_{20}O_2 \cdot C_4H_{10}O$
Guest : (±)2-Butanol
Space group : $P\bar{1}$
a = 7.990(1)Å α = 108.90(1)°
b = 8.954(1)Å β = 96.19(1)°
c = 9.007(1)Å γ = 101.37(1)°
V = 587.3(1)Å^3
Z = 1

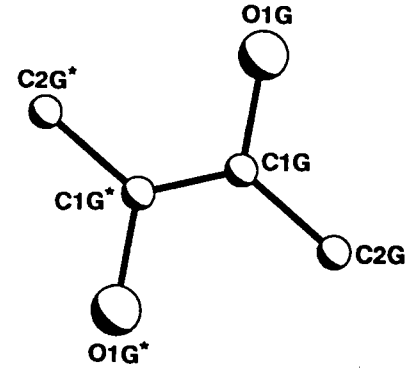

A host:guest ratio of 1:1 was established by TG (see Table 2.2). The triclinic system was indicated by $\bar{1}$ Laue symmetry of the X-ray diffraction record and the intensity statistics (mean $|E^2-1|$ for the general *hkl* reflections = 1.047) indicated $P\bar{1}$ as the correct space group rather than P1. Determination of the unit cell volume and the crystal density suggested one half of a host molecule and one half of a guest molecule in the asymmetric unit, with Z = 1.

Direct methods yielded all non-hydrogen atoms in the asymmetric unit. The guest molecule is disordered and, with reference to the guest molecule labelling scheme above, only atoms O(1G), C(1G) and C(2G) needed to be included in the model (with the oxygen atom assigned a site-occupancy factor of 0.5). The bond C(1G)-C(1G*) lies symmetrically across Wyckoff position *h* (i.e. $\frac{1}{2},\frac{1}{2},\frac{1}{2}$), and the

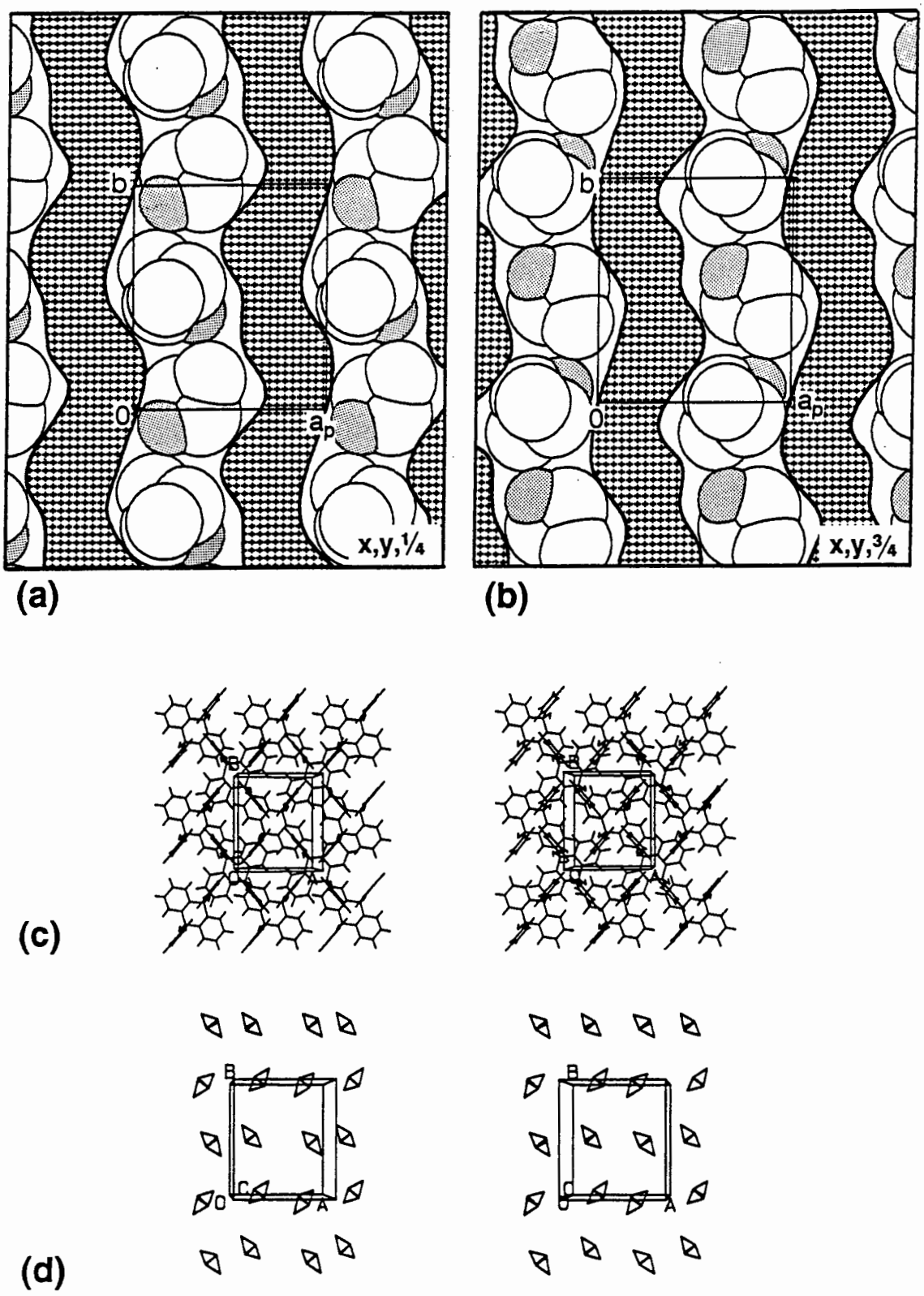

Figure 4.9 Projections of **DPdmso** along [001] showing the channels in cross section at (a) $\frac{1}{4}$,y,$\frac{1}{4}$ and (b) $\frac{3}{4}$,y,$\frac{3}{4}$ and packing diagrams of (c) the host molecules and (d) the guest molecules - in (a) and (b) the guest atoms are shown in van der Waals representation with the oxygen atoms shaded.

asterisked atoms are generated as a result of the $\bar{1}$ symmetry. The geometry of the guest molecule was fixed by introducing appropriate bond length constraints and the molecule was locked into place by constraining C(1G) at a distance of 0.70(1)Å from Wyckoff position *h*. The guest molecule was refined with isotropic thermal parameters and its hydrogen atoms were omitted from the model. The host molecule refined uneventfully. The hydroxyl hydrogen atom was located in a difference electron density map and was refined with a bond length constraint and its own temperature factor. The final R was 0.072.

Molecular structure

Figure 4.10 shows the molecular structure of **DP2bu** and hydrogen bond details are given in Table 4.1.

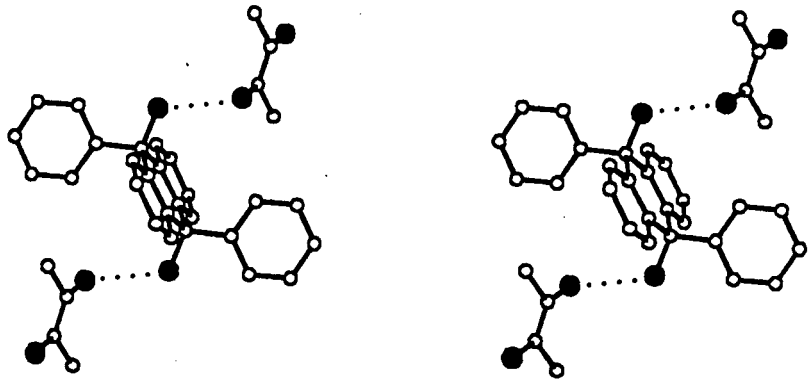

Figure 4.10 Stereoview of the molecular structure of **DP2bu** - hydrogen bonds are indicated as dotted lines.

With respect to the chosen unit cell, the host molecule is situated on the centre of symmetry at $0,0,\frac{1}{2}$ (Wyckoff position *b*). The guest molecules lie in cavities centred at $\frac{1}{2},\frac{1}{2},\frac{1}{2}$ and are held in place by the hydrogen bond O(1)–H(1O)···O(1G). These cavities can be seen in Figure 4.11 which shows the projected cross-section of the host molecules on (200) viewed along [100].

Since the geometry of the 2-butanol molecule was set by bond length constraints during refinement, any discussion about its final conformation can be considered meaningless.

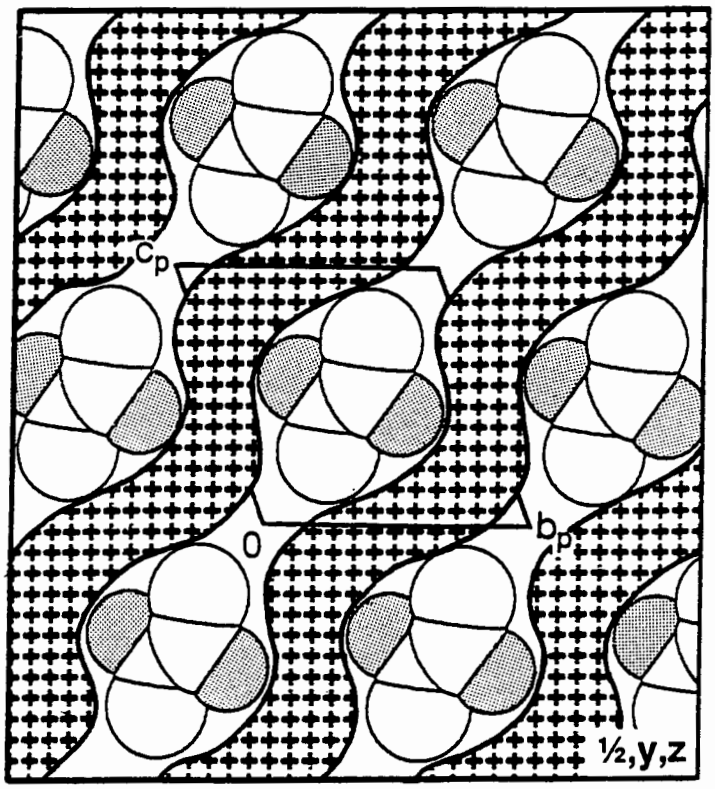

Figure 4.11 Projected cross-sections of the host molecules (hatched area) of **DP2bu** along [100] on (200) - guest molecules are shown in van der Waals representation with the oxygen atoms shaded.

Table 4.1 Hydrogen bond details for structures with Host 4

Compd.	Donor	Acceptor	O–H(Å)	O···O(Å)	H···O(Å)	O–H···O(°)
DPac	O(1)	O(1G)	0.97(2)	2.790(5)	1.83(2)	171(4)
DPdek	O(1)	O(1G)	0.98(9)	2.91(1)	2.1(1)	135(9)
DPdmso	O(1)	O(1G)	0.98(4)	2.731(6)	1.79(5)	160(6)
DP2bu	O(1)	O(1G)	0.97(5)	2.806(7)	1.95(6)	146(5)

References

1 E. Weber, K. Skobridis and I. Goldberg, *J. Chem. Soc., Chem. Commun.*, 1989,1195

2 B.M. Furphy, J.M. Harrowfield, M.I. Ogden, B.W. Skelton, A.H. White and F.R. Wilner, *J. Chem. Soc., Dalton Trans.*, 1989,2217

3 D.R. Bond, S.A. Bourne, L.R. Nassimbeni and F. Toda, *J. Crystallogr. Spectrosc. Res.*, 1989,**19**,809

4 L.R. Nassimbeni, M.L. Niven and M.W. Taylor, *J. Chem. Soc., Dalton Trans.*, 1989,119

5 I. Csoregh, M. Czugler, A. Ertan, E. Weber and J. Ahrendt, *J. Incl. Phenom.*, 1990,**8**,275

6 M.C. Etter, Z. Urbanczyk-Lipkowska, M. Zia-Ebrahimi and T.W. Panunto, *J. Am. Chem. Soc.*, 1990,**112**,8415

7 J.M. Harrowfield, M.I. Ogden and A.H. White, *Aust. J. Chem.*, 1991,**44**,1237

8 S. Tamburini, P.A. Vigato, P. Guerriero, U. Casellato and A. Aguiari, *Inorg. Chim. Acta*, 1991,**183**,81

9 Z. Asfari, J.M. Harrowfield, M.I. Ogden, J. Vicens and A.H. White, *Angew. Chem., Int. Ed. Engl.*, 1991,**30**,854

Chapter 5 Structure solution - Host 5

Crystal structures of complexes with Host 5 are discussed in this chapter. For each compound the molecular formula, space group and cell geometry are summarised together with the guest labelling scheme. This is followed by a brief description of its structure solution and refinement and then by a description of its molecular structure and guest conformation. Key bond lengths reported here can be compared with published average values based on X-ray and neutron diffraction results. Such values as are relevant to this study are reproduced in Appendix E. Crystal data, data collection and final refinement parameters for all the structures are given in Table 2.3.

The atom labelling scheme for Host 5 is shown in Figure 5.1. Where necessary, crystallographically independent guest molecules are assigned numeric suffixes after the letter "G".

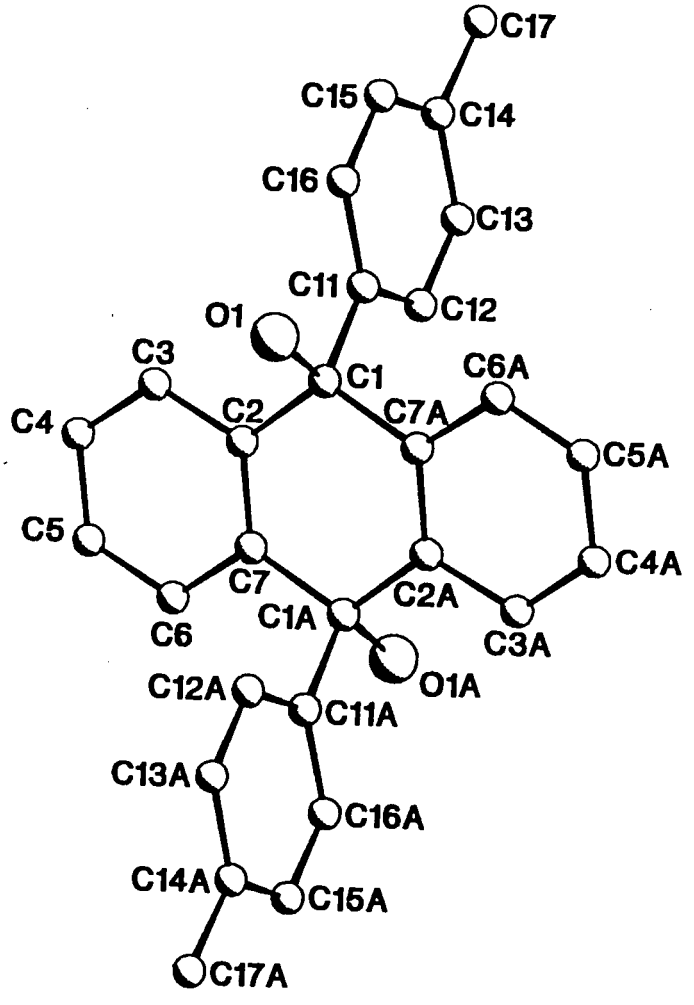

Figure 5.1 Atom numbering scheme for *trans*-9,10-dihydroxy-9,10-di-p-tolyl-9,10-dihydroanthracene.

DM $C_{28}H_{24}O_2$
Guest : None
Space group : $P2_1/c$
a = 5.876(2)Å
b = 21.349(9)Å β = 108.70(3)°
c = 8.971(2)Å
V = 1066(1)Å^3
Z = 2

Crystals were grown by slow evaporation of a solution of the compound in benzene. It was established by TG that benzene had not been included and the crystals were therefore of the pure form of the compound. Preliminary oscillation and Weissenberg photography established **DM** as belonging to the monoclinic system (2/*m* Laue symmetry). Despite several attempts at growing suitable crystals for intensity data collection, crystals were always lath-shaped. Finally a crystal of dimensions 0.06×0.19×0.25 mm was selected and intensity data were collected in the range θ = 1 to 20 °, yielding only 621 observed reflections with $I_{rel} > 2\sigma I_{rel}$. These data exhibited the following non-extinction conditions:

hkl	:	none
h0l	:	l = 2n
0k0	:	k = 2n

indicating that the space group was $P2_1/c$. Determination of the unit cell volume and the crystal density suggested two molecules per unit cell. The space group then requires the molecules to be situated on the centres of inversion with the asymmetric unit consisting of one half of a molecule.

Despite the small number of observed reflections, it was decided to proceed with the structure solution. Direct methods yielded all non-hydrogen atoms in the asymmetric unit. All the atoms with the exception of O(1) and C(17) were refined isotropically in order to increase the overdetermination ratio. The hydroxyl hydrogen atom could not be located unambiguously and was therefore omitted from the final model. The final R value was 0.076.

The purposes of this study do not necessarily require accurate modelling of thermal motion and it was therefore not deemed sufficiently critical to repeat the intensity data collection at low temperature to increase the number of observed reflections.

Molecular structure

Figure 5.2 shows the molecular structure of **DM**.

The molecules, situated at 0,0,0 and 0,$\frac{1}{2}$,$\frac{1}{2}$ (Wyckoff position *a*), pack closely in a criss-cross formation and in layers on (100). These are shown in projection along [001] and [100] in Figures 5.3 (a) and (b) respectively. There is no evidence of intermolecular hydrogen bonding and the packing factor is 17.8Å^3 per non-hydrogen atom. Further aspects of the molecular conformation will be discussed in Chapter 7.

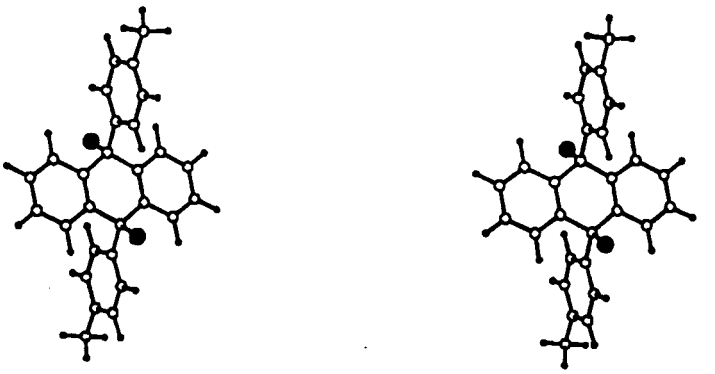

Figure 5.2 Stereoview of the molecular structure of **DM**.

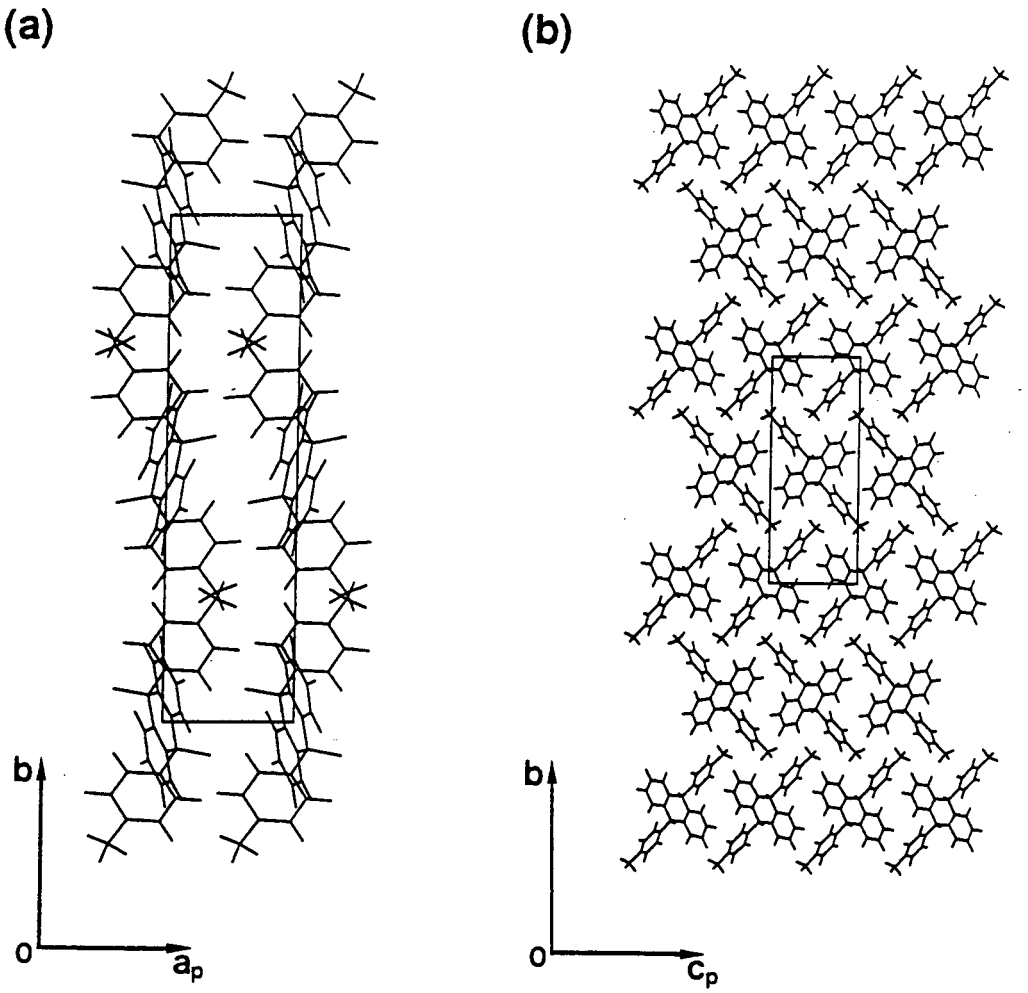

Figure 5.3 Projections of **DM** along (a) [001] and (b) [100].

DMac $C_{28}H_{24}O_2 \cdot (C_3H_6O)_2$
Guest : Acetone
Space group : $P\bar{1}$
a = 9.494(4)Å $\quad \alpha = 95.69(4)°$
b = 11.961(4)Å $\quad \beta = 101.75(4)°$
c = 12.771(8)Å $\quad \gamma = 89.80(3)°$
V = 1413(1)Å^3
Z = 2

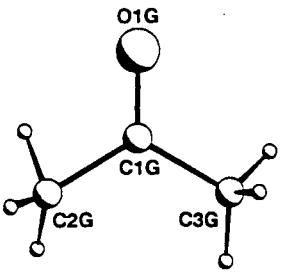

A host:guest ratio of 1:2 was established by TG (see Table 2.2). The triclinic system was indicated by $\bar{1}$ Laue symmetry of the X-ray diffraction record and the intensity statistics (mean $|E^2-1|$ for the general *hkl* reflections = 0.989) indicated $P\bar{1}$ as the correct space group rather than P1. Determination of the unit cell volume and the crystal density suggested one host molecule and two guest molecules in the asymmetric unit, with Z = 2.

Direct methods yielded all non-hydrogen atoms in the asymmetric unit and the structure refined uneventfully. All the hydroxyl hydrogen atoms were located and refined with bond length constraints and individual temperature factors. A relatively high maximum shift/e.s.d. value (ROTY[1] for C(2G1) = 1.863) was obtained in the final refinement. However, the average shift/e.s.d. value for all the parameters was 0.064 and the final R value was 0.052.

Molecular structure

The asymmetric unit is shown in Figure 5.4 and hydrogen bond details are given in Table 5.1.

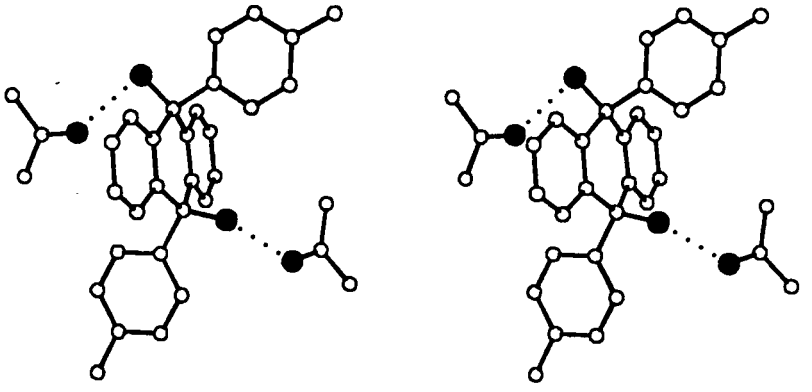

Figure 5.4 Stereoview of the asymmetric unit of **DMac** - hydrogen bonds are indicated as dotted lines.

The most interesting feature about this structure is that the central ring of the host molecule assumes the non-centrosymmetric pseudo-boat conformation and host molecule thus occupies a general position in the unit cell. This is unusual for the type of tricyclic system considered here and will be discussed in more detail in Chapter 7.

Two crystallographically unique hydrogen bonds are formed between the two hydroxyl moieties of the host molecule and the two independent acetone molecules. Figure 5.5 shows the packing between the host and guest molecules for **DMac.**. The guest molecules are situated in bulging channels running along [1-11]. The bulges are centred at $0,\frac{1}{2},0$, narrowing at the centre of inversion at $\frac{1}{2},0,\frac{1}{2}$ and bulging again at $1,-\frac{1}{2},1$. This can be seen in Figure 5.6 which shows "slices" through the unit cell (with the guest molecules omitted and the area occupied by the host molecules hatched) at intervals of 0.1c along the c-axis.

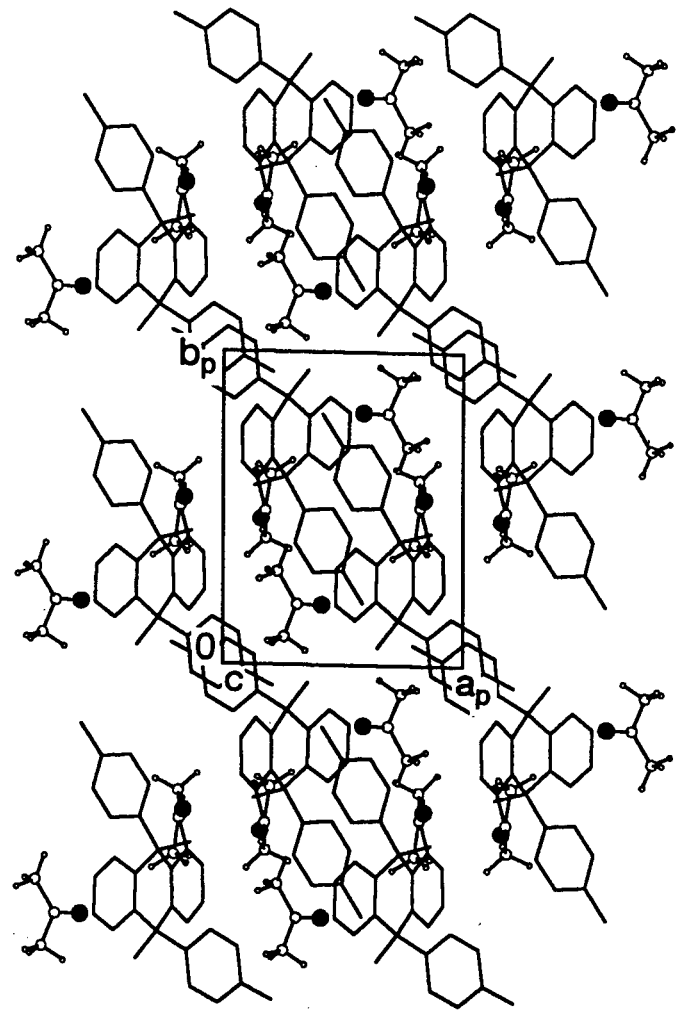

Figure 5.5 Projection of **DMac** viewed along [001] - host molecules (with hydrogen atoms omitted) are drawn in stick and guest molecules in ball-and-stick representation.

The three angles around C(1G) of the two independent guest molecules range from 117.8(4) to 121.7(4) °, the C=O bond lengths are 1.208(5) and 1.214(4) Å and the C_{sp^3}–C_{sp^2} bond lengths range from 1.471(7) to 1.490(5) Å.

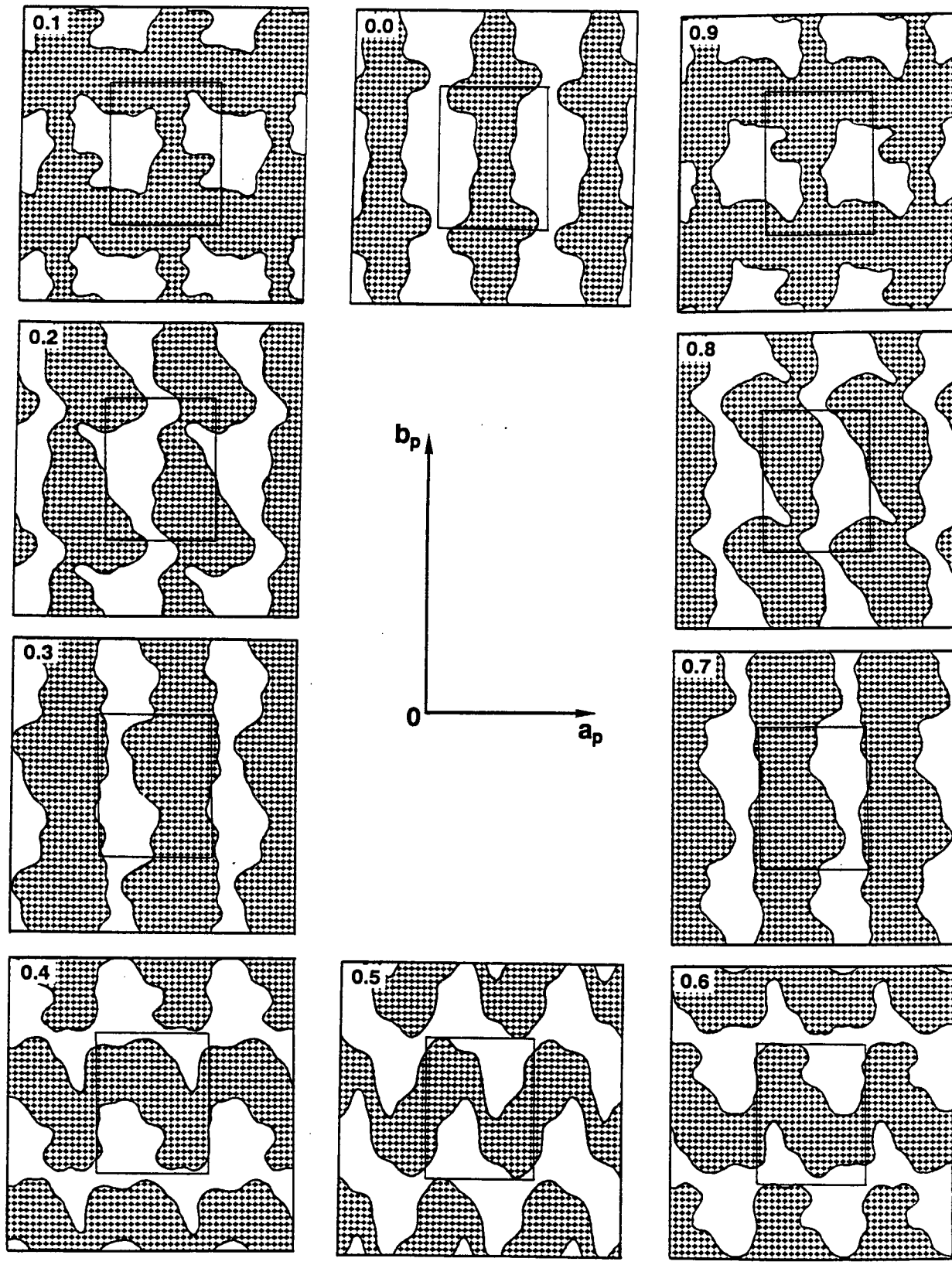

Figure 5.6 Sections through **DMac** at intervals of 0.1c viewed along [001].

DMde $C_{28}H_{24}O_2 \cdot (C_4H_{10}O)_2$
Guest : Diethyl ether
Space group : $P2_1/n$
a = 8.706(2)Å
b = 10.911(2)Å β = 94.90(3)°
c = 16.614(6)Å
V = 1572(1)Å^3
Z = 2

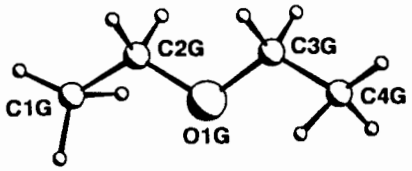

A host:guest ratio of 1:2 was established by TG (see Table 2.2). Preliminary oscillation and Weissenberg photography established **DMde** as belonging to the monoclinic system (2/*m* Laue symmetry). Crystal reflection data exhibited the following non-extinction conditions:

hkl	:	none
h0l	:	$h+l$ = 2n
0k0	:	k = 2n

indicating that the space group was $P2_1/n$. Determination of the unit cell volume and the crystal density suggested two molecules per unit cell. The space group then requires the host molecules to be situated at special positions with the asymmetric unit consisting of one half of a host molecule and one complete guest molecule.

Direct methods yielded all non-hydrogen host atoms in the asymmetric unit. The guest atoms were located in a difference electron density map and displayed a relatively high degree of thermal motion on refinement. The guest hydrogen atoms were inserted into the model and refined with fixed isotropic temperature factors. The hydroxyl hydrogen atom was located and refined with bond length constraints and its own temperature factor. Refinement of the host molecule proceeded uneventfully and the final R value was 0.057.

Molecular structure
The molecular structure of **DMde** is shown in Figure 5.7 and hydrogen bond details are given in Table 5.1.

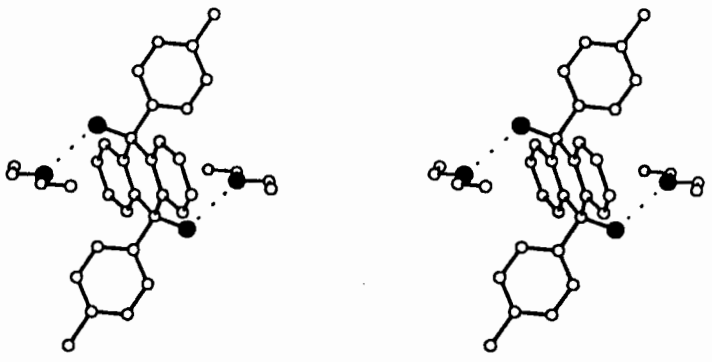

Figure 5.7 Stereoview of the molecular structure of **DMde** - hydrogen atoms are omitted and hydrogen bonds are indicated as dotted lines.

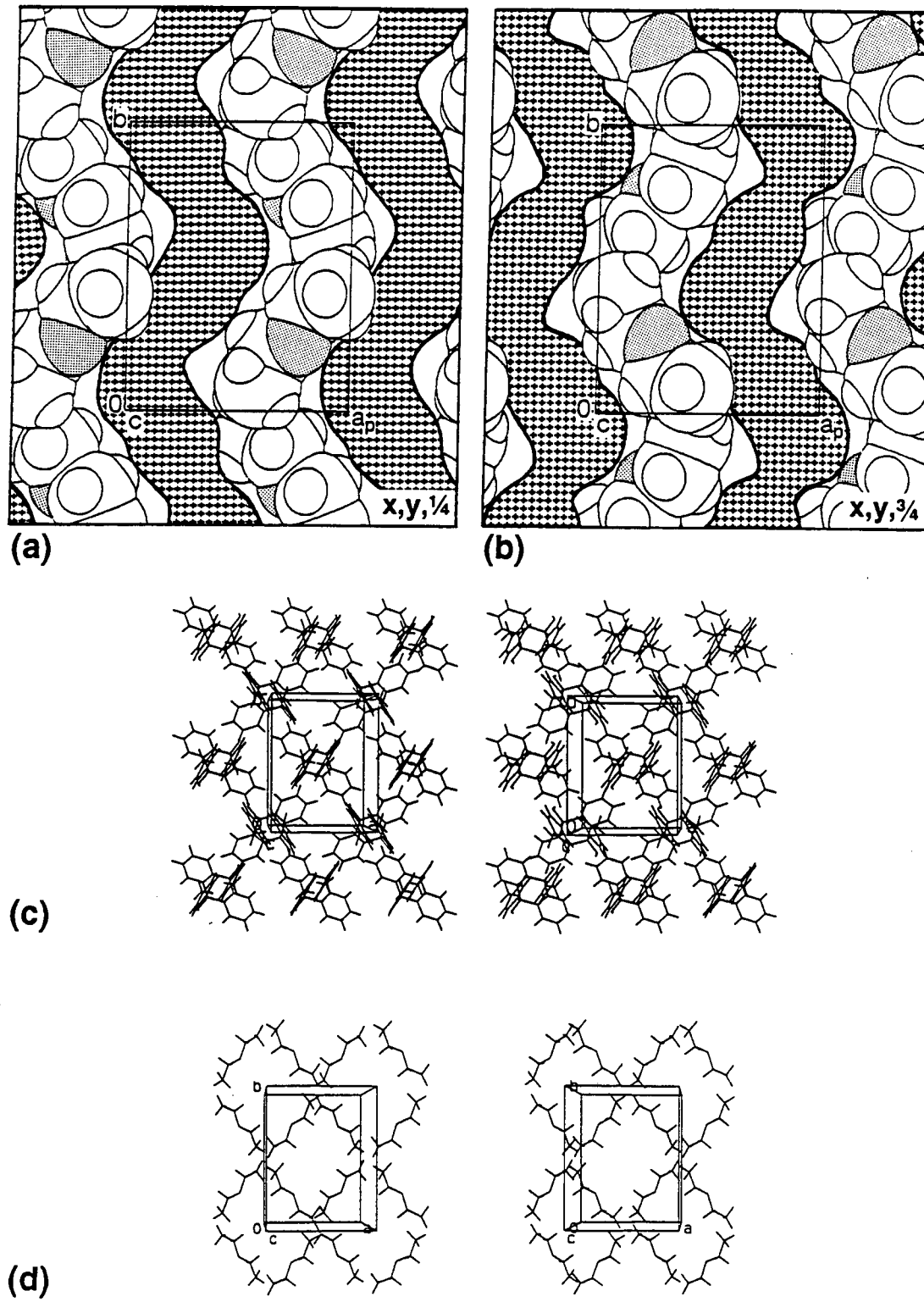

Figure 5.8 Views of **DMde** along [001] showing the channels in cross section at (a) $\frac{3}{4}$,y,$\frac{1}{4}$ and (b) $\frac{1}{4}$,y,$\frac{3}{4}$ and packing diagrams of (c) the host molecules and (d) the guest molecules.

The host molecules are situated at 0,0,½ and ½,½,0 (Wyckoff position *d*). The guest molecules are situated in undulating, symmetry-related channels running parallel to [010] at approximately ¾,y,¼ and ¼,y,¾ as shown in Figures 5.8 (a) and (b) respectively. In addition, the diethyl ether molecules are held in place by hydrogen bonding with the hydroxyl moieties of the host molecules. Figures 5.8 (c) and (d) show the packing of the host and guest molecules respectively.

The diethyl ether molecule is planar - its two torsion angles are -177.8(9)° for C(1G)-C(2G)-O(1G)-C(3G) and 178.4(8)° for C(2G)-O(1G)-C(3G)-C(4G). However, the mean C–C and C–O bond lengths are all significantly shorter than expected; 1.32(1) and 1.371(9) Å respectively in contrast to mean bond length values reported for C_{sp^3}–C_{sp^3} (1.52(2)Å overall) and C_{sp^3}–O in dialkyl ethers (1.43(2)Å).[1] The three bond angles ranged from 117.8(6)° to 122.2(9)°. The poor geometry of the diethyl ether molecule is attributed to its high degree of thermal motion. This is probably related to its relatively high volatility coupled with loose packing of the structure (the packing factor for **DMde** is 19.7Å³ per non-hydrogen atom).

DMpy $C_{28}H_{24}O_2 \cdot (C_5H_5N)_2$
Guest : Pyridine
Space group : $P2_1/n$
a = 9.661(1)Å
b = 9.724(2)Å β = 95.61(2)°
c = 16.398(4)Å
V = 1533(1)Å³
Z = 2

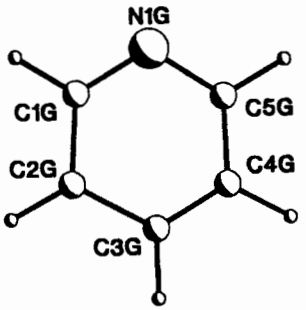

A host:guest ratio of 1:2 was established by TG (see Table 2.2). Preliminary oscillation and Weissenberg photography established **DMpy** as belonging to the monoclinic system (2/*m* Laue symmetry). Crystal reflection data exhibited the following non-extinction conditions:

hkl	:	none
h0l	:	$h+l$ = 2n
0k0	:	k = 2n

indicating that the space group was $P2_1/n$. Determination of the unit cell volume and the crystal density suggested two molecules per unit cell. The space group then requires the host molecules to be situated at special positions with the asymmetric unit consisting of one half of a host molecule and one complete guest molecule.

Direct methods yielded all non-hydrogen atoms in the asymmetric unit. The hydroxyl hydrogen atom was located and refined with bond length constraints and its own temperature factor. Refinement proceeded uneventfully and the final R value was 0.052.

Molecular structure

The molecular structure of **DMpy** is shown in Figure 5.9 and hydrogen bond details are given in Table 5.1.

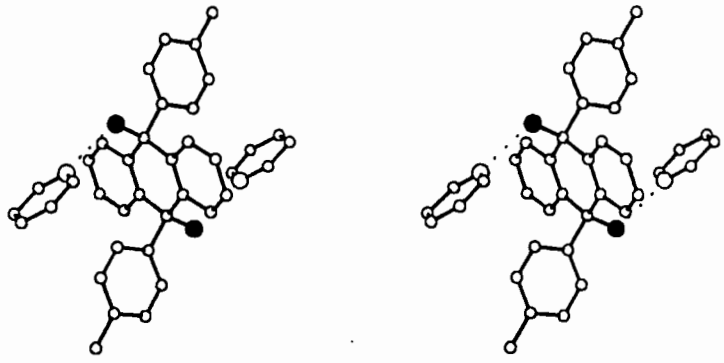

Figure 5.9 Stereoview of the molecular structure of **DMpy** - hydrogen atoms are omitted and hydrogen bonds are indicated as dotted lines.

The host molecules are situated at $0,\frac{1}{2},0$ and $\frac{1}{2},0,\frac{1}{2}$ (Wyckoff position *c*). The packing between host and guest molecules is remarkably similar to that in **DMde** (and also to **DPdmso**). The guest molecules are again located in undulating, symmetry-related channels running parallel to [010] at approximately $\frac{3}{4},y,\frac{1}{4}$ and $\frac{1}{4},y,\frac{3}{4}$ as shown in Figures 5.10 (a) and (b) respectively. In addition, the pyridine molecules are held in place by hydrogen bonding with the hydroxyl moieties of the host molecules. Figures 5.10 (c) and (d) show the packing of the host and guest molecules respectively.

The pyridine molecule is planar; the maximum deviation of any atom from the least-squares plane through the guest molecule is 0.009(8)Å.

The C≃N bond lengths are 1.328(7) and 1.319(7) Å while the C≃C bond lengths range from 1.32(1) to 1.37(1) Å. The internal angles (in °) of the pyridine molecule are: 117.8(5) for C≃N≃C, 122.0(6) and 122.6(6) for N≃C≃C and 117.9(7) to 120.2(7) for C≃C≃C. The bond length values, although relatively short, are in reaonable agreement with values reported in the literature (see Appendix E).

Table 5.1 Hydrogen bond details for structures with Host 5

Compd.	(D)onor	(A)cceptor	D–H(Å)	D···A(Å)	H···A(Å)	D–H···A(°)
DMac	O(1)	O(1G1)	0.96(2)	2.819(3)	1.89(3)	162(2)
	O(1A)	O(1G2)	0.97(3)	2.898(4)	1.94(3)	169(2)
DMde	O(1)	O(1G)	0.96(2)	2.840(4)	1.93(2)	158(3)
DMpy	O(1)	N(1G)	1.00(2)	2.826(5)	1.84(3)	168(4)

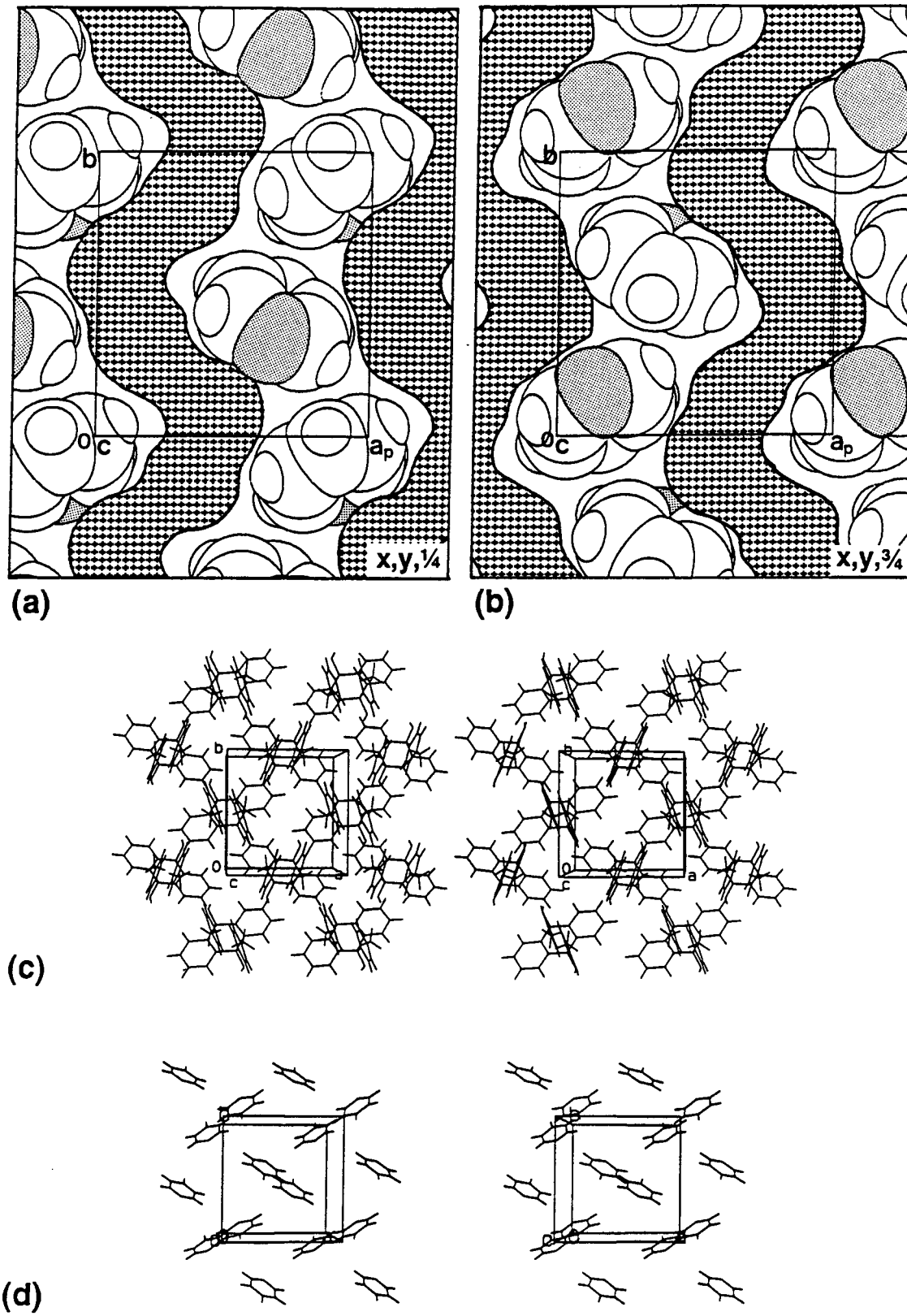

Figure 5.10 Views of **DMpy** along [001] showing the channels in cross section at (a) $\frac{3}{4}$,y,$\frac{1}{4}$ and (b) $\frac{1}{4}$,y,$\frac{3}{4}$ and packing diagrams of (c) the host molecules and (d) the guest molecules.

Reference

1 G.M Sheldrick in "Computing in Crystallography", H. Schenk, Olthof-Hazekamp, J. von Konigsveld and G.C. Bassi (Eds), Delft University Press, 34, 1978

Chapter 6 Structure solution - Hosts 6 and 7

Crystal structures of complexes with Hosts 6 and 7 are discussed in this chapter. For each compound the molecular formula, space group and cell geometry are summarised together with the guest labelling scheme. This is followed by a brief description of its structure solution and refinement and then by a description of its molecular structure and guest conformation. Key bond lengths reported here can be compared with published average values based on X-ray and neutron diffraction results. Such values as are relevant to this study are reproduced in Appendix E. Crystal data, data collection and final refinement parameters for all the structures are given in Table 2.3.

Host 6

The atom labelling scheme for Host 6 is shown in Figure 6.1. Crystallographically independent guest molecules are assigned numeric suffixes after the letter "G".

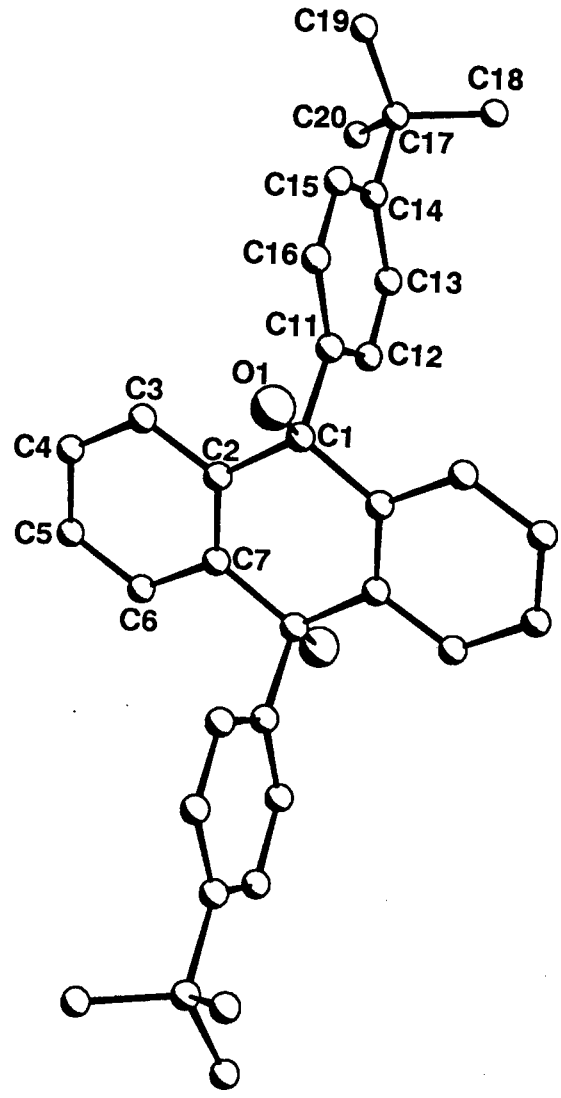

Figure 6.1 Atom numbering scheme for *trans*-9,10-dihydroxy-9,10-di-p-*tert*-butylphenyl-9,10-dihydroanthracene.

DBac $C_{34}H_{36}O_2 \cdot (C_3H_6O)_4$
Guest : Acetone
Space group : $P2_1/c$
a = 8.996(2)Å
b = 27.139(6)Å β = 109.16(3)°
c = 9.245(4)Å
V = 2132(1)Å^3
Z = 2

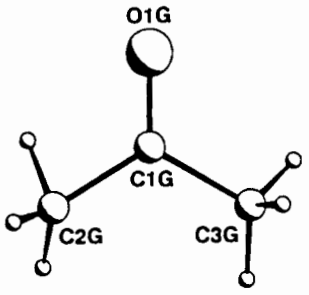

A host:guest ratio of 1:4 was established by TG (see Table 2.2). Preliminary oscillation and Weissenberg photography established **DBac** as belonging to the monoclinic system (2/*m* Laue symmetry). Crystal reflection data exhibited the following non-extinction conditions:

hkl : none
h0l : *l* = 2n
0k0 : *k* = 2n

indicating that the space group was $P2_1/c$. Determination of the unit cell volume and the crystal density suggested two molecules per unit cell. The space group then requires the host molecules to be situated at special positions with the asymmetric unit consisting of one half of a host molecule and two guest molecules.

Direct methods yielded all non-hydrogen host atoms in the asymmetric unit. The guest molecules were located in difference electron density maps and were refined with isotropic temperature factors owing to their high degree of thermal motion. No attempt was made to include the guest hydrogen atoms in the model.

A peak of approximately 1.13 eÅ^{-3} persisted in the difference Fourier map during refinement. This peak was located at about 1.52Å from C(17), the central carbon atom of the tertiary butyl group of the host molecule. An unsuccessful attempt was made to model this peak as part of a possible disorder of the tertiary butyl group. The spurious peak could not be accounted for and is tentatively attributed to poorly modelled thermal motion in the region of the tertiary butyl group. Indeed, the carbon atoms of the tertiary butyl group exhibited high thermal motion and were refined isotropically and without hydrogen atoms.

The hydroxyl hydrogen atom could not be located unambiguously in a difference electron density map and the absence of any short O···O distances precluded the existence of hydrogen bonds involving the host hydroxyl moiety. The final R value was 0.144. This R value should be regarded as unacceptable for deposition of the structure with the Cambridge Structural Database. However, the structure is sufficiently defined in order to determine the channel/cavity nature of inclusion and to make comparisons with **DBde** and **DBbz** in terms of the relative positions of the host and guest molecules.

Molecular structure

The molecular structure of **DBac** is shown in Figure 6.2 and hydrogen bond details are given in Table 6.1.

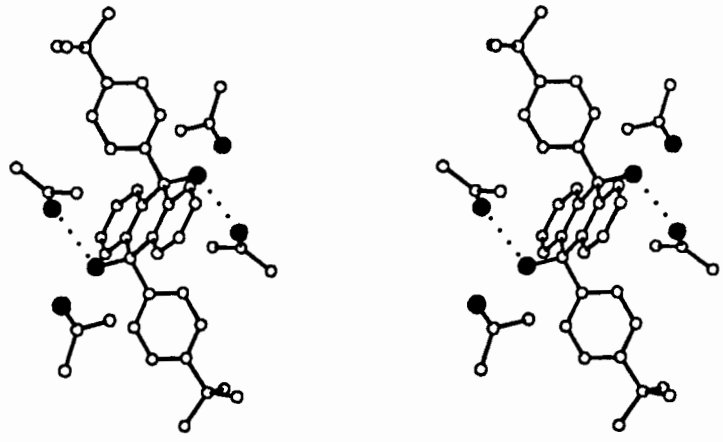

Figure 6.2 Stereoview of the asymmetric unit of **DBac** - the hydrogen atoms are omitted for clarity.

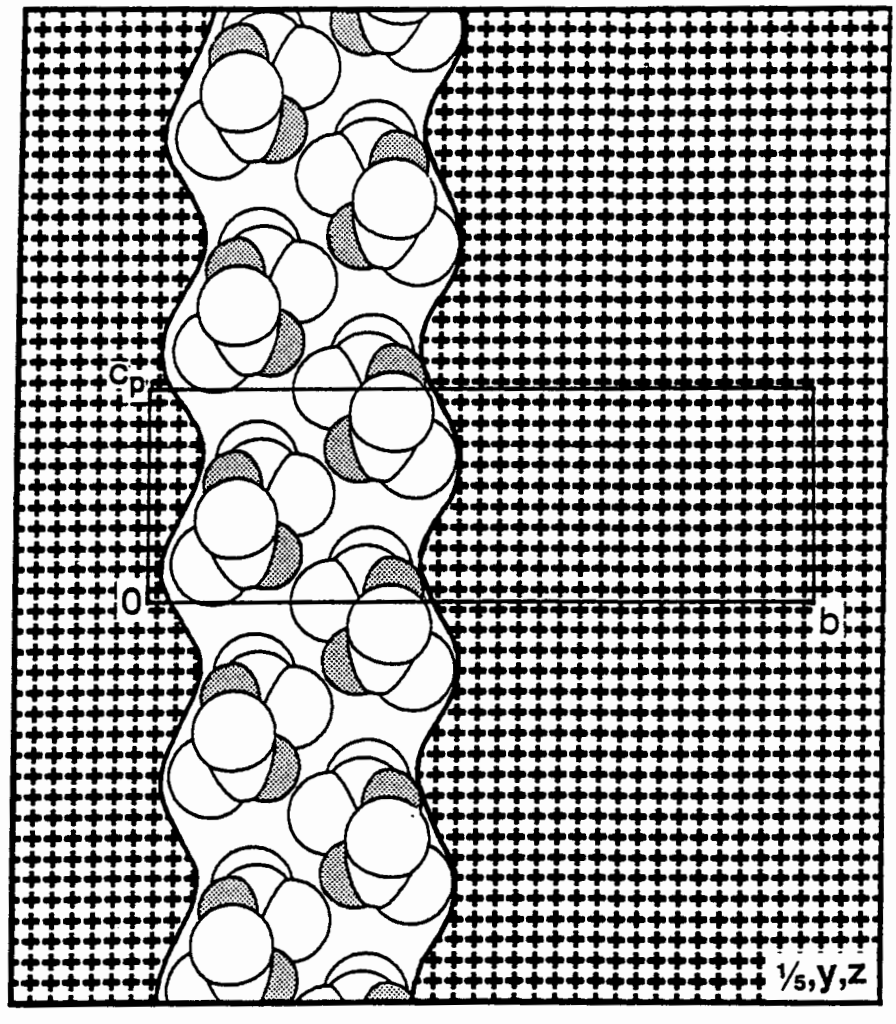

Figure 6.3 Projected cross-section of the host molecules (hatched area) of **DBac** on (500) showing the acetone molecules in channels - oxygen atoms are shaded.

The host molecules are situated at $0,\frac{1}{2},0$ and $0,0,\frac{1}{2}$ (Wyckoff position *c*) and the guest molecules lie on general positions in the unit cell. There is a hydrogen bond between O(1) and O(1G1) with an O···O distance of 2.860(8)Å. The host molecules stack to form two symmetry-related channels running parallel to [001] at $\frac{1}{5},\frac{1}{5},z$ and $\frac{4}{5},\frac{4}{5},z$. The channel at $\frac{1}{5},\frac{1}{5},z$ is shown in cross-section in Figure 6.3 and the packing diagram of **DBac** viewed down [001] (i.e. along the channels) is shown in Figure 6.4.

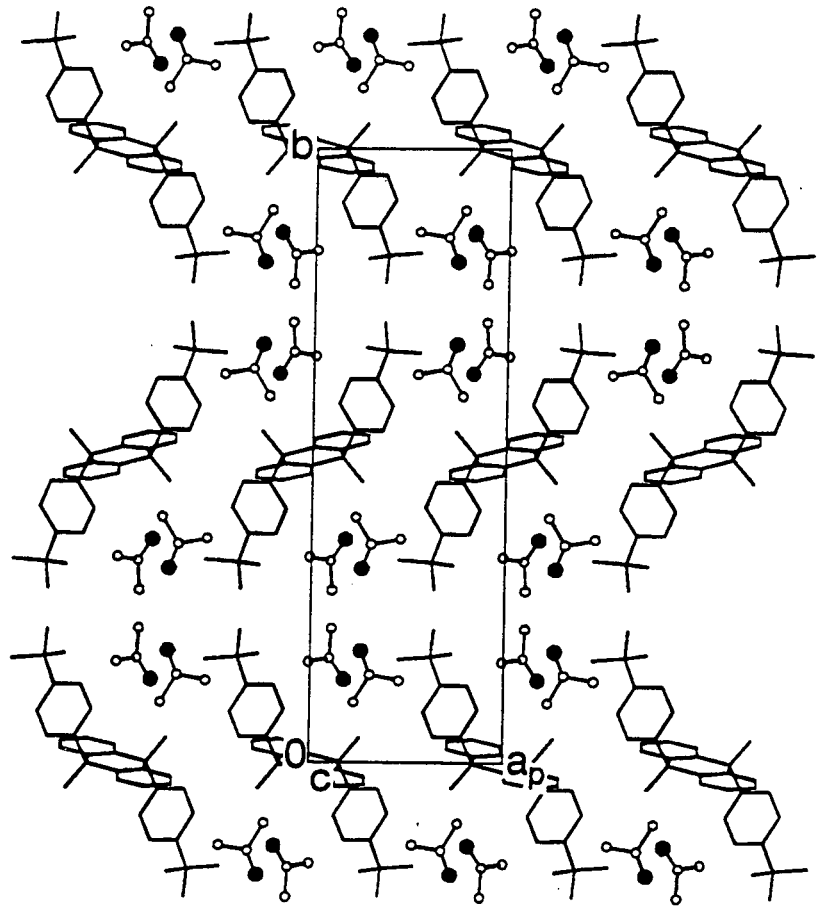

Figure 6.4 Packing diagram of **DBac** viewed along [001] - hydrogen atoms are omitted and the guest molecules are shown in ball-and-stick representation.

The three angles around the central carbon atom of the guest molecule range from 116.0(5) to 122.2(6) °, the C=O distances are 1.164(8) and 1.221(8) Å and the C_{sp^3}–C_{sp^2} bond lengths are in the range 1.434(9) to 1.488(8) Å. Despite poor refinement of the structure, these features of the guest geometry are in good agreement with values reported in the literature.

DBde $C_{34}H_{36}O_2 \cdot (C_4H_{10}O)_2$
Guest : Diethyl ether
Space group : $P2_1/a$
a = 8.771(2)Å
b = 25.132(5)Å β = 104.75(3)°
c = 9.042(3)Å
V = 1928(1)Å^3
Z = 2

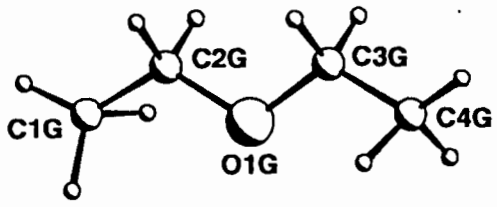

A host:guest ratio of 1:2 was established by TG (see Table 2.2). Preliminary oscillation and Weissenberg photography established **DBde** as belonging to the monoclinic system (2/*m* Laue symmetry). Crystal reflection data exhibited the following non-extinction conditions:

hkl	:	none
h0l	:	h = 2n
0k0	:	k = 2n

indicating that the space group was $P2_1/a$ (it was decided to adopt the convention of assigning the shortest axis as "a" for the inclusion compounds with this host in order to make comparisons between structures - hence the non-standard space group assignment). Determination of the unit cell volume and the crystal density suggested two molecules per unit cell. The space group then requires the host molecules to be situated at special positions with the asymmetric unit consisting of one half of a host molecule and one complete guest molecule.

During intensity data collection, periodic monitoring of three standard reflections indicated a steady overall decrease in intensity of 50.6%. The data were corrected for linear decay and it was decided to proceed with the structure solution and refinement. Direct methods yielded all non-hydrogen atoms in the asymmetric unit. Despite the relatively high degree of crystal decay during intensity data collection, refinement proceeded surprisingly uneventfully. All the non-hydrogen atoms were refined anisotropically. The aromatic hydrogen atoms were placed with appropriate geometric constraints and refined with linked isotropic temperature factors. The guest hydrogen atoms were similarly refined, while the hydroxyl hydrogen atom was located in a difference electron density map and refined with a bond length constraint and its own temperature factor. The final R value was 0.071.

Molecular structure

The molecular structure of **DBde** is shown in Figure 6.5 and hydrogen bond details are given in Table 6.1.

The host molecules are situated at $0,\frac{1}{2},\frac{1}{2}$ and $\frac{1}{2},0,\frac{1}{2}$ (Wyckoff position *b*). The guest molecules lie in linear channels running parallel to [100] at $x,\frac{1}{4},\frac{1}{2}$ and $x,\frac{3}{4},\frac{1}{2}$ as illustrated in Figure 6.6. In addition, the diethyl ether molecules are weakly hydrogen bonded to the hydroxyl moieties of the host molecules with an O···O distance of 2.948(6)Å. Figure 6.7 shows the relative packing of the host and guest molecules viewed parallel to the channels.

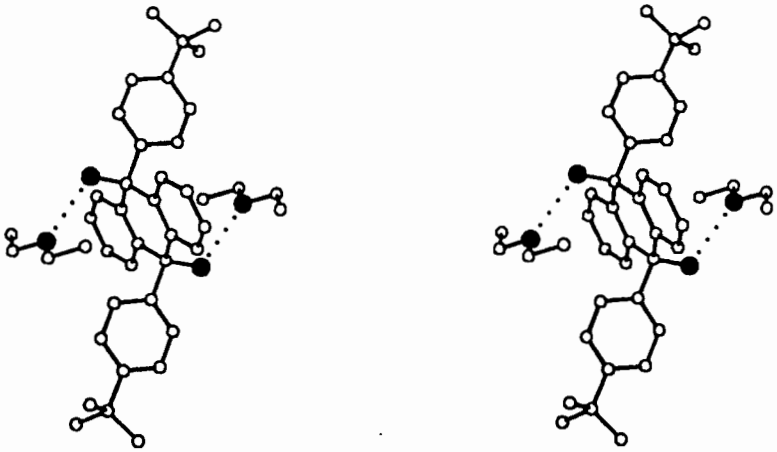

Figure 6.5 Stereoview of the molecular structure of **DBde** - hydrogen atoms are omitted and hydrogen bonds are indicated as dotted lines.

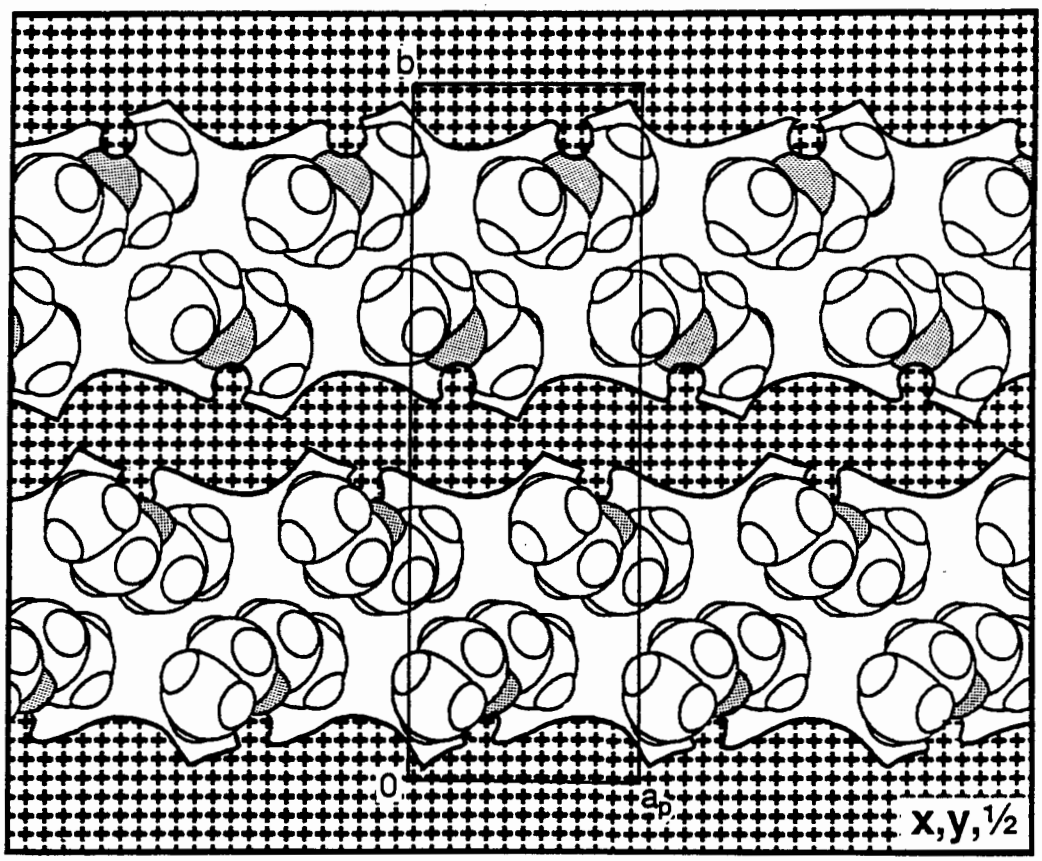

Figure 6.6 Projected cross-section of the host molecules (hatched area) of **DBde** on (002) showing the guest molecules (with oxygen atoms shaded) in channels.

The diethyl ether molecule is planar - its two torsion angles are 179.7(7)° for C(2G)-O(1G)-C(3G)-C(4G) and 179.9(7)° for C(3G)-O(1G)-C(2G)-C(1G). The mean C–C bond length is shorter than expected; 1.44(1)Å in contrast to the mean bond length value reported for C_{sp^3}–C_{sp^3} (1.52(2)Å overall). The C–O bond length of 1.41(1)Å is in good agreement with the literature value of 1.43(2)Å for C_{sp^3}–O in dialkyl ethers.[1] The three bond angles ranged from 109.4(6)° to 112.2(6)°.

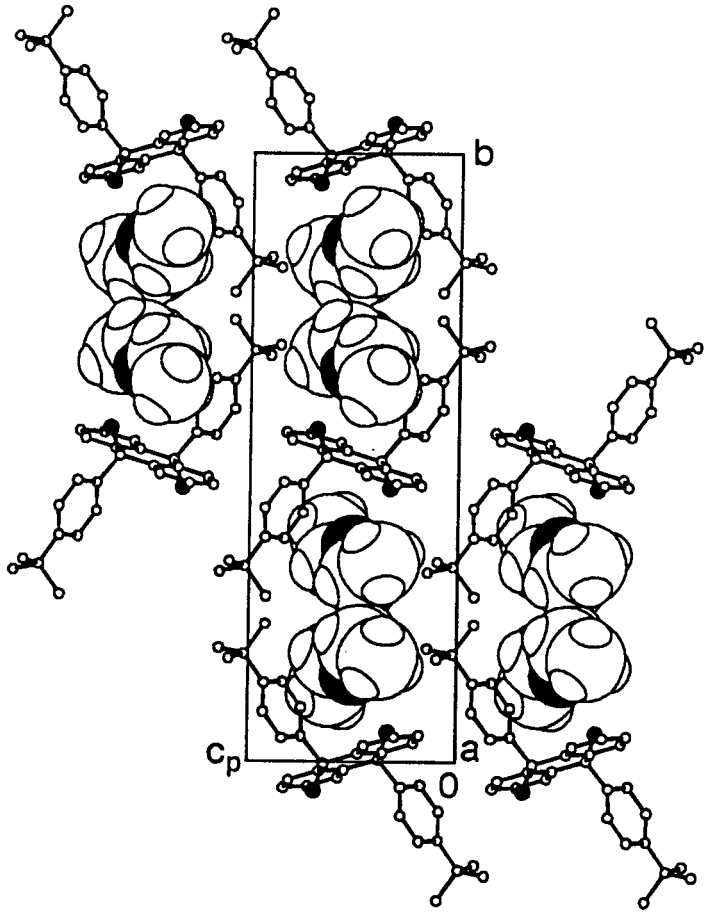

Figure 6.7 Projected view of **DBde** along [100] - the guest molecules are shown with van der Waals radii while the host molecules, with hydrogen atoms omitted are given in ball-and-stick representation (all oxygen atoms are shaded black).

DBbz $C_{34}H_{36}O_2 \cdot (C_6H_6)_3$
Guest : Benzene
Space group : $P2_1/c$
a = 8.970(4)Å
b = 17.128(2)Å β = 90.26(2)°
c = 13.275(2)Å
V = 2040(1)Å^3
Z = 2

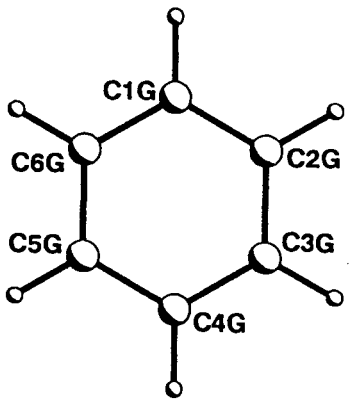

A host:guest ratio of 1:3 was established by TG (see Table 2.2). Preliminary oscillation and Weissenberg photography established **DBbz** as belonging to the monoclinic system (2/*m* Laue symmetry). Crystal reflection data exhibited the following non-extinction conditions:

hkl : none
h0l : *l* = 2n
0k0 : *k* = 2n

indicating that the space group was $P2_1/c$. Determination of the unit cell volume and the crystal density suggested two molecules per unit cell. The space group then requires the host molecules to be situated at special positions with the asymmetric unit consisting of one half of a host molecule and one and a half guest molecules. Thus one guest molecule is also expected to occupy a special position in the unit cell.

During intensity data collection, periodic monitoring of three standard reflections indicated a steady overall decrease in intensity of 14.3% and a linear decay correction was applied to the data set. Direct methods yielded all non-hydrogen atoms in the asymmetric unit. The hydroxyl hydrogen atom was located in a difference electron density map and refined with bond length constraints and individual temperature factors. Refinement proceeded uneventfully and the final R value was 0.097. The relatively poor R value may have been due to the incorrect assumption of linear crystal decay during intensity data collection.

Molecular structure

The molecular structure of **DBbz** is shown in Figure 6.8. No hydrogen bonds were observed.

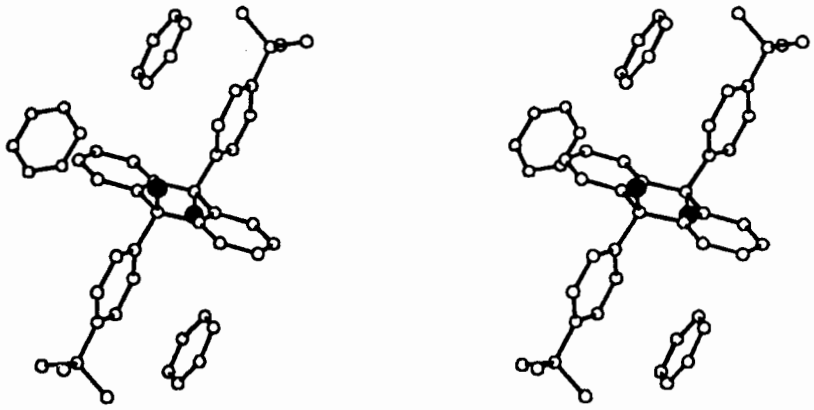

Figure 6.8 Stereoview of the molecular structure of **DBbz** - hydrogen atoms are omitted and hydrogen bonds are indicated as dotted lines.

The host molecules are situated at 0,0,0 and $0,\frac{1}{2},\frac{1}{2}$ (Wyckoff position *a*). Guest molecule G1 lies on a general position in the unit cell while G2 is situated at $\frac{1}{2},\frac{1}{2},0$ and $\frac{1}{2},0,\frac{1}{2}$ (Wyckoff position *d*) - the asymmetric unit comprises all twelve atoms of G1 and only six atoms of G2. The guest molecules G1 are situated in criss-cross channels running along [011] and [01-1] in the (100) plane (see Figure 6.9). These channels are linked from one (100) plane to the next by channels running parallel to [100] at $x,\frac{1}{2},0$ and $x,0,\frac{1}{2}$. The latter channels contain the guest molecules G2. A packing diagram of **DBbz** along [100] is shown in Figure 6.11.

The C≈C bond lengths of the guest molecules range from 1.33(1) to 1.40(1) Å while the C≈C≈C bond angles range from 118(1) to 122(1) °.

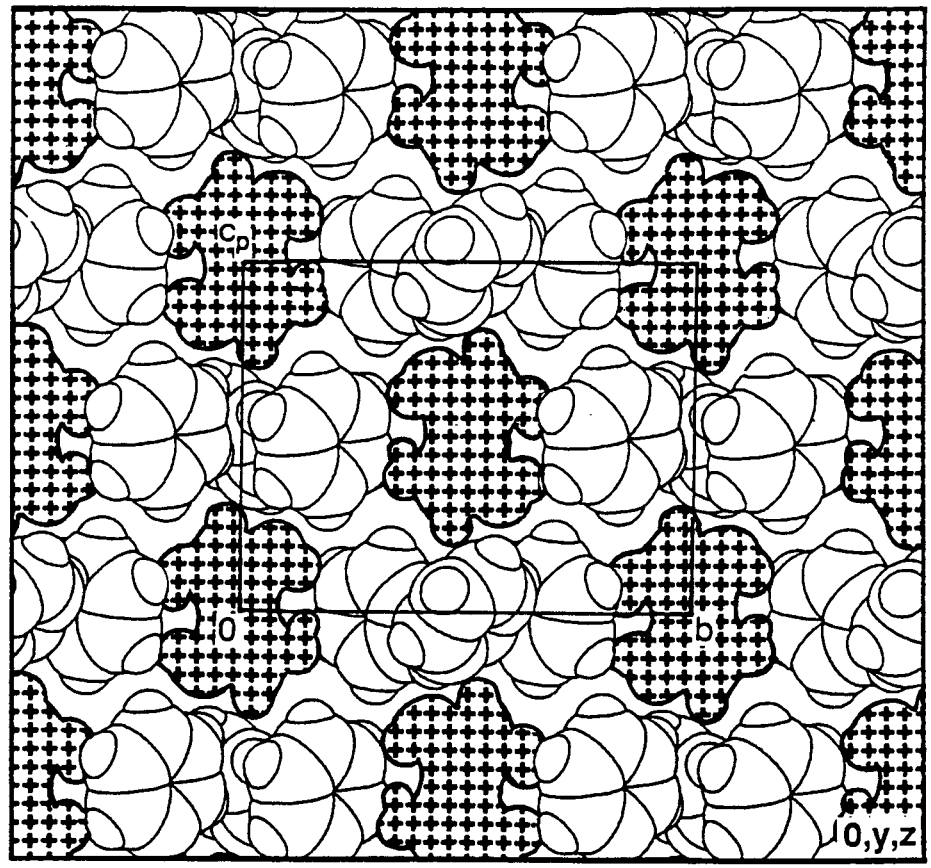

Figure 6.9 Projected cross-section of the host molecules (hatched area) of **DBbz** on (100) showing the guest molecules in channels.

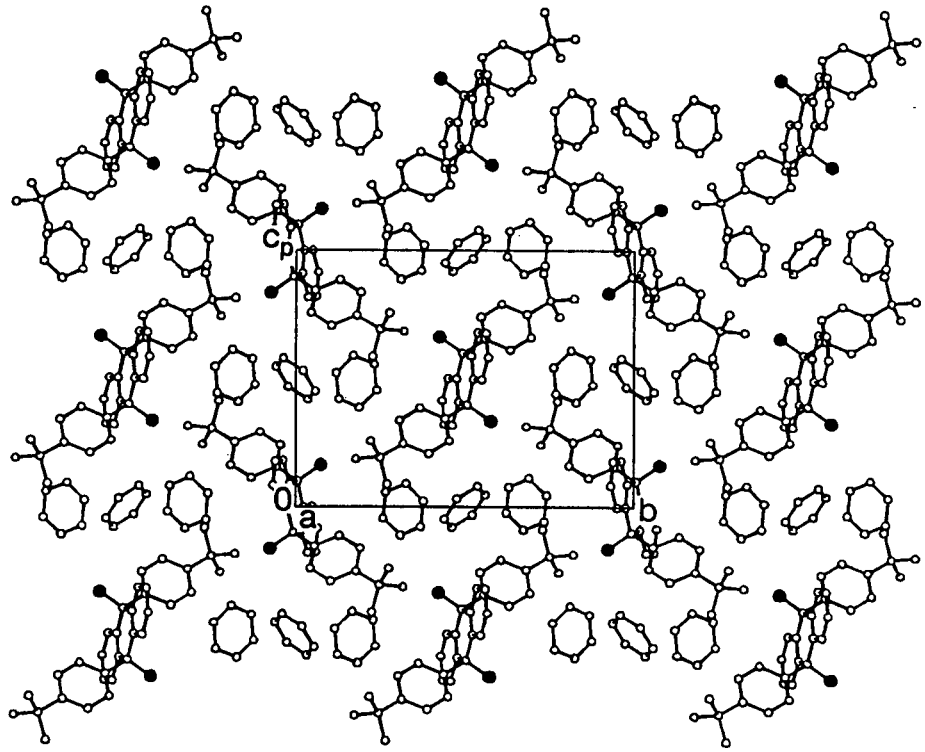

Figure 6.10 Stereoview of the guest molecules of **DBbz** viewed along [100]on (100).

Host 7

The atom labelling scheme for Host 7 is shown in Figure 6.11.

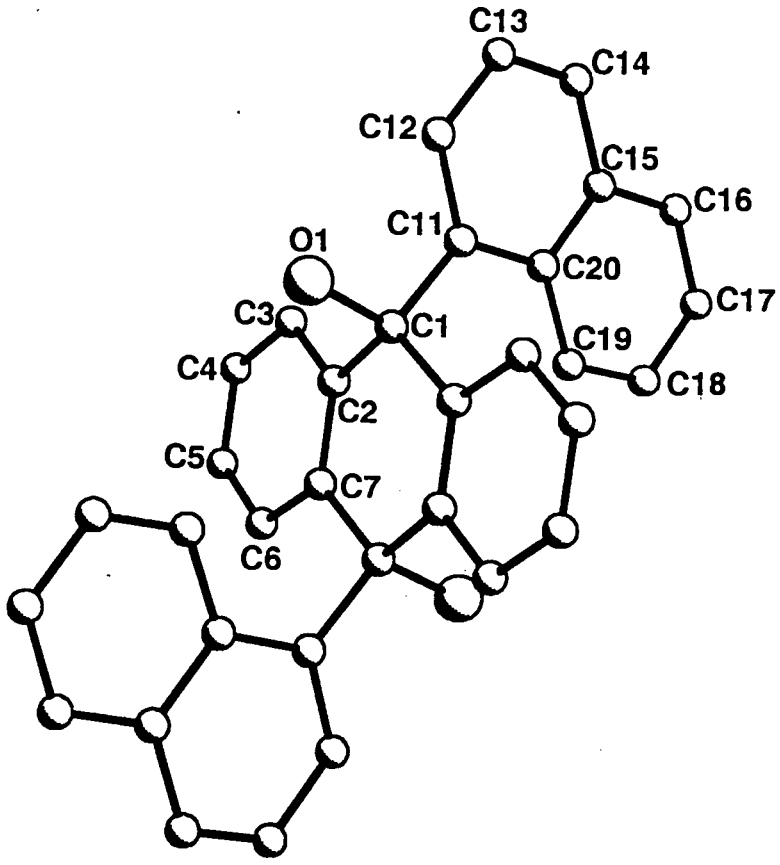

Figure 6.11 Atom numbering scheme for *trans*-9,10-dihydroxy-9,10-di-α-naphthyl-9,10-dihydroanthracene.

DNbz $C_{34}H_{24}O_2 \cdot C_6H_6$
Guest : Benzene
Space group : $P\bar{1}$
a = 7.254(2)Å
b = 9.003(3)Å
c = 11.882(3)Å
V = 708.0(3)Å^3
Z = 1

α = 108.13(2)°
β = 97.40(2)°
γ = 101.29(3)°

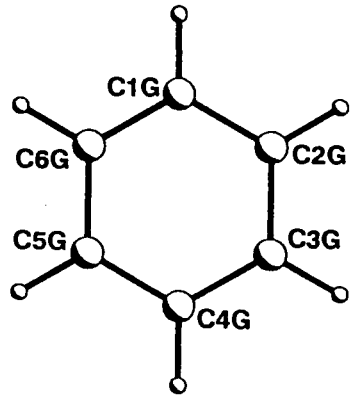

A host:guest ratio of 1:1 was established by TG (see Table 2.2). The triclinic system was indicated by $\bar{1}$ Laue symmetry of the X-ray diffraction record and the intensity statistics (mean $|E^2-1|$ for the general *hkl* reflections = 1.055) indicated $P\bar{1}$ as the correct space group rather than P1. Determination of the unit cell volume and the crystal density suggested one half of a host molecule and one half of a guest molecule in the asymmetric unit, with Z = 1. The space group symmetry then requires both the host and guest to be situated at centres of inversion in the unit cell.

Direct methods yielded all non-hydrogen host atoms in the asymmetric unit. The three crystallographically unique guest carbon atoms were located in a difference electron density map and refined isotropically. The guest hydrogen atoms were placed with geometric constraints and refined with a common isotropic temperature factor. The hydroxyl hydrogen atom was located in a difference electron density map and was refined with a bond length constraint and its own temperature factor. Refinement proceeded uneventfully and the final R was 0.068.

Molecular structure

The molecular structure of **DNbz** is shown in Figure 6.12.

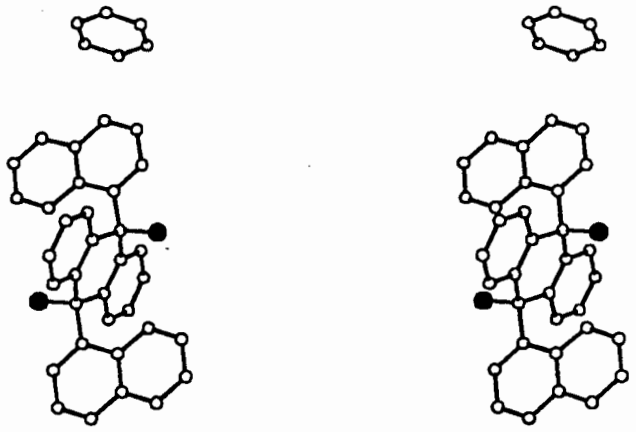

Figure 6.12 Stereoview of the molecular structure of **DNbz** - the hydrogen atoms are omitted for clarity.

With respect to the chosen unit cell, the host molecule is situated at $\frac{1}{2},0,0$ (Wyckoff position *d*) and the guest molecule at $0,\frac{1}{2},\frac{1}{2}$ (Wyckoff position). The guest molecules lie in bulging channels parallel to the relatively short "a" axis with the bulges centred at $0,\frac{1}{2},\frac{1}{2}$ as shown in Figure 6.13. Owing to the constriction of the channel at $\frac{1}{2},\frac{1}{2},\frac{1}{2}$ it could be more accurately said that the guest molecules are situated in cavities at Wyckoff position *g*. The packing between host and guest molecules can be seen in Figure 6.14.

The C=C bond lengths of the guest molecules range from 1.332(6) to 1.364(7) Å while the C=C=C bond angles range from 119.3(5) to 121.0(5) °.

Table 6.1 Hydrogen bond details for structures with Host 6

Compd.	Donor	Acceptor	O–H(Å)	O···O(Å)	H···O(Å)	O–H···O(°)
Dbde	O(1)	O(1G)	0.96(4)	2.948(6)	2.01(4)	164(4)
Dbac	O(1)	O(1G1)	-	2.860(8)	-	-

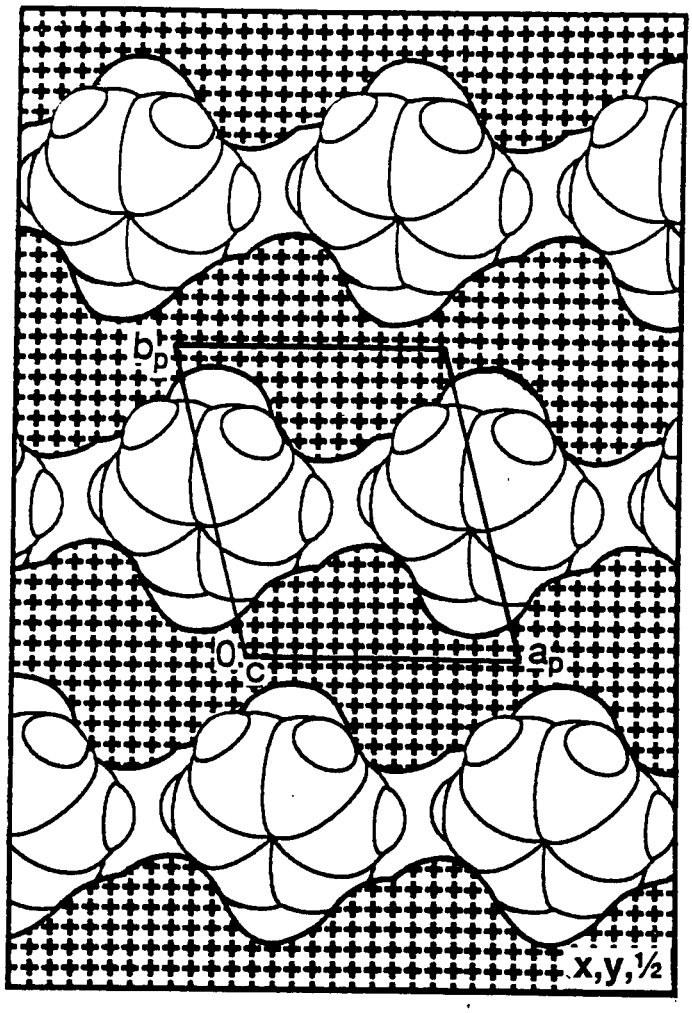

Figure 6.13 Projected cross-sections of the host molecules (hatched area) of **DNbz** viewed along [001] on (002) - guest molecules are shown in van der Waals representation.

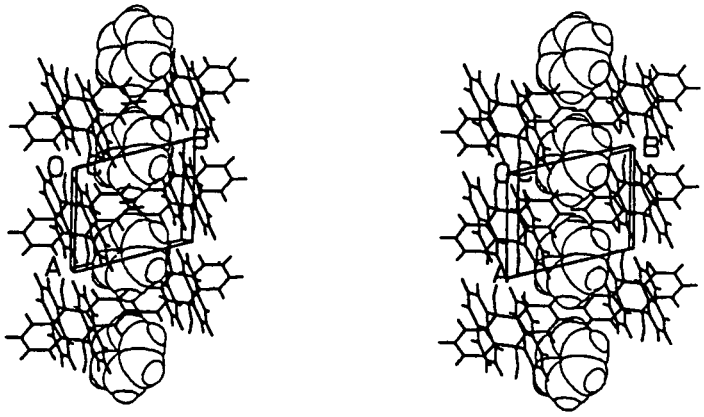

Figure 6.14 Stereoview of **DNbz** viewed along [001] - the host molecules are shown in stick representation and the guest molecules with van der Waals radii.

Chapter 7 Conformation of Host Compounds

The host conformations in the inclusion compounds whose structures have been elucidated in this study (see Chapters 3 to 6) are discussed collectively in this chapter. For ease of reference, each host numbering scheme is repeated at the beginning of the relevant sub-section. Where possible, reference will be made to previous structures with these host compounds.

Host 1

A Cambridge Structural Database[1] search (1993 version) revealed no previous structures with bis-(9,9′-dihydroxy-9,9′-difluorene) or its substituted analogues.

The two oxygen atoms of the host molecule adopt the *gauche* conformation with respect to the C(13)–C(14) bond, presumably because of steric restrictions imposed by the bulky fluorenyl moieties on rotation about the single bond. The conformation of the host molecule can be described by the torsion angle O(1)-C(13)-C(14)-O(2) about the central bond linking the fluorenyl moieties. This angle is remarkably constant in all six crystallographically uniue host molecules, varying from 58.7(2) to 60.2(7) °. The maximum deviation of any aromatic carbon atom from its phenyl ring least-squares plane is 0.033(9)Å. Each of the five-membered rings was similarly analysed to evaluate the degree of "enveloping", i.e. the distance of the sp^3 carbon atom from the least-squares plane through the four aromatic carbon atoms. The maximum distance of this type is 0.011(7)Å, indicating that the five-membered rings are essentially planar in all three structures.

The host molecule can be said to possess pseudo-symmetry in the form of a two-fold rotation axis perpendicular to, and bisecting the C(13)–C(14) bond. In this vein, bonds and angles can be classified uniquely according to Figures 7.1 (a) and (b)

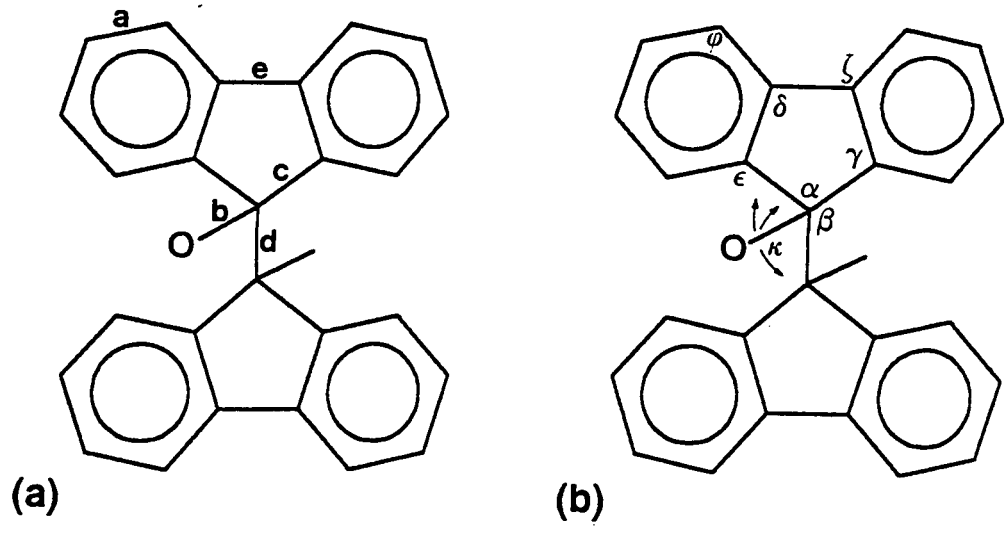

Figure 7.1 Classification of (a) bonds and (b) angles for bis-(9,9′-dihydroxy-9,9′-difluorene) - note that κ represents any of the angles O(1)-C(13)-C(1/12/14) or O(2)-C(14)-C(13/15/26).

respectively. The maximum, minimum and mean values (with the sample size, n) of these bonds and angles for the structures **W14et, W14bu** and **W14py** are tabulated in Table 7.1. The bond lengths can be compared with literature values provided in Appendix E.

Table 7.1 Cumulative host bond length and angle statistics for the structures **W14et, W14bu** and **W14py**

	Min.	Max.	Mean	n
Bond lengths (Å)				
a = C_{ar}≃C_{ar}	1.35(2)	1.43(1)	1.39(9)	144
b = C_{sp^3}–O	1.418(8)	1.454(8)	1.432(6)	12
c = C_{ar}–C_{sp^3}	1.505(7)	1.540(9)	1.524(8)	24
d = C_{sp^3}–C_{sp^3}	1.542(8)	1.581(11)	1.567(8)	6
e = C_{ar}–C_{ar}	1.447(4)	1.506(11)	1.468(8)	12
Bond angles (°)				
α = C_{ar}-C_{sp^3}-C_{ar}	101.1(5)	103.3(7)	102.0(2)	12
β = C_{ar}-C_{sp^3}-C_{sp^3}	110.0(1)	114.0(5)	112.2(2)	24
γ = C_{sp^3}-C_{ar}≃C_{ar}	108.9(8)	110.8(7)	109.9(2)	24
δ = C_{ar}≃C_{ar}-C_{ar}	107.1(6)	110.4(6)	108.9(6)	24
ϵ = C_{ar}≃C_{ar}-C_{sp^3}	127.9(7)	130.8(8)	129.5(2)	24
ζ = C_{ar}-C_{ar}≃C_{ar}	128.9(8)	132.8(10)	130.5(2)	24
κ = O-C_{sp^3}-C_{ar/sp^3}	103.8(2)	114.6(2)	110.2(6)	36
ϕ = C_{ar}≃C_{ar}≃C_{ar}	116.5(9)	123.0(10)	120.0(9)	144

The computer program PARST[2] can be used to compare the coordinates of two fragments in order to check the presence of pseudo-symmetry. The program applies a rotation matrix and a translation vector to one of the fragments in order to bring the two into coincidence. For each corresponding pair of atoms, i, the difference, Δ_i, and the associated error, σ_i, is calculated for each of the orthogonal coordinates (in Å). For each coordinate, the sum $\Sigma(\Delta_i/\sigma_i)^2$ over all atom pairs is computed, as well as the theoretical χ^2 value.

This test was applied to the two 9-hydroxyfluorene moieties of each of the six crystallographically unique host molecules. The program accepts a maximum total of eighteen atoms for each set of fragments. Thus the hydrogen atoms, as well as the atoms C(2), C(3), C(5), C(8), C(10), C(11) and their corresponding analogues were omitted from the test. For all four unique host molecules of **W14et** and **W14py**, the two 9-hydroxyfluorenyl fragments were found to have the same conformation at the 95% confidence level, indicating the presence of a two-fold rotation axis perpendicular to and bisecting the bond C(13)–C(14). This is not the case for both host molecules in the asymmetric unit of **W14bu** where the moiety conformations are significantly different.

Host 2

A Cambridge Structural Database search (1993 version) revealed no previous structures involving 1,1′-binaphthyl-2,2′-bis(diphenylhydroxymethyl).

The molecule is chiral by virtue of restricted rotation about the C(23)–C(24) bond. This is due to the presence of the bulky groups attached to the naphthyl moieties at their β-positions. As indicated in Chapter 3, the crystal structure **W12** is that of the R-enantiomer of 1,1′-binaphthyl-2,2′-bis(diphenylhydroxymethyl) while **W12Py** represents the pyridine solvate of the host racemic mixture. Although a comparison of host packing between the two crystal structures can be considered irrelevant, it is interesting to compare the geometry of the host molecule.

The conformation of the host compound remains remarkably constant in the two structures **W12** and **W12py**. The central bond C(23)–C(24), joining the two naphthyl moieties, and the bonds C(9)–C(10) and C(25)–C(26) have similar lengths in the two compounds and are recorded, together with other important molecular parameters, in Table 7.2. Figures 7.2 (a) and (b) show the two molecular structures viewed along

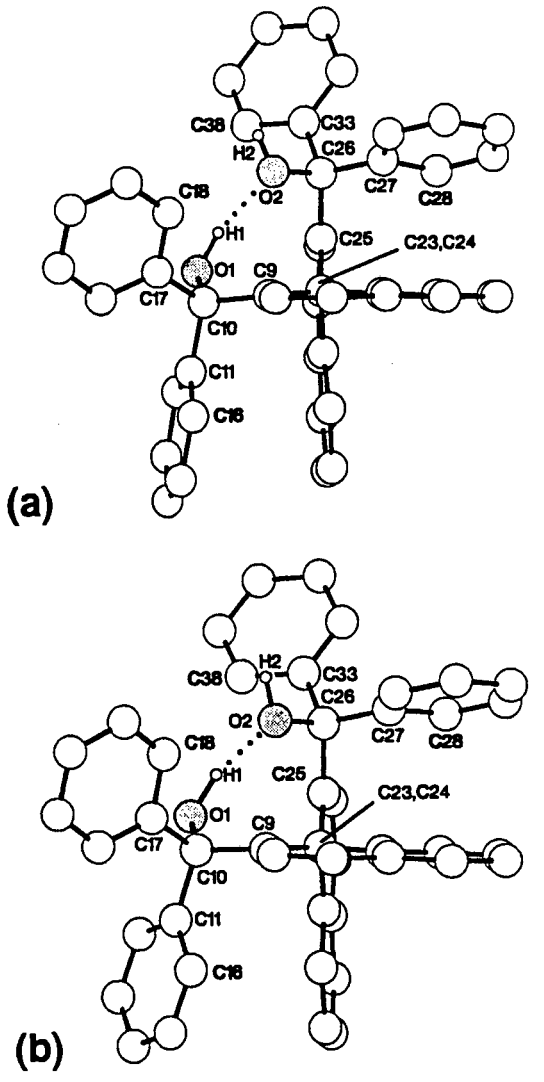

Figure 7.2 Perspective view of Host 2 along the central bond in (a) **W12** and (b) **W12Py**.

C(23)–C(24). We may take the intramolecular hydrogen bond as the most important feature which governs the conformation of the host molecule in both structures. The O(1)···O(2) distances of 2.76(1) and 2.68(1) Å in **W12** and **W12Py** show these to be moderately strong hydrogen bonds.

Table 7.2 Selected molecular parameters of **W12** and **W12Py**

Distance (Å), Angle* (°)	**W12**	**W12Py**
C_{ar}≈C_{ar}	1.352(5) - 1.447(4)	1.34(1) - 1.46(1)
C(23)–C(24)	1.503(11)	1.498(5)
C(9)–C(10)	1.554(10)	1.546(3)
C(25)–C(26)	1.534(10)	1.547(4)
C(10)–O(1)	1.428(10)	1.425(3)
C(26)–O(2)	1.455(9)	1.437(3)
∠ C_{ar}≈C_{ar}≈C_{ar}	117.0 - 123.0	117.1 - 123.7
∠ at C(10)	105.5 - 112.6	106.3 - 112.0
∠ at C(26)	106.0 - 114.0	105.8 - 112.6
τ_1 = C(9)-C(23)-C(24)-C(25)	95	97
τ_2 = O(1)-C(10)-C(9)-C(23)	-31	-31
τ_3 = C(16)-C(11)-C(10)-C(9)	59	41
τ_4 = C(18)-C(17)-C(10)-C(9)	48	57
τ_5 = O(2)-C(26)-C(25)-C(24)	-48	-44
τ_6 = C(28)-C(27)-C(26)-C(25)	51	57
τ_7 = C(9)-C(33)-C(26)-C(25)	59	63
τ_8 = H(2)-O(2)-C(26)-C(25)	-148(5)	-169(2)
O(1)···O(2)	2.759(7)	2.679(4)
O(1)–H(1)	0.97(3)	1.03(3)
H(1)···O(2)	1.81(3)	1.65(3)
∠ O(1)–H(1)···O(2)	167(6)	175(3)
O(2)–H(2)	0.84(7)	0.97(2)

* standard deviations for bond and torsion angles are in the range 0.4 to 1.2 °

It is possible for the host molecule to adopt a symmetrical conformation such that there is a two-fold rotation axis perpendicular to (and bisecting) the bond C(23)–C(24). However, this conformation seems unlikely owing to the rotational freedom (although limited) of the bonds C(9)–C(10), C(10)–C(11), C(10)–C(17) and their (potentially) pseudo-symmetrical analogues. Use of the program PARST as described above for Host 1 shows that Host 2 does not possess two-fold or pseudo-twofold symmetry.

Host 3

The molecule 2,2′-bis(9-hydroxy-9-fluorenyl)biphenyl is chiral by virtue of restricted rotation about the bond C(19)–C(20) due to the presence of the bulky fluorenyl moieties. However, crystals of **W15ch** were grown using the racemic mixture of the host compound. To date, no structure of an optically resolved form of this compound has been published.

At least five other structures with (±)2,2′-bis(9-hydroxy-9-fluorenyl)biphenyl have been elucidated. These structures include inclusion compounds with acetonitrile, di-*n*-propylamine, dimethylformamide[3], diethyl ether[4] and (-)-fenchone[5]. A Cambridge Structural Database search (1993 version) revealed no additional structures with this host compound.

Geometrical parameters of the two fluorenyl moieties are given in Table 7.3 – refer to Figure 7.1 for bond length and angle classification. The fluorenyl aromatic rings are essentially planar and the maximum deviation of any atom from their least-squares planes is 0.02(1)Å. The two phenyl rings are planar to within 0.03(1)Å and the dihedral angle between these rings is 99.3(3)°. The internal angles of the two biphenyl rings range from 117.8(7) to 123.0(8) ° while the C_{ar}–C_{ar} lengths are between 1.35(1) and 1.42(1) Å. The length of the C(19)–C(20) bond is 1.502(8)Å.

Each of the two fluorenyl five-membered rings was analysed to evaluate the degree of "enveloping" as described above. The C_{sp^3} distances from the least-squares planes through the aromatic carbons of the five-membered rings are 0.011(7) and 0.068(7) Å.

Table 7.3 Host bond length and angle statistics for the fluorenyl moieties of **W15ch**

Bond lengths (Å)	
a = C_{ar}≃C_{ar}	1.35(1) - 1.41(1)
b = C_{sp^3}–O	1.426(8) and 1.454(8)
c = C_{ar}–C_{sp^3}	1.50(1) - 1.56(1)
d = C_{sp^3}–C_{ar}	1.51(1) and 1.53(1)
e = C_{ar}–C_{ar}	1.47(10) and 1.48(1)
Bond angles (°)	
α = C_{ar}-C_{sp^3}-C_{ar}	101.2(6) and 101.7(5)
β = C_{ar}-C_{sp^3}-C_{ar}	106.6(9) - 114(1)
γ = C_{sp^3}-C_{ar}≃C_{ar}	109.9(6) - 111.4(7)
δ = C_{ar}≃C_{ar}-C_{ar}	108.3(7) - 109.6(7)
ϵ = C_{ar}≃C_{ar}-C_{sp^3}	125(1) - 132(1)
ζ = C_{ar}-C_{ar}≃C_{ar}	124(1) - 137(1)
κ = O-C_{sp^3}-C_{ar}	108.3(6) - 115.0(6)
ϕ = C_{ar}≃C_{ar}≃C_{ar}	116.6(8) 132.9(7)

If we consider the fluorenyl moieties to be rigid fragments, the overall host conformation can best be described by the torsion angles τ_1 = O(1)-C(13)-C(14)-C(19), τ_2 = O(2)-C(26)-C(25)-C(20) and τ_3 = C(14)-C(19)-C(20)-C(25) which define the orientation of the fluorenyl and biphenyl moieties. These angles for **W15ch** and other published structures are tabulated in Table 7.4. In all the structures the overall host conformation is a spiral; the two hydroxyl groups form an intramolecular hydrogen bond in the centre of the spiral and are surrounded by bulky aromatic groups.

Table 7.4 Interstructural comparison of the overall host conformation

Guest	τ_1	τ_2	τ_3
cyclohexanone[3]	26(2)	20(2)	-91(2)
acetonitrile[3]	21.8(5)	23.5(5)	-90.9(5)
di-*n*-propylamine[3]	19(2)	13(2)	-93(2)
dimethylformamide[3]	18(1)	19(1)	-93(1)
diethyl ether[4]	19.2(4)	30.0(4)	-93.2(4)

Hosts 4 to 7

Host compounds 4 to 7 are classed together since they all share the common feature of the tricyclic "template" with its *trans*-9,10-dihydroxy functional groups. These compounds differ only in the size and shape of the aromatic substituents which are intended to influence packing whilst not participating in coordination with guest molecules.

With the exception of **DMac**, all the structures with Hosts 4 to 7 have the host molecules situated on centres of inversion in the unit cell. This can only occur if the central ring of the tricyclic system assumes a planar or a pseudo-chair conformation, allowing the molecule $\bar{1}$ symmetry.

The conformational analysis of the 1,4-cyclohexadiene ring system has been the subject of a substantial number of theoretical and experimental investigations. In 1954 Ferrier and Iball[6] reported the first structure determination of 9,10-dihydroanthracene. They found the central ring to be non-planar with a folding angle (i.e. the dihedral angle between the least-squares planes through the two aromatic rings) of 145°. The following year, Beckett and Mulley[7] gave some theoretical reasons, based on chemical evidence, why 9,10-disubstituted anthracenes should be bent and they postulated structures for the *cis* and *trans* isomers which can occur when the substituents are different. However, Iball and Young[8] later reported that 9,10-dihydro-1,2,5,6-dibenzanthracene is planar, contrary to the predictions of Beckett and Mulley. This was disputed in 1961 by Herbstein[9] who, using the data of Iball and Young, showed that although the central ring is planar, the entire molecule is zigzag-shaped. In 1973 Leroy *et al.*[10] reported structures for *cis*- and *trans*-9,10-bis(trimethylsilyl)-9,10-dihydroanthracene, showing the tricyclic system for the *trans* form to be planar while that for the *cis* form is folded. In 1978 Rabideau[11] published

an in-depth study of the conformation of substituted 9,10-dihydroanthracenes and concluded that substitution can lead to a wide variation in geometry. This finding was supported by Raber *et al.*[11] using computational methods. They showed that very little energy is required to substantially distort these structures from their minimum energy conformations and that the energy of 9,10-dihydroanthracene is virtually unchanged for folding angles in the range 135 to 180 °. More recent studies[13,14] have only confirmed the conclusion arrived at by Rabideau. Thus, according to current consensus, one should not be surprised to find deviations from planarity in 9,10-substituted-9,10-dihydroanthracenes.

In the structure **DMAc** the host molecule assumes a pseudo-boat shape for the central ring of the tricyclic system, precluding its occupation of a centre of inversion

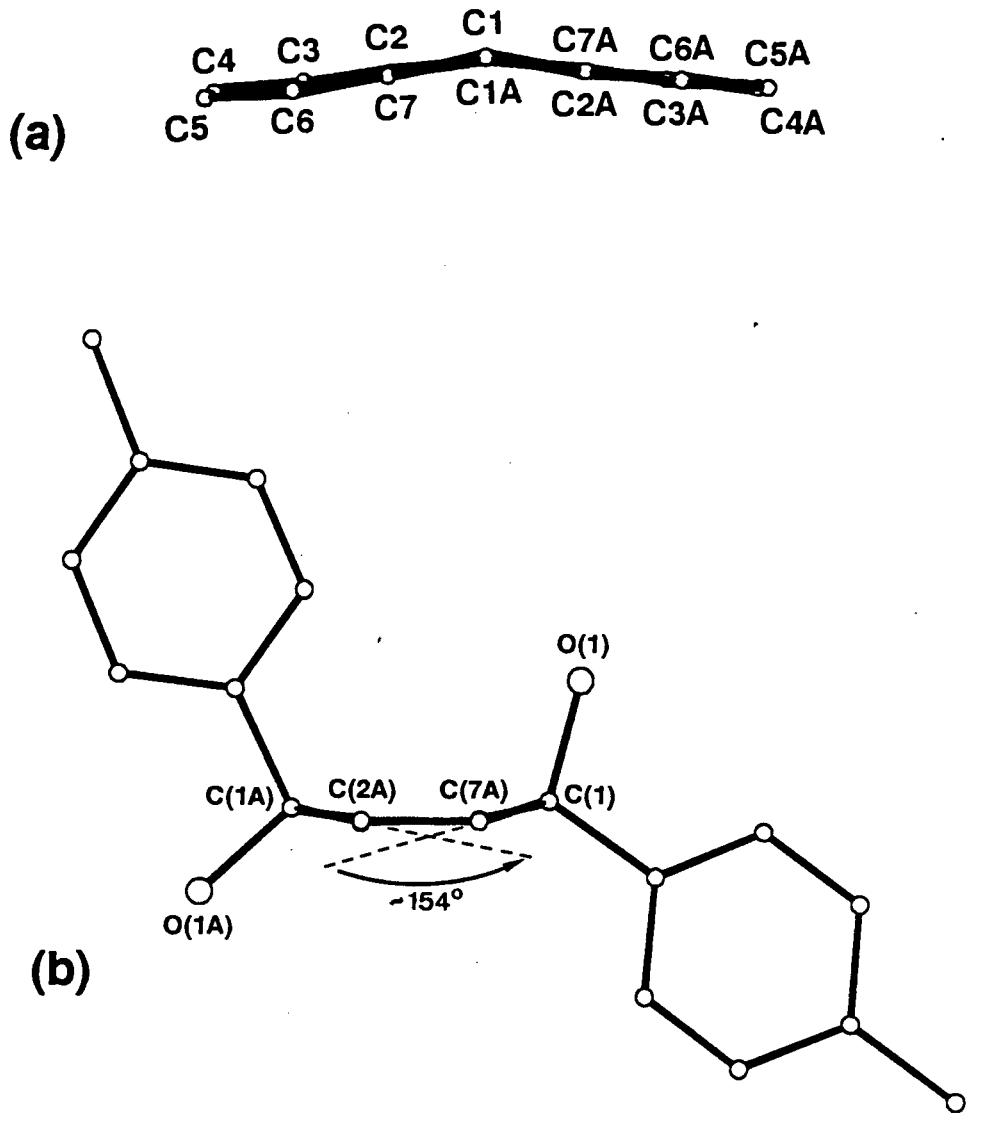

Figure 7.3 Perspective views of the host molecule of **DMac** (a) viewed along C(1A)···C(1) showing the folding of the molecule, and (b) viewed parallel to the plane through C(2), C(7), C(2A) and C(7A) showing the puckering of the central ring of the host molecule of **DMAc**. In (a) the 9,10- substituents are omitted and in (b) the peripheral rings of the tricyclic moiety are omitted.

in the unit cell. Hence the asymmetric unit contains a complete host molecule forming two unique hydrogen bonds to two crystallographically unique acetone molecules (owing to the hydroxyl moieties being pseudo-axial and pseudo-equatorial respectively). The folding angle of the host molecule is 167.9(1)° (see Figure 7.3(a)) giving it a "butterfly" shape and the puckering of the central ring can clearly be seen in Figure 7.3(b). The distances of the atoms C(1) and C(1A) from the least squares plane through the atoms C(2), C(7), C(2A) and C(7A) are 0.0220(3) and 0.166(4) Å respectively (see Table 7.5 for an interstructural comparison).

This behaviour is unusual for *trans*-9,10-dihydroxy-9,10-disubstituted-9,10-dihydroanthracene compounds whether in the pure or complexed form. Of all such structures published to date[15-21], significant deviations from planarity do occur, but in the form of "chairing" of the central ring[16] such that the molecule can still occupy a site of $\bar{1}$ symmetry within the unit cell. The structure **DMac** is the first example of an instance where complexation with a guest molecule serves to distort the molecular geometry enough to deprive it of its potential $\bar{1}$ symmetry.

For all the structures, the orientation of the aromatic substituent can be described by the dihedral angle, ϕ, between its least-squares plane and the plane through the atoms O(1), C(1) and C(11). Similarly, the orientation of the hydroxyl group can be described by the torsion angle τ_1 = H(1O)-O(1)-C(1)-C(11). For all the structures with Hosts 4 to 7, these two angles, together with bond lengths and angles, are tabulated in Table 7.6. For all the host molecules considered here, the maximum deviations from the least squares planes through an aromatic ring of the tricyclic moiety and of the aromatic substituents are 0.018(9) and 0.020(6) Å respectively.

Figure 7.4 shows a general labelling scheme for the common features of Hosts 4 to 7. For each of the structures the distance, d, of C(1) from the least-squares plane through atoms C(2), C(7), C(2*) and C(7*) was calculated (for centrosymmetric molecules, these atoms are always coplanar) as well as the angle ξ = C(2)-C(1)-C(7*). These values, together with the values of the angles ν = C(1)-C(2)-C(7) and ψ = C(1)-C(7*)-C(2*) and the corresponding sums of the three angles are given in Table 7.5.

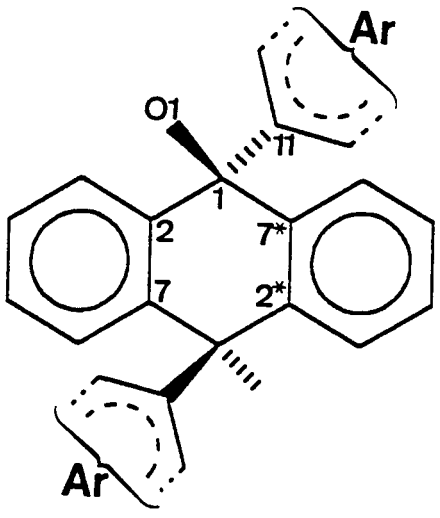

Figure 7.4 General labelling scheme for *trans*-9,10-dihydroxy-9,10-di-(Ar)yl-substituted-9,10-dihydroanthracene - C(2*) and C(7*) are related to C(2) and C(7) respectively by $\bar{1}$ symmetry.

Table 7.5 Central ring planarity of *trans*-9,10-dihydroxy-9,10-di-aryl-substituted-9,10-dihydroanthracene

	d (Å)	ξ (°)	ν(°)	ψ(°)	$\xi+\nu+\psi$(°)
DPac	0.009(3)	113.4(3)	123.4(4)	123.2(4)	360.0
DPdek	0.029(3)	113.7(3)	122.7(4)	123.6(4)	360.0
DPdmso	0.004(5)	112.9(4)	123.8(5)	123.3(5)	360.0
DP2bu	0.031(3)	113.1(2)	123.4(3)	123.5(3)	360.0
DM	0.001(7)	114.1(6)	122.8(6)	123.1(6)	360.0
DMac	0.220(3)	112.8(3)	122.2(3)	122.0(3)	357.0
	0.166(4)	112.8(3)	122.9(3)	123.0(3)	358.7
DMde	0.029(3)	112.4(3)	123.4(3)	124.2(3)	360.0
DMpy	0.052(4)	113.5(3)	123.7(3)	122.6(3)	359.8
DBac	0.059(8)	112.3(6)	125.0(7)	122.5(7)	359.8
DBde	0.029(5)	112.4(4)	123.7(4)	123.9(4)	360.0
DBbz	0.017(5)	113.0(5)	123.0(5)	124.0(5)	360.0
DNbz	0.141(2)	113.7(2)	122.5(2)	122.7(2)	358.9

The distance d is a good indication of the departure from planarity of the central ring. Based on a technique introduced by Duax and Norton[22], Schubert[21] has suggested that a value of $d \geq 0.03$Å indicates significant deviation from planarity. This is also reflected in the deviation of the sum of the three angles (see Table 7.5) from 360°. When considering the accuracy of the experimental method used, deviations from planarity as described here are unimportant since $\bar{1}$ symmetry of the molecule is still retained. The most significant consequence of deviations from planarity is seen only in the structure **DMac** where the overall symmetry of the molecule has been influenced.

Selected crystal data for all available structures involving *trans*-9,10-dihydroxy-9,10-disubstituted-9,10-dihydroanthracene are presented in Table 7.7. It can be seen that these compounds form complexes with a wide variety of guest molecules. There is also much variation in the relationship between the guest hydrogen bond accepting/donating ability and the host:guest ratio and the value for Z. For the compounds where Ar = Ph or 4-Tolyl, no inclusion compound structure has been reported where one of the guest molecules does not participate in hydrogen bonding with the host hydroxy moiety. However, it is interesting to note that where Ar = 4-*t*-BuPh or α-naphthyl, inclusion compounds are formed with benzene whereas the former two compounds, although soluble in benzene, will not include this solvent.

Table 7.6 Selected bond lengths and bond, torsion and dihedral angles for the compounds with Hosts 4 to 7

	ϕ	τ_1	*Car*=*Car*	O(1)-C(1)	C(1)-C(2)	C(1)-C(11)	C(14)-C(17)	C(17)-C (*t*-Bu)[1]
DPac	13.1(3)	167(3)	1.361(8)-1.40(1)	1.44(1)	1.51(1)	1.521(6)	-	-
DPdek	1.3(2)	177(7)	1.354(7)-1.410(7)	1.442(4)	1.519(6)	1.531(5)	-	-
DPdmso	0.4(3)	177(4)	1.36(1)-1.407(8)	1.438(6)	1.512(7)	1.538(8)	-	-
DP2bu	3.9(1)	172(4)	1.363(5)-1.405(5)	1.436(3)	1.524(5)	1.530(4)	-	-
DM	4.5(4)	-	1.35(1)-1.41(1)	1.458(8)	1.52(1)	1.523(9)	1.54(1)	-
DMac	8.7(2)	71(2)	1.366(4)-1.400(4)	1.446(3)	1.521(4)[2]	1.541(4)	1.504(5)	-
	0.9(2)	176(2)	-	1.442(4)	-	1.531(4)	1.501(5)	-
DMde	8.9(2)	179(2)	1.367(5)-1.403(5)	1.439(4)	1.526(5)	1.529(5)	1.525(5)	-
DMpy	8.1(2)	169(2)	1.353(9)-1.403(6)	1.429(5)	1.502(5)	1.535(5)	1.511(5)	-
DBac	2.8(4)	-	1.34(1)-1.43(1)	1.434(9)	1.52(1)	1.53(1)	1.555(9)	1.50(1)
DBde	10.6(2)	178(3)	1.359(6)-1.412(7)	1.436(6)	1.532(7)	1.537(7)	1.545(7)	1.52(1)
DBbz	4.8(2)	171(4)	1.35(1)-1.435(8)	1.454(6)	1.519(8)	1.530(7)	1.537(9)	1.54(1)
DNbz	2.3(1)	103(2)	1.354(5)-1.432(5)	1.461(3)	1.521(4)	1.538(4)	-	-

Angles in ° and lengths in Å

[1] mean of C(17)-C(18), C(17)-C(19), C(17)-C(20)

[2] mean of C(1)-C(2), C(1)-C(7A), C(1A)-C(2A) and C(1A)-C(7)

Table 7.6 *continued*

	Car=Car=Car	O(1)-C(1)-C(11)	O(1)-C(1)-C(2)	C(2)-C(1)-C(11)	C(2)-C(1)-C(7*)	C-C(17)-C (*t*-Bu)[3]
DPac	117.0(6)-122(1)	105.6(7)	109.3(7)	109.7(5)	113.4(3)	-
DPdek	118.6(4)-122.2(4)	106.8(3)	108.4(3)	108.6(3)	113.7(3)	-
DPdmso	118.5(5)-121.8(6)	106.5(4)	110.0(4)	108.8(4)	112.9(4)	-
DP2bu	118.7(3)-121.5(3)	106.8(2)	109.2(2)	108.8(2)	113.1(2)	-
DM	118.1(7)-121.4(8)	106.6(6)	108.5(6)	109.4(6)	114.1(7)	-
DMac	117.0(4)-122.3(4)	110.3(2)	107.5(3)[4]	111.3(2)	108.6(2)	-
		106.8(3)	-	109.4(3)	109.3(3)	-
DMde	117.3(3)-122.0(4)	105.9(3)	109.5(3)	109.2(3)	112.4(3)	-
DMpy	117.2(3)-122.2(4)	105.7(3)	110.7(3)	108.2(3)	113.5(3)	-
DBac	117.1(7)-122.0(8)	107.7(6)	109.8(6)	109.3(6)	112.3(6)	109.5(5)
DBde	116.7(5)-122.4(5)	106.1(4)	109.8(4)	108.4(3)	112.4(4)	110.0(5)
DBbz	117.3(5)-122.0(5)	106.8(4)	108.5(4)	110.1(4)	113.0(5)	109.9(6)
DNbz	118.0(3)-122.5(2)	109.3(2)	104.1(2)	112.4(2)	113.7(2)	-

Angles given in °

[3] mean of the six angles about C(17)

[4] mean of O(1)-C(1)-C(2), O(1A)-C(1A)-C(2A), O(1)-C(1)-C(7A), O(1A)-C(1A)-C(7)

Table 7.7 Selected crystal data for structures involving *trans*-9,10-dihydroxy-9,10-disubstituted-9,10-dihydroanthracene compounds where disubstitution is by Ar or R

Ar/R	Guest	H:G	Spc. Grp	Z	Ref.
$-CH_2CH_3$	-	-	$P2_1/c$	4	23
Ph	-	-	$P\bar{1}$	1	15
Ph	methanol	1:2	C2/c	4	15
Ph	ethanol	1:1	$P\bar{1}$	2	16
Ph	1,4-budanediol	1:1	C2/c	4	17
Ph	4-methylcyclohexanone	1:2	$P2_1/c$	2	18
Ph	2-methylcyclohexanone	1:2	$P\bar{1}$	1	18
Ph	Acetophenone	1:2	$P\bar{1}$	1	19
Ph	3-methylcyclopentanone	1:2	$P\bar{1}$	1	19
Ph	2-butanone	1:1	$P\bar{1}$	1	20
Ph	4-vinylpyridine	1:2	$P2_1/c$	2	20
Ph	4-methylpyridine	1:2	$P\bar{1}$	1	20
Ph	2-methylpyridine	1:1	$P\bar{1}$	2	20
Ph	3-methylpyridine	1:2	$P2_1/c$	4	21
Ph	2,4-dimethylpyridine	1:1	$P\bar{1}$	2	21
Ph	2,6-dimethylpyridine	1:2	$P\bar{1}$	1	21
Ph	acetonitrile	1:2	$P2_1/c$	2	21
Ph	3-hydroxypropionitrile	1:2	$P2_1/n$	2	21
Ph	pyridine	1:2	$C\bar{1}$ ‡	2	21
Ph	acetone	1:2	$P\bar{1}$	1	*
Ph	diethyl ketone	1:1	$P\bar{1}$	1	*
Ph	dimethyl sulphoxide	1:2	$P2_1/n$	2	*
Ph	(±) 2-butanol	1:1	$P\bar{1}$	1	*
4-Tolyl	-	-	$P2_1/c$	2	*
4-Tolyl	acetone	1:2	$P\bar{1}$	2	*
4-Tolyl	diethyl ether	1:2	$P2_1/n$	2	*
4-Tolyl	pyridine	1:2	$P2_1/n$	2	*
4-*t*-BuPh†	acetone	1:4	$P2_1/c$	2	*
4-*t*-BuPh	diethyl ether	1:2	$P2_1/a$	2	*
4-*t*-BuPh	benzene	1:3	$P2_1/c$	2	*
α-Naphthyl	benzene	1:1	$P\bar{1}$	1	*

* this study

† 4-*tert*-butylphenyl

‡ this unusual setting of $P\bar{1}$ was chosen for computational reasons

References

1 Cambridge Structural Database & Cambridge Structural Database System, Version 4.4 (January 1991) to Version 5.06 (October 1993), Cambridge Crystallographic Data Centre, University Chemical Laboratory, Cambridge, England

2 M. Nardelli, *Comput. Chem.*, 1983,**7**,95

3 L.J. Barbour, S.A. Bourne, M.R. Caira, L.R. Nassimbeni, E. Weber, K. Skobridis and A. Wierig, *Supramol. Chem.* 1993,**1**,331

4 E. Weber, K. Skobridis, A. Wierig, M.R. Caira, L.R. Nassimbeni, and N. Winder, in preparation

5 E.Weber, K. Skobridis, A. Wierig, S. Stathi, L.R. Nassimbeni and M.L. Niven, *Angew. Chem. Int. Ed. Engl.*, 1993,**32**,606

6 W.G. Ferrier and J. Iball, *Chem. Ind.*, 1954,1296

7 A.H. Beckett and B.A. Mulley, *Chem. Ind.*, 1955,146

8 J. Iball and D.W. Young, *Acta Cryst.*, 1958,**11**,476

9 F.H. Herbstein, *Acta Cryst.*, 1961,**14**,77

10 P.F. Leroy, C. Courseille, D. Daney and H. Bouas-Laurent, *Acta Cryst.*, 1976,**B32**,2792

11 P.W. Rabideau, Acc. Chem. Res., 1978,**11**,141

12 D.J. Raber, L.E. Hardee, P.W. Rabideau and L.B. Lipkowitz, *J. Am. Chem. Soc.*, 1982,**104**,2843

13 A. Sygula and T.A. Holak, *Tetrahedron Lett.*, 1983,**24**(28),2893

14 N. Ahmad, C. Cloke, I.K. Hatton, N.J. Lewis and J. MacMillan, *J. Chem. Soc., Perkin Trans. I*, 1985,1849

15 F. Toda, K. Tanaka, S. Nagamatsu and T.C.W. Mak, *Isr. J. Chem.*, 1985,**25**,346

16 F. Toda, K. Tanaka and T.C.W. Mak, *Tetrahedron Lett.*, 1984,**25**,1359

17 F. Toda, K. Tanaka and T.C.W. Mak, *J. Incl. Phenom.*, 1985,**3**,225

18 D.R. Bond, L.R. Nassimbeni and F. Toda, *J. Crystallogr. Spectrosc. Res.*, 1989,**19**,847

19 D.R. Bond, L.R. Nassimbeni and F. Toda, *J. Incl. Phenom.*, 1989,**7**,623

20 D.R. Bond, M.R. Caira, G.A. Harvey, L.R. Nassimbeni and F. Toda, *Acta Cryst.*, 1990,**B46**,771

21 W.-D. Schubert, Master's Thesis, University of Cape Town, 1991

22 W.L. Duax and D.A. Norton (Eds.), "Atlas of Steroid Structure",Vol. 1, Plenum Press, London, 1975

23 N. Ahmad, R.J. Goddard, I.K. Hatton, J.A.K. Howard, N.J. Lewis and J. MacMillan, *J. Chem. Soc., Perkin Trans. I*, 1985,1859

Chapter 8 Kinetics of Inclusion

Inclusion compounds of the type considered here are formed by evaporation of a solution of the host compound in an organic solvent. On crystallisation of the host, the solvent becomes entrapped as a guest in the lattice, resulting in the formation of a solid phase which is different from that of the pure host compound. These inclusion compounds vary widely in their stability and when removed from their mother liquor, will decompose under certain conditions of pressure and temperature. The severity of these conditions is invariably dependent on the stability of the inclusion complex which in turn depends on factors such as van der Waals interactions and geometrical aspects of molecular packing.

Figure 8.1 shows the various possible stages of inclusion compound formation and decomposition (question marks indicate uncertainty about the reversibility of a process). At elevated temperature or reduced pressure the solid inclusion complex, the β-phase, can lose all the guest molecules and revert to its original, uncomplexed

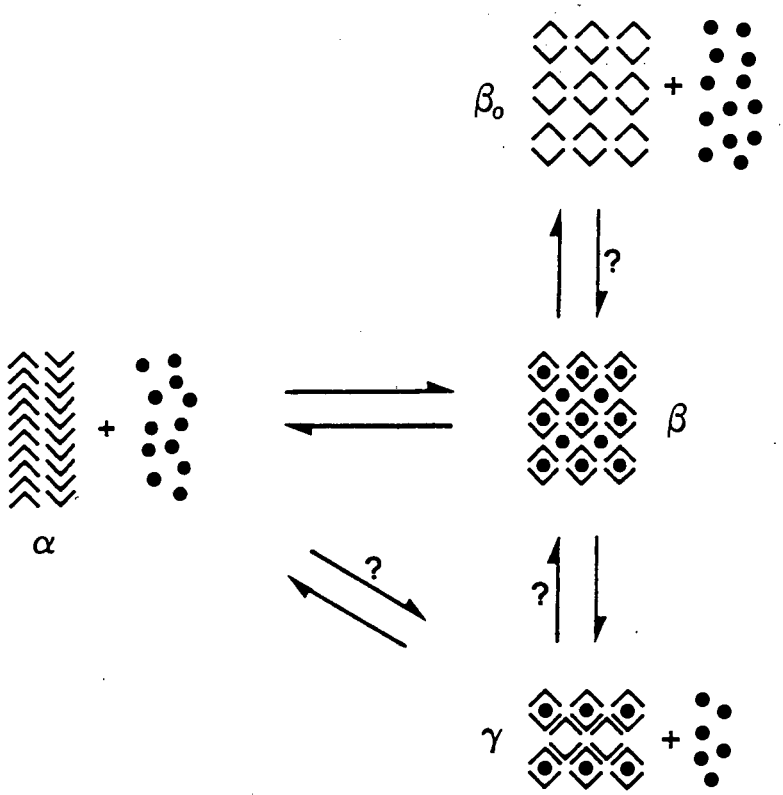

Figure 8.1 Schematic diagram showing the possible formation and decomposition pathways of inclusion compounds.

α-phase or to another polymorphic form of the host compound (the latter is not shown in the diagram since this process has not been observed for the inclusion compounds considered here). Alternatively, the β-phase could lose only *some* of the guest molecules and form a third metastable phase, the γ-phase, which can also decompose to form the α-phase. A third possibility involves loss of the guest molecules without concomitant rearrangement of the host molecules, resulting in the

formation of a so-called β_o-phase. The latter phenomenon is well known for zeolite structures which can be heated under reduced pressure to volatilise the guest molecules without modification of the alumino-silicate framework.[1] To date only one report of this type of behaviour by an organic inclusion compound has been published.[2]

For an inclusion complex where the guest is an organic solvent, the decomposition process at ambient or higher temperature is generally classified as a solid-gas reaction since organic solvents usually exert a relatively high vapour pressure at these temperatures. However, these decomposition reactions are often reversible, i.e.

$$HG_n\,(s) \rightleftharpoons H\,(s) + nG\,(g),$$

and although some effort has been expended on investigations into the kinetics of decomposition,[3-5] relatively little work has been reported on the kinetics of inclusion. Moreover, studies of the kinetics of inclusion have concentrated mainly on inorganic hosts[6] and recently a new experimental procedure has been described which allows the measurement of the velocity of intercalation reactions in systems of layered host and liquid guest.[7] However, the kinetics of inclusion between solid organic hosts and gaseous guest molecules has received little attention because the measurements are experimentally difficult and the inclusion compounds formed are often unstable at ambient conditions. Such studies would require exposure of the host compound to the gaseous guest under controlled conditions of temperature and pressure whilst measuring the extent of reaction as a function of time.

General kinetic theory

The literature involving general and specific aspects of kinetics is vast. The range of references cited here is meant merely to provide the reader with specific examples and should not be seen as an attempt to provide a comprehensive survey of work on the subject. Indeed, reaction kinetics of homogeneous systems is a particularly well established field of study.[8-13]

According to the transition state theory, the general features of how the free energy of the system changes during the course of a reaction are illustrated in Figure 8.2. At the outset of the reaction, the free energy of the system has some value which is characteristic of the reactants. As the reaction proceeds, the free energy rises to a maximum with the formation of a so-called *activated complex*. This activated complex is an intermediate stage to the formation of the products for which the free energy of the system will attain a particular value which is generally different from that of the reactants. The abscissa of the diagram represents the course of the reaction and is termed the *reaction coordinate*. The difference in free energy between the reactants and the activated complex is the activation energy, E_f, of the forward reaction. The activation energy of the reverse reaction, E_r, is similarly indicated in the figure.

For a general reaction of the form

$$A + B \longrightarrow C,$$

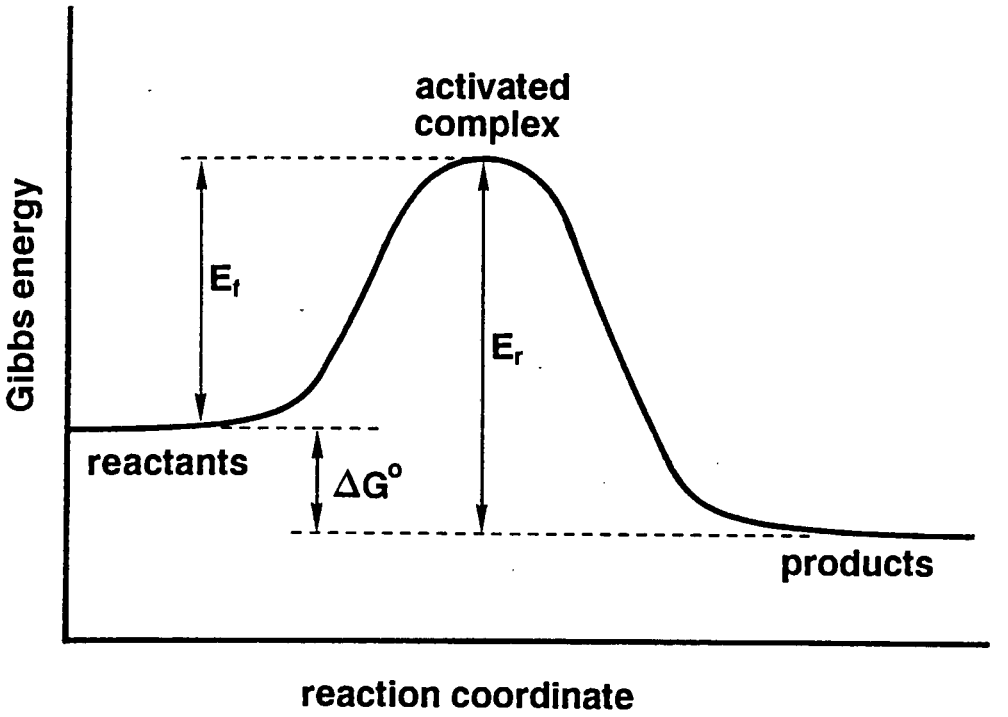

Figure 8.2 Potential energy diagram for a chemical reaction.

the change in concentration of reactants and/or products with time can be measured at constant temperature. Application of an appropriate rate equation, where

$$\text{rate} = k_T f(\text{concentration of reactants and/or products}),$$

yields a temperature-dependent rate constant, k_T which is related to the temperature by the Arrhenius equation:

$$k_T = Ae^{-E/RT}.$$

Thus a series of experiments at various temperatures can be used to determine the activation energy E, and the preexponential factor A of a particular process.

For a heterogeneous reaction of the form

$$A\,(s) \quad + \quad nB\,(g) \quad \longrightarrow \quad AB_n\,(s) \qquad (1)$$

the concept of concentration clearly no longer has the same significance and the progress of the reaction has to be followed in another way.[14] The extent of reaction, α (not to be confused with the pure α-phase of the host compound), is defined at time t as $\alpha_t = (m_t\text{-}m_0)/(m_\infty\text{-}m_0)$ where m_t is the mass of the solid sample at time t, m_0 its initial mass and m_∞ the mass after completion of the reaction. This concept applies to both formation and decomposition reactions and a kinetic study involves measurement of α as a function of time at constant temperature.

Reactions involving solids have been studied extensively and several review sources on the subject are available.[15-20] Such studies are important to solid state chemistry from the point of view of understanding the influence of structure on the chemical reactivity of solids. Gomes and Dekeyser[21] have classified solid state reactions as follows:

i solid ⟶ products, e.g. decomposition, dimerisation and polymerisation;
ii solid + gas ⟶ products, e.g. oxidation of metals;
iii solid + solid ⟶ products, e.g. the formation of solid oxides from simpler components;
iv solid + liquid ⟶ products, e.g. intercalation reactions;
v reactions at the surfaces of solids, e.g. heterogeneous catalysis.

The mechanisms of solid-state reactions are often complex and are generally considered to include two or more of the following four types of elementary steps:

a sorption phenomena (adsorption, desorption);
b reaction at the atomic or molecular scale (homogeneous or interface reactions);
c nucleation at a new phase (in the bulk or at the surface);
d transport phenomena (diffusion and migration).

Usually one of these steps is rate-determining and thus influences the overall reactivity of the system. These factors are related to the structural and energetic components associated with the chemical nature of the reacting species, e.g. lattice spacings, symmetry, surface area and lattice defects and are inherent to the reacting system considered.

Studies of solid-gas reactions of the type (1) above have concentrated almost exclusively on the tarnishing of metals by reactive gases like oxygen and halogens.[22,23] In contrast, studies of the reverse reaction have been more diverse, including the investigation of the thermal dehydration of inorganic compounds,[24-26] decomposition of intercalation compounds[3,4] and desolvation of inclusion compounds.[5] In these studies, kinetic analysis involves attempting to relate the experimentally observed α and t values with values predicted for a limited set of models based on nucleation and growth, diffusion, or simpler geometrical forms of progress of the reactant/product interface. The expressions derived from these models can all be written in their integral forms

$$f(\alpha) = kt$$

as shown in Table 8.1.

Generally, nucleation is considered to be the most important step in decomposition processes.[21] Typically, the curve of the extent of reaction as a function of time yields a sigmoid shape as shown in Figure 8.3.[18]

The type of time-dependence for the acceleratory period, CD, is usually associated with the rate of formation and growth of nuclei of the product phase. It is often presumed that the presence of the nuclei facilitates the decomposition of

Table 8.1 Theoretical models for solid-gas reactions[14]

	$f(\alpha) = kt$
1 Sigmoid α-time curves	
B1 Prout-Tompkins	$\ln[\alpha/(1-\alpha)]$
A2 Avrami-Erofeev	$[-\ln(1-\alpha)]^{1/2}$
A3 Avrami-Erofeev	$[-\ln(1-\alpha)]^{1/3}$
A4 Avrami-Erofeev	$[-\ln(1-\alpha)]^{1/4}$
2 Acceleratory α-time curves	
P1 power law	$\alpha^{1/n}$
E1 exponential law	$\ln \alpha$
3 Deceleratory α-time curves	
3.1 based on geometrical models	
R2 contracting area	$1-(1-\alpha)^{1/2}$
R3 contracting volume	$1-(1-\alpha)^{1/3}$
3.2 based on diffusion mechanisms	
D1 one-dimensional	α^2
D2 two-dimensional	$(1-\alpha)\ln(1-\alpha)+\alpha$
D3 three-dimensional	$[1-(1-\alpha)^{1/3}]^2$
D4 Ginstling-Brounshtein	$(1-2\alpha/3)-(1-\alpha)^{2/3}$
3.3 based on "order of reaction"	
F1 first order	$-\ln(1-\alpha)$
F2 second order	$1/(1-\alpha)$
F3 third order	$[1/(1-\alpha)]^2$

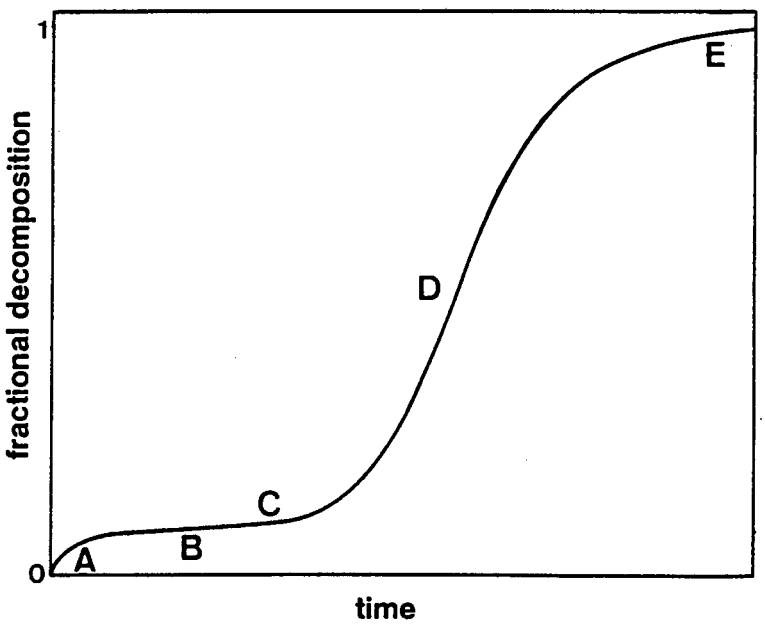

Figure 8.3 Generalised shape of an α-time curve for solid state reactions.

adjacent molecules by a kind of interface reaction. Beyond the inflection point, D, the interfacial area between reactant and product decreases as the nuclei start overlapping, thus decreasing the reaction rate. The kinetics of thermal decomposition is usually accounted for by the Prout-Tompkins model, B1, which is based on a chain branching mechanism for the nuclei, or by the Avrami-Erofeev models A2, A3 and A4 where random nucleation and three-dimensional growth of isolated nuclei is assumed. In general, the principal role of defects in decomposition seems to be to provide sites where reaction or nucleation can occur.

The rate equations R2 and R3 describe reactions which are controlled by the advancement of phase boundaries towards the centre of the particles and have been used to account for the dehydration of clathrate hydrates.[27] The diffusion-controlled equations account for processes involving one-dimensional diffusion with a constant diffusion coefficient (D1), two-dimensional diffusion in a cylinder (D2), three-dimensional diffusion in a sphere (D3) and diffusion starting at the exterior of a spherical particle (D4). For an empirical comparison of some of these models see reference 28. Equations of the form

$$d\alpha/dt = k(1-\alpha)^n$$

which are based on the concept of an order of reaction have been applied to solid state reactions mainly for analytical convenience.[28] For certain values of n, the integrated form of this equation leads to some of the equations already considered.

In order to determine which reaction mechanism is most applicable to a particular reaction, the α-time data can be used to plot $f(\alpha)$ versus time for each model in turn. The model which yields the best linear fit of the data over the greatest range of α is assumed to be correct. However, it should be kept in mind that more than one mechanism may apply through the course of the reaction owing to changes in the system caused by the formation of the product phase.[29] Values for k_T can be obtained for a series of experiments at different temperatures, and hence the activation energy and preexponential factor can be determined using the Arrhenius equation. The concept of a rate constant for solid-state reactions has been discussed briefly by Gomes[30] and the validity of applying the Arrhenius equation to heterogeneous reactions has been challenged.[31,32] However, Brown[14] suggests that the parameters E and A do have practical value even though their theoretical interpretation is questionable.

The formation of an inclusion compound as shown in reaction scheme (1) above can be considered to be analogous to its decomposition in as much as both processes involve transport of the guest vapour and interaction at the molecular scale to form nuclei of the product phase. Since the literature on the kinetics of inclusion of gaseous guests by organic solids is sparse, data for this process will be treated in accordance with the theories outlined above. Experimental aspects involved in the investigation of the kinetics of inclusion follow.

Experimental approach

The extent of reaction for a solid-gas reaction can be measured gravimetrically and kinetic studies have been conducted using a McBain balance.[11,33] With this technique, a powdered sample is placed in a pan suspended inside a glass reaction

vessel by means of a silica spring as shown in Figure 8.4. The reaction vessel can be evacuated and its temperature controlled by passing water through the outer jacket. A stoichiometric excess of the liquid guest is introduced and immediately vaporises to fill the previously evacuated reaction chamber at a pressure which is dependent on the temperature. As the sample absorbs the guest with concomitant rearrangement of the structure, the weight gain is determined by measuring the extension of the silica spring by means of a cathetometer.

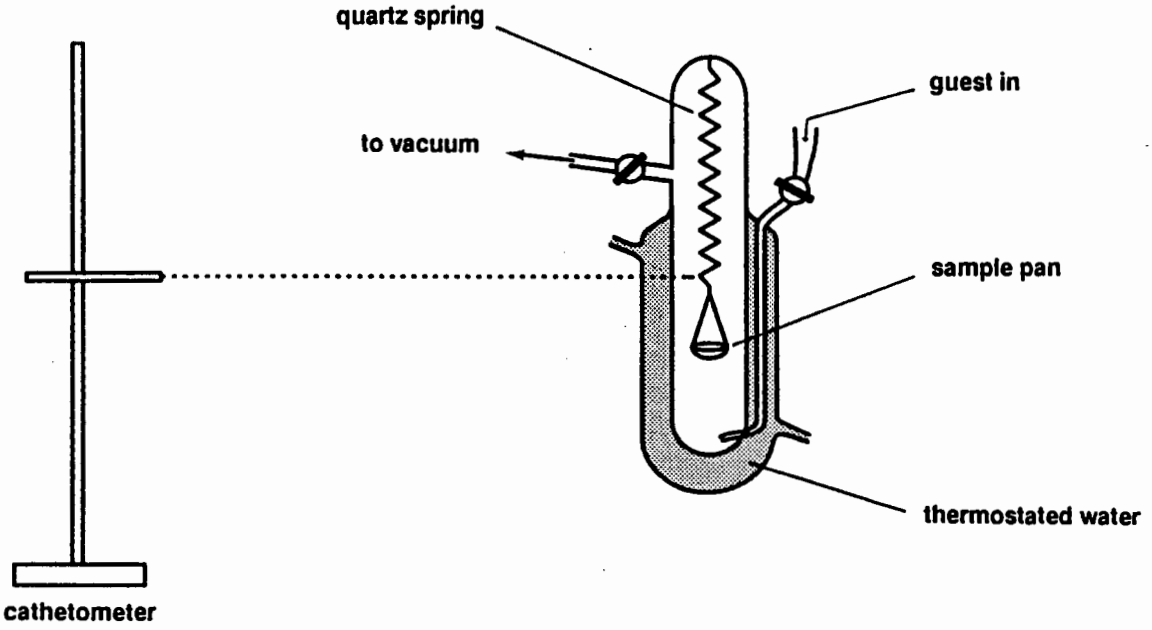

Figure 8.4 Schematic diagram of a McBain balance system used for solid-gas reaction kinetics measurements.

The main disadvantage of this method is that it is not suitable for rapid reactions, which require many measurements over a relatively short period of time. For this reason an alternative apparatus was designed and constructed as described below.

Vacuum balance techniques

A system which allows measurement of weight change with time in hermetically controlled atmospheres can be applied to a variety of interests.[33-41] Some modern electronic balances are equipped with data transfer interfaces which allow fast, automatic monitoring of mass by means of a microcomputer. The problem with weighing in controlled atmospheres is that electronic balances cannot withstand reduced pressures or corrosive gases. However, several devices have been described whereby a sample in a sealed reaction chamber can be linked to an external balance by means of free magnetic suspension.[36,40,41,43] In such systems a sample pan is attached to a permanent magnet (or an electromagnet) which is coupled across the vessel boundary to an external electromagnet suspended from an analytical balance. This coupling is effected by maintaining the equilibrium between the upward electromagnetic and downward gravitational forces acting on the permanent magnet.

Electronic feedback of the position of the permanent magnet is used to control the current through the electromagnet in order to balance the forces. Position feedback can be achieved by means of capacitive,[36,40,47,48] inductive[41,43,45,46] or optical[43,49,50] sensing. In the system described here, the optical sensing method is used since it requires the least complex electronic circuitry while the design constraint of optical passage across the system boundary is easily overcome.

Description of apparatus

Essentially, the system consists of a reaction vessel connected to a vacuum pump, a Mettler PM460 Deltarange laboratory balance, a feedback control system (which includes an electronic control circuit, an optical platform and an electromagnet), a sample support system and a microcomputer.

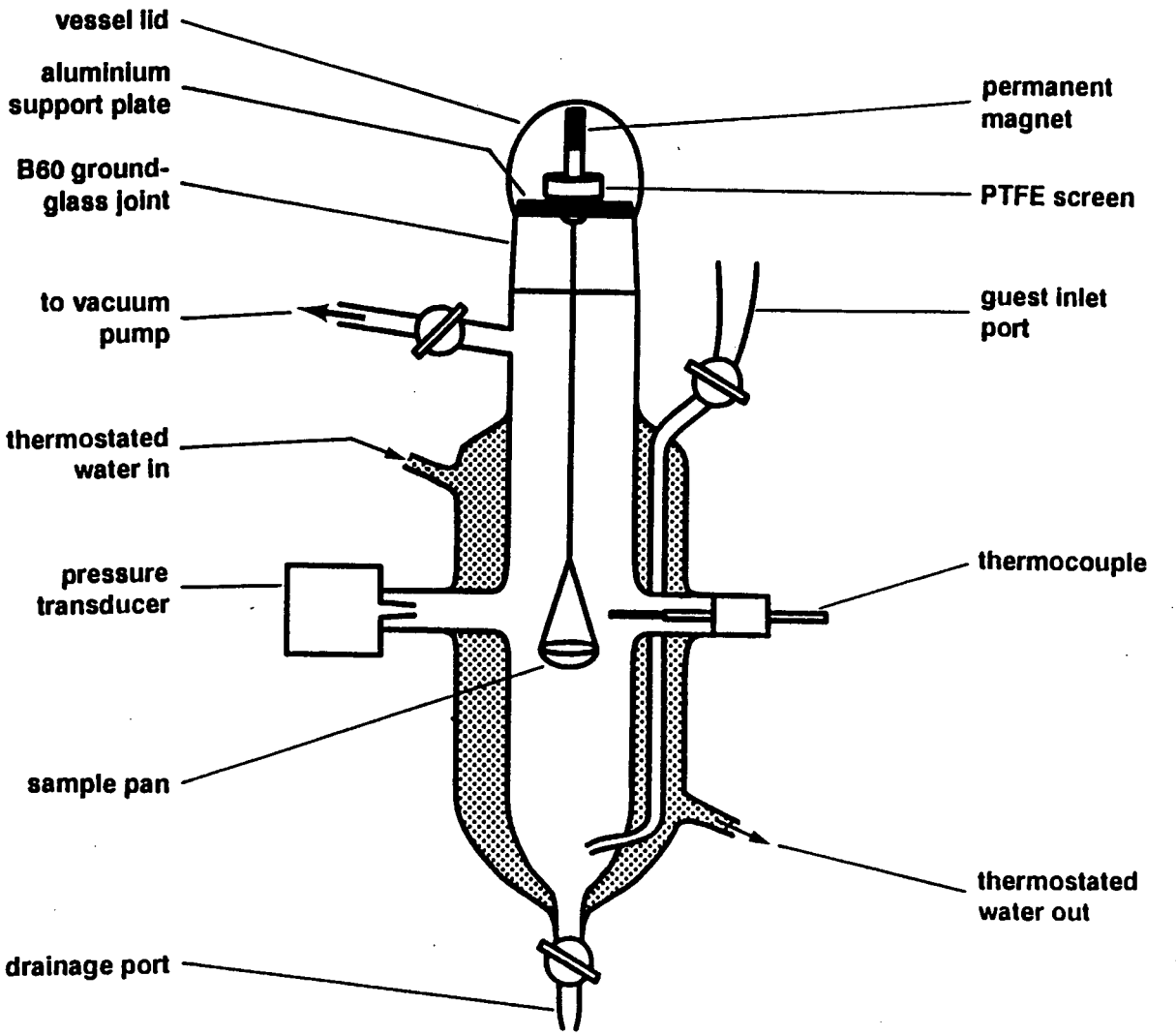

Figure 8.5 Diagram showing the main features of the reaction vessel.

The reaction vessel (Figure 8.5) is clamped vertically with its lid 2 mm below the electromagnet which is suspended from the electronic balance as shown in Figure 8.6. The sample support system consists of a permanent magnet press-fitted into a

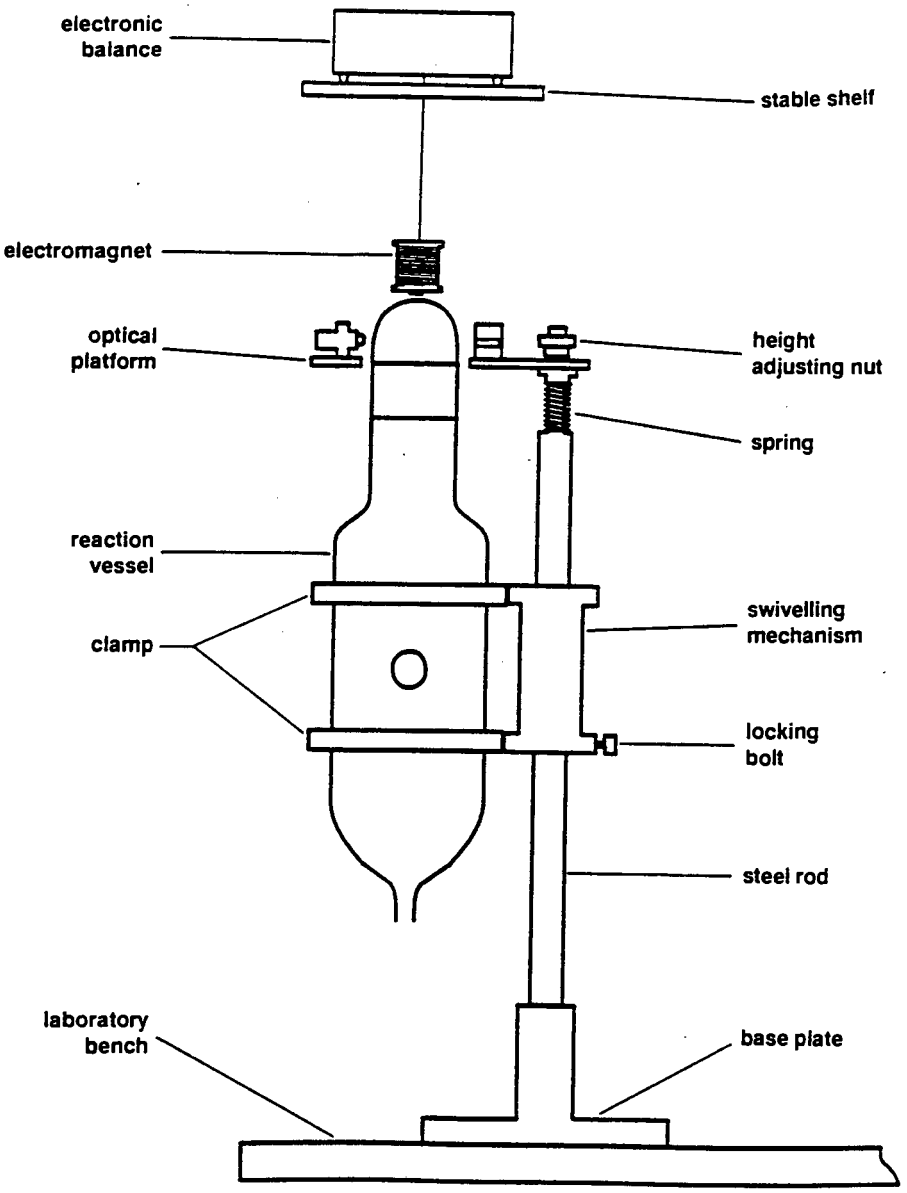

Figure 8.6 Side view of the balance system.

PTFE screen from which the sample pan is suspended at the end of a thin brass rod. The reaction vessel can be rotated horizontally, away from the electromagnet, for ease of sample loading. The pre-weighed powdered sample is placed on the sample pan and the sample support system is lowered into the reaction vessel until the screen rests on the aluminium supporting plate which in turn rests on the ground-glass socket of the vessel. The vessel head is placed over the screen and permanent magnet, sealing the reaction chamber. The vessel can then be swung into position such that the vessel head is between the light source and photodetector. The light source and photodetector are both housed on the optical platform (Figure 8.7) which is attached to the top of the vertical stand.

The reaction vessel can be evacuated and thermostated, while its internal pressure and temperature can be monitored by means of a manometer (or an electronic pressure transducer) and thermocouple respectively. A device consisting of a glass bulb and a graduated capillary was constructed to allow a measurable volume of guest liquid to be introduced via the guest inlet port. The guest liquid is

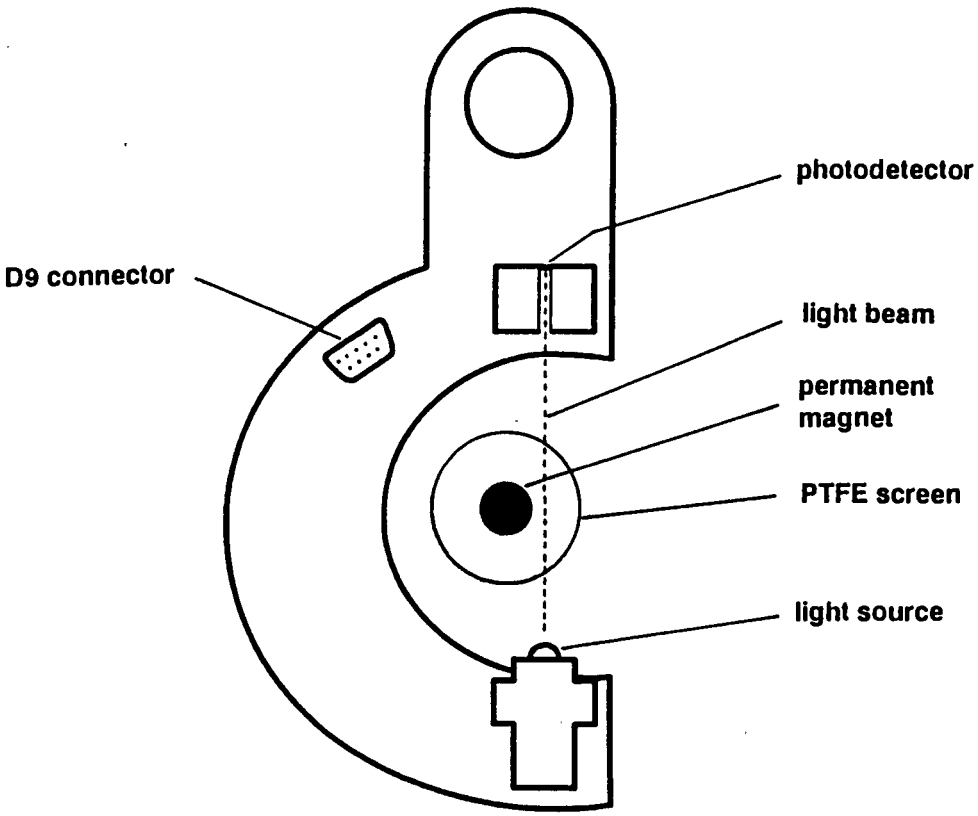

Figure 8.7 Top view of the optical platform.

tapped into the pre-evacuated reaction vessel and soon equillibrates to a vapour pressure which is dependent on the temperature of the vessel and the amount of guest introduced.

Pressing the "Lamp On" button of the control box activates the feedback control circuit. The electronic circuit is described in Appendix B but the general principle of its operation can be summarised as follows:
A light beam is projected towards the photodetector and the current passing through the electromagnet is kept proportional to the photodiode voltage. When the sample support system is in the rest position and the lamp is turned on, the current passing through the electromagnet is at a maximum because there is no interruption of the light beam. There is therefore a powerful initial force of attraction between the electromagnet and the permanent magnet. The sample support system rises towards the electromagnet, but when it passes above the correct height, part of the light beam to the detector is blocked off by the top edge of the PTFE screen, causing the electromagnetic force to weaken. An equilibrium situation is quickly reached where the shadow of the screen is approximately halfway across the aperture leading to the photodetector. In this position, the upward electromagnetic force acting on the sample suspension system is equal to the downward gravitational force. This *status quo* is maintained by the feedback control circuit, and any change in weight of the sample causes the apparent mass of the electromagnet to change accordingly.

Since the starting position of the permanent magnet is relatively far from the electromagnet, it may occur that the controlling current through the coil is not strong enough to effect initial lifting. When this situation arises, pressing the "Lift" button

on the control box causes a momentary surge of current to be passed through the coil, lifting the sample support system.

The balance is interfaced with an IBM compatible microcomputer and the data-logging software was written using the Turbo Pascal programming language[44] (and is described in Appendix A). The computer program allows entry of the duration of the experiment, the expected maximum mass gain and the desired time interval between readings. During the experiment, data are simultaneously written to the computer's hard disk and graphically displayed on the monitor in the form of a plot of mass gain (or loss) as a function of time.

Photograph 2 (see Appendix D) demonstrates the levitation of the PTFE screen and permanent magnet. The electromagnet and optical platform can be seen clearly, while the reaction vessel is not shown. Photograph 3 shows the reaction vessel in position below the electromagnet – the sample support system is enclosed in the vessel with the PTFE screen resting on the aluminium support plate.

Analysis of data

A computer program called **KINETIC** was developed as part of this study in order to analyse kinetic data quickly and conveniently. The program (which is described in more detail in Appendix A) reads an α-time data file from the computer's hard disk and displays the plot of α versus time on the graphic screen. Using the computer's mouse, any of the functions given in Table 8.1 can be selected and displayed on screen as a plot of $f(\alpha)$ versus time. In addition, the best-fit straight line for the latter plot is displayed together with the value of the slope (i.e. the rate constant, k, for the chosen model) and the correlation coefficient. The mouse can be used to "zoom in" on a subset of the data in order to evaluate the applicability of the chosen model over a particular range of α or time. Using this program, an α-time data set can be inspected visually and investigated interactively for each of the theoretical models described above.

Inclusion kinetics experiment

The kinetics of inclusion of acetone by *trans*-9,10-dihydroxy-9,10-diphenyl-9,10-dihydroanthracene was investigated (see the structure **DPac** in Chapter 4). Kinetic measurements were carried out by exposing fresh samples of finely powdered host compound (sieved fraction 63-125 μm) to acetone vapour at various pressures and three different temperatures. The acetone liquid tapped in through the guest inlet port was degassed beforehand to ensure accurate vapour pressure measurement. The vapour pressure was controlled by tapping a measured volume of acetone liquid into the vessel. A typical set of isothermal kinetic curves is shown in Figure 8.8.

The interesting and unexpected feature of the kinetics is that for a given pressure of acetone vapour, the rate of reaction **decreases** with increasing temperature. This is illustrated in Figure 8.9 which shows the kinetic results at the same acetone vapour pressure and at two different temperatures. The kinetic results most consistently obey the first order rate equation and values for the apparent rate constants k_{obs} were derived using the program KINETIC. It was noted that in order for the host in the α-phase to combine with acetone, a threshold vapour pressure, P_0, of the guest is required. Values of $P_{0,T}$ at different temperatures were obtained by

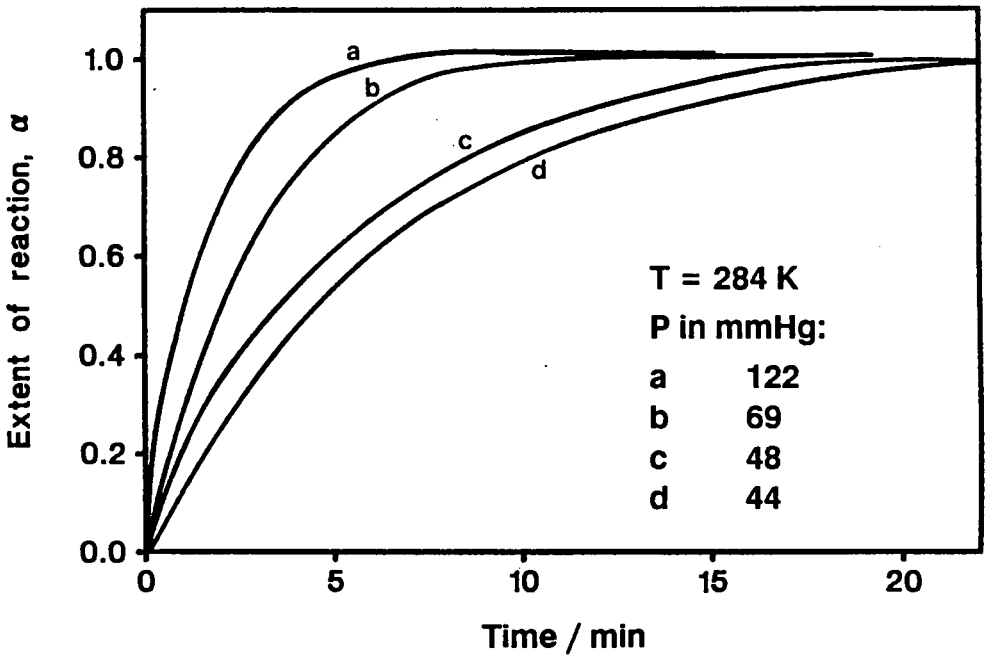

Figure 8.8 α-Time curves at various acetone vapour pressures and at 284K

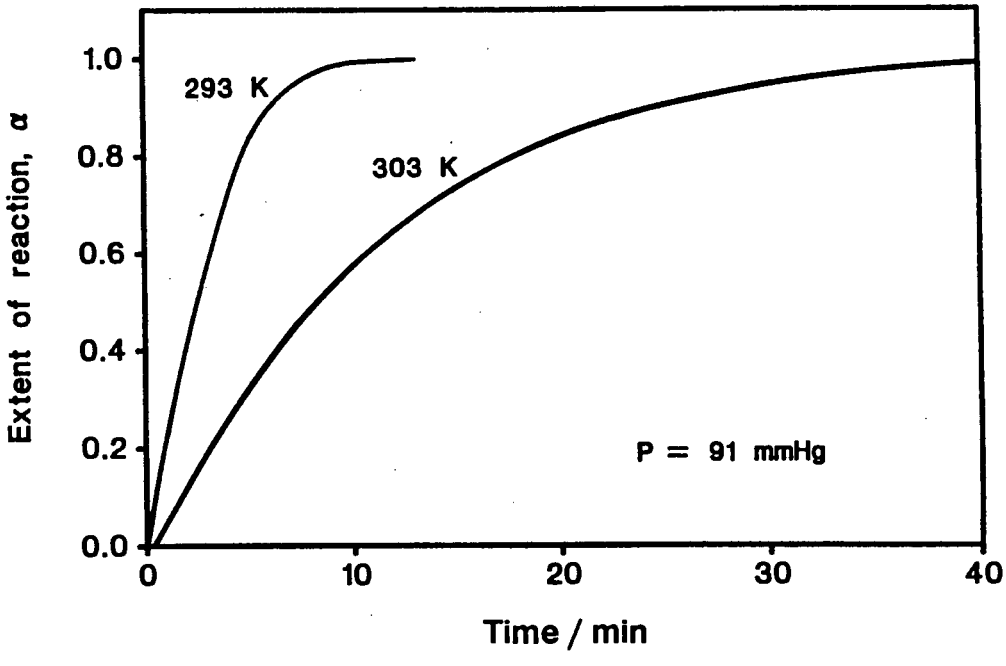

Figure 8.9 Kinetic curves at an acetone vapour pressure of 91 mmHg and at two different temperatures.

plotting the rate constant k_{obs} versus the vapour pressure P of the guest as shown in Figure 8.10 (the data are given in Table 8.2).

Table 8.2 Kinetic data relating to Figure 8.10*,†

T (°C)	P (mmHg)	k_{obs}	
11	44	0.14	r = 0.9965
	48	0.18	a = -0.13(3)
	69	0.36	b = 6.7(3)×10^{-3}
	114	0.62	P_0 = 20.2 mmHg
	122	0.67	k_f = b×P_0 = 0.273
20	56	0.14	r = 0.9902
	69	0.18	a = -0.18(4)
	71	0.22	b = 5.7(4)×10^{-3}
	91	0.37	P_0 = 30.2 mmHg
	100	0.42	k_f = 0.171
	158	0.70	
30	92	0.09	r = 0.9994
	113	0.16	a = -0.27(1)
	135	0.25	b = 3.88(8)×10^{-3}
	161	0.35	P_0 = 70.3 mmHg
	180	0.43	k_f = 0.134

* r, a and b are the correlation coefficient and linear best-fit parameters of the ordinate intercept (in min^{-1}) and the slope (in [mmHg]$^{-1}$min^{-1}) respectively

† values for k_{obs} and k_f are reported in min^{-1}

The experimental results are consistent with the rate law

$$\ln(1-\alpha) = k_f[(P-P_0)/P_0]t$$

where $k_{obs} = k_f[(P-P_0)/P_0]$ and k_f is the rate constant for the inclusion (forward) reaction. The slopes derived from Figure 8.10 are thus equated to k_f/P_0, allowing calculation of k_f for each temperature. Using the Arrhenius equation in the form

$$\ln k_f = \ln A - E/RT$$

a plot of ln k_f versus $1/T$ (Figure 8.11) yields a value of 26.8 kJmol^{-1} for the activation energy. Figure 8.11 is included here to show the general trend of ln k_f with respect to temperature and it is not suggested that the value obtained for the activation energy from only three data points is necessarily reliable.

A sub-sample of the reaction product (the β-phase) was removed from the reaction vessel and its X-ray powder diffraction pattern recorded. Care was taken to minimise the danger of guest desorption and the specially constructed sample-holder described in Chapter 2 was used. The powder diffraction pattern was successfully

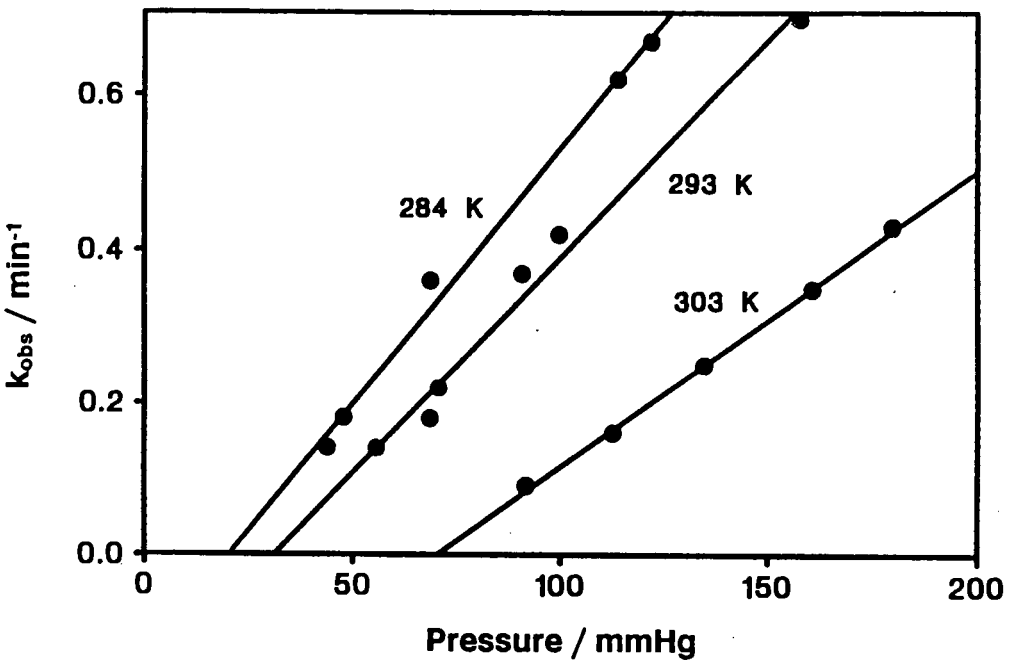

Figure 8.10 Plot of observed rate constant versus guest vapour pressure, yielding $P_{0,T}$ values.

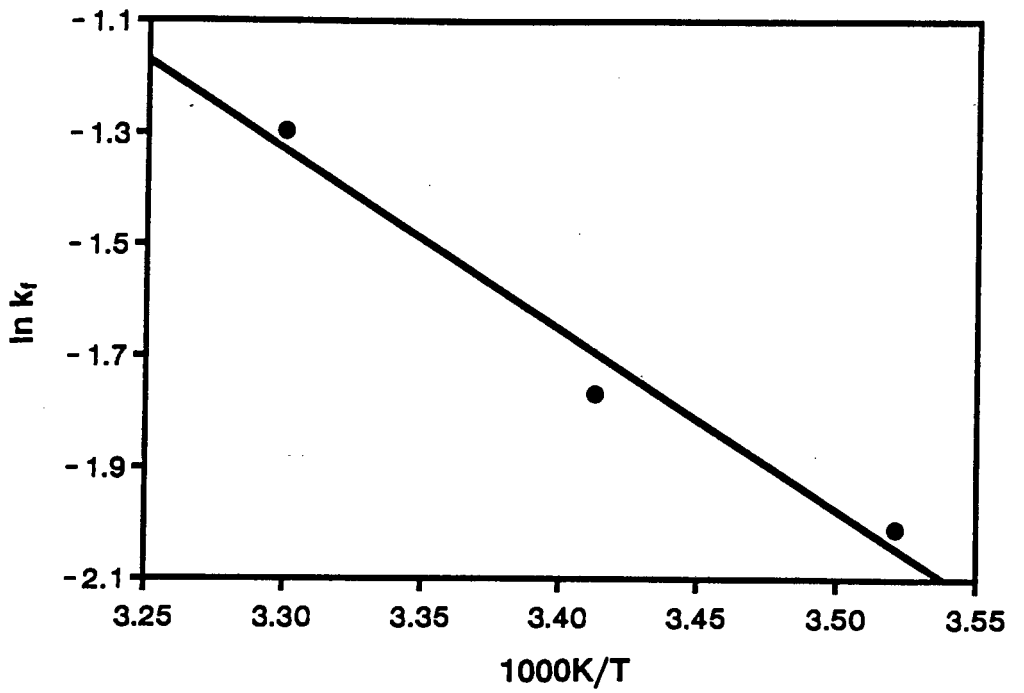

Figure 8.11 Plot of ln k_f vs $1/T$, yielding the activation energy for the forward reaction.

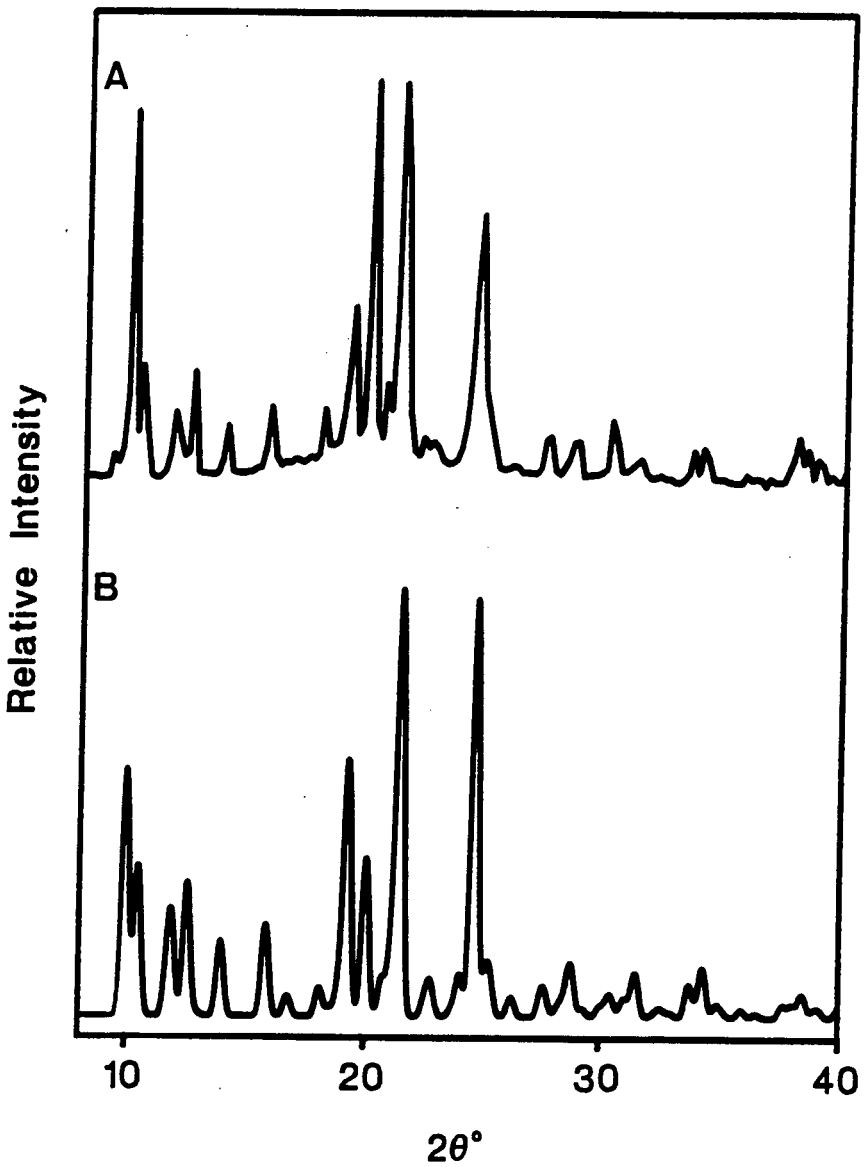

Figure 8.12 XRD traces for (A) the inclusion compound formed by guest absorption from the vapour (measured) and (B) **DPac** as calculated from the single crystal structure data.

matched with that calculated from the single crystal structure data using the computer program LAZY PULVERIX[52] as shown in Figure 8.12.

The *apparent* anti-Arrhenius behaviour has been observed with other organic host compounds which include guests from the pure vapour phase and it is suggested that this *may* be a general phenomenon when the process of inclusion is associated with a phase change to a new crystal structure.

Decomposition kinetics experiment

The kinetics of decomposition of **DPac** under reduced pressure was investigated. In each experiment, a fresh sample of the powdered host compound (α-form, sieved fraction 63-125 μm) was exposed to acetone vapour as described above. When it was evident that the inclusion reaction had effectively reached completion, the reaction vessel was evacuated and the α-time data for the decomposition reaction recorded. The α-time curves at various sample temperatures are shown in Figure 8.13 and the contracting area model, i.e. $1-(1-\alpha)^{1/2} = kt$, yields the most consistent fit to the data.

Figure 8.14 shows the plot of ln k versus $1/T$ and a value of 64(5) kJ mol^{-1} is obtained for the activation energy of the decomposition reaction. It must be emphasised here that this process is not merely the reverse of the process discussed in the preceding section since the two experiments were performed under vastly different conditions of pressure. The powder diffraction pattern of the solid decomposition product was measured and successfully matched with that calculated from the single crystal structure data (extracted from the Cambridge Structural Database) as described above. The measured and calculated XRD traces shown in Figure 8.15 indicate that the β-phase reverts back to the original α-phase on thermal decomposition under reduced pressure.

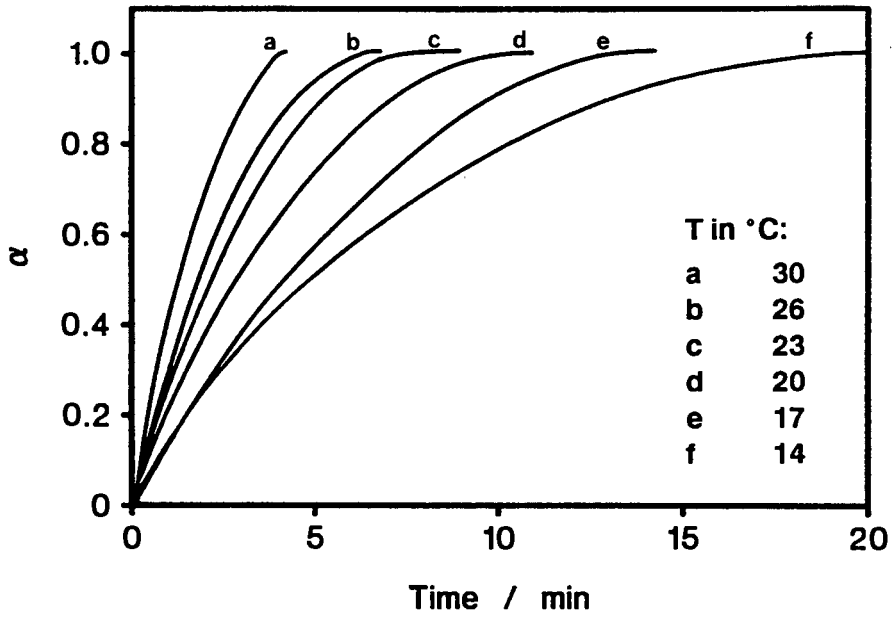

Figure 8.13 Decomposition kinetic curves at various temperatures.

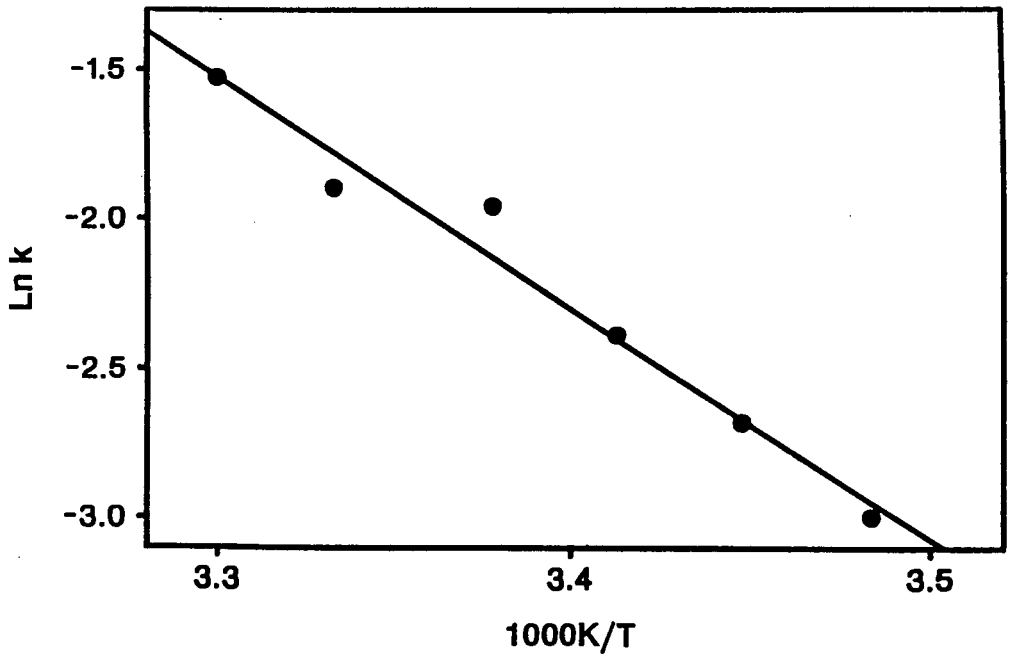

Figure 8.14 Plot of ln k vs $1/T$, yielding the activation energy for the decomposition reaction.

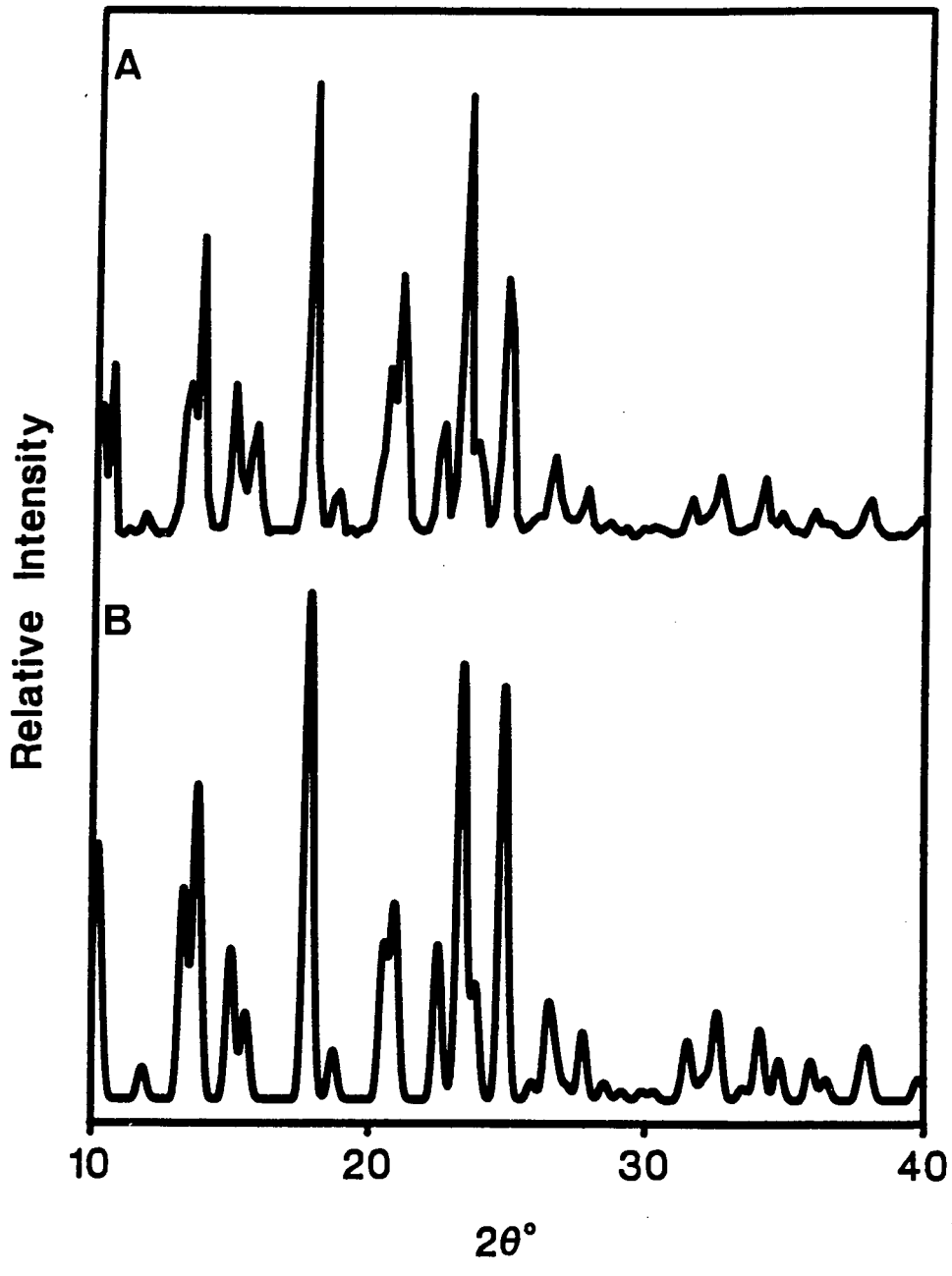

Figure 8.15 XRD traces for (A) the solid decomposition product (measured) and (B) the α-phase of the host compound *trans*-9,10-dihydroxy-9,10-diphenyl-9,10-dihydroanthracene as calculated from the single crystal structure data.

The effect of particle size

The influence of particle size distribution on solid state reactions is well known, especially in relation to thermal analysis.[53-55] Lahiri[53] even suggests that changes in particle size distribution due to fragmentation may lead to an erroneous conclusion about multiple mechanisms during the course of a reaction.

A sample of large single crystals of *trans*-9,10-dihydroxy-9,10-diphenyl-9,10-dihydroanthracene (about 2 to 3 mm across) grown from benzene was exposed to acetone vapour at 19°C as described above and its α-time curve recorded. On

completion of the inclusion reaction, the reaction vessel was evacuated and the desorption curve recorded. This process was repeated four more times without disturbing the sample. The α-time curves for the first, second and third experiments are shown in Figure 8.16 as curves a to c respectively (the fourth and fifth curves are omitted for clarity as they were nearly coincident with curve c). Fragmentation of the crystals was clearly visible after the first inclusion experiment. Further fragmentation occurred with the subsequent experiments as evidenced by gradual "creeping" of the sample towards the edge of the aluminium pan. After the fifth desorption experiment, the sample was removed and inspected. By this stage the sample consisted of fine flake-like particles.

Figure 8.16 shows that there is a marked increase in the rate of reaction after the first inclusion experiment after which the absorption isotherm, with repetition of the reaction, rapidly appears to converge to a particular shape. This suggests that although particle size distribution is an important consideration, there is a limit beyond which a further decrease in particle size does not significantly increase the reaction rate.

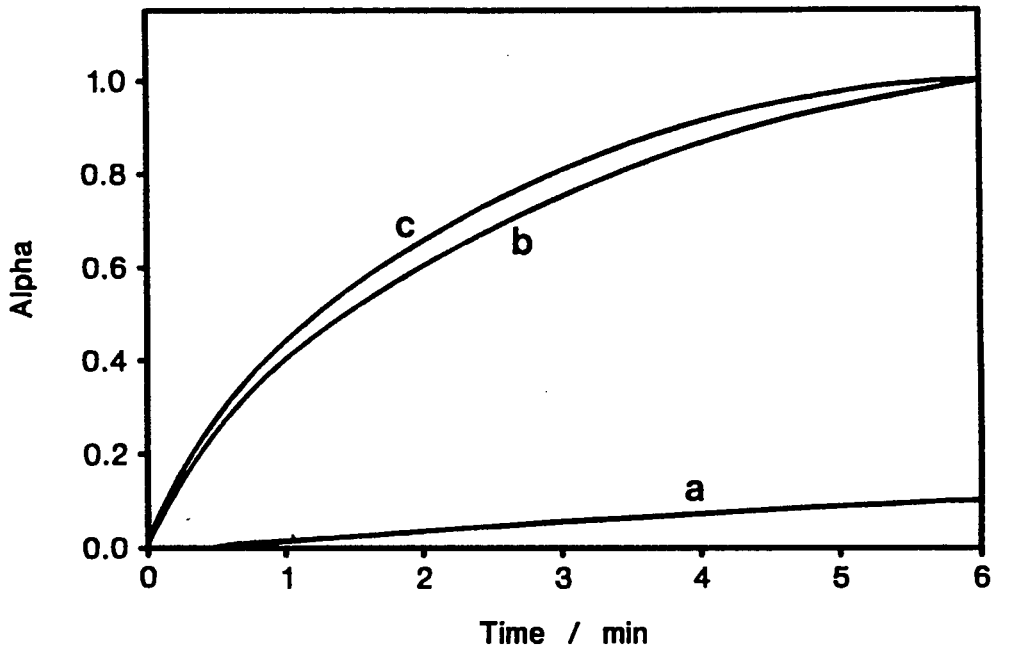

Figure 8.16 Three successive absorption α-time curves for a sample initially consisting of large single crystals.

Self-heating

The inclusion reaction is an exothermic process and it is possible that self-heating may cause the temperature of the sample to increase by several degrees during a reaction. This may lead to erroneous evaluation of experimental data since the sample temperature is generally assumed to be constant and equal to that of the surrounding atmosphere. Self-heating has not been taken into account here and it is suggested that this effect (and indeed self-cooling for endothermic processes) be investigated in future studies. Such investigations would require a temperature probe to be in constant contact with the sample. Fixing a temperature device to the levitating sample pan presents some practical difficulties. However, a second host sample, identical to that in the sample pan, could be placed in the reaction vessel,

but not in contact with the sample support system. This sample would undergo the same changes as the weighed sample and its temperature could be monitored without disturbing the levitating sample.
The effects of self-heating during surface oxidation of pyrophoric iron have been studied by Galwey and Gray.[56] Although the reaction is not highly temperature-dependent, these authors reported temperature increases of up to 150°C of the solid sample, depending on the pressure of the oxygen gas.

The influence of other gases

An experiment was conducted in order to test whether the rate of the absorption reaction is affected by the presence of gases which do not become included. A series of eight absorption runs were recorded at 17°C using *trans*-9,10-dihydroxy-9,10-diphenyl-9,10-dihydroanthracene as the host and acetone as the guest. For each run a freshly sieved (63-125 μ) and weighed (95 to 100 mg) host sample was used and the pre-evacuated reaction vessel was filled with nitrogen gas at different pressures before introduction of the acetone. From Figure 8.17, which shows the absorption isotherms at different nitrogen partial pressures, it can be seen that the nitrogen gas has a marked affect on the rate of the inclusion reaction. At higher nitrogen pressures the rate of the reaction is slower and the induction period is longer. Since the inclusion reaction is thought to start with surface adsoprion of the guest molecules onto the solid surface of the host compound, two possible explanations are suggested for the influence of the nitrogen gas on the rate of the reaction :

1 the nitrogen molecules compete with the guest molecules for adsorption sites, and
2 the nitrogen molecules collide with surface-adsorbed guest molecules, removing them from the surface thereby raising the activation energy of the inclusion reaction.

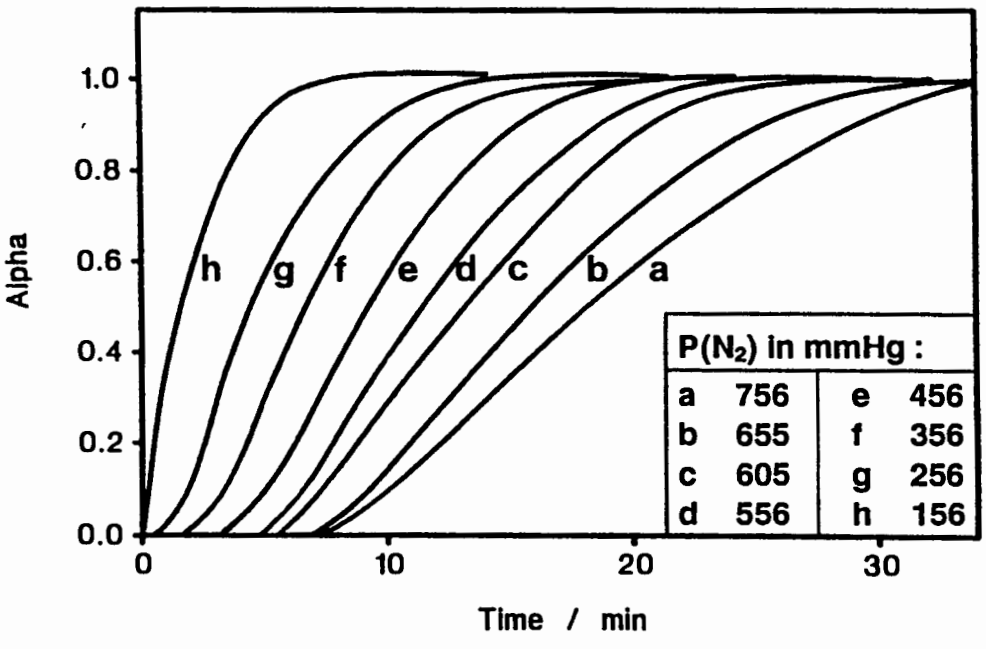

Figure 8.17 The effect of nitrogen gas at various partial pressures on an inclusion reaction.

References

1 R.M. Barrer, "Zeolites and Clay Minerals as Sorbents and Molecular Sieves", Academic Press, London, 1978

2 S.A. Talipov, B.T. Ibragimov, G.B. Nazarov, T.F. Aripov, A.S. Sadikov, *Khim. Prir. Soed.*, 1985,835

3 J.M. Adams and G. Waltl, *Clays and Clay Minerals*, 1980, **28**(2),130

4 C. Breen and S. Lynch, *Clays and Clay Minerals*, 1988, **36**(1),19

5 C.M. Wyandt and D.R. Flanagan, *Thermochim. Acta*, 1992,**196**,379

6 M.S. Whittingham and A.J. Jacobson (Eds), "Intercalation Chemistry", Academic Press, New York, 1982

7 J. Votinsky, J. Kalousova, L. Benes, I. Baudysova and V. Zima, *J. Incl. Phenom. Mol. Recog. Chem.*, 1993,**15**,71

8 S. Glasstone and K.Y. Laidler, "The Theory of Rate Processes", McGraw-Hill, New York, 1941

9 S. W. Benson, "Thermochemical Kinetics", Wiley, New York, 1968

10 K.J. Laidler, "Chemical Kinetics", McGraw-Hill, New York, 1965

11 G. Pannetier and P. Souchay, "Chemical Kinetics", translated by H.D. Gesser and H.H. Emond, Elsevier, Amsterdam, 1967

12 H. Eyring, S.H. Lin and S.M. Lin, "Basic Chemical Kinetics", Wiley, New York, 1980

13 C.H. Bamford and C.F.H. Tipper, (Eds), "Comprehensive Chemical Kinetics", Vol 22, Elsevier, Amsterdam, 1980

14 M.E. Brown, "Introduction to Thermal Analysis", Chapman and Hall, London, 1988

15 W.E. Gardner, (Ed.), "Chemisorption", Butterworths, London, 1957

16 D.O. Hayward and B.M.W. Trapnell, "Chemisorption", Butterworths, London, 1964

17 J.S. Anderson, M.W. Roberts and F.S. Stone, (Eds), "Reactivity of Solids", Chapman and Hall, London, 1972

18 N.B. Hannay (Ed.), "Treatise on Solid State Chemistry", Vol. 4, "Reactivity of Solids" and Vol. 5, "Changes of State", Plenum Press, New York, 1976

19 H. Schmalzried, "Solid State Reactions", Verlag Chemie, Weinheim, 1981

20 C.N.R. Rao and J. Gopalakrishnan, "New Directions in Solid State Chemistry", Cambridge University Press, Cambridge, 1986

21 W.P. Gomes and W. Dekeyser, in "Treatise on Solid State Chemistry", N.B. Hannay (Ed.), Vol. 4, "Reactivity of Solids", Plenum Press, New York, 1976

22 K. Hauffe, in "Treatise on Solid State Chemistry", N.B. Hannay (Ed.), Vol. 4, "Reactivity of Solids", Plenum Press, New York, 1976

23 Smeltzer and D.J. Young, *Prog. Solid State Chem.*, 1975,**10**,17

24 J.A. Lumpkin and D.D. Perlmutter, *Thermochim. Acta*, 1992,**202**,151

25 Y. Masuda, K. Hirata and Y. Ito, *Thermochim. Acta*, 1992,**203**,289

26 X. Gao and D. Dollimore, *Thermochim. Acta*, 1993,**215**,47

27 O. Yamamuro and H. Suga, *J. Thermal Anal.*, 1989,**35**,2025

28 J.H. Sharp, G.W. Brindley and B.N Narahari Achar, *J. Amer. Ceram. Soc.* 1966,**49**(7),379

29 A.M. Mulokozi, *Thermochim. Acta*, 1992,**197**,363

30 W. Gomes, *Nature*, 1961,**192**,865

31 M. Arnold, G.E. Veress, J. Paulik and F. Paulik, *Thermochim. Acta*, 1982,**52**,67; *Anal. Chim. Acta*, 1981,**124**,341

32 P.D. Garn, *Crit. Rev. Anal. Chem.*, 1972,3,65

33 A.W. Czanderna and S.P. Wolsky (Eds), "Methods and Phenomena", Vol. 4, "Microweighing in vacuum and controlled environments", Elsevier, Amsterdam, 1980

34 Th. Gast and K. Koppe, *J. Vac. Sci. Technol.*, 1978,**15**(2),813

35 J.L. Garcia Fierro and A.M. Alvarez Garcia, *Vacuum*, 1980,**31**,79

36 Th. Gast and K.-P. Gebauer, *Thermochimica Acta*, 1981,**51**,1

37 A.J. Ashworth, *Thermochimica Acta*, 1981,**51**,17

38 H.L. Eschbach, I.V. Mitchell and E.Louwerix, *Thermochimica Acta*, 1981,**51**,33

39 A.J. Ashworth and G.J. Price, *Thermochimica Acta*, 1984,**82**,161

40 R. Masui, W.M. Haynes, R.F. Chang, H.A. Davis and J.M.H. Levelt Sengers, *Rev. Sci. Instrum.*, 1984,**55**(7),1132

41 Th. Gast, E. Hoinkis, U. Muller and E. Robens, *Thermochimica Acta*, 1988,**134**,394

42 D.R. Bond, L. Johnson, L.R. Nassimbeni and F. Toda, *J. Solid State Chem.*, 1991,**92**,68

43 Th. Gast, *Thermochimica Acta*, 1986,**103**,5

44 Turbo Pascal, Version 6.0, 1990, Borland International Inc., Scotts Valley, CA, USA

45 J.L. Hales, *J. Phys.*, 1970,**E3**,855

46 J.L. Hales, *J. Phys.*, 1983,**E16**,91

47 W.M. Haynes, M.J. Hiza and N.V. Frederick, *Rev. Sci. Instrum.*, 1976,**47**,1237

48 W.M. Haynes, *Rev. Sci. Instrum.*, 1977,**48**,39

49 J.W. Beams, C.W. Hulbert, W.E. Lotz, Jr. and R.M. Montague, Jr., *Rev. Sci. Instrum.*, 1955,**26**,1181

50 J.P. Senter, *Rev. Sci. Instrum.*, 1969,**40**,334

51 F. Toda, K. Tanaka, S. Nagamatsu and T.C.W Mak, *Isr. J. Chem.*, 1985,25,346

52 K. Yvon, W. Jeitschko and E. Parthe, *J. Appl. Cryst*, 1977,10,73

53 A.K. Lahiri, *Thermochim. Acta*, 1980,**40**,289

54 M. Ochiai and R. Ozao, Th*ermochim. Acta*, 1992,**198**,279

55 M. Ochiai and R. Ozao, Th*ermochim. Acta*, 1992,**198**,289

56 A.K. Galwey and P. Gray, "Self-heating During the Surface Oidation of Pyrophoric Iron" in Reference 17, Page 733

Chapter 9 Thermal stability studies

The majority of studies involving inclusion compounds deal with their synthesis, structure and uses while relatively little work has been devoted to their kinetics of formation or thermodynamic stabilities. For the general reaction

$$HG_n\,(s,\beta) \rightleftharpoons H\,(s,\alpha) + nG\,(g),$$

the enthalpy change ΔH of the guest-release reaction is a measure of the strength of the interactions between host and guest molecules. Thus ΔH is expected to increase with increasing thermal stability of the inclusion compound.

Thermal Analysis

Most of the thermal stability studies of inclusion compounds have employed techniques such as TG and DSC. Since these techniques are well-established (e.g. references 1 to 4) they will not be described here.

An important application of TG is the determination of host:guest ratios. However, much effort has been expended on extending this method for isothermal and non-isothermal decomposition kinetics (e.g. see references 5 to 13). DSC has been widely used to measure ΔH of the guest-release reaction, and has been successfully employed in the thermal decomposition of urea-n-paraffin inclusion compounds[14] and β-quinol clathrates.[15] Although DSC methods have been used to measure the enthalpy of decomposition of a number of inclusion compounds with volatile guests, where the enthalpy changes have been correlated with decomposition onset temperatures and non-bonded energies of the host-guest compounds,[16,17] this method has several inherent disadvantages. In order to obtain reproducible results, the inclusion compounds should be crushed and sieved so as to work with a narrow band of crystallite sizes. This is generally not possible if the guest is volatile, owing to prompt decomposition of the inclusion compound. The enthalpy values obtained are also dependent on the heating rates, the purge gas flow rate, the type of specimen holder employed and the geometry of the calorimeter.

For the purposes of this study, TG has been used primarily for the determination of host:guest ratios. Since sieving of the inclusion compounds considered here is generally not feasible owing to their instability, no attempt was made to study decomposition kinetics or to use DSC for the determination of ΔH. However, inspection of the thermal traces can still be of qualitative value for inferences about the decomposition process. In general, the onset temperature of the guest-loss process, when compared with the boiling point of the guest, is used as a crude measure of the stability of the inclusion compound.

Figure 9.1 shows a schematic DSC trace for the decomposition of an inclusion compound and can be interpreted in several different ways (refer also to Figure 8.1; note that an endotherm (or an exotherm) is generally indicative of a phase-change). The following three interpretations are usually related to the types of inclusion compounds considered here:

i As the β-phase decomposes, *some* of the guest compound is volatilised with concomitant formation of the so-called γ-phase (endotherm A) which is more

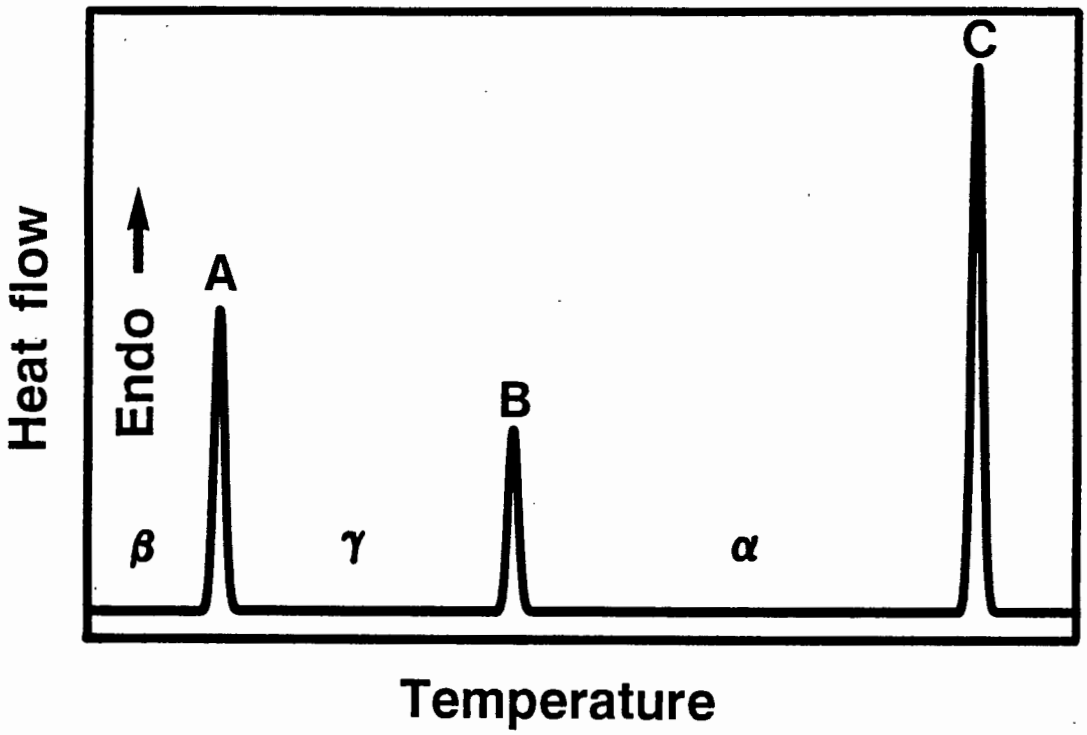

Figure 9.1 Schematic DSC trace showing various possible phase-changes (as endotherms) associated with the decomposition of an inclusion compound.

stable at higher temperatures. On further heating, the γ-phase also decomposes and the host compound reverts to its α-phase (endotherm B). Endotherm C represents melting (or sublimation) of the host compound.

ii The host compound loses *all* the guest molecules (endotherm A) and reverts to an intermediate, desolvated phase (either the β_0 structure, or another polymorphic form). The compound then undergoes a molecular rearrangement to form the α-phase or a polymorph of the α-phase (endotherm B), and melts (endotherm C).

iii In many cases there is no perceivable intermediate stage between the β- and α- phases, and endotherm B is absent.

In Figure 9.1 the endotherms are shown as Gaussian peaks. However, it should be noted that peaks are not always well defined, and may assume complex shapes owing to the complex nature of phase-change mechanisms. It is useful to consider the DSC and TG traces in a complimentary fashion. For example, TG will allow one to distinguish between (i) and (ii) above since a guest-loss gives rise to a weight-change, whereas a phase-change involving only the solid state does not. When considering TG and DSC traces together, it is apparent that the onset temperatures of events do not necessarily coincide. This is due to differences in the system

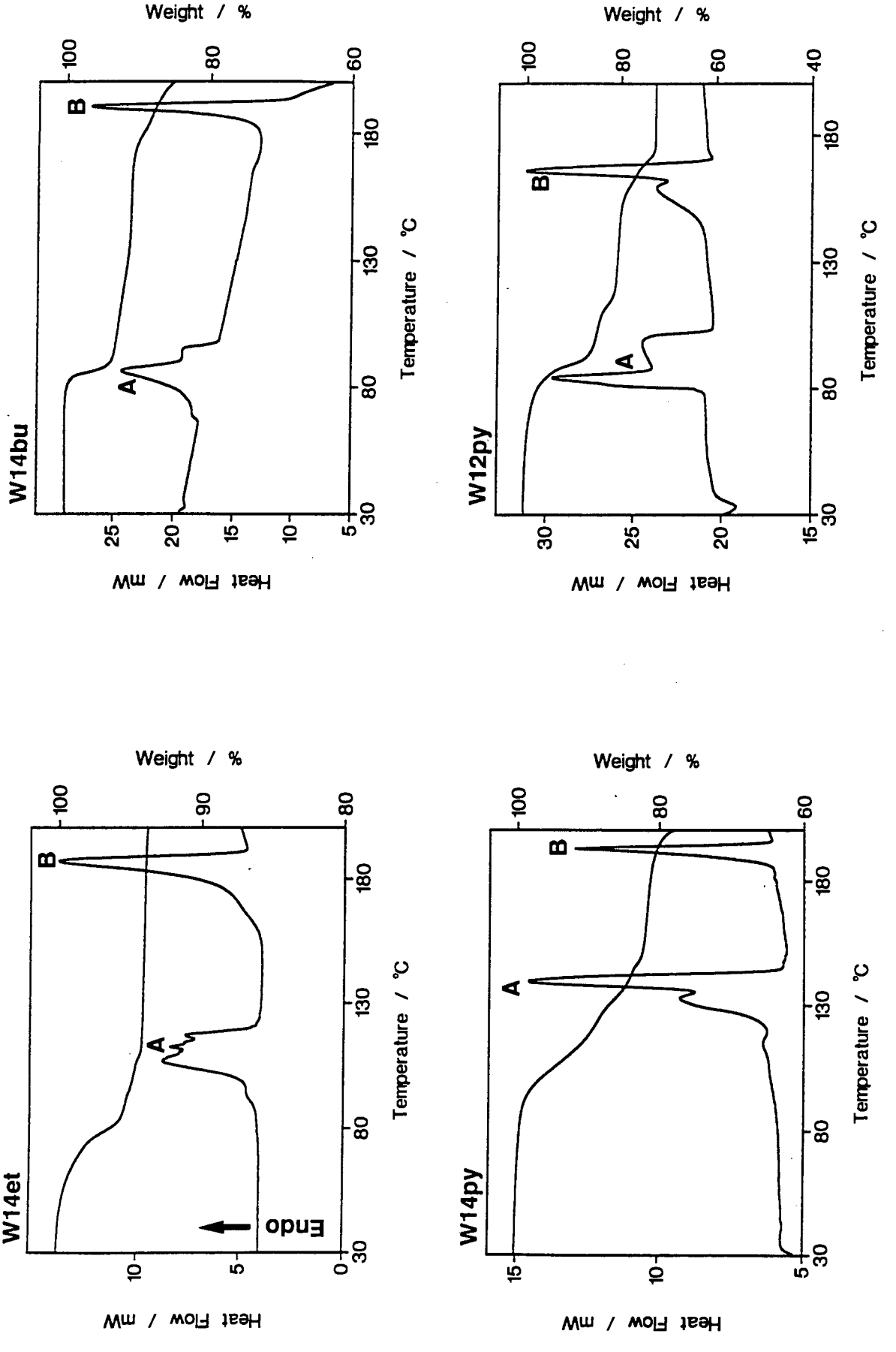

Figure 9.2 DSC and TG traces for all the inclusion compounds considered in the present study.

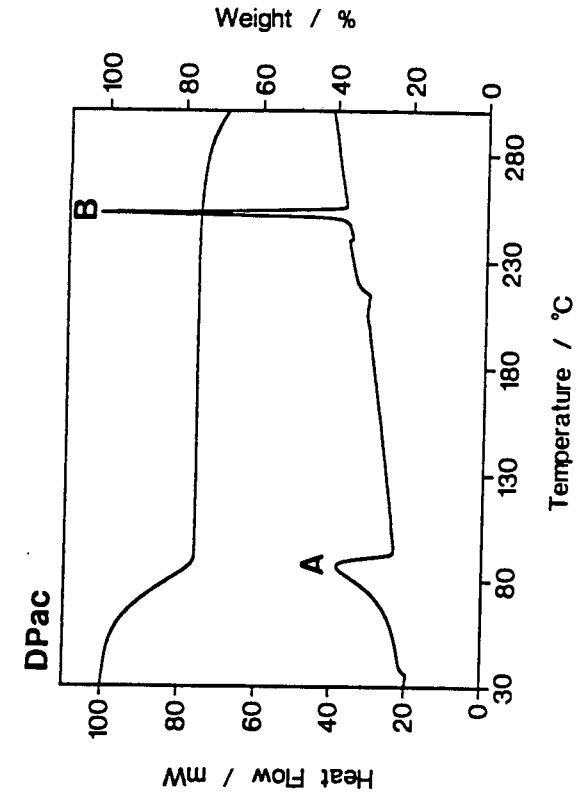

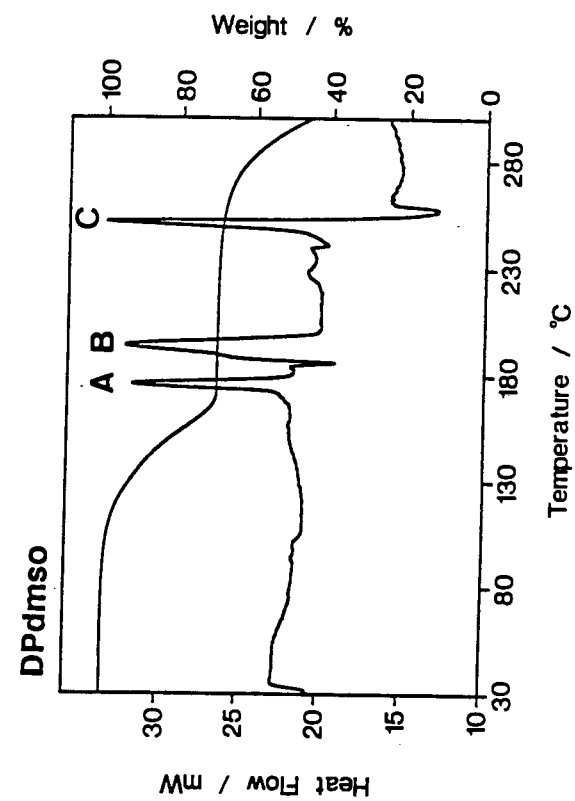

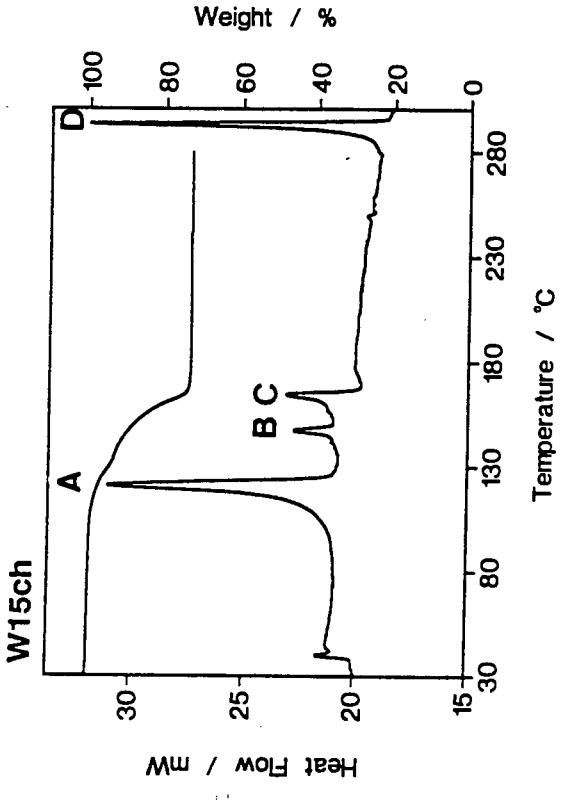

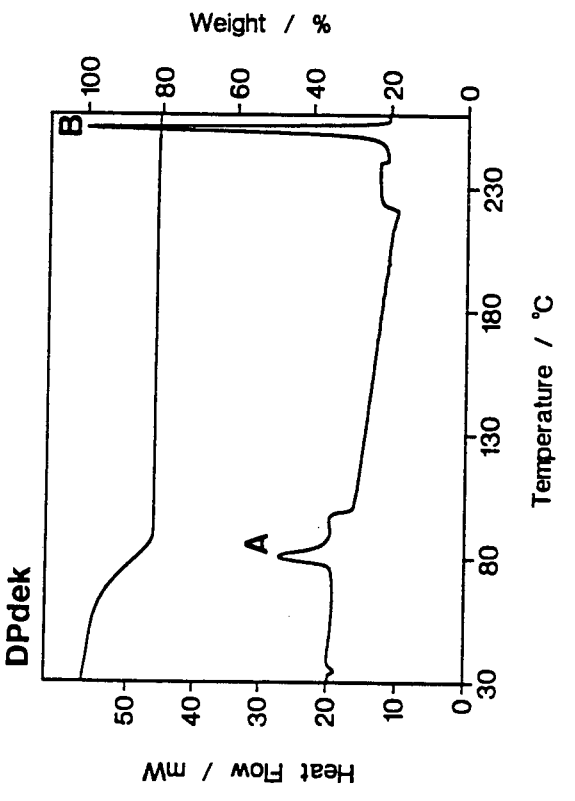

Figure 9.2 *continued*

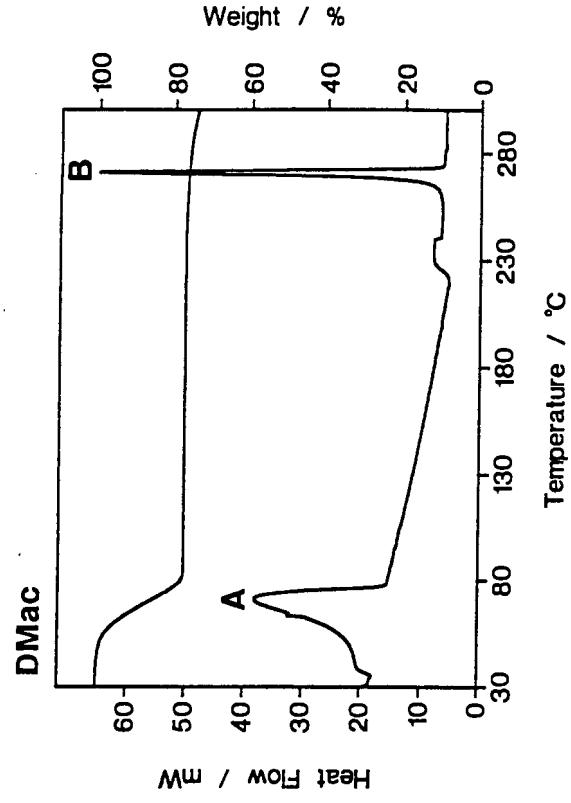

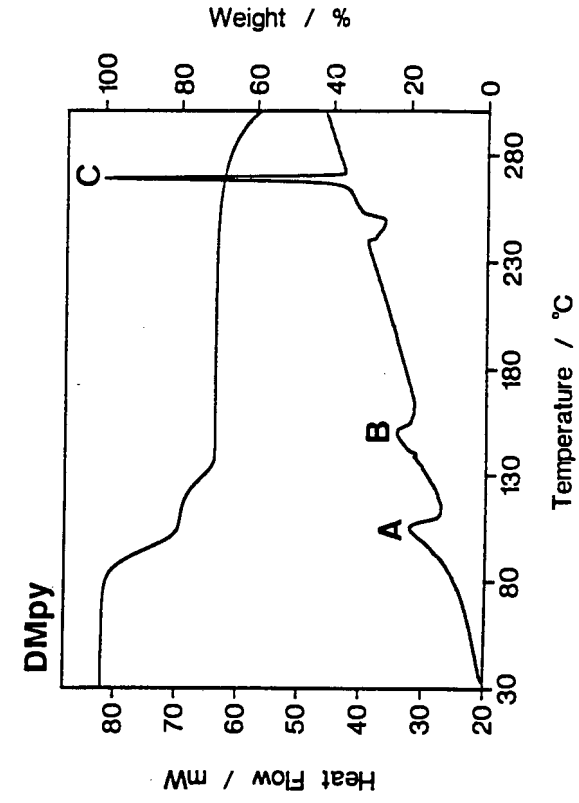

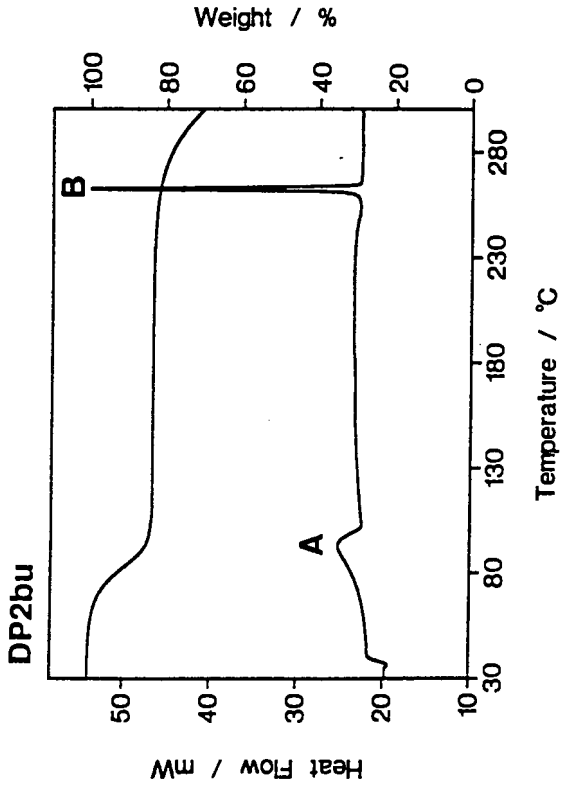

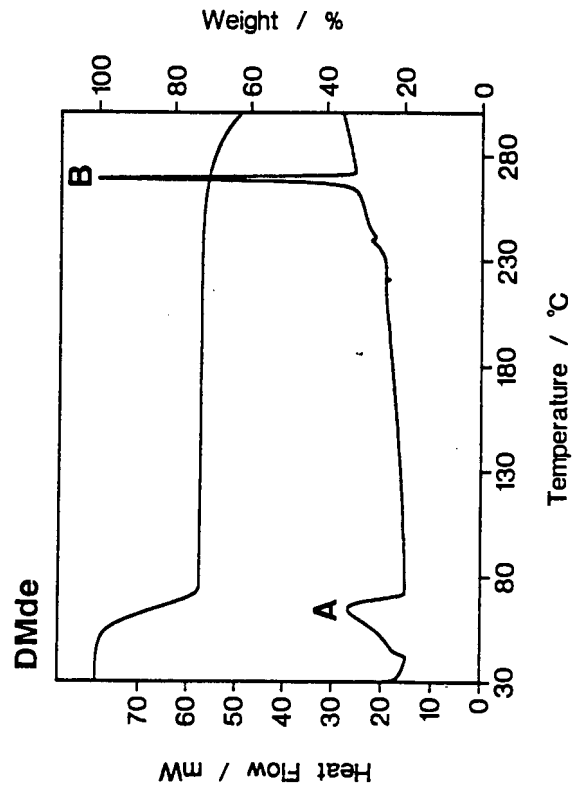

Figure 9.2 *continued*

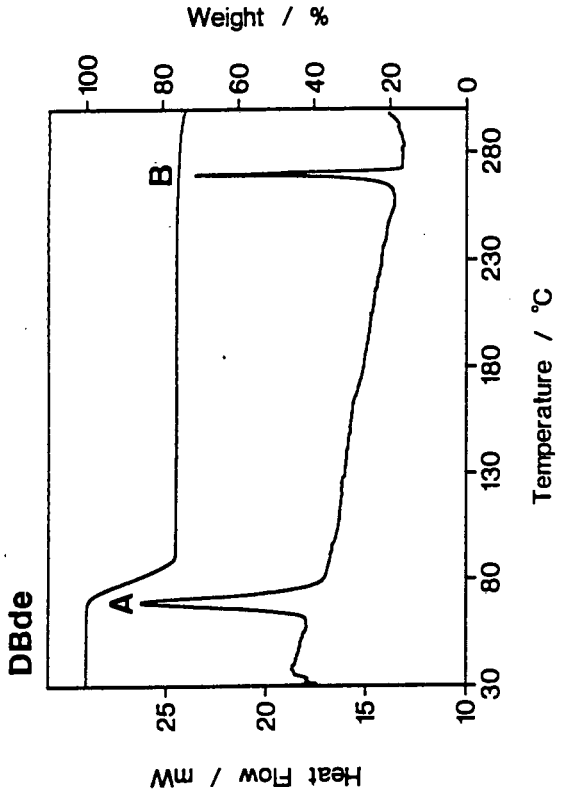

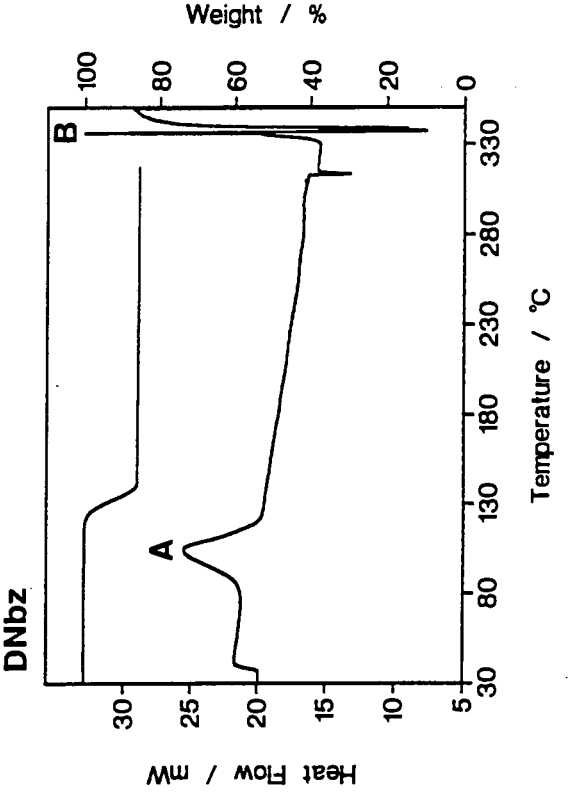

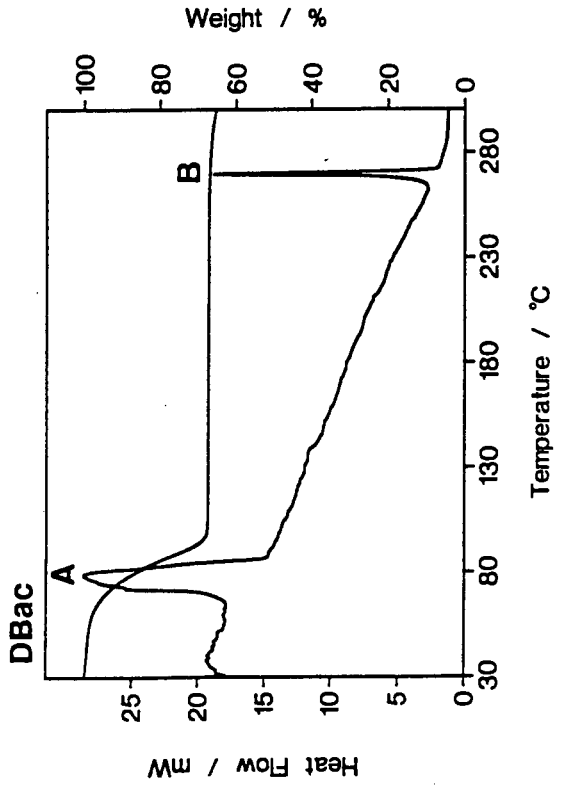

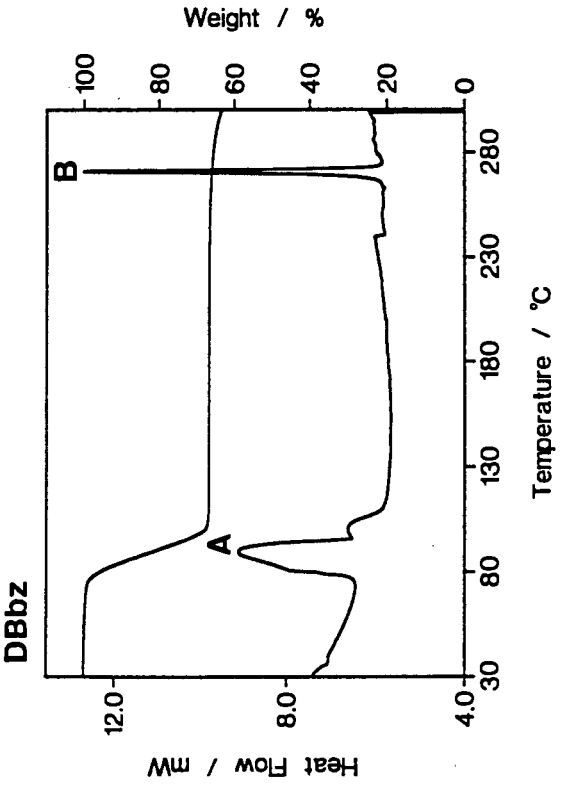

Figure 9.2 *continued*

geometries – the DSC experiments are performed with the sample in a crimped, vented aluminium pan while the TG experiments employ an open platinum sample pan.

The TGA and DSC traces for all the inclusion compounds studied here are shown in Figure 9.2 and are discussed below. The host melting or sublimation endotherm is not commented on in each case, but can be identified as the last peak, unless otherwise stated.

The three inclusion compounds **W14et**, **W14bu** and **W14py** appear to have complex guest-release mechanisms as evidenced by the multiple- or double-peak endotherms A. Endotherm B, in each case, corresponds to the sublimation of the host compound.

The compound **W12py** experiences two well-separated, complex guest-loss events (endotherms A and B) – the endotherm associated with the melting of the host (299-302 °C)[18] is not within the temperature range shown. The host:guest ratio of the inclusion compound is 1:3. Inspection of the TG trace shows that endotherm A corresponds to the loss of two guest molecules per host molecule as a two-step process. The resulting phase appears to be stable from 104 to 140 °C after which the remaining guest molecule is lost (endotherm B). The program HEENY (see Chapter 2) was used to calculate the potential energy environment of each of the three crystallographically independent guest molecules of **W12py**, yielding values of -15.39, -19.19 and -16.61 kcal mol^{-1} for Guests 1, 2 and 3 respectively. As noted in Chapter 3, the nitrogen atom of Guest 2 acts as a hydrogen bond acceptor to one of the host hydroxyl groups. From the above evidence, it is surmised that endotherm A represents the loss of guest molecules 1 and 3 which are less-tightly held within the structure. A rearrangement of the structure occurs to yield a so-called γ-phase inclusion compound with a host:guest ratio of 1:1. The XRD traces of the α-, β- and γ- phases are shown in Figure 9.3. The patterns for the α- and γ- phases were recorded using a Debye-Scherrer powder camera (the film was scanned photometrically) while the β-phase trace was calculated using the program system LAZY PULVERIX. The γ-phase was obtained by heating the β-phase (i.e. crushed crystals of **W12py**) to 130 °C at 10 °C min^{-1} using the TG analyser in order to remove two pyridine molecules per host molecule. Inspection of the three traces confirms that the γ-phase structure indeed differs from that of the α- and β- phases.

Three endotherms (A to C) are associated with the guest-loss process of **W15ch**. Analysis of the TG trace shows that endotherm A corresponds to a phase-change from a 1:2 to a 2:3 (host:guest ratio) inclusion compound. The relatively small endotherms B and C relate to the loss of the remaining guest molecules, while the corresponding TG trace does not resolve the multiplicity of the process.

From their TG traces, the remaining inclusion compounds, with the exception of **DMpy**, do not appear to experience multi-step decomposition processes, . However, two distinct, but relatively closely spaced endotherms (A and B) are observed in the DSC trace for **DPdmso**. It is not known how these endotherms may be associated with the guest-loss process since the TG trace is not stepped. The inclusion compound **DMpy** appears to decompose from a 1:2 (host:guest ratio) β-phase to a 3:2 γ-phase with an onset temperature of about 75 °C. Soon afterwards, this phase reverts to the α-phase with the loss of the remaining guest molecules.

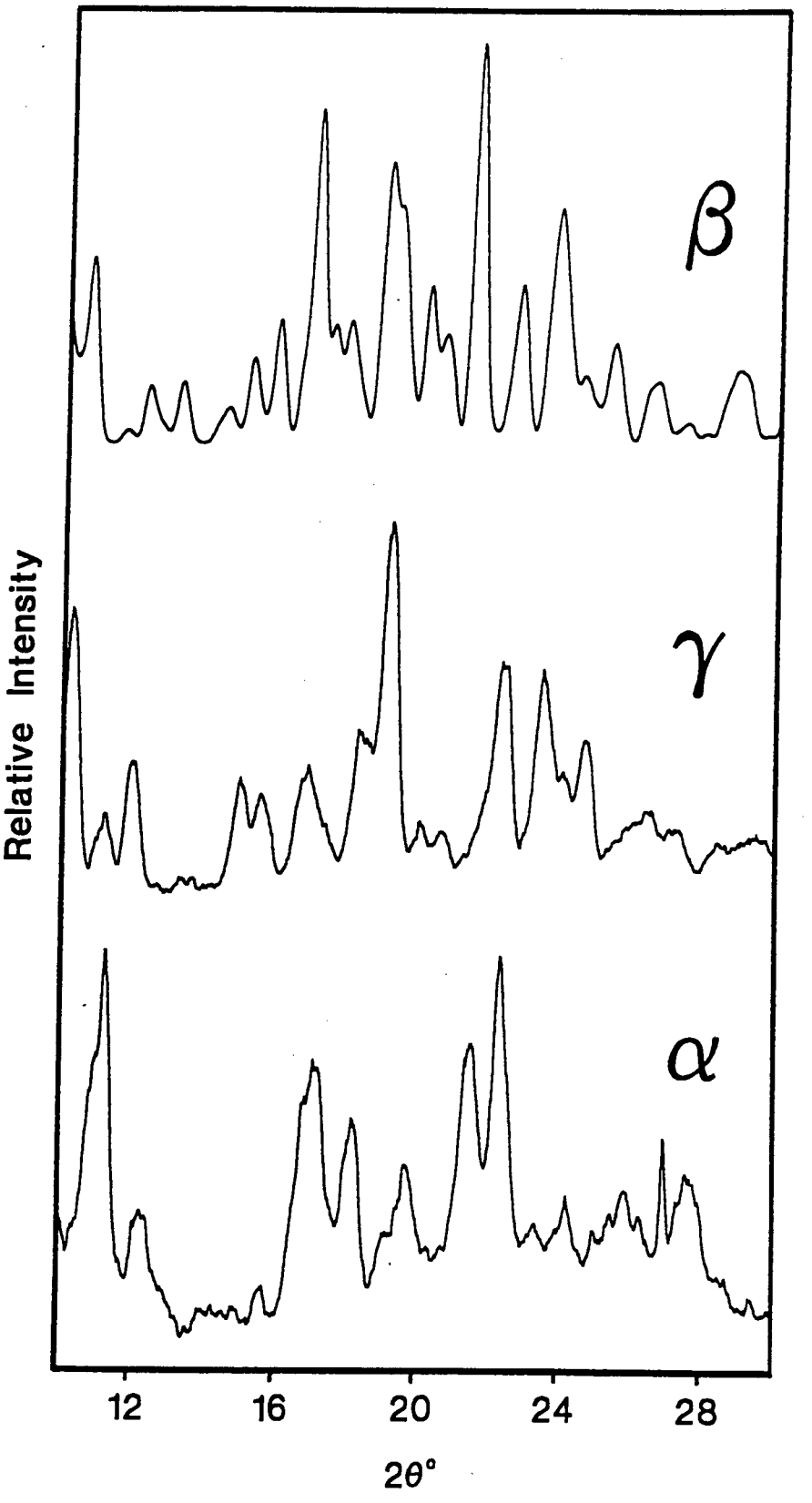

Figure 9.3 XRD traces of the α-, β- and γ- phases formed during the decomposition stages of **W12py**.

Determination of ΔH

A general problem with the determination of thermodynamic and kinetic parameters for a solid-gas reaction is that these parameters are highly dependent on the physical and chemical nature of the atmosphere surrounding the solid. It is postulated that this is so because the surrounding atmosphere influences the mechanism of the reaction. For instance, when an inclusion compound is heated in a vented DSC pan, the guest is volatilised and lost. In a closed pan, the evolved gas exerts a back-pressure on the solid, and the guest-release process may become reversible. As demonstrated in Chapter 8, the influence of atmospheric gases on the reaction cannot be ignored either. Thus, when reporting kinetic or thermodynamic values for a solid-gas reaction, it is imperative that the conditions of measurement be specified.

For the reaction

$$HG_n\,(s,\beta) \quad \rightleftharpoons \quad H\,(s,\alpha) \quad + \quad nG\,(g),$$

we have $K = P^n$ where K is the equilibrium constant and P is the vapour pressure of the guest. So, by combining this relationship with the equations

$$\Delta G^\circ = \Delta H^\circ - T\Delta S^\circ$$

and

$$\Delta G^\circ = -RT \ln K,$$

we get the Clausius-Clapeyron equation:

$$n \ln P = -\Delta H^\circ/RT + \Delta S^\circ/R.$$

Thus a plot of $n \ln P$ vs $1/T$ yields ΔH° and ΔS°.

In order to determine ΔH° using the Clausius-Clapeyron equation as shown above, it is necessary to know the pressure exerted on the host by the guest and to exclude extraneous gases from the system. A dewpoint apparatus has been described to measure the equilibrium of addition compounds of urea with organic guests[18] and vapour pressure measurements have also been carried out on inclusion compounds of deoxycholic acid by means of a torsion-effusion apparatus.[19] However, as part of this study, an apparatus has been devised to allow measurement of the vapour pressure with temperature of a volatile guest resulting from the thermal decomposition of a solid inclusion compound.

Description of apparatus

The system described here uses a personal computer to monitor the guest vapour pressure as a function of temperature when an inclusion compound is heated and cooled. Pressure can be measured electronically by means of a transducer which produces a voltage signal proportional to the pressure at its aperture. This signal can be amplified with a suitable circuit and fed to a computer *via* an analogue-to-digital converter (ADC) interface card. Similarly, temperature can be monitored using a thermocouple. The electronic circuits used to convey the pressure and temperature signals to the microcomputer are described in Appendix C.

The prototype of the system employed a piezoresistive absolute pressure sensor (Sensym LX06015A) with its aperture fixed by means of silicone sealant into a glass tube which was in turn joined to a sample flask (see Photograph 4, Appendix D). However, exposure of these sensors to organic vapours (e.g. diethyl ether, acetone) caused them to fail irreparably. On opening a failed sensor, it was discovered that the thin gold wire contacts to the silicon crystal, which are imbedded in a silicone-based gel, had been pulled free from the crystal thereby causing an open circuit. This was apparently caused by swelling of the gel under the influence of the organic solvent.

Piezoresistive transducers have been used because they are highly sensitive and linear, do not suffer from hysteresis effects and are inexpensive. Their disadvantages include non-suitability for organic vapours and susceptibility to temperature variations. Although transducers which employ a steel membrane are impervious to organic solvents, they suffer from hysteresis effects and are thus not suitable for experiments which require the detection of small changes in pressure.

An indirect method of measuring the pressure, based on the isoteniscope principle, was therefore devised by utilising a U-tube containing mercury which separates the sample flask from the pressure transducer. This design has the double advantage of exposing the transducer only to air and of keeping the transducer outside the oven, thus avoiding the need for temperature compensation of the output signal. The final design of the apparatus is shown diagramatically in Figure 9.4. (also see Photographs 5 and 6 in Appendix D).

Experimental procedure

The sample is placed in the round-bottomed flask (about 2 cm^3 in volume) and cooled on solid CO_2 to prevent its premature decomposition under reduced pressure. Taps 1 and 2 are opened and tap 3 is slowly opened to allow simultaneous evacuation of limbs A and B of the apparatus. When the pressure in the limbs has been reduced to between 0 and 1 mmHg, taps 1 and 2 are closed, the solid CO_2 is removed and the pressure of the sample is allowed to equilibrate to its ambient temperature value. An electronic circuit, the operation of which is described in detail in Appendix C, was designed in order to ensure that the pressure in limb B is always equal to that in limb A. Essentially, the circuit consists of a window comparator which controls the venting and evacuation of limb B to compensate for changes in pressure in limb A.

Limb A of the apparatus is situated in an oven consisting of a wooden box lined internally with polystyrene foam covered with aluminium foil. The oven also contains a 500W lamp as a heat-source, a circulating fan and a K-type thermocouple (T_1). A computer program (described in more detail in Appendix A) was written to partially control the apparatus and to monitor the thermocouple and pressure transducer .

During an experiment the temperature in the oven is read via T_1 and controlled by appropriate switching of the lamp. It had been established, using a specially designed sample flask with a thermocouple sealed into its interior, that the temperature-difference between the oven and the sample flask is negligible.

An experiment always starts with the heating cycle. The temperature of the oven is incremented by a fixed amount (software-selectable) and this new temperature is

A sample limb
B transducer limb
C 500W lamp
D oven
E pressure transducer
F circulating fan
G optical source and detector unit
H solenoid valve 1
J solenoid valve 2
K buffer flask
L to vacuum pump
M sample flask
T1 thermocouple

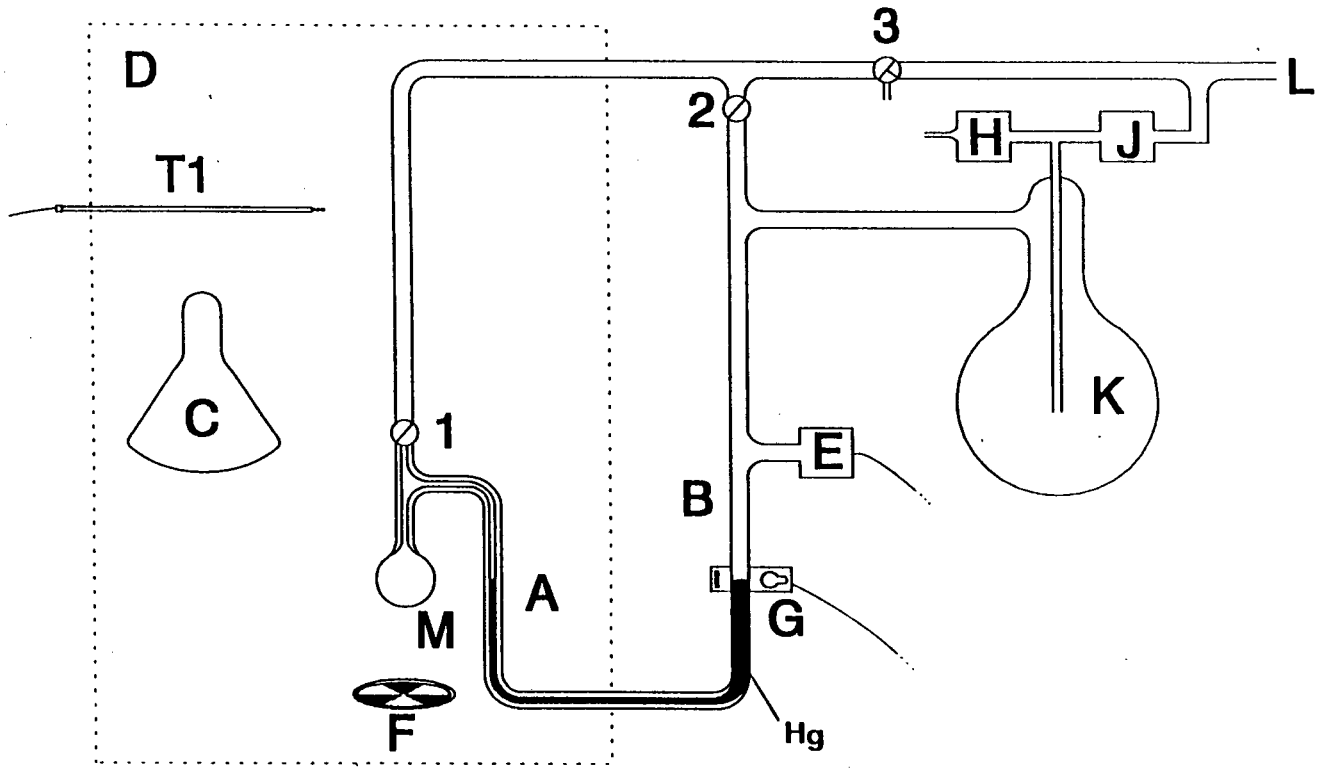

Figure 9.4 Diagram showing the apparatus used to measure pressure-temperature relationships for reversible solid/gas inclusion reactions.

maintained for a fixed period of time (also selectable) after which the pressure and temperature are recorded. This process is repeated until the pressure of the system exceeds 700 mmHg, or a maximum temperature (selectable) has been reached. The software then reverses the process and records the pressure/temperature data for cooling. Thus a typical run would consist of pressure/temperature readings for both heating and cooling. If the pressure versus temperature curves for both the heating and cooling cycles are significantly similar, they can be assumed to represent true equilibrium of the process being investigated. During an experiment, the pressure versus temperature values are displayed graphically (in real-time) on the computer monitor as well as the plot of ln P vs 1/T. These values are also written to the hard disk of the computer for subsequent analysis. The precision of the apparatus is ±1 mmHg in pressure and 0.2°C.

Experimental results

In order to test the accuracy of the apparatus, a small quantity of carbon tetrachloride was placed in the sample flask and degassed by exposure to low pressure for several minutes. The vapour pressure vs temperature curve was recorded continuously whilst heating from 30 to 65 °C at 0.5 °C min^{-1} and then cooling at the same rate to 30 °C again. Figure 9.5 shows the plot of ln P vs $1000/T$ which has a correlation coefficient of 0.99994 and yields a value of 29.81(7) kJ mol^{-1} for the enthalpy of vapourisation. This is in excellent agreement with the value of 30.0 kJ mol^{-1} reported by Kaye and Laby.[21]

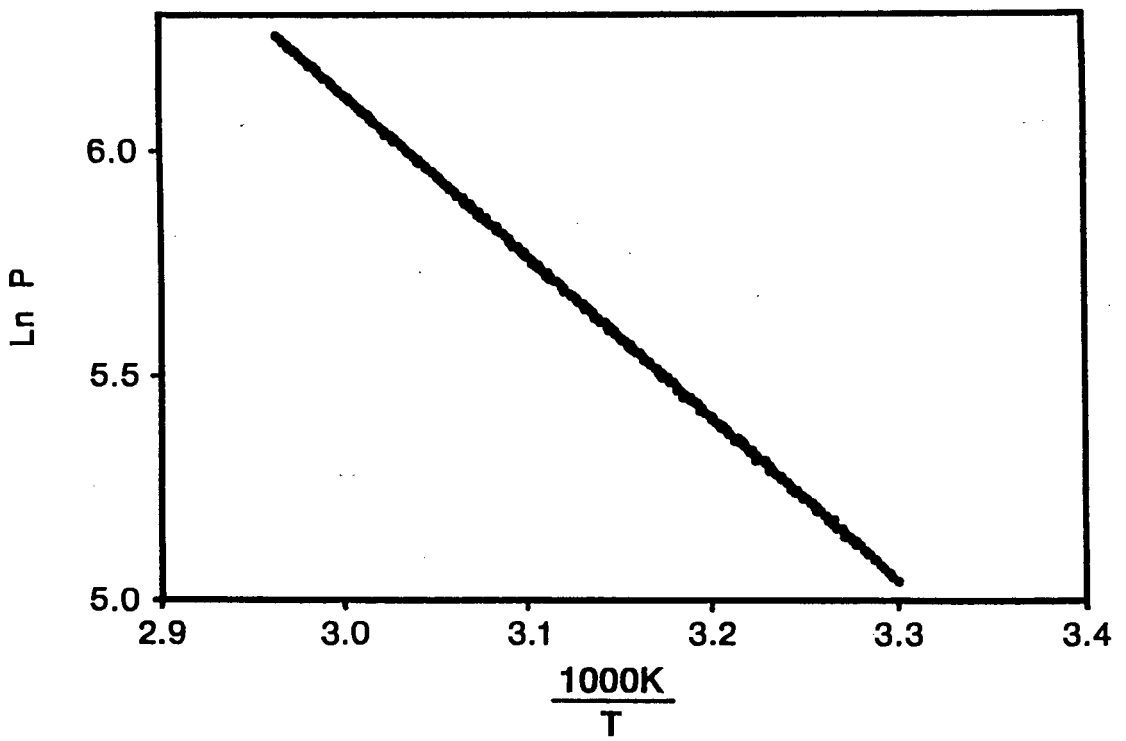

Figure 9.5 Plot of ln P vs $1000/T$ for carbon tetrachloride – several hundred data points are shown.

Slow evaporation of a solution of *trans*-9,10-dihydroxy-9,10-diphenyl-9,10-dihydroanthracene in acetone yielded crystals of **DPac** in the size range 0.1 to 0.5 mm. These crystals were dried and placed in the sample flask of the apparatus and cooled on solid CO_2. The system was evacuated and then allowed to warm to room temperature (c.a 28 °C). After several hours, the pressure equilibrated to about 165 mmHg. The sample was heated to 52 °C and cooled again to room temperature. Temperatures were incremented or decremented by 4 °C and kept at each temperature for 180 minutes before recording the pressure. The plot of 2 ln P versus $1/T$ for this experiment is shown in Figure 9.6.

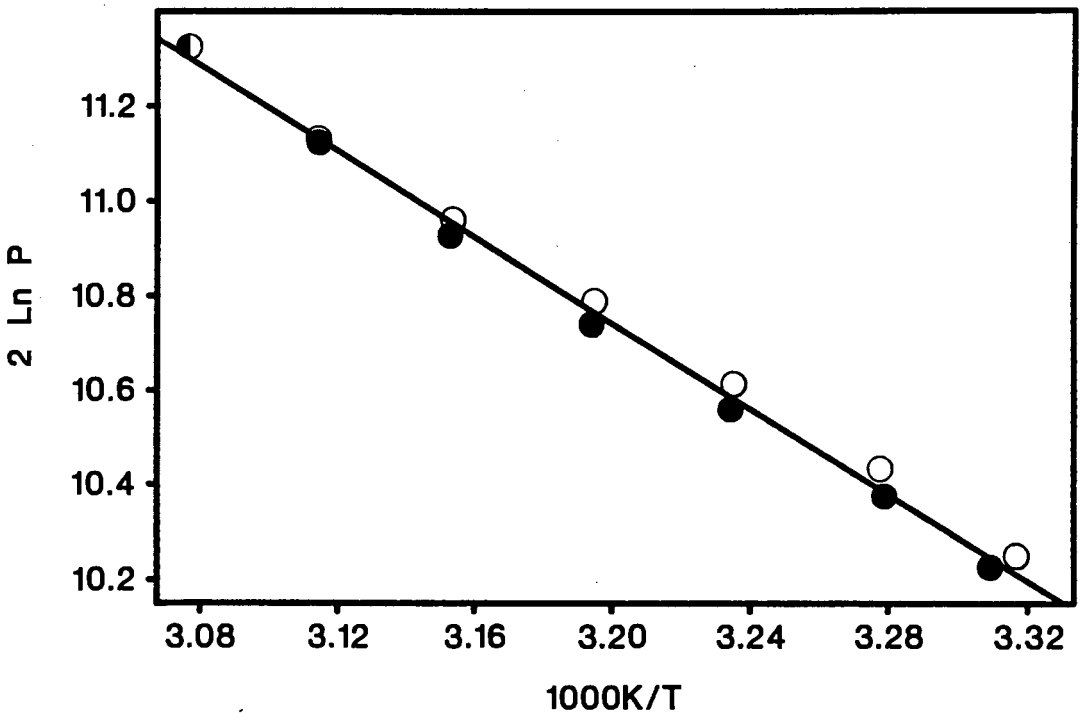

Figure 9.6 Plot of 2 ln P vs $1000/T$ for **Dpac** - black circles, heating; clear circles, cooling.

It is evident that equilibrium conditions were not completely maintained during the course of the experiment since the points recorded whilst heating are not coincident with those for cooling. Nevertheless, the heating and cooling data were analysed together using the Clausius-Clapeyron equation for the reaction

$$H \cdot Acetone_2\ (s,\beta) \rightleftharpoons H\ (s,\alpha) + 2Acetone\ (g),$$

yielding apparent values of ΔH° = 37.3(8) kJ mol^{-1} and ΔS° = 209(3) J K^{-1} mol^{-1} for the guest-release reaction.

This experiment had been performed several times using a temperature increment of two degrees and hold times of 30, 60 and 120 minutes. However, the resulting heating and cooling data showed that these hold times are not long enough to allow true equilibrium to be reached. Intact rather than ground crystals were used

because grinding results in rapid guest loss. However the problem with large crystals is that they take longer to reach equilibrium.

The crystals were removed from the sample flask and inspected under a microscope. They appeared to have clear cores which were surrounded by an opaque crust which could easily be flaked off. It is suggested that the crusts consist of decomposed outer layers of the original crystals, while the clear cores are the unreacted β-form of the inclusion compound.

The apparatus described yields enthalpy (and entropy) values for the guest-release reaction of inclusion compounds with volatile guests. Modification to measure pressures greater than one atmosphere and temperatures of up to 300°C can easily be made by using a different transducer and an appropriate oven. The apparatus could also be improved by developing a method of crushing the crystals once they have already been loaded into the sample flask and the system degassed.

Structure-reactivity relationships of the compound DPac

The inclusion compound **DPac** has been subjected to a kinetic analysis of both its inclusion and decomposition reactions (see Chapter 8). In addition, ΔH^{o} for the guest-release reaction has been evaluated in this chapter. In order to attempt to relate the structure of the compound to its reactivity in the solid-state, it is necessary to inspect the relative positions of the host molecules before and after the reaction. It has been shown, using XRD methods, that the solid-gas decomposition product of the β-form is identical to that of the α-form grown by slow evaporation of a solution of *trans*-9,10-dihydroxy-9,10-diphenyl-9,10-dihydroanthracene in benzene (see Figure 8.15).

The atomic coordinates of the α-form[22] were extracted from the Cambridge Structural Database in order to produce a packing diagram. Figure 9.7 shows the packing, viewed from the same direction with respect to the host molecule, of the structures (a) **DPac**, the β-phase inclusion compound with acetone as the guest, (b) the α-form of the host compound and (c) the β-phase of **DPac** with the guest molecules omitted (i.e. the speculative β_0-phase) . Both the α- and β-phase structures crystallise in the space group $P\bar{1}$ with one host molecule per unit cell. Careful inspection of the diagram shows that the host molecules in the α-phase pack with their phenyl rings arranged to form an undulating column. For the purposes of this discussion, the host molecules themselves can be said to form columns parallel to the plane of the page in the vertical direction. When the β-phase is formed, the shaded column of host molecules moves relative to the unshaded column in order to accommodate the guest molecules, but the relative orientation of the host molecules within a column does not change significantly. The formation of the β-phase is also accompanied by a small rotation about the bond C(1)–C(11) (see Chapter 4 for the numbering scheme of the host molecule). The torsion angle C(16)-C(11)-C(1)-O(1) changes from 2° in the α-phase to -12° in the β-phase.

The movement of one column of host molecules relative to another, with concomitant twisting of the phenyl moiety, may be regarded as the reaction pathway of the phase change from the α- to the β-phase. It has been demonstrated that this phase change is reversible since the α-phase gives rise to the β-phase on exposure to acetone vapour and this phase in turn reverts to the α-phase when the inclusion compound decomposes.

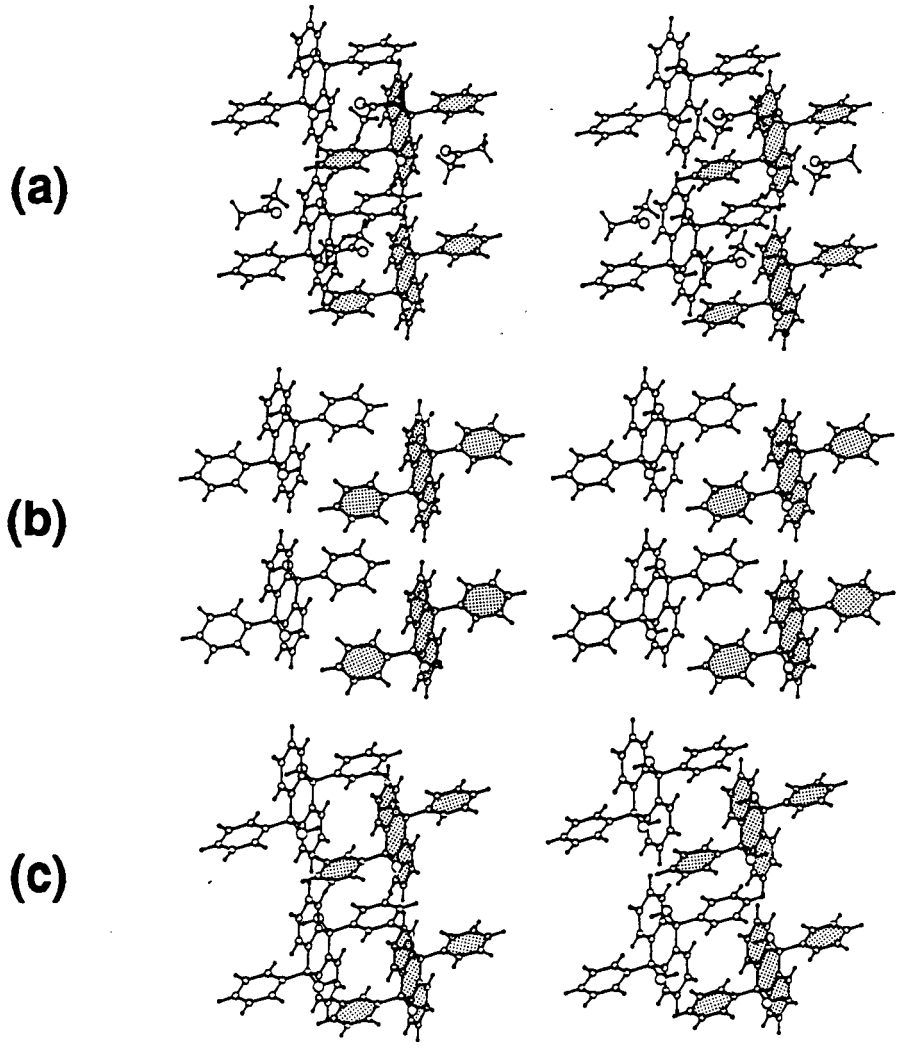

Figure 9.7 Stereoviews showing the molecular structures of (a) **DPac**, the β-phase of Host 4 with acetone as the guest, (b) the α-phase of Host 4 and (c) **DPac** with the guest molecules omitted.

References

1 W.W. Wendlandt, "Thermal Analysis", Third Edition, Wiley-Interscience, New York, 1986

2 M.E. Brown, "Introduction to Thermal Analysis", Chapman and Hall, London, 1988

3 B. Wunderlich, "Thermal Analysis", Academic Press, Boston, 1990

4 E.L. Charsley and S.B. Warrington (Eds), "Thermal Analysis - Techniques and Applications", The Royal Society of Chemistry, Cambridge, 1992

5 M.E. Brown and A.K. Galwey, Anal. Chem., 1989,61,1136

6 H. Anderson, *Thermochim. Acta*, 1992,**203**,515

7 A.R. Salvador and E.G. Calvo, *Thermochim. Acta*, 1992,**203**,67

8 J. Malek, *Thermochim. Acta*, 1992,**200**,257

9 R.K. Agrawal, *Thermochim. Acta*, 1992,**203**,93

10 R.K. Agrawal, *Thermochim. Acta*, 1992,**203**,111

11 T.P. Prasad, S.B. Kanungo and H.S. Ray, *Thermochim. Acta*, 1992,**203**,503

12 I.C. Hoare and H.J. Hurst, *Thermochim. Acta*, 1992,**203**,127

13 J. Malek and J.M. Criado, *Thermochim. Acta*, 1992,**203**,25

14 H.G. McAdie, *Can. J. Chem.*, 1963,**41**,2137

15 H.G. McAdie, *Can. J. Chem.*, 1960,**44**,1373

16 S.A. Bourne, L.R. Nassimbeni, E. Weber, and K. Skobridis, *J. Org. Chem.* 1992,**57**,2438

17 S.A. Bourne, L. Johnson, C.F. Marais, L.R. Nassimbeni, E Weber, K. Skobridis and F. Toda, *J. Chem. Soc. Perkin Trans* 2,1991,1707

18 E. Weber, K. Skobridis, A. Wierig, L.J. Barbour, M.R. Caira and L.R. Nassimbeni, *Chem. Ber.*, 1993,**126**,1141

19 O. Redlich, C.M. Gable, A.K. Dunlop, and R.W. Millar, *J. Amer. Chem. Soc.*, 1950,**72**,4153

20 V. Piacente, and G. De Maria, *Ric. Sci.*, 1960,**39**,545

21 G.W.C. Kaye and T.H. Laby, "Tables of Physical and Chemical Constants", Longman, London, 1973

22 F. Toda, K. Tanaka, S. Nagamatsu and T.C.W. Mak, *Isr. J. Chem.*, 1985,**25**,346

Chapter 10 Discussion and Conclusion

As stated in Chapter 1, the host molecules selected for this study possess molecular planes with bulky substituents and opposing hydroxyl moieties as probes for possible coordination by means of hydrogen bonding. Selected characteristics of the inclusion compound structures elucidated here are summarised in Table 10.1.

Table 10.1 Selected characteristics of the inclusion compound structures elucidated in this study

Cmpd.	Guest	H:G	Spc. grp	guest encapsulation
W14et	ethanol	2:1	$P\bar{1}$	cavities
W14bu	*n*-butanol	2:1	$P\bar{1}$	cavities
W14py	pyridine	1:1	P2/n	channels
W12py	pyridine	1:3	$P\bar{1}$	cavities and channels
W15ch	cyclohexanone	1:2	$P2_1/c$	channels
DPac	acetone	1:2	$P\bar{1}$	channels
DPdek	diethyl ketone	1:1	$P\bar{1}$	cavities
DPdmso	DMSO	1:2	$P2_1/n$	channels
Dp2bu	(±)2-butanol	1:1	$P\bar{1}$	cavities
DMac	acetone	1:2	$P\bar{1}$	channels
DMde	diethyl ether	1:2	$P2_1/n$	channels
DMpy	pyridine	1:2	$P2_1/n$	channels
DBac	acetone	1:4	$P2_1/c$	wide channels
DBde	diethyl ether	1:2	$P2_1/a$	wide channels
DBbz	benzene	1:3	$P2_1/c$	crisscross channels
DNbz	benzene	1:1	$P\bar{1}$	cavities

In an attempt to identify general trends relating to the inclusion properties of some of the host compounds, the effects of two types of structural modifications were investigated:

1 The same host was used to form inclusion compounds with structurally related guest molecules. The inclusion compounds **W14et** and **W14bu** both crystallise in the space group $P\bar{1}$ with the alcoholic guest molecules situated in cavities. However, in the former structure the ethanol molecules pack with their oxygen atoms close together with only one guest molecule per cavity, whereas in the latter structure the oxygen atoms are well-separated and each cavity accommodates two guest molecules. Furthermore, few similarities exist between the structures **DPac**, **DPdek** and **DPdmso**. However, inspection of Figures 4.7(a)

and 4.11 shows that the packing of the guest molecules is remarkably similar in the structures **DPdek** and **DP2bu.**

2 The same guest was included by different 9,10-substituted-9,10-anthracenediols. Inclusion compounds of acetone were formed with Hosts 4, 5 and 6 and these again yielded few structural similarities. Diethyl ether was included by Hosts 5 and 6 and, although the orientation of the guest molecule relative to that of the host molecule is similar in the two structures, the guest channels in the two structures are geometrically different. Comparison of Figures 6.9 and 6.13 shows that the inclusion compounds **DBbz** and **DNbz** have vastly different structures, while it is interesting to note that Hosts 4 and 5 do not include benzene.

Thus the evidence presented here indicates that the crystal structure of an inclusion compound employing the type of host compound considered in this study cannot easily be predicted. Since hydrogen bonding generally does occur when the guest has donating or accepting ability, the presence of the host hydroxyl moiety indeed has a stabilising influence on the resulting structure. This is illustrated by the observation that although diethyl ether and pentane are of similar size and shape, Host 6 forms a relatively stable inclusion compound with the former (even as a solid-gas reaction) while the latter is not included. However, since Hosts 6 and 7 include benzene and Hosts 4 and 5 do not, it is suggested that the introduction of bulky substituents also plays a major role in the inclusion process.

Much of the current work in inclusion chemistry is devoted to the synthesis of targeted host compounds which will include a specific guest molecule. The host compounds are tested simply by establishing whether they form inclusion compounds. However, this thesis addresses the more fundamental problem of relating the structure of an inclusion compound to the strength of the host-guest interactions. The enthalpy change which accompanies the decomposition of an inclusion compound is fundamental to the understanding of the host-guest interaction and is a composite function made up of the endothermic term of the guest release and the concomitant change in the structure of the host, which almost invariably occurs. These terms cannot generally be separated and most physical methods measure a combined enthalpic change. Differential scanning calorimetry is often used for this purpose, but the results are inaccurate because the method suffers from various experimental difficulties. An apparatus was therefore devised to yield accurate ΔH° and ΔS° values of the guest-release reaction. This device was used to determine ΔH° and ΔS° of the guest-release reaction of a selected inclusion compound and shown to be a practical solution to the known problems related to the measurement of these quantities.

In addition to their decomposition, this thesis discusses aspects of the kinetics of formation of inclusion compounds as solid-gas reactions. One such example was studied in detail and proved to be particularly rewarding because it showed apparent anti-Arrhenius behaviour (i.e. the reaction occurred faster as the temperature was decreased). The decomposition of this same inclusion compound was also studied by isothermal kinetic methods and the activation energy of decomposition estimated.

Finally, an attempt was made to explain thermal decomposition in terms of structure. Molecular mechanics was employed to estimate the relative energies of

guest molecules which are crystallographically non-equivalent. Using the technique of atom-pair potentials it has been demonstrated that the different guest energies can be related to their topologies and their decomposition patterns have thus been explained. It has been shown that it is possible to evaluate host-guest interactions and to justify the subsequent thermal stability of inclusion compounds in terms of the topology of the crystal structures.

This thesis therefore makes a contribution to the understanding of structure-reactivity relationships of organic inclusion compounds.

Molecular recognition in the form of a solid-gas inclusion reaction has far-reaching implications for the development of sensing devices in the future. This area of research depends firstly on the success of synthesising guest-specific host compounds and secondly on a better understanding of the solid-gas inclusion process. Although the former aspect has received much attention, relatively little is known about vapour inclusion. This is mostly due to the difficulties involved in making the necessary measurements. However, it is suggested that the balance apparatus described in Chapter 8 can be used to test whether or not a host compound will form an inclusion compound with a specific gaseous guest. Using this apparatus, the effects of different atmospheric conditions on the inclusion reaction can also be evaluated. Reference is made in Chapter 1 to recent experiments which employ a quartz crystal coated with a suitable host compound. It is reported that inclusion of a gaseous guest by the host causes the oscillation frequency of the crystal to change. It may be possible to exploit this phenomenon as an alternative to the balance apparatus described here. In order to study the kinetics of a solid-gas inclusion reaction, the oscillation frequency of the quartz crystal could be monitored as a function of time, thus yielding α-time data for the reaction.

Appendix A

During the course of this study it was necessary to develop several computer programs to aid in the acquisition, analysis and presentation of data. The most useful of these programs, written using the Turbo Pascal Version 6 programming language,[1] are described here. At least a rudimentary understanding of the IBM personal computer system by the reader is assumed.

In order to run any of these programs, one requires an IBM compatible PC (preferably 80286 or faster) with VGA graphics capability, a Microsoft or Mouse Systems (or compatible) mouse and a hard disk. The programs BALANCE and PT require additional interfacing equipment for full operation and details will be provided in the relevant sections below. A numeric co-processor, a pen-plotter or laser printer able to interpret Hewlett-Packard Programming Language (HPGL) commands and/or an Epson compatible dot-matrix printer are also desirable.

These programs are included on the diskette attached at the end of this volume. The source code, compiled programs and sample data are provided where applicable (see the final section of this appendix for access instructions).
The programs are all mouse-menu driven and the options, which are generally self-explanatory, are selected by placing the mouse pointer on the desired menu "button" and clicking the left mouse button.

A useful feature of the Turbo Pascal programming language is that it can be extended using *units* (see Turbo Pascal Version 6 Programmer's Guide). These units consist of often-used definitions, functions and procedures, in compiled form, which can be created by the programmer. Several units have been developed by the author in order to deal with mouse input, general graphics mode operations, data acquisition etc. The units required to compile the programs described below are also included on the diskette.

A comprehensive description of all the programs would be a substantial undertaking. Thus, for the sake of brevity, only essential details regarding their operation will be discussed below.

MOLMAP was developed in order to explore the shapes of the voids resulting from the removal of the guest atom coordinates from an inclusion compound crystal structure. The program reads a SHELX-76 (see Chapter 2) input file-type (with minor changes) and allows one to plot "slices" through the unit cell. A slice is a plane parallel to any of the cell faces and can be plotted as viewed along its normal direction or in projection along the cell axis which is cut by the slice.
A typical use of the program involves prior deletion of the guest atom cards from a SHELX-76 input file. In addition, MOLMAP requires the SYMM card of the input file to be edited in order to generate *all* the symmetry-related atoms from the asymmetric unit. Each symmetry operation for the space group (other than x,y,z) must be represented by a SYMM card which defines the appropriate (4 × 4) transformation matrix $\mathcal{Q}$. The required SYMM card format is as follows:

"SYMM Q_{11} Q_{12} Q_{13} Q_{21} Q_{22} Q_{23} Q_{31} Q_{32} Q_{33} q_1 q_2 q_3"

such that

$$\mathcal{Q} = \begin{pmatrix} Q_{11} & Q_{12} & Q_{13} & q_1 \\ Q_{21} & Q_{22} & Q_{23} & q_2 \\ Q_{31} & Q_{32} & Q_{33} & q_3 \\ 0 & 0 & 0 & 1 \end{pmatrix}$$

and the transformed coordinates x′,y′,z′ are obtained by

$$\begin{pmatrix} x' \\ y' \\ z' \\ 1 \end{pmatrix} = \mathcal{Q} \begin{pmatrix} x \\ y \\ z \\ 1 \end{pmatrix}$$

Using the program, the axis to be cut is selected and the height of the cut (or the fractional height) above the cell origin is entered. The slice can then be plotted on screen or to a file which can later be plotted using a pen plotter or a laser printer. Each slice shows the intersection of the unit cell (as lines) and atoms (as circles) with the chosen plane. Thus a series of slices through the unit cell can show the three-dimensional shape of channels or cavities formed by the host molecules.

These results can also be achieved using the computer program OPEC[2] which primarily performs organic packing energy calculations. However, using OPEC to produce maps of occupied space in a crystal structure can be tedious since its output consists of distorted maps which need to be transformed manually to account for the unit cell geometry. In addition to being interactive, fast and user-friendly, MOLMAP produces maps with little or no distortion and was used in the preparation of many of the diagrams shown in Chapters 3 to 6 as follows:

> A unit cell projection with only the guest molecules included is produced using PLUTO (see Chapter 2). A MOLMAP projection viewed from the same direction (and at a suitable height above the cell origin) is then plotted to show the space occupied by the host molecules. The two projections can be overlaid on a light box and the channels or cavities formed around the guest molecules can be traced out.

The menu options include:

QUIT	exits the program;
Data File	allows selection of a *filename*.INS data file, reads the cell data and the atomic coordinates and assigns van der Waals radii to the atoms;
View Height (Å)	sets the height in Å of the slice above the cell origin;
Cut Axis at:	sets the height of the slice above the cell origin as a fraction of the view-axis, i.e. the axis to be cut;

Scale (p/Å)	sets the scale of the diagram in screen pixels per Å (a scale of 25 p/Å is equivalent to 1 cm/Å for a hard-copy plot on A4 paper - see *PLOT* option);
H-Pack	sets the range of unit cells to be displayed in the horizontal direction;
V-Pack	sets the range of unit cells to be displayed in the vertical direction;
View down	toggles the view-axis;
Cell	toggles the drawing of the intersection of the cell with the plane;
Labels	toggles the labelling of the atoms;
Projected	toggles between plotting the slice in projection down the view-axis or down the normal to the plane of the slice;
SHOW	displays the slice in the diagram box;
PLOT	prompts the user for a plot-file name and plots the slice to this file in HPGL format;
PrnScrn	prints the image in the diagram box to an Epson compatible dot-matrix printer attached to the computer's parallel port LPT1.

The atoms in a crystal structure are assumed to be spheres, and the intersection of a sphere and a plane is a circle of radius $a = (r^2 - d^2)^{½}$ where r is the van der Waals radius of the atom and d the distance of the atomic centre from the plane. The centre of the circle will be at the intersection of the normal from the atom centre to the plane. The program recognises the following elements : H, B, C, N, O, F, Si, P, S, Cl, As, Se, Br, Te and I, and their van der Waals radii are taken from OPEC.[2] Up to 800 atoms per unit cell can be accommodated.

When plotting a slice in projection, the intersection of the unit cell with the plane is shown with the two cell axes and the angle between them corrected for non-orthogonal viewing. No correction is made for the intersection of the plane with the atoms which should then be represented as ellipses instead of circles. However for angles of 90 ± 20 ° between the plane and the view-axis the overall shape of the cavity or channel should not be affected significantly.

BALANCE serves as the data-logging software for the vacuum balance apparatus described in Chapter 8. The Mettler balance must be configured to send weight readings continuously at a baud rate of 9600 bit per second with even parity, seven data bits and one stop bit per byte. In addition, the program assumes that the mouse is connected to COM2 and the balance to COM1 of the PC. Before envoking the program, the following MS-DOS MODE command *must* be executed:

"MODE COM2:9600,n,7,1"

in order to synchronise communication between the balance and the PC.
Once **BALANCE** has been envoked, the following menu options are available:

QUIT	exits the program;
Data File	to enter a name for the disk file to which the data will be saved (this values defaults to "NONE" in which case the data are written to a file called "DEFAULT.M");
S/Reading	the time interval in seconds between readings written to disk;
Offset/mg	the mass in mg to be added to the reading sent from the balance (used to counter the buoyancy effect);
Gain/Loss	toggles between plotting weight gain or loss as a function of time;
Start Expt.	starts reading the balance and plotting weight change with time;
Redraw	redraws the plotting area with the current axis limits;
PrnScrn	prints the graphics screen to a Epson-compatible dot-matrix printer;
Other Files	allows selection of up to six data files from disk and displays them in the plotting area with the current axis settings;
Title	to enter a title for the experiment which will also be written to the first line of the data file;
Min Mass	the ordinate minimum for the plotting area;
Max Mass	this should be the maximum expected mass change for the experiment and will be written to the second line of the data file for subsequent rescaling of weight readings to α-values (the ordinate maximum will be 110% of this value);
Max Time	the maximum duration of the experiment in minutes (and the maximum abscissa value for the plotting area).

Before starting an experiment, a data file name must be entered as well as the values which define the plot area. The balance is tared when the sample pan is levitating and after the balance displays a stable reading. When the guest liquid is tapped into the reaction vessel, the *Start Expt.* option is selected and the program continuously monitors the balance until the escape key is pressed or the desired maximum time has been reached. Weight change with time is displayed in real-time on the computer monitor. The data files created by this program are given the extension ".M" and can be converted to α-time data by dividing each weight reading by the maximum mass value.

KINETIC was written in order to evaluate the α-time data produced by the program BALANCE described above. the menu options are as follows:

QUIT	exits the program;
Data File	reads an α-time data file and plots the values on screen;
PrnScrn	prints the graphics screen to a Epson-compatible dot-matrix printer;
Fit Data	displays another menu where the options represent the different kinetic functions given in Table 8.1. Choosing any of these options results in a display of $f(\alpha)$ versus time with its linear best-fit line and the parameters r, a and b (the correlation coefficient, the ordinate intercept and the slope

respectively). The results of the application of the functions to the data can thus be inspected visually, and when the most-acceptable function has been selected, the main menu can be reinstated using the *EXIT* option;

Reset Data re-plots the α-time curve;

Reset fn. re-plots the selected function over the entire time range;

Window Allows "zooming" of the function plot. The mouse pointer is confined to the plot area and pressing the left mouse button selects the first corner of the zoomed window. The button is held down while the mouse is moved to select the opposite corner of the window. On releasing the mouse button, the zoomed portion of the plotted function is replotted together with its best-fit line and parameters. The best-fit line is applicable only to the portion of the function within the plotting area, so this option is used to evaluate the linearity of selected sections of the plot of $f(\alpha)$ versus time.

The interactiveness of the program makes it fast and easy to use. In addition, visual inspection of the f(α) vs time curves is desirable since possible changes in mechanism during the course of the reaction can thus be identified.

PT serves as the data-logging and partial-control software for the pressure/temperature measuring apparatus described in Chapter 9. The microcomputer must be installed with a PC-30 (Boston Technology) interface card which has sixteen ADC input channels and twenty four I/O switching channels. Two ADC channels are used to read the thermocouple and pressure transducer signals while switching of the light bulb and disabling/enabling of the solenoid valves is effected via three of the I/O lines. A Turbo Pascal unit was written to conveniently control the functions of the interface card.

The following menu options are available:

QUIT exits the program;

Data File to enter a name for the disk file to which the data will be saved (this values defaults to "NONE" in which case the data are written to a file called "DEFAULT.PT");

Start Expt. starts reading the pressure and temperature and controls the heating of the sample;

Redraw redraws the plotting area with the current axis limits;

PrnScrn prints the graphics screen to a Epson-compatible dot-matrix printer;

Other Files allows selection of up to six data files from disk and displays them in the plotting area with the current axis settings;

Title to enter a title for the experiment which will also be written to the first line of the data file;

Min Temp. the abscissa minimum for the plotting area;

Max Temp	the abscissa maximum and the temperature at which the cooling cycle should start;
Min Press.	the ordinate minimum;
Max Press	the ordinate maximum.

When *Start Expt.* is selected, the user is prompted to enter the temperature increment for the pressure readings and the hold-time (see Chapter 9). The program disables the vacuum valve and starts the heating the oven until the first multiple of the temperature increment higher than the starting temperature has been reached. This temperature is maintained for the specified hold-time after which the pressure and temperature are recorded. The temperature increment and hold procedure is repeated until the pressure exceeds 700 mmHg, or the maximum desired temperature has been reached. The vacuum valve is disabled and the vent valve enabled as the cooling procedure starts. The cooling cycle is the reverse of the heating cycle and the oven is allowed to cool by convection when necessary. When the initial temperature has once again been reached, both valves are enabled and the data file is closed. The vacuum and vent valves are disabled during the heating and cooling cycles respectively to prevent oscillation of the mercury column as a result of slight over-venting or over-evacuation of the system.
During an experiment, data are displayed on the computer monitor as a plot of pressure vs temperature and as a plot of ln(pressure) vs 1000/(temperature).

BONDS reads a SHELX-76 output file and allows quick evaluation of bond lengths and angles and torsion angles using the mouse. Up to 99 positions of atoms and peaks (from the difference Fourier map) are read by the program and the origin of the cell is appended as an extra position. The following main menu options are available:

QUIT	exits the program;
LST File	allows selection of a SHELX-76 output file with the extension ".LST". The cell geometry is read together with the refined atomic positions of the asymmetric unit and peak positions from the difference Fourier map. The names of the atoms and peaks are printed in a large rectangle on screen for later selection as menu "buttons";
Bond length	confines the mouse pointer to the atom rectangle and allows selection of two positions. The distance between these positions is then displayed and the user is once again prompted to select positions. The right-hand mouse button is pressed to exit this function and return to the main menu;
Bond angle	as above, but three positions (p1, p2 and p3) are selected and the angle p1-p2-p3 displayed;
Torsion angle	as above, but four positions (p1, p2, p3 and p4) are selected and the torsion angle p1-p2-p3-p4 displayed;
XFORM	Allows transformation of the coordinates of any position according to the simple transformation matrix shown in the upper right corner of the screen. This matrix can be defined by

	the changing the "+" and "×" coefficients which operate on the three cell coordinates of the original position as read from the data file;
RESET	Resets the coordinates of positions to their original values;
Co-ords	Displays the current coordinates of positions;

This program proved to be useful during structure solution since peaks in the difference Fourier map could easily be evaluated as being possible positions of atoms missing from the structure model.

LINESCAN monitors the voltage output of a METEX M-3650CR multimeter equipped with a serial communication interface. The meter is used to monitor the photodetector voltage while XRD film is continuously scanned using an Enraf-Nonius densitometer to which is attached a motor drive from an old chart recorder. The mode switch of the multimeter must be set to the 0-200 mV DC range and its serial interface attached to COM2 of the PC. The PC must be set (using the DOS MODE command) to expect communication at 1200 bps, no parity, seven data bits and two stop bits. The function relating voltage (V in millivolts) to peak intensity (I) is

$$I = 298.3/\ln(V) - 64.2;$$

and was derived empirically by scanning a Kodak projection print scale. The 2θ scale is a function of the scanning time and the selected gear of the motor drive. Seven different scanning speeds can be accommodated. Since the resulting intensity vs 2θ data are based on an unknown starting value of 2θ owing to difficulties in synchronising the start of a scan with a specific position on the film, another program was written to correct the data.

SCANCON reads a LINESCAN output file (with the extension ".FLM") and displays the data on screen as a plot of intensity versus the incorrect 2θ values. It is necessary for the film to have been scanned across the $2\theta = 0$ point to yield two sets of matching, approximately mirrored peaks. The user is prompted to indicate the positions of two corresponding (preferably strong) peaks using the mouse. The point midway between these peaks corresponds to $2\theta = 0$. Of the two potential traces on either side of this zero point, the most distinct one can be chosen. The corrected data is then written to disk as a 2-column ASCII file with the extension ".XRD'. This file can be read and displayed using the program XRDPLOT.

XRDPLOT reads calculated and/or experimental XRD data files and produces publication-quality plots in HPGL format (e.g. Figures 8.12, 8.15 and 9.3). Three types of input data are supported - one of calculated and two of experimental data. One calculated and one experimental file can be displayed and plotted together for the purposes of comparison. The calculated input file is produced using LAZY PULVERIX. XRDPLOT reads the peak intensities and fits Gaussian peaks to the

data. These peaks are summed to produce a traces. The experimental input files can be either of the type produced by the computer-controlled XRD system housed in the Geochemistry Building at the University of Cape Town, or of the type produced using the program SCANCON which corrects data from LINESCAN. XRDPLOT detects the difference between the two types of experimental data files.

Files on diskette

The attached diskette contains the following files (in self-extracting format) relating to this appendix:

\APNDX-A\MOLS.EXE contains :

MOLMAP.EXE	executable MOLMAP as described above
MOLMAP.PAS	source code of MOLMAP.EXE
PLOTTER.INC	include file for MOLMAP.PAS
GEOMTOOL.INC	include file for MOLMAP.PAS
DBDE.INS	sample data file (structure **DBde**)
W12PY.INS	sample data file (structure **W12py**)

\APNDX-A\KIN.EXE contains :

KINETIC.EXE	executable KINETIC as described above
KINETIC.PAS	source code of KINETIC.EXE
A11_044.DAT	sample data*
A11_048.DAT	" "
A11_069.DAT	" "
A11_114.DAT	" "
A11_122.DAT	" "
A20_056.DAT	" "
A20_069.DAT	" "
A20_071.DAT	" "
A20_091A.DAT	" "
A20_091B.DAT	" "
A20_100.DAT	" "
A20_158.DAT	" "
A30_092.DAT	" "
A30_113.DAT	" "
A30_135.DAT	" "
A30_161.DAT	" "
A30_180.DAT	" "

* the sample data files are those for the experiment described in Chapter 8 for the inclusion of acetone by *trans*-9,10-dihydroxy-9,10-diphenyl-9,10-dihydroanthracene at three different temperatures and at different pressure of acetone vapour. The generalised name of the data file is "Ax_y.DAT" where x is the temperature in °C and y the pressure in mmHg.

\APNDX-A\BONDING.EXE contains :

BONDS.EXE	executable BONDS as described above
BONDS.PAS	source code of BONDS.EXE
DMET.LST	sample data file for BONDS.EXE
DPAC.LST	sample data file for BONDS.EXE

\APNDX-A\SCAN.EXE contains :

LINESCAN.EXE	executable LINESCAN as described above
LINESCAN.PAS	source code of LINESCAN.EXE
SCANCON.EXE	executable SCANCON as described above
SCANCON.PAS	source code of SCANCON.EXE
W12GAMMA.FLM	sample data file for SCANCON.EXE (scanned **W12py** decomposition γ-phase)

\APNDX-A\XRD.EXE contains :

XRDPLOT.EXE	executable XRDPLOT as described above
XRDPLOT.PAS	source code of XRDPLOT.EXE
XRDPLOT.FON	HPGL font file for XRDPLOT.PAS
DDDA.LIN	LAZY PULVERIX simulated XRD pattern for Host 4 α-phase structure retrieved from CSD
DDDA.XRD	experimental XRD trace of Host 4 α-phase
DPAC.LIN	LAZY PULVERIX simulated XRD pattern for the structure **DPac**
W12ALPHA.XRD	scanned XRD trace of Host 2($\pm$) α-phase
W12BETA.LIN	LAZY PULVERIX simulated XRD pattern for the structure **W12py**
W12GAMMA.XRD	scanned XRD trace of **W12py** decomposition γ-phase

\APNDX-A\UNITS.EXE contains :

BGIDRIV.UNT	links graphics drivers to the EXE file
BGIFONT.UNT	links the fonts to the EXE file
DISK.UNT	disk-related utilities
FILTER.UNT	data noise filtering functions
GRAPHER.UNT	screen graph plotting handling utilities
GSCREEN.UNT	graphics utilities
HPGL.UNT	HPGL-related utilities
METEX.UNT	reads the Metex multimeter
MISC.UNT	miscellaneous definitions, procedures and functions
MMOUSE.UNT	mouse-control
MOUSEBUT.UNT	menu button utilities
PC30.UNT	reads the PC-30 interface card
PM460.UNT	reads the Mettler PM460 balance
TSCREEN.UNT	text screen utilities
TIMER.UNT	timing utilities
HPGL.FON	HPGL font file

EGAVGA.OBJ	EGA/VGA graphics driver object file
HERC.OBJ	Hercules graphics driver object file
LENF.OBJ	graphics font object file
LITT.OBJ	graphics font object file
TRIP.OBJ	graphics font object file

In order to test or view any of the above files, copy the self-extracting EXE file (shown in bold above) to an empty subdirectory of the hard disk. Enter the name of the file to extract its contents. Provided that the computer conforms to the requirements described above, the executable programs can be evaluated using the sample data files. In addition, the source code files for the programs BALANCE and PT are provided as \APNDX-A\BALANCE.PAS and \APNDX-A\PT.PAS respectively. All the sources for the programs are supplied, together with the sources of the units required by them. These sources can be compiled using Turbo Pascal Version 6.0 or higher.

References

1 Turbo Pascal, Version 6.0, 1990, Borland International Inc., Scotts Valley, CA, USA

2 A. Gavezotti, *J. Am. Chem. Soc.*, 1983,**105**,16

Appendix B

The vacuum balance system described in Chapter 8 employs an electronic circuit which controls the levitation of the sample. This circuit was designed and constructed by Mr K. Achleitner and is described here since it is an essential part of the apparatus. Details of the data logging software are provided in Appendix A.

Description of the circuit

The circuit (Figure B1; Note : the power supply circuit is not shown) is a voltage controlled current source, the voltage level being a function of the light intensity striking photodiode D_1. The 1.8 volt light bulb (with built-in lens) gives rise to a quasi parallel light beam which passes over the top edge of the PTFE screen, striking the large area silicon photodiode. A photocurrent is produced which is a linear function of the light intensity. The photodiode is reverse biased and connected to a transimpedance amplifier, U_{1A}, which ensures that the photodiode is operating in a short-circuit mode, thereby producing a current proportional to the incident irradiance.

The output voltage, $V_P = -R_F.I_P$ where R_F is the feedback resistor and I_P is the photodiode current. The voltage V_P then feeds into a phase-lead amplifier, U_{1D}, that ensures stability of the control loop by compensating for lags in the system. The levitating magnet experiences a low frequency oscillation if C_4 is removed and the optimum value for C_4 can be empirically selected for maximum stability. The transfer function of the phase-lead amplifier is given by

$$\frac{V_C}{V_P} = \frac{-R_4 (1 + jR_3C_4)}{-R_4 (1 + jR_3C_4)} \qquad (1)$$

where jR_3C_4 and jR_4C_3 are complex numbers. The transfer function may also be expressed in terms of the complex frequency, s, as

$$T(s) = \frac{-C_4[s + 1/(R_3C_4)]}{C_3[s + 1/(R_4C_3)]} \qquad (2)$$

Equation 2 indicates that $1/(R_4C_3)$ is a pole of T(s) and that $1/(R_3C_4)$ is a zero. With the values shown, the first break-point frequency, f_1, is 60.3 Hz. A second break-point (f_2 = 13,3 kHz) is due to a pole created by C_3 and R_4. The ten-turn potentiometer, R_{V1}, and resistor R_4 are used to set the current through the coil, L_1, when the PTFE screen blocks approximately 50% of the light projected at the photodiode. The length of the magnet protruding from the screen must be optimised to ensure that the barrier blocks the correct amount of light, at the same time making sure that the gap between the permanent magnet and the electromagnet permits stable levitation to take place. These two adjustments are critical but once set, need no further attention. The output of U_{1D} is given as

$$V_c = R_4(V_o/R_5 + R_fI_D/R_3) \qquad (3)$$

where V_o = offset from potentiometer R_{V1} and the voltage V_P due to photodiode current = $R_f + I_D$. However, $R_4 = R_5 = R_3$. Therefore

$$V_c = V_o + V_P \quad (4)$$

The voltage V_c at pin 10 of U_{1C} is identical to the voltage at pin 9, which is the voltage across resistor R_7 (proportional to the current). The action of the negative feedback loop, comprising the MOSFET transistor, R_7, and the operational amplifier, ensures that I_{coil} is directly proportional to V_c. This section therefore acts as a voltage controlled current source:

i.e. $I_{R7} = V_c/R_7 = I_{L1}$ = coil current

The 5.1 volt zener diode protects the MOSFET transistor from excessive gate-source voltage and the capacitor C_5 is used to suppress a high frequency oscillation due to the inductance of L_1.

Specifications

The balance has a weighing range of 410 grams and features subtractive taring with a readability of 1 milligram. The electromagnet weighs approximately 78 grams and the tare weight of the levitating system (comprising the permanent magnet, PTFE screen, brass connecting rod and the sample pan) is 25.2 grams. An additional weight of up to 16 grams can be supported by the electromagnet. The gap between the electromagnet and the permanent magnet is maintained at between 4 and 7 mm. Since a compensating beam balance (for which there is no perceptible vertical displacement of the weighing mechanism) is used, fluctuating forces due to elastic deformation of the electric lead (double strand of 0.1 mm diameter copper wire) to the electromagnet are not detected.

Once in operation, the levitating system quickly gains sufficient stability to allow accurate mass readings, restricted only by the detection limit of the analytical balance. Typically, 100 to 500 milligrams of host sample is used for an expected stoichiometric mass increase in the range 30 to 200 milligrams of absorbed guest. This is well within the capabilities of the free suspension system.

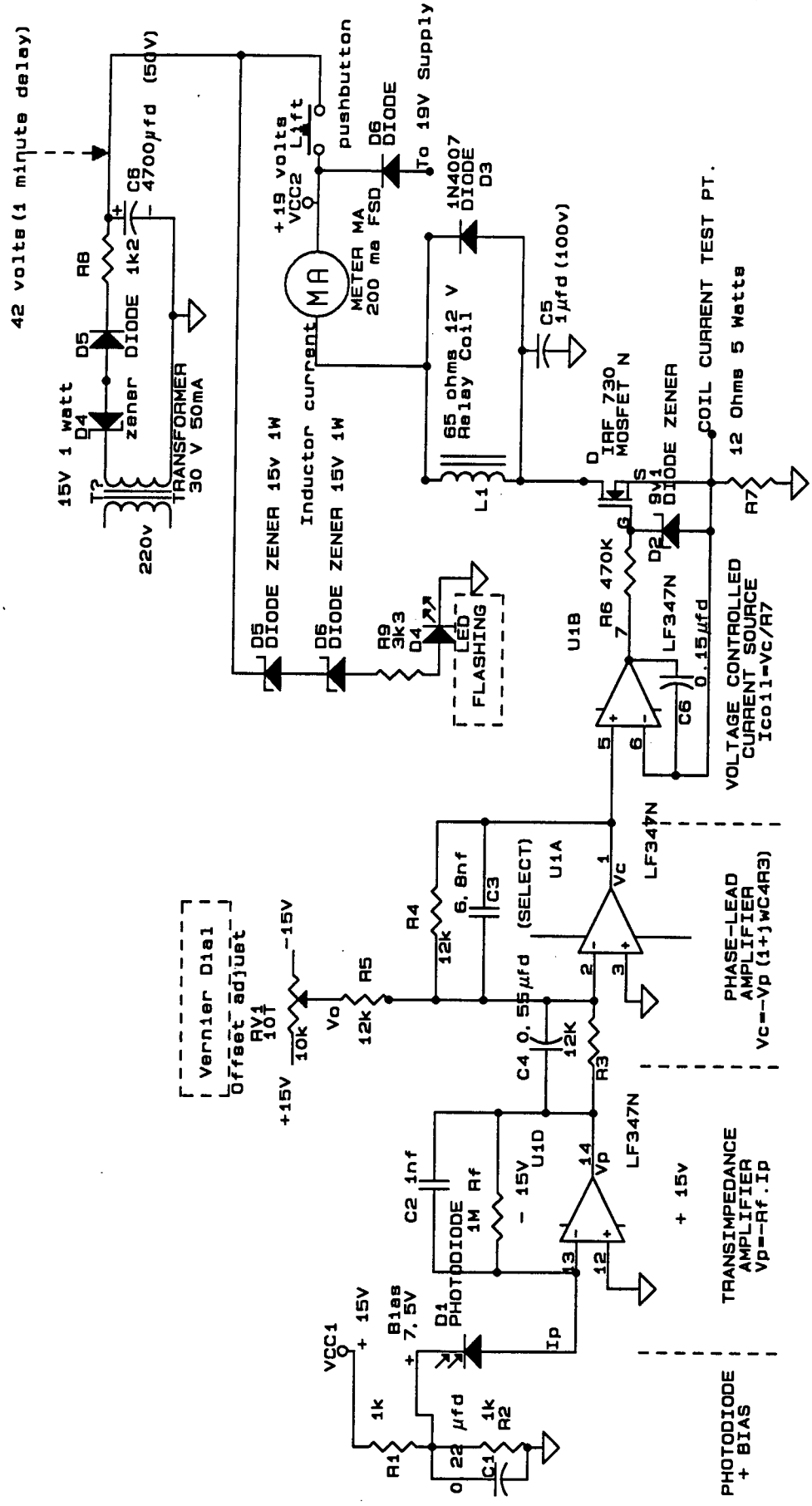

Figure B1 Levitation control circuit.

Appendix C

The pressure/temperature measuring apparatus described in Chapter 9 employs two electronic circuits. The first circuit transmits the pressure and temperature signals to the PC-30 interface card of the microcomputer while the second controls the pressure compensation system which separates the pressure transducer from the sample. These circuits were designed and constructed by Mr K. Achleitner and are described here since they are essential to the apparatus. Details of the data logging software are provided in Appendix A.

Pressure/temperature amplifier circuit

The pressure transducer and thermocouple amplifier circuits are shown in Figures C1 and C2 respectively. The former employs a true differential instrumentation amplifier to produce 0 to 10 volts for the pressure range 0 to 800 mmHg, while the latter produces the same voltage range for the temperature range 0 to 100 °C. Both voltage signals are linear with respect to the pressure and temperature.

The two circuits are housed in the same box together with a common power supply and a liquid crystal display which can be switched to display either the temperature or the pressure.

Window comparator circuit

As noted in Chapter 9, an electronic circuit (Figure C3) was designed in order to balance the pressure differential in the two limbs of the U-tube (refer to Figure 9.4). A beam of light from the bright LED is passed over the mercury meniscus in limb B and its intensity measured by the large area photodiode D_1. The photodiode operates with zero bias and is connected to a transimpedance amplifier U_{1A} which ensures that the photodiode is operating in short-circuit mode, thereby producing a current I_P, proportional to the incident light. The output voltage from the photodetector is V_P, where $V_P = - R_1 I_P$ and feeds into a window comparator. When the pressure in limb A increases, the mercury level in limb B rises, resulting in a decrease in light intensity. At a predetermined intensity value V_1, solenoid valve 1 is opened, causing venting of limb B to the atmosphere until the light signal is again greater than V_1. Similarly, if the sample pressure decreases, the light intensity increases until it reaches V_2, causing activation of valve 2 which opens limb B to the vacuum pump. V_1 and V_2 can be set using the two potentiometers pot. 1 and pot. 2. Thus, with suitable adjustment of V_1 and V_2, a narrow window can be set to ensure pressure readings of acceptable accuracy (better than 1 mmHg). However, with a narrow window setting, the problem arises where even slight over venting causes activation of valve 2 which in turn again activates valve 1, causing the system to 'hunt' for the equilibrium pressure. For this reason valve 2 is disabled during sample heating (since only an increasing pressure trend is expected) using another I/O line fed to the circuit. During the cooling cycle, valve 1 is similarly disabled and valve 2 again enabled. The PC-30 interface card of the microcomputer is used to inhibit (with software) either of the valves as shown in Figure C3. C_3 and C_4 were added to the circuit in order to desensitise the comparator to vibrations. These capacitors

introduce a half-second delay before the triggering of either valve. A flask of volume 3L is attached to limb B and acts as an air-movement buffer to the solenoid valves.

Specifications

The resolution of the ADC of the PC-30 card is 2.44 mV. Thus pressure and temperature changes of 0.2 mmHg and 0.02 °C can be resolved. However, owing to limitations relating to the response of the thermocouple and the ability of the window comparator to keep the two limbs of the U-tube at equal pressure, the realistic precision of the apparatus is ±1 mmHg in pressure and 0.2°C. Using the 500W light bulb as the heating source for the oven, heating rates up to 7 °C min^{-1} can be maintained and an oven temperature exceeding 100 °C can be reached. The advantage of using a lamp is that its thermal inertia is small, thus enabling rapid and relatively accurate control of the oven temperature.

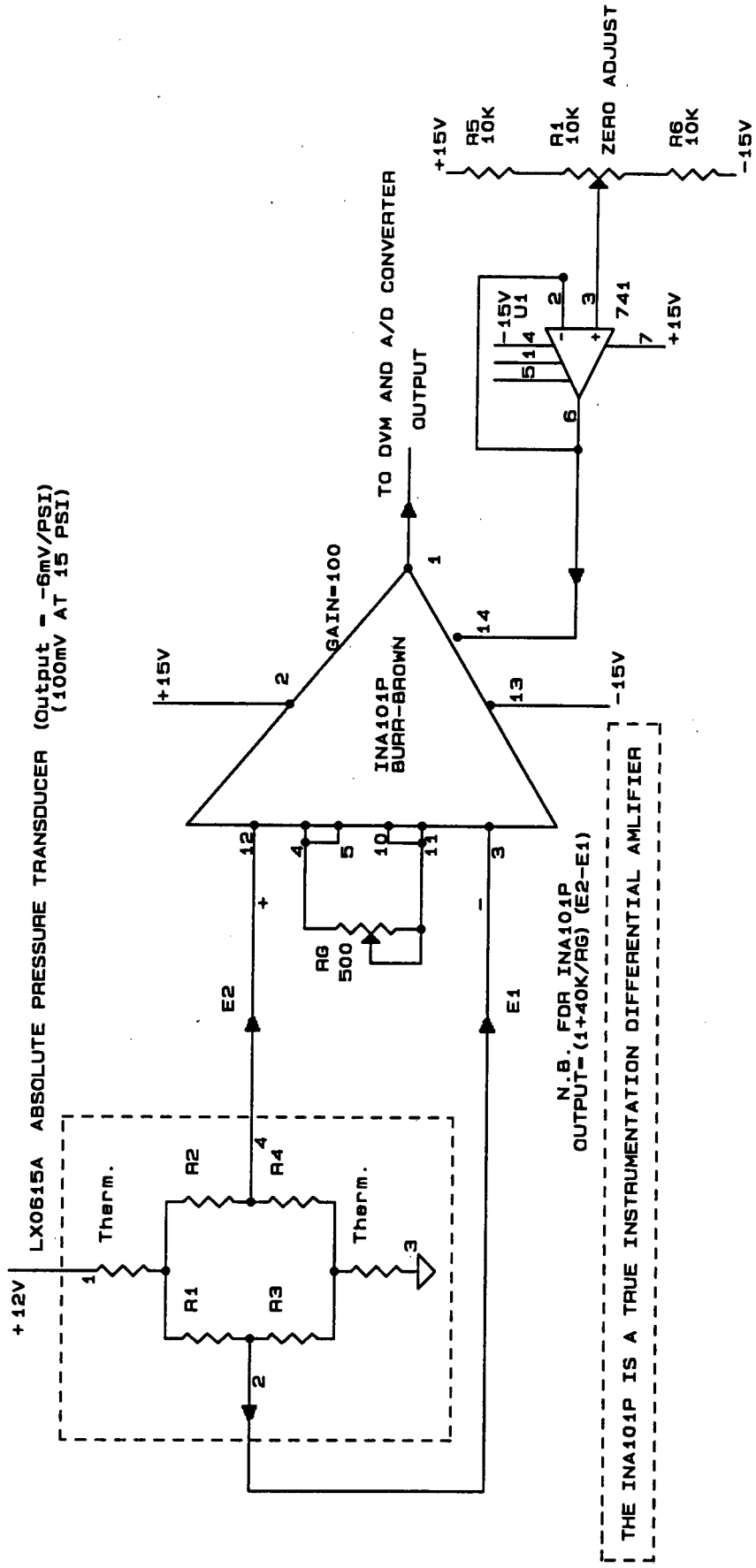

Figure C1 Pressure transducer amplifier circuit for LX06015A.

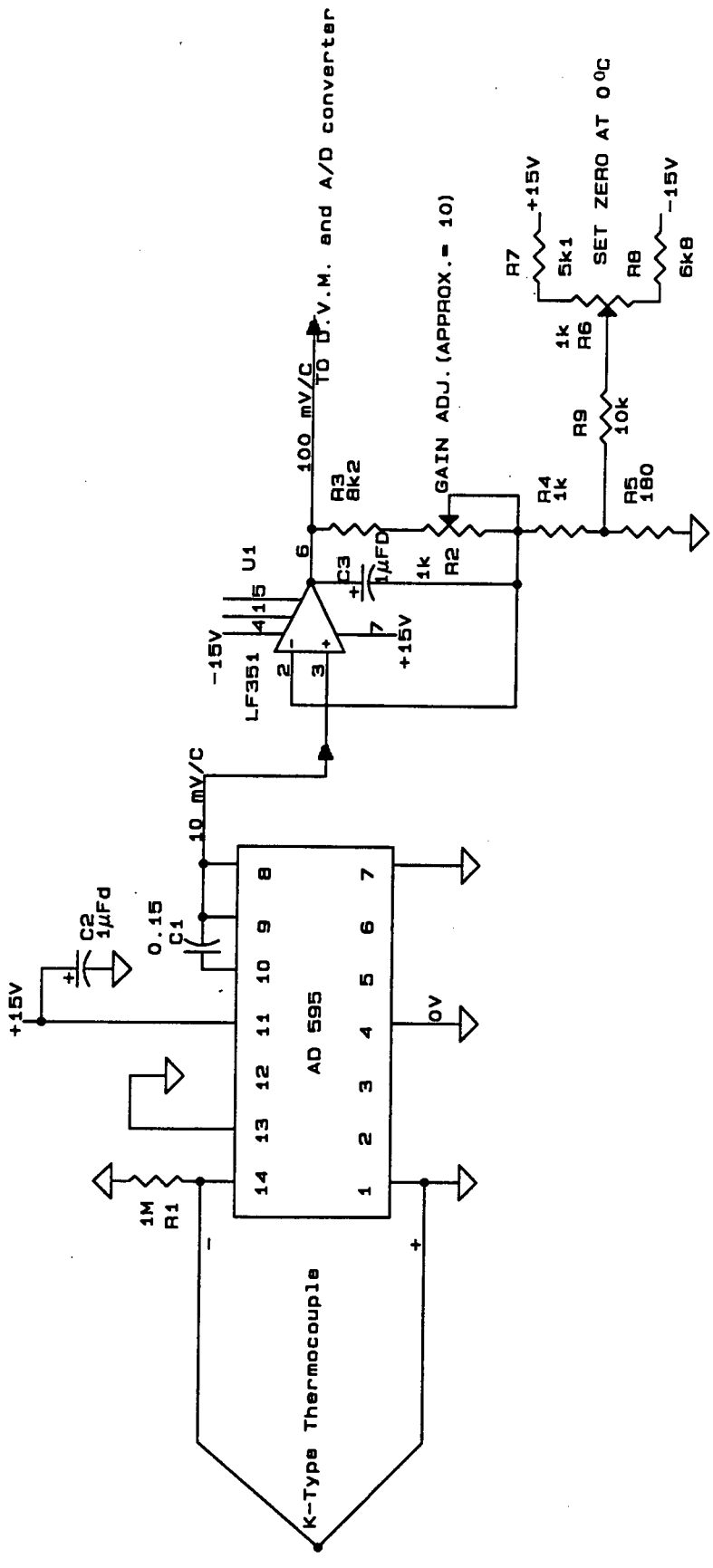

Figure C2 Thermocouple amplifier circuit.

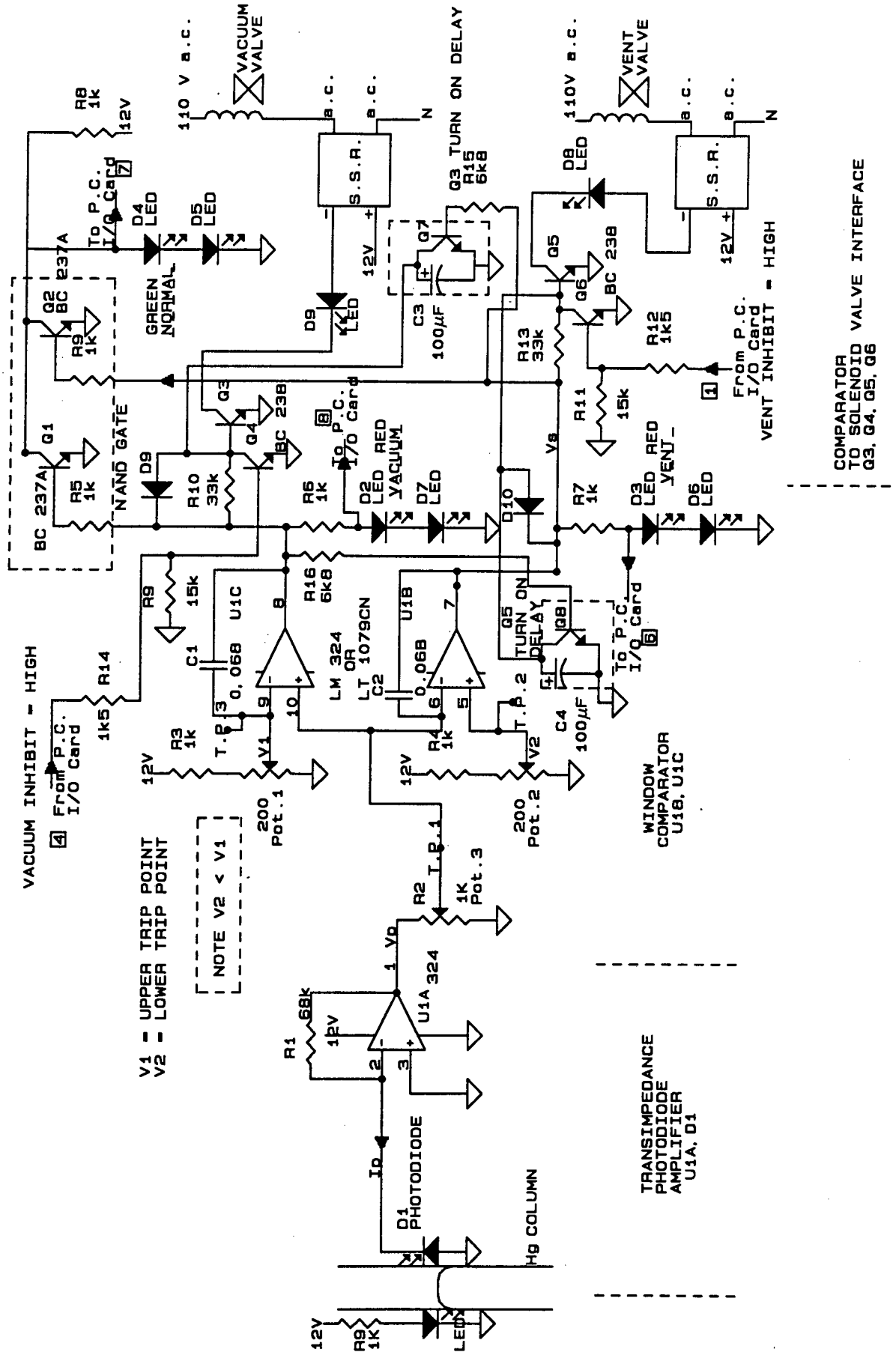

Figure C3 Window comparator circuit.

Appendix D

The photographs shown on the next page are :

Photograph 1
A crystal of **DBde** sealed with mother liquor in a Lindemann glass tube. The tube is glued into a brass pin with the crystal approximately 8 mm from the flange of the pin.

Photograph 2
The sample support system (the PTFE screen, permanent magnet and part of the connecting rod to the sample pan can be seen) levitating below the electromagnet of the vacuum balance system.

Photograph 3
The reaction vessel containing the sample support system clamped in position below the electromagnet.

Photograph 4
Part of the prototype of the pressure/temperature apparatus. The pressure transducer (top left) is sealed into a ground glass joint which is linked to the sample flask *via* a capillary. The system can be evacuated through the side-arm (top) and sealed using the PTFE tap (top right).

Photograph 5
Inside the oven (left half of photograph) are shown the 500W heating lamp, the circulating fan and the sample flask attached to limb A of the apparatus described in Chapter 9. Limb B is shown (right half) with the light source and detector unit.

Photograph 6
Shown are the oven (left), the box containing the pressure and temperature amplifier circuit (top left), the box containing the window comparator circuit (bottom) and limb B (with attachments) of the apparatus. Attached to limb B are the pressure transducer, the 3L buffer flask the two solenoid valves and tubing leading to the vacuum pump.


1


4

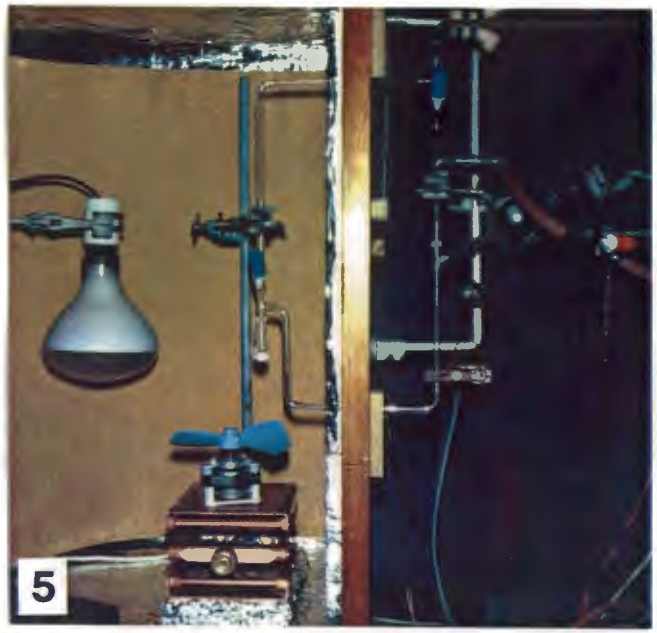
5

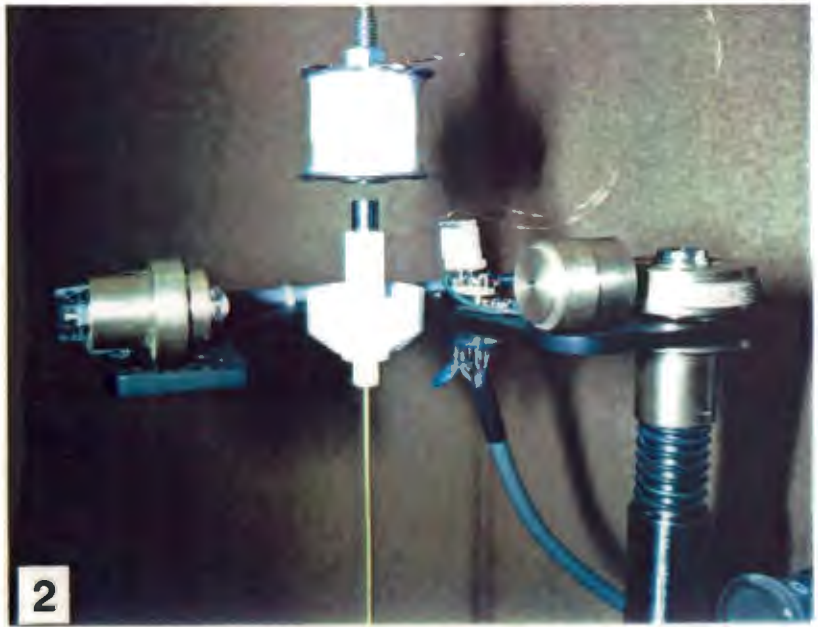
2


3


6

Appendix E

In 1987, Allen *et al.** published mean bond lengths in organic compounds as calculated using X-ray and neutron diffraction results retrieved from the September 1985 version of the Cambridge Structural Database. The following table lists such values for the types of bonds encountered in the present study:

Type of bond		Mean distance (Å)
$C_{sp^3} - C_{sp^3}$	overall	1.53(2)
$C_{sp^3} - C_{sp^2}$	ketones	1.51(2)
$C_{ar} \simeq C_{ar}$	phenyl rings, overall	1.38(1)
$C_{ar} \simeq C_{ar}$	pyridine	1.38(1)
$C_{ar} - C_{sp^3}$	overall	1.51(1)
$C_{ar} - C_{ar}$	biphenyls, *o*-subst.	1.49(1)
$C_{ar} \simeq C_{ar}$	in naphthalene:	
	$C_1 - C_2$	1.37(1)
	$C_2 - C_3$	1.41(1)
	$C_1 - C_{8a}$	1.42(1)
	$C_{4a} - C_{8a}$	1.42(1)
$C_{sp^3} - O$	alcohols, overall	1.43(1)
$C_{sp^2} = O$	ketones	1.210(8)
$C_{sp^3} - O$	ethers, overall	1.43(2)
$C_{ar} \simeq N$	pyridine	1.34(1)
$C_{sp^3} - S$	overall	1.81(3)
O = S	in $C_2S{=}O$	1.50(1)

* F.H. Allen, O. Kennard, D.G. Watson, L. Brammer, A.G. Orpen and R. Taylor, *J. Chem. Soc., Perkin Trans. 2*, 1987,S1

Appendix F

The attached diskette contains relevant data relating to the final refinement of the structures elucidated here. These data are stored in three self-extracting MS-DOS formatted EXE files in the "\APNDX-F" subdirectory:

ANALVAR.EXE contains the analysis of variance tables as described in Chapter 2.

STRUCDAT.EXE contains tables of the fractional atomic coordinates, anisotropic thermal parameters, bond lengths and angles, torsion angles and fractional atomic coordinates of hydrogen atoms in calculated positions.

STRUCFAC.EXE contains the observed and calculated structure factors.

To access the data, copy the relevant EXE file to the hard disk of an IBM-compatible PC and enter its name. The data files for all the structures will self-extract. They can be viewed by means of any text-editing program (e.g. a word processor).